THE UNIVERSITY *of* EDINBURGH

Experimental Studies on Resistance to Fluid Displacement in Single Pores

Stephen Okachukwu Kwelle

A thesis submitted for the degree of Doctor of Philosophy

The University of Edinburgh

April 2016

Declaration

I declare that the research reported in this thesis has been conducted by me, Stephen Okachukwu Kwelle, and the work contained in it is my own, except where stated otherwise. Further, this thesis has not been submitted for the award of any other degree or professional qualification except as specified. Where other sources are quoted full references are given.

Stephen Okachukwu Kwelle

April 2016

Thesis Supervisors

Dr. Xianfeng Fan, University of Edinburgh, School of Engineering, Edinburgh, United Kingdom

Prof. Stefano Brandani, University of Edinburgh, School of Engineering, Edinburgh, United Kingdom

Abstract

Understanding the resistance to displacement of one fluid by another in multiphase transport in a porous medium is very beneficial in hydrocarbon exploration and production as well as geological storage of carbon dioxide. Pore resistance behaviour of a porous medium controls the fluxes of fluids through the caprocks over the geological times and therefore directly determines the volume and localization of the hydrocarbons trapped (best locations for exploration) and also the overpressured formation (zone of drilling hazard). In the design for enhanced oil recovery and geological storage, it sets a limit on both the injection pressure and storage capacity of the reservoir to avoid an upward migration of the injected fluid into the overlaying formations. Many investigations have been carried out on the resistance to porous media flows for decades, yet the understanding of the individual factors affecting it is not complete, because most studies were carried out on core samples, whereas flow resistance depends on the flow details at the pore scale. For example, two core samples may have same porosity but different pore size.

This research focused on advancing the understanding of resistance to multiphase displacement in a porous medium, using the pressure profile of interface flow through single pores, to measure the resistance to two-phase flow and then link the impact of pore geometry, surface tension, fluid properties, and wettability, on the pressure profile to the displacement process, in order to fill the noticed gap of knowledge.

Experiments conducted in this research using tapered capillaries revealed that the resistance to two-phase flow is significantly higher than the single phase resistance

and the pore throat of a porous medium is not just determined by a group of smallest pore sizes as understood using core samples, but by response of critical effective pore diameter to resistance to two-phase interface flow. The initiation of a pore throat is characterised by a drastic increase in the resistant pressure at the effective pore size. The effective pore diameter is generally less than 500 μm and increases with the pore tip diameter and the capillary gradient, interfacial tension, but decreased by surfactants. Viscosity does not have any significant effect on the effective pore diameter. The study also revealed a relationship between pore contact angle and pore throat; pore contact angle is maximum and remains fairly constant at the pore throat.

The overall outcome of this research is a significant contribution to the influence of pore geometry on the resistance to porous media flows.

Lay summary

Understanding the resistance to flow is very useful because it controls how fluids move across caprocks (seals) over time and so determines the volume of oil and gas trapped, where in the rocks they are trapped, and also zones of possible danger (too much resistance) during drilling. In preparing for enhanced oil recovery and underground storage of carbon dioxide this resistance helps us to determine the maximum pressure that can be applied and the amount of gas or liquid that can be stored in order to avoid leakage of the injected fluid. Many researches have been carried out on the resistance to fluid flow in porous media but the effects of each factor have not been fully understood, because most of these researches were carried out on large rock samples (core samples). As a result, the details of the events occurring in the pores which manifest in the properties of the large samples are not properly understood. An example is the case where two core samples of same size store the same amount of fluids, yet their resistances differ.

In this research, in order to understand better the effect of the factors affecting two-phase flow resistance, a single capillary is used to represent the single pore and the resistant force profile to two-phase flow through this single pore was measured. The impact of pore geometry, surface tension, fluid properties, and wettability on the force profile was then used to explain their effects on the displacement process.

Results of the experiments conducted with tapered capillaries showed that the resistance offered when two immiscible fluids flow is much higher than that by flow of single fluid, which remains constant once it reaches its maximum value. The pore

throat of a porous medium for two-phase flow is not only determined by a group of pores of small sizes, but also by the response of the pore to resistance to flow of the two fluids. The beginning of a pore throat is identified by a sharp increase in the resistant pressure at the effective pore size. The exact effect of pore geometry, interfacial tension, surfactant, viscosity and wettability on the fluid flow resistance is now established. In particular, this research has shown the exact impact of pore size on the resistance to fluid flow in porous media.

Dedication

To all who contribute to knowledge

Acknowledgment

I thank the Almighty God for his mercy and grace that saw me through the challenges of this journey. I give Him all the glory, honour, and adoration for the successful completion of this programme.

I owe a lot of gratitude to my supervisor, Dr. Xianfeng Fan, for his unwavering and untiring support that has made this work successful. His constructive criticisms, invaluable advice, guidance, and encouragement have added so much value to this work and contributed immensely to my personal development and scientific maturity.

I would also express my deepest gratitude to my second supervisor, Prof. Stefano Brandani, for his relentless support throughout the course of this study. My discussions with him sincerely stimulated my analytical reasoning and gave me deeper insights into this research.

I am indebted to all the staff of the Institute for Materials and Processes for providing me with the necessary support at all times. The School of Engineering technical support staff namely, Steve Gourlay, Bryan Mitchell, Douglas Carmichael, David Stewart and Kevin, just to mention a few, are highly appreciated for attending promptly to my research demands.

I would like to thank friends and colleagues whom I met in the course of this programme and who made my experience in Edinburgh an enjoyable one namely, Ares Gomez, Dursun Can Ozcan, Stephen McGurk, Ebraheam Al-Zaidi, Mia Mohd-Ismail, Dimitrios Mamalis, Sofia Korniliou, Nelly Vasileiadou, Yunning Li, Andrea

Dávidné, Esme Anderson, Mengyu Cao, Jiaxian Zhang, Yu Guo, Weiwei Wang, and many others not mentioned. I would not forget the special support of my colleague, Sena Peace Hounkpe at critical times during my research.

My friends outside the University who always encouraged and supported me during my research are highly appreciated.

My sincere appreciation goes to my parents, Hart N. Kwelle (late) and Janet Kwelle for their inspiration that has brought me to this enviable height. I thank my siblings and other family members for their support during this period.

My special thanks go to my amiable wife, Miya and son, Excel, who sacrificed their precious time and inspired me to complete this programme. Without your unalloyed support and constant love this feat would not have been possible. I would always remember the encouragement from my son for his thoughtfulness to dissuade any form of noise while I worked by posting a notice for silence at my study.

Contents

List of abbreviations

General

CCS	Carbon Capture and Storage
EOR	Enhanced Oil Recovery
FEP	Fluorinated Ethylene Propylene
GHG	Green House Gas
HP	Hagen Poiseuille
MICP	Mercury Injection Capillary Pressure
$MtCO_2$	Metric ton of Carbon dioxide
NMR	Nuclear Magnetic Resonance

Parameters

K	Absolute permeability (md, cm^2, m^2)
ϕ	Porosity (fraction)
R_X	Radius corresponding to x% mercury saturation of rock
R, r	Pore radius (mm, µm)
T	Temperature (^oC)
P	Pressure (mbar, Pa)
γ	Surface tension (mN/m)
θ	Contact angle (deg)
µ	Viscosity (µPa.s, mPa.s, cp, cst)
D,d	Diameter (mm, µm)

Units

µm	Microns (micrometer)
mm	Millimeter
m	Meter
km	Kilometer
mbar	Millibar
mN/m	MilliNewton per meter
md	Millidarcy
Pa	Pascal
MPa	MegaPascal

List of figures

List of tables

Chapter 1: Introduction

1.1 General overview

Displacement of fluids in pore spaces has its wide applications in many natural and industrial processes, such as oil and gas recovery (Kovscek and Cakici, 2005, Chen *et al.,* 2012; Dehghan *et al.,* 2009; Shad *et al,* 2013), geological storage of carbon dioxide (Bachu and Bennion, 2009; Juanes *et al,* 2006; Orr, 2004; Bachu, 2003; Wang *et al.,* 2013), underground water remediation (Tsakiroglou and Payatakes, 2000), filtration (Grismer, 1986; Hammecker *et al*, 2004), chemical microreactors (Juncker *et al.,* 2002), microfluidic technologies *(Yang et al.,* 2011), nanofluidic devices (Wang *et al.,* 2010; Liu *et al.,* 2011), and proton exchange membrane fuel cells (He *et al.,* 2000; Qi *et al.,* 2009; Wang *et al,* 2001, Koido *et al,* 2008). The basic phenomenon is that the multiphase transport involves the displacement of one fluid by another. For example, the injection of carbon dioxide for underground storage or for enhanced oil recovery, involves the displacement of water and/or oil by CO_2 during injection and the displacement of CO_2 by either water or oil after cessation of injection by influx of fluids from adjacent aquifers or hydrocarbon sources (Kumar *et al,* 2005; Bennion and Bachu, 2006b). The injection process and its efficiency are dependent on the resistance to the flow of the fluids in the porous medium.

Fluid flow in a porous medium is opposed by the resistance of the porous medium and the constituent fluids, and this resistance is measured by the pressure drop that occurs in the medium (Despois and Mortensen, 2005; Endo *et al,* 2009). Accurate prediction of porous media flows, therefore, crucially depends on the evaluation of

flow resistance, defined as the relationship between the driving force and the resulting fluid momentum. The lower the resistance, the lesser the energy needed to displace the fluid through the porous medium. In many applications this is very desirable; for example, in the migration of hydrocarbons to conventional reservoir rocks and recovery of the hydrocarbons from the same rocks, the resistance of the porous medium should be low enough to store and deliver economic quantities of oil and gas. On the other hand, high resistance to flow may also be beneficial. For example, to trap the stored fluids in the reservoir rocks the resistance of the seal rock should be high enough to block the passage of the fluids (Nelson, 2009). Steam foams, as displacing fluids for enhanced oil recovery, improve oil recovery by increasing the resistance to flow of the steam through the underground oil-bearing porous medium, thus improving mobility control and decreasing gravity override (Dilgren and Deemer, 1982; Gauglitz *et al,* 1987). High resistance to flow in compact heat exchangers is known to increase the effectiveness of heat transfer between fluid and solid (Kim *et al,* 2000), and also yields a desirable transition in reactant mass transport mode in fuel cells (Kumar and Reddy, 2003).

Flow resistance in a porous medium is usually characterised by bulk flow properties, such as permeability, capillary pressure, fluid saturation, resistivity, conductance, but the fundamental behaviours of multi-phase porous media systems are governed by physical processes acting at the pore scale (Al-Raoush and Wilson, 2005; Celia *et al.,* 1995; Andrew *et al,* 2014), so flow resistance depends on the flow details at the microscopic scale. These properties are controlled by the interplay of capillary and viscous forces (Melrose and Brandner, 1974) and, in some cases, buoyancy and inertial forces. Viscous forces are always resistive forces trying to slow down flow,

while capillary forces usually dictate the pore-scale distribution of each fluid phase (Perkins, 1957; Silina and Patzek, 2006), which eventually dictate the bulk properties such as residual saturation and relative permeability. Pore level displacement is influenced by the pore structure (pore geometry and distribution, pore topology or connectivity, and porosity), fluid properties (surface tension, viscosity), fluid-fluid interaction, fluid-solid interaction such as wettability, and porous media conditions such as pressure and temperature (Chen *et al,* 2012; Hammond and Unsal, 2009; Jamaloei *et al.,* 2011; Anderson, 1986; Blunt, 1997; Chalbaud *et al,* 2009; Plug and Bruining, 2007). The effects of all of these factors are inter-related. Although porous media flows have been investigated for many decades, the exact impact of the individual factor on the resistance to displacement is not fully understood, neither is their relative importance clearly understood. For example, the detailed flow structure at the pore-scale is not fully understood. A proper understanding of the significance of these factors could enhance the understanding of the processes that occur in the porous medium, such as in geological storage of CO_2 and improved oil recovery.

For some decades, studies in understanding the mechanisms of multiphase flow in porous media have progressed from macroscopic studies, involving the measurement of averaged quantities, such as relative permeability and residual saturations, in samples that are large compared with pore scale, to microscopic studies focusing on individual pores (Lenormand *et al,* 1983; Mohanty *et al*, 1987; Dullien, 1979; Payatakes and Dias, 1984; Chen and Koplik, 1985). Until date, studies of transport mechanisms (Colombani *et al,* 2002; Ellis and Bazylak, 2012; Ma *et al,* 2012) at the pore scale have continued to attract attention because of their importance in many engineering applications, especially in the energy field where the oil/gas is found in

formations which consist of solid matrix and pore space (Joseph *et al,* 2013). Researchers have consistently agreed that the mechanisms involved in transport phenomena in porous media are usually described by macroscopic laws applicable to systems whose dimensions are large compared with the dimensions of the pores (Dullien, 1979; Lin and Miller, 2000). Microscopic studies involved associating a description of the fluid behaviour at a pore scale with a representation of the structure of the porous medium using an interconnected pore network (Lenormand *et al,* 1983). The bulk behaviour was then determined from the local scales either by computer simulations (Fatt, 1956; Dodd and Kiel, 1959; Wardlaw and Taylor, 1976; Androutsopoulos and Mann, 1979; Mann *et al,* 1981) or using a statistical 'percolation-type' approach (Chatzis and Dullien, 1977; Larson *et al,* 1981).

Unfortunately, because of the complexity of the pore geometry, it is difficult to predict macroscopic (effective) properties from microscopic (pore level) properties. Generally, no linear or non-linear rule for the use of microscopic physical properties to predict the macroscopic scale properties exists. As a result, it becomes essential to develop appropriate experimental techniques and theoretical models to describe in detail the pore-level flow which occurs through a porous medium (Lin and Miller, 2000). Researchers have tried to create micromodels (Karadimitriou and Hassanizadeh, 2012) which consist of simple and regular geometric features, fractal patterns and irregular patterns with characteristic length-scale comparable with the average pore diameter, quite different than the pore geometry of a natural porous media (Er *et al,* 2010; Jamaloei and Kharrat, 2010; Wu *et al,* 2012a). Visual micromodels are now used commonly to enhance pore scale studies. As defined by Sayegh and Fisher (2008), visual micromodels are flow apparatuses that enable

visual observation of multiphase flow behaviour in porous media at the pore level. Mattax and Kyte (1962) used chemically etched networks on glass plates to study waterflood. These micromodels give clear observations, but the shape of the section of the ducts is not well defined. In addition, adhesion between the glass plates poses a problem, especially for studies of imbibition; the wetting fluid enters the space between the plates (Lenormand *et al,* 1983). Generally, engineered micromodels have proved to be very useful for studying a variety of displacement processes, especially in oil recovery processes, such as surfactant floods (Paterson *et al,* 1984; Hornof and Morrow, 1988), foam injection (Owete and Brigham, 1987; Chang *et al,* 1994), immiscible displacements (Wardlaw, 1980; Chatzis and Dullien, 1983; Mahers and Dawe, 1985;Touboul *et al,* 1987), gels or conformance control (Bai *et al,* 2007), microbial EOR (Soudmand-Asli *et al,* 2007), and solution gas drive (Grattoni and Dawe, 2003; George *et al,* 2005). Micromodels have also been used to study specific aspects relating to flow in porous media, including wettability (Morrow *et al,* 1986; Romero-Zeron and Kantzas, 2007); capillary pressure (Smith *et al,* 2005); and interfacial tension (Mackay *et al,* 1998). However, micromodels typically have uniform or homogeneous wetting and geometrically simple pore shapes that do not represent the multiple solid phases, pore sizes, and pore shapes of the porous medium (Heath *et al,* 2012).

Single glass capillaries of circular cross-sections are among visual micromodels that have been used by numerous researchers for experimental (Fairbrother and Stubbs, 1935; Schwartz *et al,* 1986; Tzimas *et al,* 1997, Lucas *et al,* 2006; Argüelles-Vivas and Babadagli, 2014), theoretical (Bretherton, 1961; Cox 1962), and simulation (Park and Homsy, 1984; Ratulowski and Chang, 1989; Giavedoni and Saita, 1997)

studies at the pore level. Most of these studies were focused on film thickness (residual saturation) in the tube, with no significant attention to the resistance to fluid flow. From the available literatures, apart from a few experimental studies by Goldsmith and Mason (1963), Roof (1970), and Olbricht and Leal (1983) on constricted circular capillaries, most other investigations were conducted with circular capillary tubes of uniform cross-sections. For the constricted capillaries, the diameter of the constriction showed a sharp departure from the other parts of the capillary. Lenormand et al (1983) had observed that models for fluid behaviour obtained from experiments using circular capillary tubes remained simplistic. Blunt *et al* (1995) and Dong and Chatzis (2004) suggested that circular capillary tubes are not the best option to mimic the network of pores in a real reservoir due to their low retention power. However, Argüelles-Vivas and Babadagli (2014) used circular capillary tubes to study residual oil saturation in gas-oil displacement on the basis of their availability for relatively small diameters and ease of use in visualisation, especially with heavy crude oil. They suggested that the shape of the capillaries can be changed, having made initial attempts using square capillaries (Argüelles-Vivas and Babadagli, 2014).

Despite their shortcomings, circular glass capillary tubes still remain good options for pore-scale studies, especially if their geometries can be modified, because of ease of visualisation and monitoring of the events. Circular glass capillary tubes fabricated from borosilicate glass offer a good option as their geometry can be modified. Using this type of modified circular single glass capillary tubes, the impact of each factor affecting fluid displacement, such as pore geometry, fluid properties (surface tension, viscosity) and wettability can be studied at the pore level. For

instance, pore contact angle which used to be measured on flat surface can be measured in a pore. It is hoped that using these capillary tubes, a lot of useful and essential information will be revealed to enhance our understanding of the pore-scale processes and also provide fundamental data for designing EOR processes and CO_2 storage. With current research focus on techniques for scale changes, this study in single pores will stimulate further interest in pore scale studies and also provide data that can be used to develop better network models and enhance our understanding of the multiphase flow in porous media.

1.2 Porous medium morphology

A porous medium is a material consisting of a solid matrix with interconnected void. Porous media in nature are always made up of numerous irregular pores of different sizes spanning several orders of magnitude in length scales, such as soil, sandstones in oil reservoir, matrix pores in coal, packed beds in chemical engineering, fabrics used in liquid composite moulding and wicks in heat pipes (Wang *et al,* 2014). Figure 1.1 shows photomicrographs of some natural porous media, namely, beach sand, sandstone, lime stone, rye bread, wood, and the human lung (Dullien, 1992). They are called fractal porous media because they possess pore microstructures, including both pore sizes and pore interfaces, and exhibit fractal characteristics.

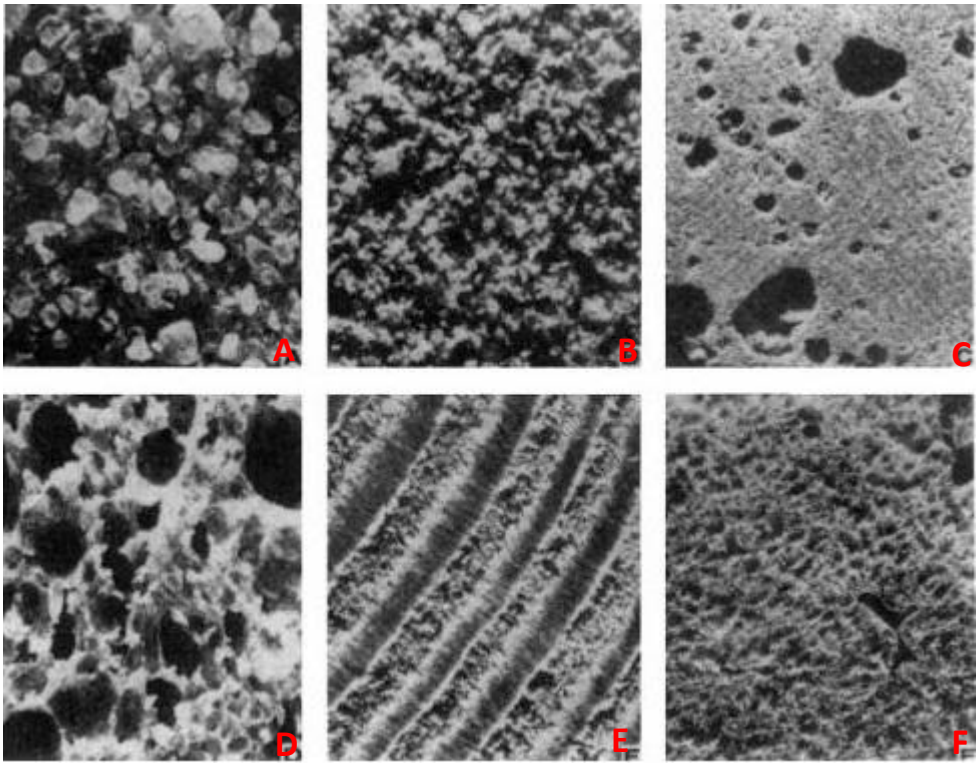

Figure 1.1 – Examples of natural porous materials (x 10): (A) beach sand; (B) sandstone; (C) limestone; (D) rye bread; (E) wood; (F) human lung (Dullien, 1992).

The pore spaces are also irregularly multiply connected. Pore throats are constrictions or smaller spaces connecting pore bodies which are the larger spaces. The pore bodies determine the porosity, while the pore throats control the movement of fluids and the permeability.

Scanning electron micrographs of cross sections show the non-uniform curvature and roughness of the pore walls. For network modelling, even if it is possible in principle to find both the equivalent network and the distribution of a characteristic radii in a systematic way (Figure 1.2), there is a degree of arbitrariness in deciding when elementary branch points or nodes are close enough together to count as multiple branching and when pore bodies are so small as not to warrant counting (Mohanty *et*

al., 1987). Therefore, for a detailed understanding of the porous medium multiphase flow, study at the pore level is very important.

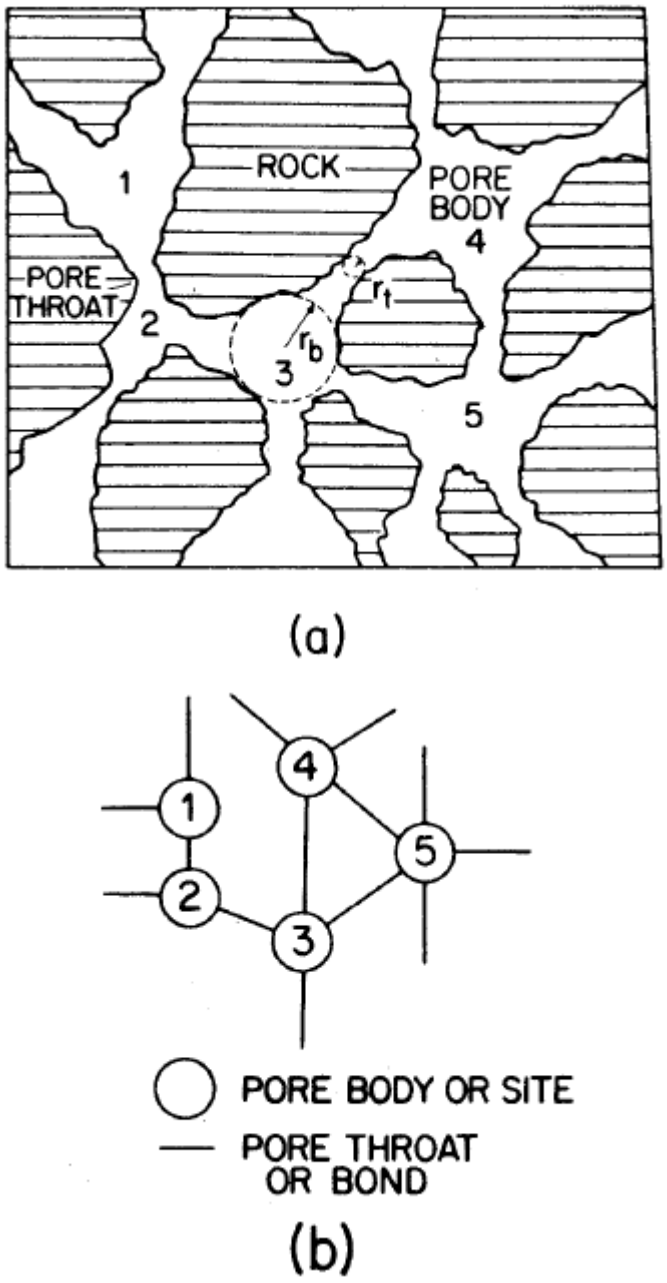

Figure 1.2 – (a) A porous medium and (b) its network analogue (Mohanty, 1987).

1.3 Previous work on pore resistance in porous media

Resistance to two-phase flow has been studied extensively in highly porous and permeable porous media, such as in coarse-grained sedimentary systems like reservoir rocks and unsaturated soils. Pore size distribution by mercury porosimetry, using Washburn equation (Washburn, 1921), is a routine experiment on a large number of core samples. Thomas *et al* (1968) performed breakthrough measurements on eight samples of sand and limestones using a step-wise increase of nitrogen gas pressure until the threshold pressure was reached, characterized by a slow continuous flow of water from the core eventually followed by a free gas phase. The average water flow from the core was measured after each increment until flow ceased. At the threshold pressure, a continuous flow of water resulted, ultimately followed by a free gas phase. Schowalter (1979) showed that pore resistance is the main resistant force to secondary hydrocarbon migration and the magnitude of this resistance is determined by the radius of the pore throats of the rock, hydrocarbon-water interfacial tension, and wettability. The hydrocarbon/water/solid rock contact angle was assumed to be zero.

For low-porosity low-permeability porous media, such as fine-grained rocks, processes such as pressure-driven volume flow and the molecular diffusion of hydrocarbon and non-hydrocarbon gases through water-saturated rocks have been investigated **(**Schlömer and Krooss, 1997). Earlier studies aimed at the assessment of the quality of geological barriers for radioactive waste storage were carried out on migration mechanisms of gases in fine-grained rocks (Horseman *et al,* 1999; Gallé, 2000). Horsemann *et al* (1999) using helium gas showed that because of high pore

resistance, it is impossible for the gas (non-wetting) to breakthrough fully water-saturated samples of pre-compacted bentonite without increasing pressure.

Recently, the focus of interest has shifted to the sealing efficiency of fine-grained sedimentary rocks for the geological storage of carbon dioxide in depleted oil and gas reservoirs and deep saline aquifers. The caprock sealing efficiency is often measured by the resistance of the pore space to the fluid-fluid interface; the higher the resistance the better the sealing efficiency. This resistance has been expressed by several authors with terms such as displacement pressure (Hildenbrand *et al,* 2002), capillary entry pressure, threshold pressure (Hildenbrand *et al,* 2004) and breakthrough pressure (Hildenbrand *et al,* 2004; Li *et al,* 2005), bubbling pressure or sealing pressure (Li *et al,* 2005), among others. Pore resistance measurements on initially water-saturated rock samples have been carried out using either a continuous (Rudd *et al,* 1973; Horseman *et al,* 1999; Gallé, 2000, Hildenbrand *et al,* 2002) or step-by-step (Thomas *et al,* 1968; Schowalter, 1979; Al-Bazali *et al,* 2005; Li *et al,* 2005) increase of the gas pressure until breakthrough was observed.

Hildenbrand *et al* (2002) performed 28 gas breakthrough experiments on completely water-saturated samples by imposing instantaneously a high gas-pressure gradient (i.e. exceeding the expected gas breakthrough pressure) across the fine-grained rock samples with nitrogen, to obtain capillary displacement pressure, maximum effective gas permeability after breakthrough and pore size distribution of the conducting pore system. They observed that gas breakthrough and flow in mudrocks can occur at pressures much lower than fracture pressure or the minimum principal stress. Therefore, using the fracture pressure as the basis for injection may be misleading, hence the need for studying the accurate behaviour of the gas. These investigations

were extended to carbon dioxide experiments for the purpose of geological storage (Hildenbrand *et al*, 2004), and in order to compare the breakthrough behaviour of N_2, CO_2 and CH_4, additional data from CH_4 experiments performed by Schlömer (1998) (In: Hildenbrand *et al*, 2004) using the same technique were included. While the experiments with N_2 and CO_2 were performed under the same conditions (controlled axial stress) at 50^oC, the experiments with CH_4 were performed under different conditions (no controlled axial stress) at 30^oC. Based on statistics, they concluded that the CO_2 and CH_4 capillary displacement pressures tend to be generally lower than the corresponding N_2 values. They simply explained that for the same pore size, the observed differences in their displacement pressures was attributed to differences in the interfacial tension and the wetting angles of the three gases without any experimental evidence. Also, a gas-water contact angle of 0^o (complete wetting) was assumed in comparing the results. This could be correct but need to be further investigated by subjecting all the gases to exactly same experimental conditions.

Li *et al* (2005) measured the breakthrough pressures of N_2, CH_4 and supercritical CO_2 in brine-saturated seal rock samples from Midale Evaporite formation using a step-wise increase in pressure. All the breakthrough tests were performed at Weyburn reservoir temperature of 59^oC. To compare the breakthrough pressure of N_2 and CO_2, measurements were conducted on two separate samples for CO_2 after using the samples for N_2 breakthrough tests. It was observed that the breakthrough pressures of CO_2 in the two samples were 9.2 MPa and 11.2 MPa while the corresponding breakthrough pressures with N_2 were 27.9 MPa and 29.7 MPa, respectively. In both cases the breakthrough pressure of CO_2 was much lower than the nitrogen breakthrough pressure. To compare the breakthrough pressure of CH_4

and CO_2, measurements were made on one sample with both gases, without prior measurement of N_2 breakthrough on the same sample. The breakthrough pressure of CO_2 was 5 MPa, which was much lower than the breakthrough pressure of CH_4 (12.8 MPa). Again, using statistics of their IFT values they concluded that the ratio of measured N_2 and CH_4 breakthrough pressures to CO_2 breakthrough pressure is approximately the same as the ratio of their IFTs; the IFTs for N_2/brine and CH_4/brine are about two to three times that of CO_2/brine systems. The minor difference between these two ratios was attributed to the difference between the contact angles of the CO_2/water system and the N_2 (or CH_4)/water systems and experimental errors.

This also may be correct but need to be verified. For instance, the contact angles need to be measured in pore space instead of on a flat surface, and all experiments need to be conducted under the same conditions to give a better insight into the breakthrough behaviour of the gases. Furthermore, breakthrough pressure is a macroscopic property of the porous medium involving measurement on core samples, which may not represent the exact impact of the pore structure. For instance, the breakthrough pressure on the core samples measures the resistance of a series of largest interconnected pores of the sample and only the effective radius (of all the radii of the interconnected pores) will have the significant influence on the breakthrough pressure. It is well-known that the continuum properties are controlled by the pore level activities, so it is important to measure the resistance to two-phase flow at the pore level to have a better understanding of the fluid flow behaviour in porous media. We have developed a method to measure pressure resistance to two-phase flow in single pores and using this method we are able to interpret precisely

the impact of parameters such as pore geometry, pore wettability, fluid properties and interfacial tension on multiphase flow.

Although it can be seen from the Young-Laplace equation (or capillary pressure equation) that the capillary pressure (or resistance to interface) is influenced significantly by very small pore throats (permeability) (Al-Bazali *et al*, 2005), the actual impact of the throat size has not been demonstrated experimentally. In most investigations the resistance to two-phase flow considered at the pore level is that offered by the interconnected largest pore throats, as the nonwetting phase tends to displace the wetting phase contained in the largest pore throat within the water-wet formation (Hildenbrand *et al*, 2004; Li *et al*, 2005).

1.4 Motivation and justification

In a highly heterogeneous porous medium fluid will normally flow through low resistance path (high permeability zones), making it impossible to sweep substantial amounts of fluid located in the high resistance (low-permeability) zones. This is the so-called conformance problem, which is common in heterogeneous reservoirs (Sang *et al*, 2014). In oil recovery process, for instance, this will lead to a substantial amount of the oil being trapped in the high resistance zone, and for the low resistance (high permeability) zone, it will lead to water channelling resulting in a high water cut, low oil production rate, a rapid reaching of the economic limit, and high residual oil saturation. Long-term erosion caused by water injection in the low resistance layers after an oil field reaches a high water-cut period also leads to the increased heterogeneity of the reservoir. It is estimated that about 65-77% of remaining oil is

left in unswept (high resistance) areas and only 23-35% of remaining oil is confined in the waterflood area (Liu *et al,* 2010). Thus, sweeping remaining oil from unswept areas is crucial to EOR in heterogeneous reservoirs.

While the global characteristics of the porous medium are very important, a good knowledge of their individual elements is very essential to enhance our understanding of the multiphase processes. For example, numerous studies have revealed that flow and transport properties in each pore are strongly influenced by the roughness of the walls and the spatial variations of their local aperture (Keller *et al.*, 1999, Matsuki *et al.*, 2006, Méheust and Schmittbuhl, 2000, Boschan *et al,* 2011). Owing to the fractal nature of porous media it is essential to devise a method to study the processes that occur at the pore level. Studies in single pores will, therefore, provide data to interpret the impact of pore size, pore wettability, pore surface chemistry, physical and chemical property of pore fluids on fluid transport in the pores and provide a clearer understanding of the exact impact of each of these factors on multiphase flow in the porous media. This technique can be used not only to study the leakage risk of stored carbon dioxide and enhanced oil recovery by carbon dioxide flooding, but will provide fundamental data for pore-level modelling.

1.5 Thesis outline

This thesis contains seven chapters, the contents of which are described subsequently.

Chapter 1 introduces the subject matter by describing the background, motivation and justification of the study, as well as, the morphology of the porous medium. The relevance and the significance of this study are briefly highlighted.

Chapter 2 provides the relevant theoretical background and literature review on this study. An overview on resistance to multiphase porous media displacement and resistant forces to the displacement is presented. Concepts of displacement pressure, interfacial phenomenon, flow geometry, wettability and the related empirical equations are explained.

Chapter 3 deals on the materials and the main experimental methodologies used, including a novel method of measurement of resistant pressure in micron-sized single pores developed in this project, in addition to measurement of pore wetting in micron-sized pores.

Chapters 4 to 6 form the core of this research, presenting the experimental results and discussions on resistant forces to two-phase flow in micron-sized single pores.

In Chapter 4 the results and discussions on the resistant pressure profiles of air-liquid and liquid-liquid interface motions through a single pore are presented, and indicates that the characteristics of the resistant pressure profiles are similar for all the interfaces. They all show a section of constant pressure followed by a sharp increase in resistant force.

Chapter 5 investigates the relationship between the resistant pressure and the pore geometry and summarizes that the point of sharp increase in resistant pressure in the pore channel corresponds to the effective pore size, from where the pore throat starts. This finding elucidates the actual influence of the pore geometry on the resistance to displacement. The results of the influence of pore gradient, surface tension and constituent components of the interface on the resistant pressure, and consequently on the effective pore size are presented.

Chapter 6 presents the results and discussions on pore wettability and resistance to two-phase flow in micron-sized pores. The results of analyses of contact angles measured from various micron-sized pores are presented and linked to the resistant pressure profiles. The transitional point on the resistant pressure profile is explained using pore wetting.

Finally, Chapter 7 presents the main findings of this research and highlights the relevance of this study. The limitations and weaknesses of this work are highlighted and future work is recommended.

1.6 References

Al-Bazali, T. M., Zhang, J., Chenevert, M. E., and Sharma, M. M., 2005. Measurement of the sealing capacity of shale caprocks. Paper SPE 96100 presented at the 2005 Annual Technical Conference and Exhibition held in Dallas, 9-12 October.

Al-Raoush, Riyadh I., Clinton S. Willson., 2005. A pore-scale investigation of a multiphase porous media system. Journal of Contaminant Hydrology 77 (2005) 67–89.

Anderson, W. G., 1986. Wettability Literature Survey – Part 2: Wettability Measurement, J. Pet. Technol. 1986,37,1246 – 1262.

Andrew M, Bijeljic B, Blunt MJ, 2014. Pore-scale contact angle measurements at reservoir conditions using X-ray microtomography. Advances in Water Resources. 2014; 68:24-31.

Androutsopoulos, G. P. and Mann, R. 1979. Evaluation of mercury porosimetry experiments using a network pore structure model. Chem. Engineering Sci., Vol. 34, Issue 10, 1979, 1203-1212.

Argüelles-Vivas, F.J. and Tayfun Babadagli, 2014: Drainage type oil and heavy-oil displacement in circular capillary tubes: Two- and three-phase flow characteristics and residual oil saturation development in the form of film at different temperatures. Journal of Petroleum Science and Engineering 118 (2014) 61–73.

Bachu, Stefan and D. Brant Bennion, 2009. Interfacial Tension between CO_2, Freshwater, and Brine in the Range of Pressure from (2 to 27) MPa, Temperature from (20 to 125) ^{o}C, and Water Salinity from (0 to 334 000). J. Chem. Eng. Data 2009, 54, 765-775.

Bachu, S., 2003. Sequestration of CO_2 in geological media in response to climate change: Capacity of deep saline aquifers to sequester CO_2 in solution, Energy Convers and Manage, 44(2003)20, 3151-3175.

Bai, B., Liu, Y., Coste, J., and Li, L., 2007. Preformed Particle Gel for Conformance Control: Transport Mechanism through Porous Media, SPERE, v.10, n.2, 176-184, April.

Bennion, D. B. and S. Bachu, 2006b. Dependence on Temperature, Pressure, and Salinity of IFT and Relative Permeability Displacement Characteristics of CO_2 Injected in Deep Saline Aquifers. Paper SPE 102138 presented at the SPE Annual Technical Conference and Exhibition held in San Antonio, Texas, U. S. A., 24 – 27 September.

Blunt M., D. Zhou, D. Fenwick, 1995. Three-phase flow and gravity drainage in porous media. Transp. Porous Media, 20 (1995), pp. 77–103.

Blunt Martin J., 1997. Pore Level Modelling of the Effects of Wettability, SPE Journal, Volume 2, December, pp. 494 – 510.

Boschan A., I. Ippolito, R. Chertcoff, J.P. Hulin, H. Auradou, 2011. Characterization of fracture aperture field heterogeneity by electrical resistance measurement. Journal of Contaminant Hydrology 123 (2011) 65–74.

Bretherton, F. P., 1961. The Motion of Long Bubbles in Tubes. J. Fluid Mech. (1961) 10, 166.

Celia, Michael A., Paul C. Reeves and Lin A. Ferrand., 1995. Recent advances in pore scale models for multiphase flow in porous media. Reviews of Geophysics, Supplement, Pages 1049-1057, July 1995.

Chalbaud C, Robin M, Lombard JM, Martin F, Egermann P, Bertin H., 2009. Interfacial tension measurements and wettability evaluation for geological CO2 storage. Adv. Water Resource 2009; 32:98-109.

Chang, S.-H., Martin, F.D., Grigg, R.B., 1994. Effect of Pressure on CO_2 Foam Displacements: A Micromodel Visualization Study, Proceedings SPE Symposium on Improved Oil Recovery, Tulsa, OK, v. 2, pp. 11-22, 17-20 Apr 1994.

Chatzis I, and Dullien F. A. L., 1977. Modelling pore structure by 2-D and 3-D networks with applications to sandstones. J Can Petrol Techno 1977; 16(1):97–108.

Chatzis, I. and Dullien F.A.L., 1983. Dynamic Immiscible Displacement Mechanisms in Pore Doublets. Theory versus Experiment, J. Coll. Int. Sci., v. 91, n.1, pp. 199-222, 1983.

Chen, Lin Zhuang, Xuefeng Li, Jinfeng Dong, and Juntao Lu., 2012. A Many-Body Dissipative Particle Dynamics Study of Forced Water Oil Displacement in Capillary. Langmuir 2012, 28, 1330–1336

Chen, Jing-Den and Joel Koplik, 1985. Immiscible Fluid Displacement in Small Networks. Journal of Colloid and Interface Science, Vol. 108, No. 2, December 1985.

Colombani, J., Galliéro, G., Duguay, B., Caltagirone, J., Montel, F., Bopp, P., 2002. A molecular dynamics study of thermal diffusion in a porous medium. Phys. Chem. Chem.Phys.4, 313–321.

Cox, B. G., 1962. On driving a viscous fluid out of a tube. J. Fluid Mech. 14, 81–96.

Dehghan A., R. Kharrat, M. H. Ghazanfari, S. A. Farzaneh, 2009. Studying the Effects of Pore Geometry, Wettability and Co-Solvent Types on the Efficiency of Solvent Flooding to Heavy Oil in Five-Spot Models. Paper SPE 123315 presented at 2009 SPE

Asia Pacific Oil and Gas Conference and Exhibition held in Jakarta, Indonesia, 4-6 August, 2009.

Despois Jean-François, Andreas Mortensen, 2005. Permeability of open-pore microcellular materials. Acta Materialia 53 (2005) 1381–1388.

Dilgren, R.E. and Deemer, A.R., 1982. The Laboratory Development and Field Testing of Steam/Noncondensible Gas Foams for Mobility Control in Heavy Oil Recovery. Paper SPE 10774 presented at the 1982 SPE California Regional Meeting, San Francisco, March 24-26.

Dodd, C. G. and Kiel, G. O. 1959. Evaluation of Monte Carlo Methods in Studying Fluid-Fluid Displacements and Wettability in Porous Rocks. J. Phys. Chem., Vol. 63, 1646-1652.

Dong, M., Chatzis, I., 2004. An experimental investigation of retention of liquids in corners of a square capillary. J. Colloid Interface Sci. 273, 306–312.

Dullien, F. A. L., 1979. Porous Media: Fluid Transport and Pore Structure. Academic Press, New York, 1979.

Dullien, F. A. L., 1992. Porous Media: Fluid Transport and Pore Structure. 2nd Edition, Academic Press, London, p. 21.

Ellis, J., Bazylak, A., 2012. Dynamic pore network model of surface heterogeneity in brine-filled porous media for carbon sequestration. Phys. Chem. Chem. Phys.14, 8382–8390.

Endo Yoshiyuki, Caroline L. Y. Ngan, Asep B. D. Nandiyanto, Ferry Iskandar, Kikuo Okuyama, 2009. Analysis of fluid permeation through a particle-packed layer using an electric resistance network as analogy. Powder Technology 191 (2009) 39-46.

Er, V., Babadagli, T., Xu, Z., 2010. Pore-scale investigation of the matrix–fracture interaction during CO2 injection in naturally fractured oil reservoirs. Energy Fuels 24, 1421–1430.

Fairbrother, F., Stubbs, J., 1935. Studies in electro-endosmosis. Part VI. The 'Bubble Tube' method of measurement. J. Chem. Soc. 1, 527–529.

Fatt, 1956. The Network Model of Porous Media. Petroleum Trans., AIME, Vol. 207, 1956, 144-181.

Gallé, C., 2000. Gas breakthrough pressure in compacted Fo-Ca clay and interfacial gas overpressure in waste disposal context. Applied Clay Science 17 (2000) 85-97.

Gauglitz, P. A., St. Laurent, C. M., Radke, C. J., 1987. An Experimental Investigation of Gas-Bubble Breakup in Constricted Square Capillaries, JPT, September 1987, 1137 – 1146.

George, D.S., Hayat, O., and Kovscek, A.R., 2005. A Microvisual Study of Solution-Gas-Drive Mechanisms in Viscous Oils, J. Pet. Sci. Eng., v. 46, n.1-2, pp. 101-119, February 2005.

Giavedoni, M. D., Saita, F. A., 1997. The axisymmetric and plane cases of a gas phase steadily displacing a Newtonian liquid – a simultaneous solution of the governing equations. Phys. Fluids 9 (8), 2420–2428.

Goldsmith, H. L. and Mason, S. G., 1963: The flow of suspensions through tubes: II. single large bubbles. J. Colloid Sci. 18, 237-261

Grattoni, C. A. and Dawe, R. A., 2003. Gas and Oil Production from Waterflood Residual Oil: Effects of Wettability and Oil Spreading Characteristics, J. Pet. Sci. Eng., v. 39, n. 3-4, pp. 297-308, September 2003.

Grismer, M. E.: 1986, Pore size distribution and infiltration, Soil Sci. 14, 249–260.

Hammecker, C., L. Barbiero, P. Boivin, J. L. Maeght and E. H. B. Diaw, 2004. A Geometrical Pore Model for Estimating the Microscopically Pore Geometry of Soil with Infiltration Measurements. Transport in Porous Media 54: 193–219, 2004.

Hammond, P. S. and Unsal, E., 2009. Spontaneous and Forced Imbibition of Aqueous Wettability Altering Surfactant Solution into an Initially Oil-wet Capillary. Langmuir 2009, 25(21), 12591-12603.

He W, Yi JS, Van Nguyen T., 2000. Two-phase flow model of the cathode of PEM fuel cells using interdigitated flow fields. AIChE J 2000;46 (10):2053–64. http://dx.doi.org/10.1002/aic.690461016.

Heath, Jason E., Thomas A. Dewers, Brian J.O.L McPherson, Martin B. Nemer, Paul G. Kotula, 2012. Pore-lining phases and capillary breakthrough pressure of mudstone caprocks: Sealing efficiency of geologic CO2 storage sites. International Journal of Greenhouse Gas Control 11 (2012) 204-220.

Hildenbrand, A., Schlömer, S., Kroos, B. M., 2002. Gas breakthrough experiments on fine-grained sedimentary rocks. Geofluids (2002) 2, 3 – 23.

Hildenbrand, A., Schlömer, S., Kroos, B. M., and Littke, R., 2004. Gas breakthrough experiments on pelitic rocks: comparative study with N_2, CO_2 and CH_4. Geofluids (2004) 4, 61 – 80.

Hornof, V. and Morrow, N.R., 1988. Flow Visualization of the Effects of Interfacial Tension on Displacement, SPERE, v. 3, n. 1, pp. 251-256. 1988.

Horseman, S. T., Harrington, J. F. and Sellin, P., 1999. Gas migration in clay barriers. Engineering Geology, 54 (1999) 139-149.

Jamaloei Benyamin Yadali, Koorosh Asghari, Riyaz Kharrat, 2011. Pore-scale flow characterization of low-interfacial tension flow through mixed-wet porous media with different pore geometries. Experimental Thermal and Fluid Science 35(2011)253 – 264.

Jamaloei, B., Kharrat, R., 2010. Analysis of pore-level phenomena of dilute surfactant flooding in the presence and absence of connate water saturation. J. Porous Media 13, 671–690.

Joseph, Jerry, Naga Siva Kumar Gunda, Sushanta K. Mitra., 2013. On-chip porous media: Porosity and permeability measurements. Chemical Engineering Science Volume 99, 9 August 2013, 274-283.

Juanes, R., Spiteri, E. J., Blunt, M. J., 2006. Impact of Relative Permeability Hysteresis on Geological CO_2 Storage. Water Resour. Res. 2006, 42, W12418.

Juncker, D.; Schmid, H.; Drechsler, U.; Wolf, H.; Wolf, M.; Michel, B.; de Rooij, N.; Delamarche,2002. E. Anal. Chem. 2002, 74, 6139.

Karadimitriou, N. K., Hassanizadeh, S., 2012. A review of micromodels and their use in two-phase flow studies. Vadose Zone J. 11, 1–10.

Keller, A., Roberts, P.V., Blunt, M. J., 1999. Effect of fracture aperture variations on the dispersion of contaminants. Water Resources Research Vol 35(1), 55–63.

Kim, S. Y., Paek, J. W., Kang B. H., 2000. Flow and Heat Transfer Correlations for Porous Fin in a Plate-Fin Heat Exchanger. Journal of Heat Transfer, August 2000, Vol. 122, 572-578.

Koido, Tetsuya, Toru Furusawa, Koji Moriyama, 2008. An approach to modelling two-phase transport in the gas diffusion layer of a proton exchange membrane fuel cell. Journal of Power Sources 175 (2008) 127–136.

Kovscek A. R. and M. D. Cakici, 2005. Geologic Storage of Carbon dioxide and Enhanced Oil Recovery. II. Cooptimisation of Storage and Recovery. Energy Conversion and Management 46(2005) 1941-1956.

Kumar Atul, Reddy R. G., 2003. Modelling of polymer electrolyte membrane fuel cell with metal foam in the flow-field of the bipolar/end plates. Journal of Power Sources 114 (2003) 54-62.

Kumar, A., R. Ozah, M. Noh, G. A. Pope, S. Bryant, K. Sepehrnoori, and L. W. Lake, 2005. Reservoir Simulation of CO_2 Storage in Deep Saline Aquifers. SPEJ, September, 336-348.

Larson, R. G., Scriven, L. E. and Davis, H. T., 1981. Percolation theory of two phase flow in porous media. Chem. Engineering Sci., Vol. 36, Issue 1, 1981, 57-73.

Lenormand, R., C. Zarcone, and A. Sarr, 1983: Mechanisms of the displacement of one fluid by another in a network of capillary ducts, J. Fluid Mech., 135,337-353, 1983.

Li, S., Dong, M., Li, Z., Huang, S., Qing H. and Nickel, E., 2005. Gas breakthrough pressure for hydrocarbon reservoir seal rocks: implications for the security of long-term CO_2 storage in the Weyburn field. Geofluids (2005) 5, 326-334.

Lin, C.L., J.D. Miller, 2000. Network analysis of filter cake pore structure by high resolution X-ray microtomography. Chemical Engineering Journal 77 (2000) 79–86.

Liu, Y. Z., Bai, B. J., Wang, Y. F., 2010. Applied Technologies and Prospects of Conformance Control Treatments in China. Oil and Gas Science and Technology Vol. 65(6), 859-878.

Liu, Y.; Wang, W.; Hu, W.; Lu, Z.; Zhou, X.; Li, C., 2011. Highly sensitive poly [glycidyl methacrylate-co-poly (ethylene glycol) methacrylate] brush-based flow through microarray immunoassay device. Biomedical Microdevices 2011, Vol. 13, Issue 4, 769-777.

Lucas, Yann, Mikhail Panfilov, Michel Buès, 2006. Prolongation of two phases in the model of fluid displacement through a capillary. C. R. Mecanique 334 (2006) 196–204.

Ma, K., Liontas, R., Conn, C., Hirasaki, G., Biswal, S., 2012. Visualization of improved sweep with foam in heterogeneous porous media using microfluidics. Soft Matter 8, 10669–10675.

Mackay, E. J., Henderson, G. D., Tehrani, Dabir H. and Danesh, A., 1998. The Importance of Interfacial Tension on Fluid Distribution during Depressurization, SPERE, v. 1, n. 5, pp. 408-415, October 1998.

Mahers, E.G. and Dawe, R.A., 1985. Visualization of Microscopic Displacement Processes within Porous Media in EOR Capillary Pressure Effects, presented at the 3rd European Meeting on Improved Oil Recovery, Rome, 16-18 April 1985.

Mann, R., Androutsopoulos, G. P. and Golshan, H. 1981. Application of stochastic network pore model to oil-bearing rock with observations relevant to oil recovery. Chem. Engineering Sci., Vol. 36, Issue 6, 1981, 337-346.

Matsuki, K., Chida, Y., Sakaguchi, K., Glover, P. W. J., 2006. Size effect on aperture and permeability of a fracture as estimated in large synthetic fractures. International Journal of Rock Mechanics and Mining Sciences Vol. 43(5), 726–755.

Mattax, C. and Kyte, J., 1962. Imbibition Oil Recovery from Fractured, Water-Drive Reservoir. SPEJ 2 (2): 177-184.

Méheust, Y., Schmittbuhl, J., 2000. Flow enhancement of a rough fracture. Geophysical Research Letters Vol. 27(18), 2989–2992.

Melrose, J. C. and Brandner, C. F., 1974: Role of Capillary Forces in Determining Microscopic Displacement Efficiency for Oil Recovery by Waterflooding. J. Cdn. Pet. Tech. (Oct. 1974) 13, 54-62.

Mohanty, K.K., Davis, H.T. and Scriven, L. E., 1987. Physics of oil entrapment in water-wet rock. Soc. Pet. Eng. Reservoir Eng., 2: 113-128.

Morrow, N.R., Lim H.T. and Ward, J.S., 1986. Effect of Crude Oil Induced Wettability Changes on Oil Recovery, SPE Formation Evaluation, v. 1, n. 1, pp. 89-103, 1986

Nelson, Philip H., 2009. Pore-throat sizes in sandstones, tight sandstones, and shales. AAPG Bulletin, v. 93, no. 3 (March 2009), pp. 329–340.

Olbricht, W. L. and Leal, L. G., 1983. The creeping motion of immiscible drops through a converging/diverging tube. J. Fluid Mech. 134, 329-355.

Orr, F. M., Jr., 2004. Storage of carbon dioxide in geologic formations. J. Pet. Technol., 2004 56(9), 90-97.

Owete, O.S. and Brigham, W.E., 1987. Flow Behaviour of Foam: A Porous Micromodel Study, SPERE, v. 2, n. 3, pp. 315-323, 1987.

Park, C.W., Homsy, G. M., 1984. Two phase displacement in Hele-Shaw cell: theory. J. Fluid Mech. 139, 291–308.

Paterson, L., Hornof, V. and Neale, G., 1984. Visualization of a Surfactant Flood of an Oil Saturated Porous Medium, SPEJ, v. 24, n.3, pp. 325-327, 1984.

Payatakes, A. C., and Dias, M. Madalena, 1984. Immiscible Microdisplacement and Ganglion Dynamics in Porous Media. Reviews in Chemical Engineering, Vol.2, Issue 2, 85-174 (June 1984).

Perkins, F. M., Jr., 1957. An Investigation of the Role of Capillary Forces in Laboratory Water Floods. Journal of Petroleum Technology, November, 1957, pp. 49-51.

Plug WJ, Bruining J., 2007. Capillary pressure for the sand–CO2–water system under various pressure conditions. Application to CO2 sequestration. Advances in Water Resources 2007; 30:2339-53

Qi R, LaForce T. C, Blunt M. J., 2009. Design of carbon dioxide storage in aquifers. Int J Greenhouse Gas Control March 2009; 3(2):195–205. http://dx.doi.org/10.1016/j.ijggc.2008.08.004.

Ratulowski, J., Chang, H. C., 1989. Transport of gas bubbles in capillaries. Phys. Fluids A 1(10), 1642–1655.

Romero-Zeron, L. and Kantzas, A., 2007. The effect of Wettability and Pore Geometry on Foamed-Gel-Blockage Performance, SPERE, v. 10, n. 2, pp. 150-163, April 2007.

Roof, J.G., 1970. Snap-off of Droplets in Water-Wet Cores. SPEJ (March 1970) 85-90; Trans., AIME, 249.

Rudd, N., and Pandey, G. N., 1973. Threshold pressure profiling by continuous injection. Paper SPE 4597 presented at the 1973 Annual Technical Conference and Exhibition held in Las Vegas, Nevada, 30 September-3 October.

Sang, Qian, Yajun Li, Long Yu, Zhenquan Li, Mingzhe Dong, 2014. Enhanced oil recovery by branched-preformed particle gel injection in parallel-sandpack models. Fuel 136 (2014) 295–306.

Sayegh, S. G. and D. B. Fisher, 2008. Enhanced Oil Recovery by CO_2 Flooding in Homogeneous and Heterogeneous 2D Micromodels. SPE paper 2008-005presented at the Canadian International Petroleum Conference/SPE Gas Technology Symposium held in Calgary, Alberta, Canada, 17-19 June 2008.

Schlömer (1998) (In: Hildenbrand et al, 2004).

Schlömer, S, Krooss, B. M., 1997. Experimental characterisation of the hydrocarbon sealing efficiency of cap rocks. Marine and Petroleum Geology, 14, 565–80.

Schowalter, T. T., 1979. Mechanics of secondary hydrocarbon migration and entrapment. AAPG Bulletin, 63, 723-760.

Schwartz, L.W, Princen, H. M., Kiss, A. D., 1986. On the motion of bubbles in capillary tubes. J. Fluid Mech.172, 259–275.

Shad Saeed 1, Brij B. Maini, Ian D. Gates, 2013. Effect of gap and flow orientation on two-phase flow in an oil-wet gap: Relative permeability curves and flow structures. International Journal of Multiphase Flow 57 (2013) 78–87.

Silina Dmitriy, Tad Patzek, 2006. Pore space morphology analysis using maximal inscribed spheres. Physica A 371 (2006) 336–360.

Smith, J.D., Chatzis, I., and Ioannidis, M.A., 2005. A New Technique to Measure the Breakthrough Capillary Pressure, J. Can. Pet. Tech., v. 44, n. 11, pp. 25-31, November 2005.

Soudmand-Asli, A., Ayatollahi, S. S., Mohabatkar, H., Zareie, M., and Shariatpanahi, S. F., 2007. The in Situ Microbial Enhanced Oil Recovery in Fractured Porous Media, J. Pet. Sci. Eng., v. 58, n. 1-2, pp. 161-172, August 2007.

Thomas, L. K., Katz, D. L., and Tek, M. R., 1968. Threshold pressure phenomena in porous media. SPE Journal, 174-184.

Touboul, E., Lenormand R. and Zarcone, C., 1987. Immiscible Displacements in Porous Media: Testing Network Simulators by Micromodel Experiments, paper SPE 16954, presented at the 62nd Annual Technical Conference and Exhibition of SPE, Dallas, TX, 27-30 September 1987.

Tsakiroglou, Christos D.; Alkiviades C. Payatakes, 2000. Characterization of the pore structure of reservoir rocks with the aid of serial sectioning analysis, mercury porosimetry and network simulation. Advances in Water Resources 23 (2000) 773-789.

Tzimas, G. C., T. Matsuura, D. G. Avraam, W. Van Der Brugghen, G. N. Constantinides, A. C. Patyatakes, 1997. The combined effect of the viscosity ratio and the wettability during forced imbibition through nonpolar porous medium. Journal of Colloid and Interface Science 189 (1997) 27-36.

Wang Baoyu, Yi Jin, Qing Chen, Junling Zheng, Yibo Zhu, Xiaobing Zhang, 2014. Derivation of Permeability–Pore Relationship for Fractal Porous Reservoirs using Series–Parallel Flow Resistance Model and Lattice Boltzmann Method. Fractals, Vol. 22, No. 3 (2014) 1440005 (15 pages), World Scientific Publishing Company. DOI: 10.1142/S0218348X14400052.

Wang Shibo, Ian M. Edwards, and Andres F. Clarens., 2013. Wettability Phenomena at the CO2−Brine−Mineral Interface: Implications for Geologic Carbon Sequestration. Environ. Sci. Technol., 2013, 47 (1), pp 234-241. DOI: 10.1021/es301297z.

Wang, Z.H., Wang, C.Y., Chen, K.S., 2001. Two-phase flow and transport in the air cathode of proton exchange membrane fuel cells. J Power Sources 2001; 94(1):40–50. http://dx.doi.org/10.1016/S0378-7753(00)00662-5.

Wang, W.; Yang, C.; Liu, Y.; Li, C., 2010. On-demand droplet release for droplet-based microfluidic system. Lab Chip 2010, 10, 559-562.

Wardlaw N. C. and Taylor R. P. 1976. Mercury capillary pressure curves and the interpretation of pore structure and capillary behaviour in reservoir rocks. Bull. Can. Pet. Geol., Vol. 24, 1976, No. 2 (June), 225-262.

Wardlaw, N.C., 1980. The Effects of Pore Structure on Displacement Efficiency in Reservoir Rocks and in Glass Micromodels, paper SPE 8843, presented at the 1st Joint SPE/DOE Symposium on Enhanced Oil Recovery, Tulsa, OK, 20 April 1980.

Washburn, E.W., 1921. Note on a method of determining the distribution of pore sizes in a porous material. Proceedings of the National Academy of Science, 115–116.

Wu, M., Xiao, F., Johnson-Paben, R., Retterer, S., Yin, X., Neeves, K., 2012a. Single- and two-phase flow in microfluidic porous media analogues based on Voronoi tessellation. Lab Chip 12, 253–261, Miniaturisation for Chemistry and Biology.

Yang Die, Marta Krasowska, Craig Priest, Mihail N. Popescu, and John Ralston., 2011. Dynamics of Capillary-Driven Flow in Open Microchannels. J. Phys. Chem. C 2011, 115, 18761–18769.

Chapter 2: Theoretical Background and Literature Review

2.1 Introduction

The need for a clearer understanding of the resistance to pore level fluid displacement is becoming of increasing importance. This can be attributed to the increasing awareness of CO_2 geological storage as an option to reduce the atmospheric concentration of anthropogenic CO_2 (Orr, 2004; Hitchon *et al*, 1999; Bachu, 2000). In addition, in the oil and gas industry, there is the gain in global prominence of the recognition of the injection of CO_2 for enhanced oil recovery, due to its potential for mitigating greenhouse gas emissions (Moritis, 2006), and more particularly by the promise of CO_2–EOR as a profit–making option (Chiquet *et al,* 2007b; Bennion and Bachu, 2006b). Among the target formations for this purpose are depleted oil and gas reservoirs (Kovscek and Cakici, 2005; Kovscek and Wang, 2005), deep saline aquifers (Pruess *et al*, 2003; Bachu, 2003; International Energy Agency, 2004; Socolow, 2005) and unminable coal beds (Bromhal *et al,* 2005).

Resistance to displacement of fluids is very important in characterisation of a caprock for its sealing capacity. Parameters used to characterise the resistance to fluid displacement include capillary pressure (breakthrough pressure, etc.), fluid saturation, permeability or conductance, and these depend on the pore structure, fluid properties and composition, and wettability. All of these factors are interrelated, for example, several researchers (Yang *et al*, 2008a; Chalbaud *et al*, 2006; Juanes *et al*, 2006) have reported that wettability depends on pore geometry, fluid composition

and properties, and the interfacial tension, and has strong effect on capillary pressure (Yang *et al,* 2008a; Chalbaud *et al,* 2006; Juanes *et al,* 2006), relative permeability (Juanes *et al,* 2006), and fluid saturation (Morrow, 1990). The exact impact of each of these factors on resistance to flow needs more experimental work to be verified (Lin and Miller, 2000). For instance, both contact angle on a flat surface and in a pore were treated as the same, but recently, Li *et al* (2013, 2014) developed a new experimental method to measure the contact angles of fluids in micro-sized pores and found out that contact angles on a flat borosilicate glass surfaces are different from their contact angles on pore surfaces of same materials. Li *et al* (2014) observed that the contact angle in a pore tends to approach the value measured on a planar substrate once the pore size is large enough, approximately 1000 μm (1 mm). Using a similar method, pore contact angles will be measured and used to study its impact and other factors' impacts on resistance to displacement.

2.2 Fundamentals of Porous Media Resistance

2.2.1 Porous media resistant pressures

Pore resistance characterizes the ability of the porous medium saturated with a wetting phase to block the flow of a non-wetting phase (Li *et al*, 2005; Egermann *et al,* 2006). This property has been found to be very important in petroleum and natural gas exploration and production, repository for radioactive and non-radioactive wastes, and more recently for geological CO_2 sequestration, which is considered to be the most immediately effective and economically viable of the various CO_2 emission reduction methods so far proposed (Bachu, 2000; Perera *et al,*

2012). The character of the gas/water pore resistance affects relative permeability and therefore the way the fluids will flow and distribute in the pores (Pini *et al,* 2012). In addition, pore resistance is responsible for the displacement mechanisms at the pore-scale that lead to the break-up of the nonwetting phase into bubbles and ganglia, which eventually become immobile (Lenormand *et al,* 1983; Gauglitz *et al,* 1987).

Pore resistant pressure is also a key parameter to design enhanced oil recovery and geological storage, and avoid an upward migration of the injected fluid (hydrocarbon gases and non-hydrocarbon gases) into the overlaying formations (Horsemann *et al,* 1999; Marshall *et al,* 2005), because it sets a limit on both the injection pressure and the storage capacity of the reservoir (Li *et al,* 2006; Chiquet *et al,* 2007a). For example, the sealing capacity of a caprock for hydrocarbon reservoirs and for CO_2 underground storage is provided by the resistance across the interface of the wetting phase (usually brine) which saturates the seal rock, and the non-wetting phase (oil or gas) which accumulates in the reservoir (Li *et al, 2005;* Hildenbrand *et al,* 2002 and 2004; Li *et al,* 2006; Andreas and Nadja, 2011; Egermann *et al,* 2006, Chiquet *et al,* 2007a and 2007b).

Vavra *et al* (1992) defined a seal generally as a sediment, rock or immobile fluid with high capillary entry pressure (also known as capillary breakthrough or capillary entrance pressure) that acts to stop the flow of hydrocarbon. Some common seal lithologies are shales, clays, claystones, mudrocks, siltstones, and anhydrites. The ability of caprocks to exhibit good sealing characteristics arises from their small, water-wet pores, which are responsible for generating high capillary pressures, which

excludes hydrocarbons and stop the flux of CO_2 through it (Al-Bazali *et al*, 2009). This ability is complicated by the partial solubility of CO_2 in the water. The capillary pressure is given by the Young-Laplace equation (Moore and Slobod, 1956; Stegemeier, 1974) (Equation 2.1):

$$P_c = P_{nw} - P_w = \frac{2\gamma \cos\theta}{R} \tag{2.1}$$

where P_c is capillary pressure in Pa or N/m^2, P_{nw} is the pressure in the nonwetting phase in Pa, P_w is the pressure in wetting phase in Pa, γ is the interfacial tension between the nonwetting and wetting phase in N/m or dyne/cm, θ is the contact angle in degrees and R is the pore throat radius (m). The differential pressure between the nonwetting phase (hydrocarbon or CO_2) and the wetting phase (brine) must exceed the minimum capillary entry "threshold" pressure of the caprock in order for the nonwetting phase to enter the seal. The minimum capillary entry pressure is the capillary pressure at which the non-wetting phase, usually oil, gas, or CO_2, starts to displace the wetting phase, usually brine, contained in the largest pore throat within a water-wet formation. Equation (2.1) shows that the capillary entry pressure can be significant, especially for porous media with very small pore throats (low permeability).

The height of a hydrocarbon column that can be trapped by a seal rock can be estimated using the minimum capillary entry pressure (Figure 2.1). The hydrocarbon column height, h (m) (also called the hydrocarbon capacity) at equilibrium, is given by Equation (2.2):

$$h = \frac{P_{c_{min}}}{(\rho_w - \rho_o)g} \tag{2.2}$$

where $P_{c_{min}}$ is the minimum capillary entry pressure in Pa, ρ_w (kg/m^3) and ρ_o (kg/m^3) are the densities of water and oil, respectively and g is the acceleration due to gravity in m/s^2. As shown in Equation (2.1), capillary pressure depends on the interfacial tension between the wetting fluid and the non-wetting fluid, the contact angle and the pore throat radius, and must be known to estimate the hydrocarbon capacity of a seal rock.

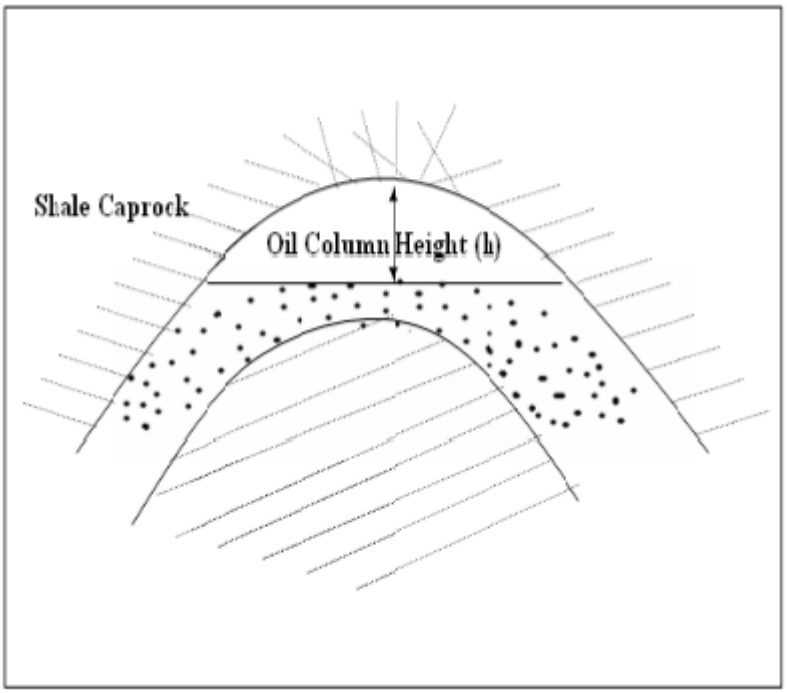

Figure 2.1: Hydrocarbon column trapped by a shale caprock (Al-Bazali *et al.*, 2009).

In basin modelling reliable pore resistance behaviour of a porous medium is important because they control the fluxes of fluids through the caprocks over the geological times and therefore determine directly the volume and localization of the hydrocarbons trapped (best locations for exploration) and also the over-pressured formation (Egermann *et al,* 2006). Formation of overpressure zones in the petroleum

reservoir is known to be due to the increased resistance of the reservoir rock pore to flow of the reservoir fluids (Hildenbrand *et al*, 2002). This may constitute a drilling hazard during petroleum exploration and production activities, it is therefore very useful to locate such resistant zones for proper design of drilling programmes (Thomas *et al, 1968;* Katz and Ibrahim, 1971). Moreover, it is a critical parameter for reservoir simulators used to design field-scale injection projects (Doughty, 2007).

Resistance to fluid flow, is a complex interplay of the pore geometry, fluid properties, fluid-fluid interaction and fluid-pore surface interaction, but it is conventional to consider the pore structure. It is measured by the pressure drop (ΔP) that occurs in the medium. This is expressed by Darcy's law (Endo *et al*, 2009).

2.2.2 Trapping of fluids

The trapping and storage processes of the reservoir fluids in the reservoir rocks could provide more information for understanding the resistance of the porous media for fluid flow processes, such as oil recovery and geological storage of carbon dioxide.

2.2.2.1 Oil and gas reservoir rocks

A petroleum reservoir is a trap that contains gas, oil, and water in varying proportions, in the pore spaces or fractures of the reservoir rock (Figure 2.2). The pore spaces are interconnected so that the fluids can move through the reservoir. Accumulation of oil and gas in significant quantities in the reservoir rock, after its formation in the source rock, involves migration of the hydrocarbon through water-filled pores. Migration is promoted by buoyancy forces but it is inhibited by the

capillary forces which must be overcome for the oil globule to pass through an adjacent pore throat (Berg, 1975; Gluyas and Swarbick, 2004). For a conventional reservoir rock (high permeability), the pore body size and pore throats are large enough to store and deliver economic quantities of petroleum (Nelson, 2009), while unconventional resources, such as tight-gas sandstones and shale gas are low-permeability systems with small pore body and throat sizes. Both situations pose different degree of resistance to the fluid flow through the porous rock. Unconventional resources would require fracturing or stimulation to increase their pore and throat sizes, as well as their permeability.

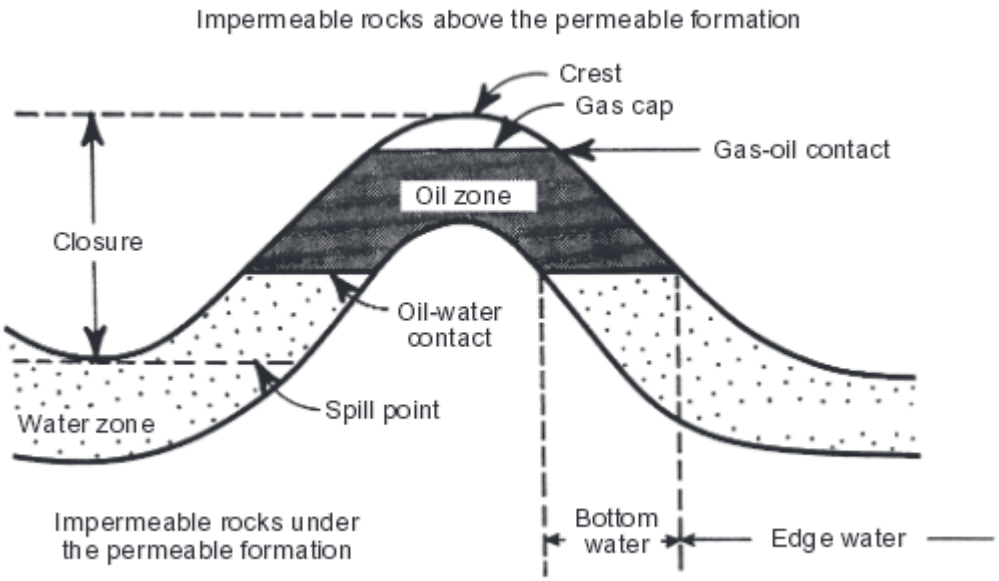

Figure 2.2: Idealized cross-section through an anticlinal trap formed by a porous, permeable, formation surrounded by impermeable rocks. Oil and gas are trapped at the top of the anticline (Tiab and Donaldson, 2015).

2.2.2.2 Cap rock

Cap rock or seal rock is a formation with extremely low porosity and permeability overlaying an oil or gas reservoir, and it constitutes the barrier against the volume flow of hydrocarbons into the upper layers. When the capillary pressure is greater than or equal to the buoyancy pressure of the migrating hydrocarbons (or CO_2) a capillary seal is formed. That is, the sealing capacity of the seal rock is provided by the capillary forces across the interface of the wetting phase (usually brine), which saturates the seal rock, and the nonwetting phase (oil or gas), which accumulates in the reservoir (Li *et al*, 2005). The pore throats in this case are small enough to block the passage of petroleum at the applied level of buoyant pressure (Nelson, 2009).

Seals do not allow fluids to migrate across them until their integrity is disrupted, causing them to leak. A capillary seal may be a hydraulic seal or a membrane seal (Watts, 1987).

2.2.3 Capillary sealing mechanism

The membrane seal will leak whenever the pressure differential across the seal exceeds the threshold displacement pressure, allowing fluids to migrate through the pore spaces in the seal. Ortoleva (1994) showed that the leakage will just be enough to reduce the pressure differential lower than the displacement pressure and will reseal. This implies that the membrane seal provides a self-pressure maintenance mechanism. The hydraulic seal occurs in rocks that have a significantly higher displacement pressure such that the pressure required for tension fracturing is actually lower than the pressure required for fluid displacement – for example, in

evaporates or very tight shales. The rock will fracture when the pore pressure is greater than both its minimum stress and its tensile strength, then reseal when the pressure reduces and the fractures close.

Krooss *et al* (1992) have recognised molecular diffusion and slow Darcy flow as two main mechanisms responsible for migration of hydrocarbon gases through seal rocks into adjacent upper layers. Molecular diffusion is a ubiquitous and slow process that involves the diffusion of the hydrocarbon molecules through the water-saturated pore space of the seal rock. Slow Darcy flow occurs when the pressure difference across the seal rock is sufficiently high to overcome the sealing capacity of the seal rock. It depends strongly on the geologic and hydrodynamic conditions of the system, including the reservoir, the seal rock, and the overburden formations, as well as the properties of the fluids in both the reservoir and the seal rock (Li *et al,* 2005).

For an oil or gas-water interface in a pore throat adjacent to a pore body, the penetration of the nonwetting fluid (oil or gas) into the seal rock by slow Darcy flow is prevented by the capillary pressure (Figure 2.3). The nonwetting phase will advance along the channel when the pressure difference between the nonwetting and the wetting phase, ($P_{nw} - P_w > P_c$), exceeds the capillary pressure at the pore throat. The displacement will continue until it reaches the next smaller pore throat where the capillary pressure is higher. A continuous filament of nonwetting phase will be formed when the differential pressure across the seal rock overcomes the capillary pressure of a series of interconnected pore throats of arbitrarily large sizes and, consequently, a slow Darcy flow will occur. This differential pressure is the breakthrough pressure of the seal rock (Berg 1975; Schowalter 1979; Dullien 1992;

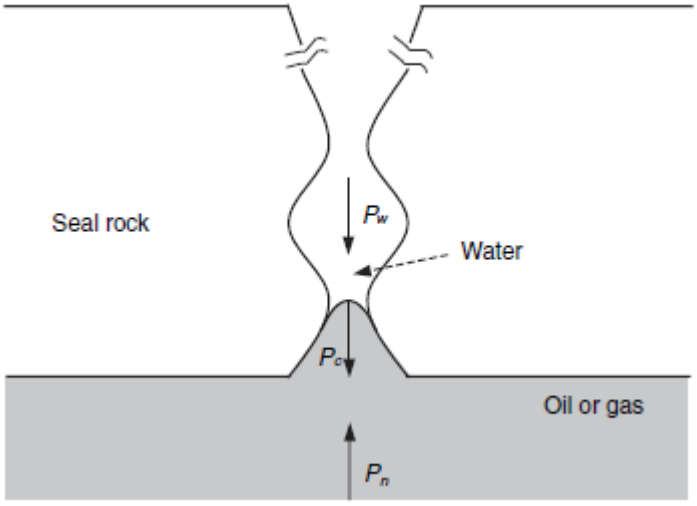

Figure 2.3: Schematic of capillary sealing mechanism in a pore throat of seal rock. (Li *et al*, 2005)

P_{nw} = pressure in the nonwetting phase,
P_w = pressure in the wetting phase,
P_c = capillary pressure across the nonwetting/wetting meniscus in a pore throat.

Hildenbrand *et al*., 2002). Breakthrough pressure is also referred to as the bubbling pressure or sealing pressure, and is an important parameter for assessing the sealing capacity of a seal rock of a hydrocarbon trap. It also has its applications in different areas, such as oil and gas reservoir evaluation prior to exploitation, basin analysis, hydrocarbon secondary migration assessment, as well as the selection of geological sites to store natural gas, CO_2 or industrial waste gases. The magnitude of the breakthrough pressure is determined by the highest capillary pressure of an interconnected network of pore throats that are first invaded by the nonwetting phase. The capillary pressure P_c in a pore throat is expressed by the Young-Laplace equation (Equation 2.1). Several investigators (Keller *et al.*, 1999, Matsuki *et al.*, 2006, Méheust and Schmittbuhl, 2000) have observed that for a heterogeneous

porous medium it may be misleading to use an equivalent radius as flow and transport properties in each pore differ greatly and strongly influenced by spatial variations of their local aperture and the roughness of the walls. Boschan *et al.* (2011) concluded that the determination of the geometrical and transport properties of individual pores is therefore a key issue in view of practical applications. They noted that although elaborate laboratory techniques have been developed to characterize the heterogeneity of porous media, methods that allow the characterisation of a single pore and then predict accurately the displacement of fluids are lacking. In this study we have developed a method to characterise a single pore of the porous medium.

2.3 Immiscible Displacement Processes

2.3.1 Drainage and Imbibition

The two main processes involved in the immiscible displacement of fluids in porous media are drainage and imbibition, and both processes are controlled by the capillary pressure, which depends on the surface tension, interface curvature (wettability), and capillary radius (Hammond and Unsal, 2009).

2.3.1.1 Drainage

Drainage, which is the displacement of a wetting phase by a nonwetting phase, occurs if the pressure in the nonwetting phase is larger than the pressure in the wetting phase. The nonwetting phase invades the pore or throat (large) with the lowest threshold capillary pressure and it is characterized by a piston-like

displacement (Figure 2.4). The nonwetting fluid may only fill pores and throats adjacent to pores already occupied by wetting fluid.

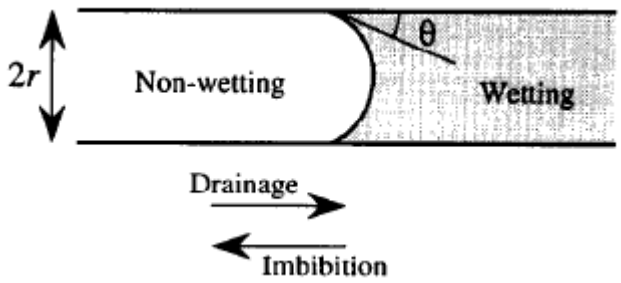

Figure 2.4: Piston-like displacement in a pore of radius r with contact angle θ between the phases (Fenwick and Blunt, 1998).

The pressure difference between the invading (nonwetting) phase and invaded (wetting) phase is the capillary pressure given by the Young-Laplace equation.

2.3.1.2 Imbibition

Imbibition is the displacement/invasion of a nonwetting phase by a wetting phase. In this case, the wetting fluid fills pores or throats (small) with the highest threshold capillary pressure. Previous studies by Fairbrother and Stubbs (1935), Bretherton (1961), Tzimas *et al* (1997) and Argüelles-Vivas and Babadagli (2014) have shown that the wetting phase is connected throughout the pore space by thin films or layers. The presence of these connected thin films in the pores makes it possible for the wetting fluid to displace the nonwetting fluid in every pore or throat. As the wetting fluid invades the smaller pore throats more easily than it does the larger pore bodies, this process is controlled by the connected small pores. Using the mechanism of snap-off, where the wetting fluid in films and wedges may coalesce to fill the narrow throats, Lenormand *et al* (1983) have shown that pore throats influence imbibition

strongly. Hysteresis between drainage and imbibition arises naturally from the size differences between pore bodies and pore throats, because pore-body radii influence imbibition while pore throats control drainage (Celia *et al,* 1995).

If the pressure at the inlet and outlet ends of the capillary is the same, primary (spontaneous) imbibition will occur. The driving force for displacing the non-wetting phase is the capillary pressure, which depends on the surface tension, interface curvature, and capillary radius. Spontaneous imbibition will occur only if the contact angle, θ, between the wetting phase and capillary surface is less than 90º (water wet). In cases where the pressure at both ends of the capillary is different, imbibition will be forced (forced imbibition), in which the displacement of the nonwetting phase by the wetting phase from the capillary tube or porous medium occurs under an externally applied pressure difference.

For oil recovery from naturally fractured reservoirs by spontaneous imbibition of water in strongly water-wet rock, the capillary forces allow water to imbibe and push the oil out of the rock pores. However, in a mixed- or oil-wet reservoir the capillary forces are weak or act in wrong direction. The rate of recovery from such reservoirs can be improved by dissolving low concentrations of surfactants in the injected water to alter the wettability of the reservoir rock to be more water-wet. The surfactant lowers the oil-water interfacial tension and alters the wettability of the rock surfaces.
In the displacement of oil by water or a surfactant solution for oil recovery, the water or surfactant solution is applied under a force (injection), which gives rise to a pressure gradient. Forced imbibition is potentially much faster than the spontaneous case, particularly when the applied pressure is large enough to overcome the

capillary pressure threshold for entrance into the oil-wet capillary. If the applied pressure is less than the threshold pressure for entry, penetration of the meniscus is only possible if the surfactant acts to change the contact angle. It is worthy of note here that both diffusion and adsorption of surfactant molecules are very slow processes and cannot be made faster by the applied differential pressure; it only speeds up the meniscus. The surfactant might lag behind the moving meniscus under very high differential pressures, and as a consequence may not have the desired effects on wettability alteration (Hammond and Unsal, 2009).

2.3.2 Displacement Mechanisms

The two main mechanisms that characterise the displacement of two immiscible fluids by imbibition are snap-off or choke-off and piston-like motion.

2.3.2.1 Snap-off or Choke-off

Snap-off will occur at a critical capillary pressure and curvature which are dependent on throat size and wettability**.** In snap-off the fluid interface ruptures at the pore throat due to the increase in the radius of curvature of the fluid interface up to a point of instability, arising from decrease in capillary pressure. Chatzis *et al* (1983) and Lenormand *et al* (1983) have applied this mechanism to events during imbibition, and described by Li and Wardlaw (1986). During the displacement of nonwetting fluid by wetting fluid collars of wetting fluid may form at the pore throat, with interfaces having elements of negative as well as positive curvature. That is, the interface is selloidal or saddle-shaped with the radii of curvature occurring on both sides of the interface as shown in Figure 2.5. The curvature of the collar changes to a

critical value as capillary pressure is lowered causing the fluid-fluid interface to become unstable and suddenly rupture. Before it ruptures, the interface is stable and can advance or retreat in response to small decreases or increases of capillary pressure.

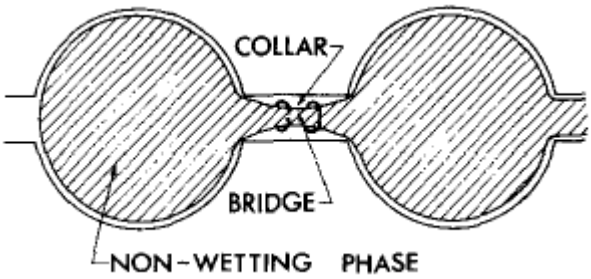

Figure 2.5: Two pore bodies with connecting throat to illustrate nonwetting phase bridge (shaded) and wetting phase collar (plain) in the throat. Interface is selloidal. (Thickness of the continuous wetting film is greatly exaggerated) (Li and Wardlaw, 1986).

It is important to note that the difference between smooth circular capillaries and those of rectangular cross section is that the former only have a thin film of wetting fluid separating the nonwetting fluid from the solid over the entire surface whereas, in the latter case, there are larger wedges of wetting fluid associated with the corners of the rectangle as well as thin films elsewhere (Figure 2.6). Li and Wardlaw (1986) suggest that since sediments and rocks typically have spaces defined by irregular surfaces, a rectangular section, or better still, a triangular or star shape section, provides a more realistic model than a cylindrical tube.

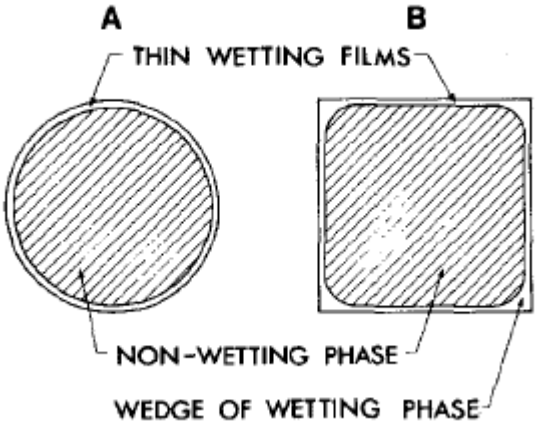

Figure 2.6: Conduits of circular and square cross section to illustrate positions of thin films and wedges of wetting phase (Li and Wardlaw, 1986).

The critical capillary pressure at which snap-off occurs for a throat of square cross-section and inscribed radius r, is (Lenormand and Zarcone, 1984; Fenwick and Blunt, 1998):

$$P_c = \frac{\sigma(\cos\theta - \sin\theta)}{r} \qquad (2.3)$$

Snap-off results in a sudden invasion of the throat by the wetting fluid leading to the discontinuity of the nonwetting phase. If the nonwetting phase is completely surrounded by wetting fluid, it is trapped in the pore body and in this case, no further displacement is possible. These trapped or isolated nonwetting blobs are said to be at residual satura*tion* (Mayer and Miller, 1992; Al-Raoush and Wilson, 2005; Li and Wardlaw, 1986; Roof, 1970). At residual saturation, the shapes assumed by the nonwetting blobs are influenced by the pore geometry and topology, and their sizes can range over several orders of magnitude. The viscous force required to remove the blob is directly related to the blob size. The mass transfer characteristics of the system are affected by the blob volume and surface (Al-Raoush and Wilson, 2005).

The term snap-off has also been used by Pickell *et al* (1966) and Roof (1970) to apply to events during drainage.

2.3.2.2 Piston-like motion

Convex interfaces with only positive elements of curvature also occur, apart from selloidal interfaces (Figure 2.7a and Figure 2.7b). The advance or retreat of a convex interface in a pore body or throat is referred to as "piston-type" motion (Lenormand *et al*, 1983). It can only occur if an adjacent pore body or pore throat is already completely filled with wetting phase.

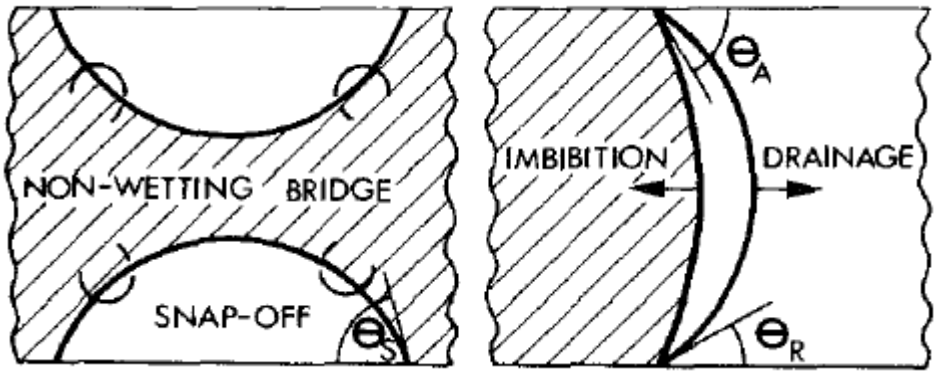

Figure 2.7a: Selloidal interface (left) and convex interfaces (right) in cylindrical tube with horizontal axis. Two convex interfaces indicate the advancing and retreating positions with contact angle hysteresis ($\theta_A > \theta_R$) (piston-type motion) (Li and Wardlaw, 1986).

Piston-like invasion has a higher capillary pressure (Equation 2.1) than snap-off, for a given throat, and so is favoured. Because snap-off occurs when the pressure difference between the nonwetting phase and wetting phase is decreased. The critical pressure for piston-like pore filling depends on the number of adjacent throats that are completely filled with wetting fluid (Fenwick and Blunt, 1998). Since pore

bodies are always larger than the adjacent throats, piston-like advance in pore bodies is always favoured over snap-off.

Chen and Koplik (1985) identified piston-like displacement, Haines' jumps, bubble displacement, and the spreading, rupture, and coalescence of thin films as microscopic displacement mechanisms which can occur in a random pore space and contribute to the flow. The relative importance of these various possibilities will depend on the external boundary conditions (e.g., flow rate), the microscopic geometry of the porous medium, and the physical properties of the fluids and solids present. They observed that for two-phase flow studies of imbibition, pistonlike effect dominate at high flow rates and in low aspect ratio systems, while thin film or interfacial displacement dominate at low flow rates and in high aspect ratio systems. The aspect ratio is defined as the ratio of pore body size to pore throat size. Motion at very low flow rates is controlled by the local geometry, so that motion occurs at the point of least capillary resistance. At low flow rates capillary forces are dominant while at high flow rates viscous forces are dominant.

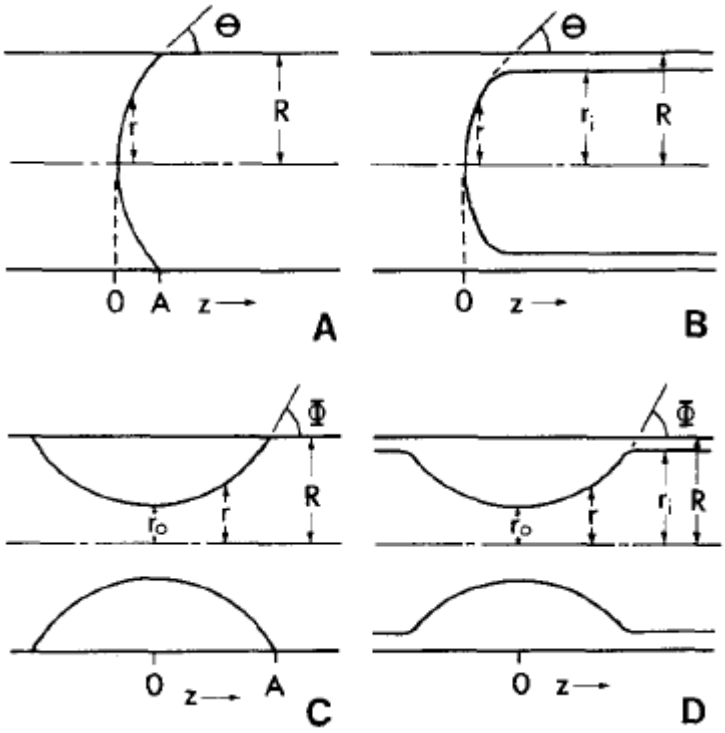

Figure 2.7b: Convex interfaces (convex to nonwetting phase): (A) with a contact angle; (B) with thin film. Selloidal interfaces: (C) with a contact angle;(D) with thin film (Li and Wardlaw, 1986).

2.4 Enhanced Oil Recovery and CO_2 Storage

2.4.1 Enhanced Oil Recovery

Enhanced oil recovery processes influence the resistance to flow commonly through one of the following mechanisms: (i) reduce interfacial tension and/or modify wettability to increase capillary number and mobilise residual oil, (ii) increase the viscosity of water by adding polymer, thus decreasing the mobility ratio, (iii) reduce the permeability of high permeability zones or streaks and improve conformance in heterogeneous reservoirs for better sweep efficiency (Almohsin *et al.*, 2014; Hite *et al.*, 2005; Fletcher and Davis, 2010), and (iv) reduce oil viscosity, such as in thermal

recovery. Initial recovery of oil from a porous medium such as an oil reservoir, referred to as primary recovery), involves flowing the oil under the natural reservoir pressure or by assisted flow, such as artificial lift or the use of pumping devices. This reservoir pressure is in the form of the energy stored in the reservoir in the form of gas or water. Gas in solution lowers the viscosity of the oil, making it easier to displace to the wellbore under the natural reservoir pressure. After a period of production, the natural reservoir pressure decreases, and vast amounts of the hydrocarbons remain unrecovered. Stosur (2003) estimated that only less than 30% of oil-originally-in-place (OOIP) can be recovered by primary recovery leaving 70% unrecovered.

Secondary oil recovery involves immiscible gas or water injection into the reservoir to improve the natural gas or water to drive oil out. Water flooding is the most common method of secondary recovery, in which large quantities of water is injected into the reservoir to displace additional oil in front of it to the wellbores where it can be recovered. Water flooding is inefficient because of conformance problem, a situation in a highly heterogeneous porous medium in which fluids flow through the low resistance path (high permeability zones) and make it impossible to sweep substantial amounts of fluid located in the high resistance (low-permeability) zones. This results in substantial amounts of oil unswept in the low-permeability zones (Sang *et al*, 2014), as well as water channelling and its associated problems for the high-permeability zones.

It is estimated that about 65–77% of remaining oil is left in unswept areas and only 23–35% of remaining oil is confined in the waterflooded area (Liu *et al*, 2010). Thus, sweeping remaining oil from unswept areas is crucial to enhanced oil recovery

About 30-40% (one-third) of the OOIP is generally recovered after secondary recovery, leaving a substantial amount of about 60-70% (two-third) as a target for EOR (Stosur, 2003; Kokal and Al-Kaabi, 2010).

Enhanced oil recovery (tertiary recovery) is the additional recovery over and above what could be recovered by secondary recovery methods. It involves methods designed to displace residual oil (immobile oil) trapped in the pores of the reservoir after both primary and secondary recovery methods have become ineffective. EOR methods include thermal recovery (steam, hot water, combustion), gas injection (carbon dioxide, hydrocarbon, nitrogen/flue gas), chemical flooding (surfactant, alkali, polymer). "Water Alternating Gas" (WAG) is a commonly used flood method that has volumes of water injected between volumes of CO_2 to displace the oil more uniformly out of reservoir (Sweatman *et al,* 2011). Injecting water alternately with gas affects the gas/oil relative permeability and reduces gas mobility, while improving oil mobility. Recent study shows that EOR contributes about 3 million barrels (about 3.5%) of world oil per day, compared to about 85 million barrels of the daily production (Moritis, 2010). The bulk of this production comes from thermal recovery, contributing about 2 million barrels of oil per day. EOR by CO_2 injection contributes to about a third of a million barrels of oil produced per day, and this is expected to rise with the increasing awareness of sequestering CO_2 and at the same time producing incremental oil. Most of the current CO_2-EOR productions are from the Permian basin in the US and the Weyburn field in Canada. Hydrocarbon gas injection is employed where the gas supply cannot be monetised, and contributes another one third of a million of barrels per day. Production from chemical EOR

contributes to total worldwide production of another third of a million barrels per day with China practically contributing all.

Mobilization of oil on a microscopic scale is affected by the geometric and topological properties of the pores, by fluid properties, and by properties related to fluid-rock interaction such as wettability (Wardlaw, 1980). The capillary forces which act on this microscopic scale control the distribution of oil and water under static equilibrium conditions. Even during flow the capillary forces continue to control the microscopic distribution of oil and water within the pores of a porous material for all practical reservoir and laboratory flow rates (Moore and Slobod, 1955). Because of the microscopic nature of the displacement of oil by water, it is necessary to consider the flow and the fluid distribution in individual pores (Perkins, 1957). Using individual micron-sized pores (pore diameter < 1000 μm) provide suitable examples of micro level displacements. Hammond and Unsal (2009) also agree that better insight into displacement processes is required than is afforded by experiments such as tests in rock cores, where it is impossible to see individual pores. It is therefore necessary to carry out laboratory experiments concerned with specified system parameters and to link the results of these experiments with displacement tests. This study is focused on the relationship between pore geometry, interfacial tension, interface composition, and contact angle and the resistance to displacement. A better understanding of the displacement phenomena in the pores will help to improve the average worldwide recovery factor from hydrocarbon reservoirs beyond current limits and ultimately alleviate a number of issues related to global energy supply.

2.4.2 CO_2 Storage

CO_2 geological storage has been proposed as a long-term solution to limiting the emission of anthropogenic CO_2 to the atmosphere (Lackner, 2003). The increasing concentration of atmospheric CO_2 attributed mainly to the combustion of fossil fuels for power generation (Kovscek and Cakici, 2005; Herzog *et al.,* 2000), has received attention because of the well documented fact that carbon dioxide is a greenhouse gas, and one of the major contributors to global warming (Ghedan, 2009; Cox *et al.,* 2000). As fossil fuel presently supplies 85% of primary power, a drastic reduction in CO_2 emissions represents a major challenge (Orr, 2004).

Achieving CCS by injecting CO_2 into saline formations or for EOR in mature oil reservoirs (Figure 2.8) is considered to be a safe and effective method to reduce greenhouse gas (GHG) emissions (Sweatman et al, 2011). The most significant anthropogenic CO_2-EOR is at Weyburn in south eastern Saskatchewan, Canada which uses approximately 1 $MtCO_2$/year, pipelined from the North Dakota Coal Gasification Plant in Beulah, North Dakota. A much smaller operation at Joffre in Alberta uses CO_2 produced at a nearby petrochemical plant. Since 2005 several oil producers in Alberta have started CO_2-EOR pilot operations using CO_2 from gas plants (Bennion and Bachu, 2006a).

In both miscible and immiscible form CO_2 can improve oil production. Injected CO_2 under miscible and near-miscible pressure and temperature conditions dissolves in oil, thins and expands oil to help displace oil out of reservoirs and pushes oil to producing wells through use of injection flow pressure (Figure 2.9).

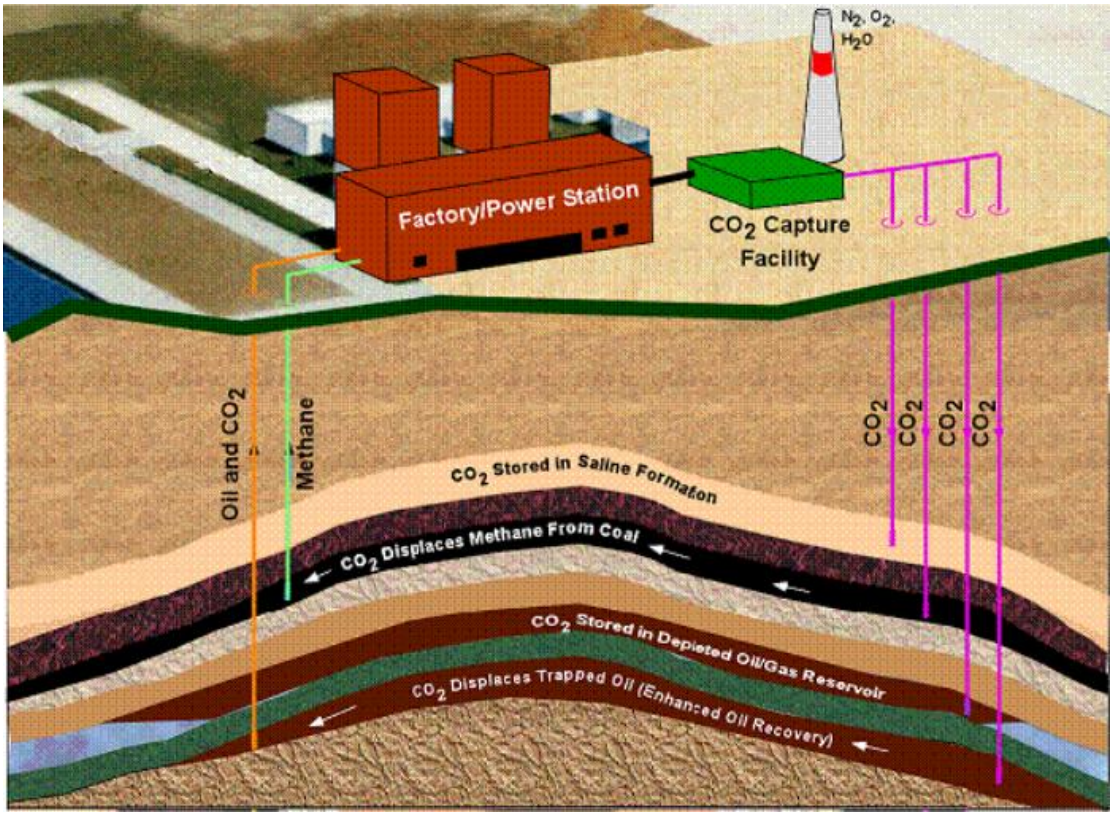

Figure 2.8: CCS process combined with enhanced hydrocarbon recovery (Sweatman *et al*., 2011).

The displacement mechanism of gas is also a non-wetting phase displacement, similar to oil. Under the immiscible pressure and temperature conditions, injected CO_2 floats above the oil due to its lighter density, supporting gas assisted gravity displacement (GAGD) of oil out of lower depths, helps improve oil production when GAGD (Figure 2.10) is combined with horizontal wells (Rao *et al.*, 2004)**,** pushes oil down to producing depths in the lower sections of reservoirs using gas injection flow pressure. It is therefore very crucial to study the characteristics of the displacement process involving the injected gas and in-situ fluids (Bennion and Bachu, 2008; Kumar *et al.*, 2005). These characteristics affect injectivity, and flow rate, spread of

the plume of the injected gas, and residual trapping of gas in the pore space (Kumar *et al*, 2005).

The injected CO_2 can be stored securely by a number of mechanisms, namely structural/stratigraphic or hydrodynamic trapping, capillary or pore-level trapping, solution trapping and mineral trapping. The importance of each storage mode depends on the characteristics of the formation, injected fluid and time period after injection (Shah *et al.*, 2008). The residence time of CO_2 in aquifers for sequestration applications is of the order of 10,000 years and different time scales for the different processes must be considered. CO_2 has a critical temperature of 31 ^{o}C (88 ^{o}F) and a critical pressure of 7.38 MPa (1070 psia). Therefore, at typical reservoir pressures and temperatures carbon dioxide will behave as a supercritical fluid. At injection depths greater than ~800 m, assuming a geothermal gradient of 30^{o}C/km and a pressure gradient of 10.5 MPa/km, CO_2 can be stored as a supercritical fluid (Bruant *et al*, 2002; Bachu and Gunter, 1994; Bachu, 2002; Holloway and van der Straaten, 1995). The density of supercritical CO_2 at 800 m depth is approximately 260 kg/m^3 and this permits far greater quantities of CO_2 to be stored per unit volume than as a gas at shallower depths (Bruant *et al*, 2002). At this depth, the density of water with 15% total dissolved solids by mass is ~1100 kg/m^3 (McCain, 1991; Bachu and Gunter,1994). This density difference generates buoyancy forces that drive injected CO_2 upward.

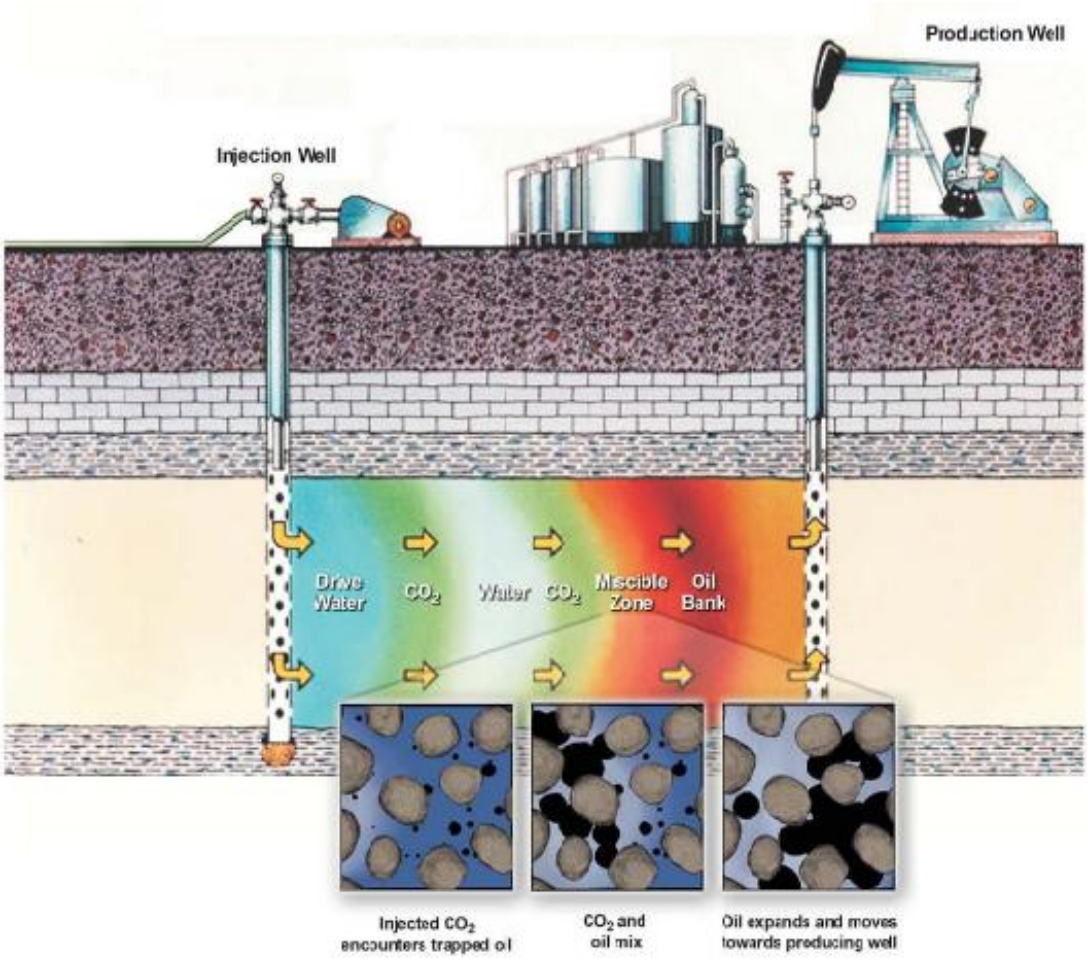

Figure 2.9: CO_2 EOR process and downhole mechanisms (NETL, 2010 – In: Sweatman *et al.*, 2011).

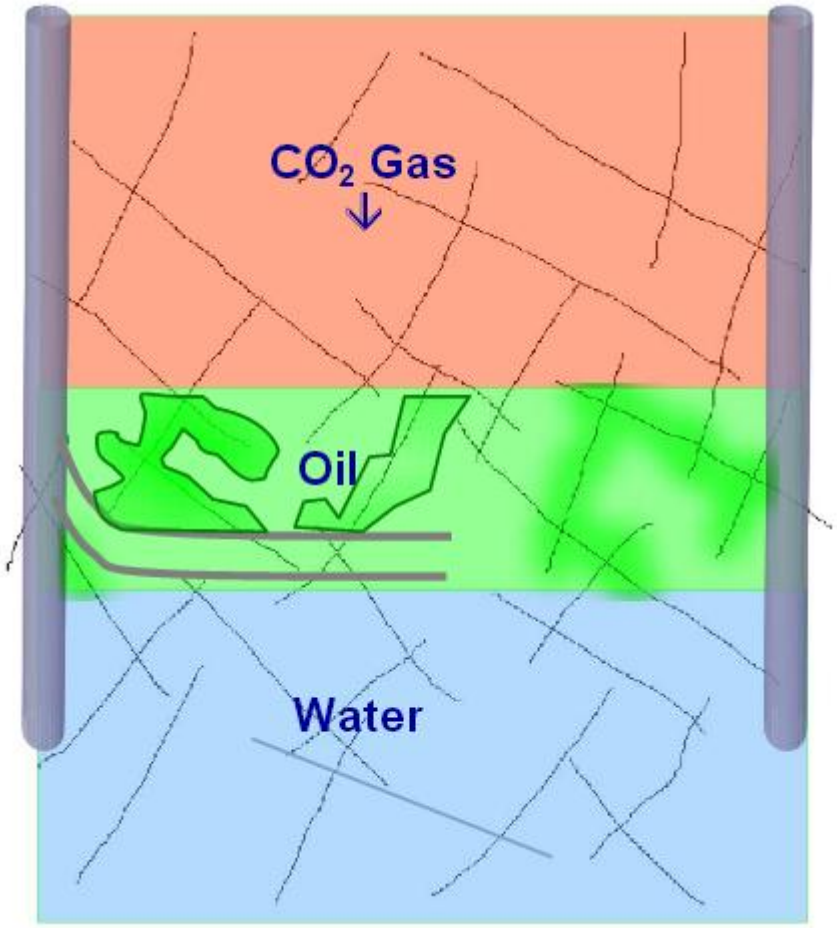

Figure 2.10: Horizontal well at a lower depth provides best oil drainage for gravity displacement by immiscible CO_2 (Sweatman *et al*., 2011).

In hydrodynamic trapping the buoyant CO_2 is trapped under impermeable caprock. During and shortly after the injection period, a significant fraction of the injected gas rises buoyantly and accumulates beneath the geological seal (caprock), a low-permeable (most often clayey or evaporite) porous medium usually saturated with water. This process relies on an intact barrier to upward flows (Bachu *et al*, 1994; van der Meer, 1995; Shah *et al.*, 2008).

Capillary trapping is the form in which the residual part of the gas phase is stored as disconnected gas droplets; the CO_2 is stranded in pore-space bubbles surrounded by water (Shah *et al.,* 2008; Juanes *et al.,* 2006; Al-Mansoori *et al.,* 2010). It is the fastest and secure way to immobilise the CO_2 in porous media without relying on sealing caprock. A way of maximizing the trapped CO_2 by this method is to engineer the process, by the injection of additional brine into the formation after CO_2 injection (Juanes *et al,* 2006; Qi *et al,* 2009). During the injection period, the less wetting CO_2 displaces the more wetting brine in a drainage-like process. However, after injection, the buoyant CO_2 migrates laterally and upward, and water displaces CO_2 at the trailing edge of the plume in an imbibition-like process. This leads to disconnection of the once-continuous plume into blobs and ganglia, which are effectively immobile.

Solution trapping is the dissolution of CO_2 in the formation water (aquifer brine) or residual oil. This fraction is stored permanently, as the injected CO_2 will not reach the surface any sooner than the other fluid species originally present in the formation (Shah *et al,* 2008). The CO_2 saturated brine is denser than the surrounding brine leading to convective mixing where the denser brine migrates deeper into the formation over hundreds of thousands of years (Lindeberg and Wessel-Berg, 1997; Ennis-King and Paterson, 2005). The solubility of CO_2 decreases with increasing temperature and salinity, and increases with increasing pressure.

CO_2 and its aqueous derivatives on reaction with aquifer solids may be stored as precipitated and adsorbed phases. This is known as mineral trapping (Bachu *et al,* 1994; Gunter *et al,* 2000). An example is the precipitation of calcium, magnesium,

and iron carbonate on reaction with silicate minerals. This process is a method of permanently sequestering the CO_2 injected into the formation. This is the ultimate desirable form of sequestration, because once geochemical equilibrium is reached, it is unlikely that mineralised CO_2 will be able to leak into the atmosphere. For long-term CO_2 storage, these slow reactions may proceed to an appreciable extent (Gunter *et al*, 2000; Lin *et al*, 2008).

A major issue in CO_2 geological storage is to ensure that the CO_2 will remain stored in the geological formation where it is injected (Chiquet *et al*, 2007a; Li *et al*, 2006). For optimization of the CO_2 storage efficiency, reservoirs are commonly selected to ensure that CO_2 will be injected and stored as a dense phase. In most cases this dense phase, being lighter than the formation brine and most oils, will rise buoyantly to the top of the reservoir structure and accumulate beneath the seal rock (or caprock), a low permeability (usually shale) porous medium saturated with brine (salted water) (Chiquet *et al*, 2007b). The caprock is susceptible to capillary failure, and storage safety is therefore dependent on the caprock ability to prevent or seriously hinder CO_2 leakage. Study on leakage of seals for CO_2 geological storage has consequently become a recent focus of research interest on the porous media. In the presence of two or more immiscible fluid phases in the caprock rock, multiphase flow will occur, which is associated with capillary effects. Fluid transport is then controlled by the interfacial tension of the fluids involved, the wettability of the solid surface with respect to the fluids, and the structure of the pore system (Hildenbrand *et al*, 2002). A clearer understanding of this pore-level event will be needful in making accurate assessments of the leakage risks of stored CO_2. Although a lot of investigations have been carried out on the sealing integrity of caprocks (Hildenbrand *et al*, 2004;

Chiquet *et al,* 2007; Li *et al,* 2005; Chalbaud *et al,* 2009), the results so far suggest that some fundamental data for accurate interpretation of seal leakage are still lacking. For example, the contact angle used in estimating the capillary resistance are measured on flat surface and most times assumed to be constant. Also, the exact impact of the pore geometry is not fully understood. This may be due to the fact that the measurement of petrophysical and fluid transport properties of fine-grained rocks is time consuming and the corresponding data base is relatively small (Hildenbrand *et al,* 2002). In this study we have developed a method to measure contact angle in a pore and also measure the resistance to two-phase flow in the single pore.

2.5 Characterisation of Porous Media Resistance

2.5.1 Permeability

Resistance to flow in porous media is usually measured by its permeability**,** a measure of the capacity of the porous medium to transmit fluid (API Code 27, 1952). It is one of the most important parameters in reservoir studies, and a measure of the fluid conductivity of the particular material. It is a complex interplay of porosity, pore connectivity, grain packing, grain size, pore size, and rock diagenesis (Rezaee *et al,* 2012).

Permeability of petroleum reservoir rocks may range from 0.1 to 1000 or more millidarcy as shown in Table 2.1.

Table 2.1: Permeability and Porosity of Selected Oil Sands (Tiab and Donaldson, 2015)

Name of Sand	Porosity (%)	Permeability (mD)
"Second Wilcox" (Ordovician) Oklahoma Co., OK	12.0	100.0
Clinch (Silirian) Lee Co., VA	9.6	0.9
Strawn (Pennsylvanian) Cook Co., TX	22.0	81.5
Bartlesville (Pennsylvanian) Anderson Co., KS	17.5	25
Olympic (Pennsylvanian) Hughes Co., OK	20.5	35.0
Nugget (Jurassic) Fremont Co., WY	24.9	147.5
Cut Bank (Cretaceous) Glacier Co., MT	15.4	111.5
Woodbine (Cretaceous) Tyler Co., TX	22.1	3,390.0
Eutaw (Cretaceous) Choctaw Co., AL	30.0	100.0
O'Hern (Eocene) Dual Co., TX	28.4	130.0

Conventional petroleum reservoirs have permeability more than 1 md, near tight reservoirs have permeability between 1 and 0.1 md and tight reservoirs have permeability less the 0.1 md, based on the in-situ permeability values (Figure 2.11).

Permeability may be absolute, effective or relative. Absolute permeability is the capacity of a porous medium to conduct fluid when saturated with a single fluid (permeability of a fluid at 100% saturation). Effective permeability is the capacity of the porous medium to conduct a fluid in the presence of other fluids. Relative permeability is the ratio of the effective permeability of a given fluid at a partial saturation to the permeability at 100% saturation. That is, the ratio of effective permeability to absolute permeability. By analogy with electrical conductors, permeability represents the reciprocal of the resistance which the porous medium permits flow.

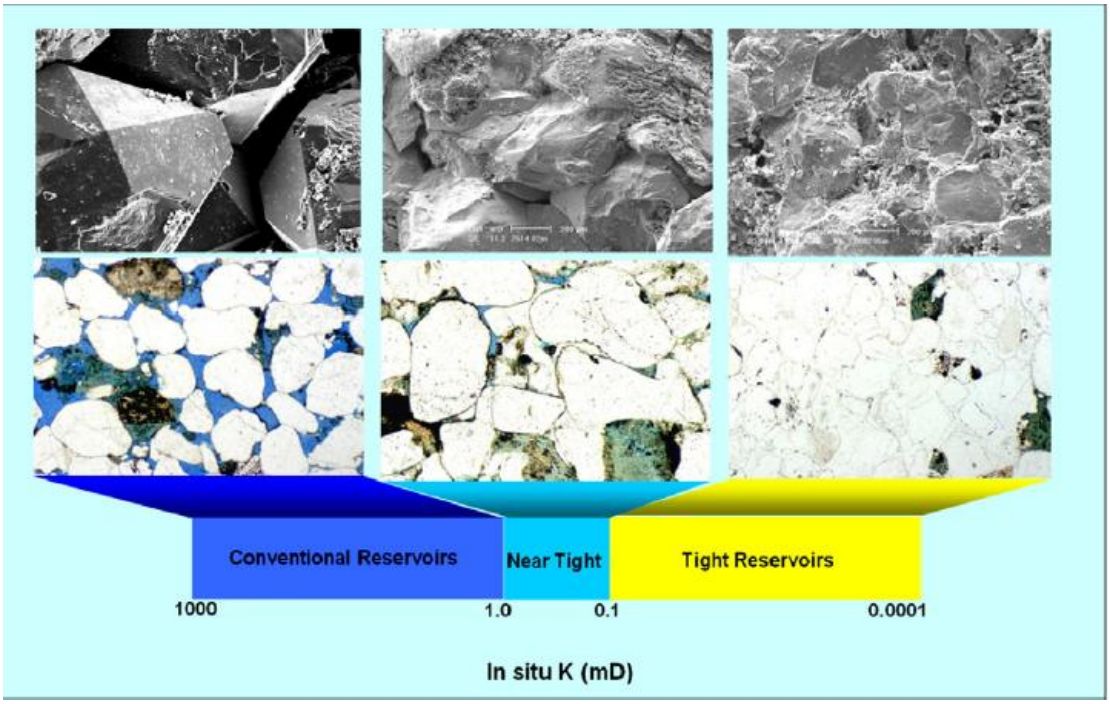

Figure 2.11: Conventional, near tight and tight gas sand definition based on the in-situ permeability. The tight sand matrix is primarily composed of micro-pores where average pore throat aperture might be less than 1 μm in diameter (Rezaee *et al*., 2012).

Rezaee (2012) stated that one of the main controlling parameters for permeability, in addition to pore connectivity, is the pore throat which is a very tiny element in the rock, and any reduction in the pore throat size will affect the permeability significantly. Thompson *et al* (1987) had suggested earlier that permeability can be expressed in terms of a single effective pore diameter measured from mercury injection capillary pressure and this permeability relation is valid for essentially all porous rock and for a broad class of porous media.

2.5.1.1 Permeability from pore throat parameter and porosity

Permeability of porous media is usually expressed to depend on some physical properties of the interconnected pore system such as porosity and tortuosity. The natural assumption would be that permeability depends on porosity, but it is not simple to determine appropriate permeability-porosity relationship (Costa, 2006). For example, two porous systems can have same porosity but different permeability.

Many investigations have established that permeability of the porous media is mainly dependent on the pore throat radius, with the pore space contributing a little.

One of the most widely accepted and simplest model for the permeability-porosity relationship is the Kozeny-Carman (KC) model (Kozeny, 1927; Carman, 1937), which provides a link between media properties and flow resistance in pore channels (Costa, 2006). The starting point of the KC equation is the comparison between the average fluid velocity as given by Darcy's law and that obtained from the Poiseuille formula for capillary tube. The capillary tube model considers the porous medium as consisting of straight cylindrical capillary tubes with an average inside diameter.

The Kozeny-Carman (1937) equation is expressed as:

$$k = \frac{\phi}{8}\frac{r^2}{\tau^2} \qquad (2.4)$$

where k is absolute permeability (cm^2), ϕ is porosity (%), τ is tortuosity (dimensionless), and r is radius (cm) of capillary tube.

Equation (2.4) shows the dependence of permeability on both of the pore geometry segments; pore spaces and pore throats. For constant porosity, permeability is directly proportional to pore throat radius.

Salah (2011) made a porosity-permeability plot of 219 samples of sandstones and carbonates studied and observed that the regression coefficient was very low (R^2 = 0.376) (Figure 2.12). For better accuracy, the permeability was plotted against porosity and pore throat from R35, and the regression coefficient increased from 0.376 to 0.9469 (Figure 2.13). R35 was chosen to represent the pore throat as most studies had shown that R35 dominate the flow within the measured sample and it is commonly used to predict the flow units of reservoir rocks. This increase of regression coefficient on introduction of R35 confirms that the pore throat is the main effective parameter in the fluid flow through the reservoir rock pore space configuration.

.

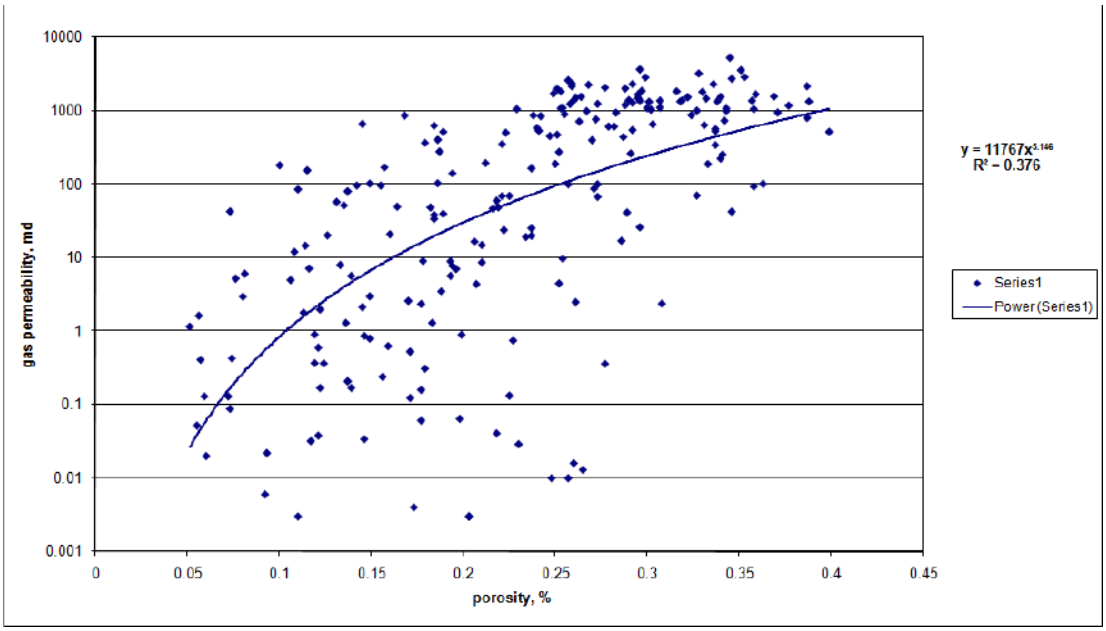

Figure 2.12: Permeability vs Porosity (Salah, 2011)

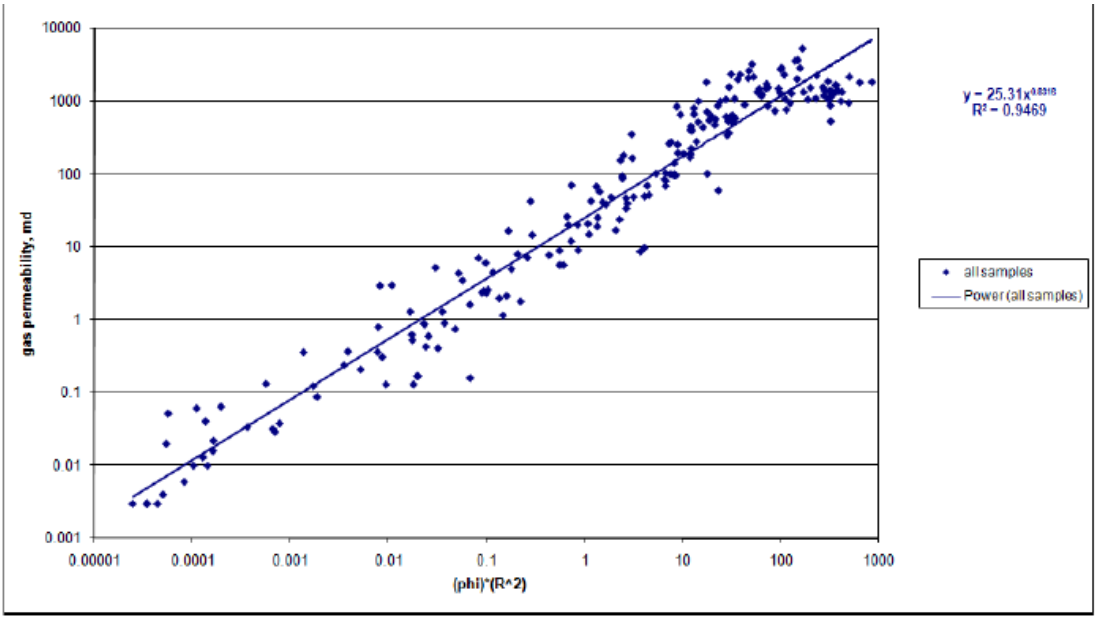

Figure 2.13: Permeability vs Porosity and R35 (Salah, 2011)

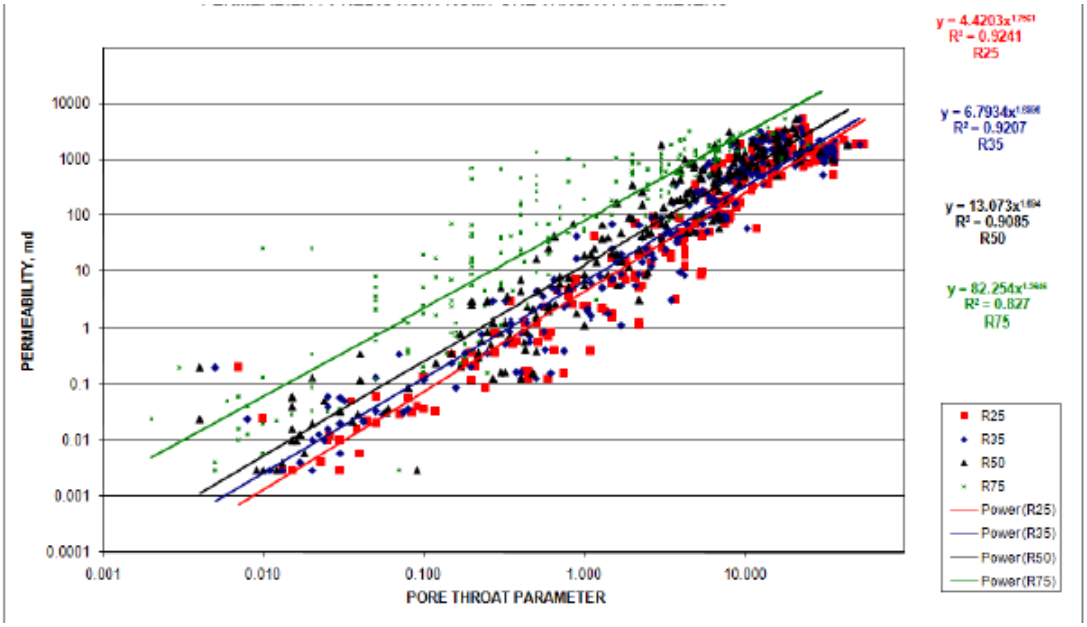

Figure 2.14: Permeability prediction from pore throat parameters (Salah, 2011)

Scheidegger (1974) expressed a relationship between permeability and pore throat diameter based on the capillary tube model, from Hagen-Poiseuille and Darcy laws.

The flow rate for a bundle of straight parallel capillaries is given by Hagen-Poiseuille equation as:

$$Q = \frac{\pi r^4 \Delta P}{8\mu L} \quad (2.5)$$

where Q is the flow rate (m^3), r is the radius of the capillary (m), L is length of capillary (m), μ is the fluid viscosity (Pa.s or $N.s/m^2$), and ΔP is the pressure drop across the capillary (Pa).

The total area,A, available to flow is

$$A = \pi r^2 \quad (2.6)$$

So that Equation 2.5 reduces to

$$Q = A\frac{r^2}{8}\frac{\Delta P}{\mu L} \quad (2.7)$$

It is known from Darcy's law that

$$Q = Ak\frac{\Delta P}{L\mu} \quad (2.8)$$

where k is the permeability of the medium (m^2). Therefore, equating Darcy's and Poiseuille's equations for fluid flow in a uniform and smooth-walled tube (Amyx *et al*, 1960; Oritz-Arango and Kantzas, 2011; Salah, 2011),

$$k = \frac{r^2}{8} \quad (2.9)$$

where k and r are in consistent units (k in m^2 for r in m).

Equation (2.9) shows also that permeability is mainly a function of the tube radius which is represented by the pore throat radius in reservoir rocks. This again shows the principal role of pore throat size in permeability estimation. Salah (2011) also attempted to establish the relationship between pore throat diameter and permeability using pore throat radius corresponding to a mercury saturation of 25% (R25), 35% (R35), 50% (R50) and 75% (R75) for the mixed suite of sandstones (179 samples)

and carbonates (40 samples) (Figure 2.14). The regression coefficients using the four different mercury saturations were 0.92, 0.92, 0.91 and 0.83 for R25, R35, R50 and R75, respectively. These are excellent demonstrating the high dependence of the measured permeability on pore throat size. However, it should be noted from Figure 2.14 that the pore throat size correlation has very high uncertainty, 5 orders magnitude variance. This implies that pore topology is the first order control. Salah (2011) suggested that any of the four equations can be used to estimate permeability from pore throat size. This could be very useful for uncored wells where the pore throat size can be measured on cutting samples to estimate permeability, especially in tight reservoir rocks.

Scheidegger (1974) also expressed permeability as:

$$k = \frac{\phi \bar{d}^2}{32} \tag{2.10}$$

where k is permeability in cm^2 and $\bar{d}$ is the average diameter of the capillary in cm. For $\bar{d}$ in microns, porosity ϕ in fraction, and permeability k in md (Permadi and Susilo, 2009), Eq. (2.10) becomes:

$$k = 31.6875 \phi \bar{d}^2 \tag{2.11}$$

This is similar to a correlation (practical) obtained for sandstone samples:

$$k = 20.464 \phi d_H^{1.646} \tag{2.12}$$

where d_H is effective (mean) hydraulic diameter in microns.

They suggested that the power for d_H in Eq. (2.12) is less than 2.0, probably due to irregular shape of the pore throats. According to fractal theory, a plane with a perfectly smooth, regular shape must have a fractal dimension of less than 2.0. The cross-sectional area of rock pores, from investigation, ranges from 1.5800 to 1.8120,

with the fractal dimension increasing with the permeability. For tortuous capillary tubes with tortuosity τ, Eq. (2.11) may be written as (Scheidegger, 1974):

$$k = 31.6875\phi\bar{d}^2/\tau \quad (2.13)$$

where $\tau = L_a/L$, L_a is the actual distance travelled by the fluid through the tubes from the inlet to the outlet, and L is the straight length of the medium. As natural porous rocks have τ mostly greater than 1.0, the constant in Eq. (2.13) should be less than 31.6875.

Porosity for the capillary tube model (Scheidegger, 1974) is:

$$\phi = \frac{nA\pi\bar{r}^2T\Delta l}{A\Delta l} = n\pi\bar{r}^2\tau \quad (2.14)$$

where n is the number of capillaries in the bundle, Δl is the pore length, and $\bar{r}$ is mean effective pore radius. For a uniform capillary, $\tau = 1$, and

$$\phi = n\pi\bar{r}^2 \quad (2.15)$$

or

$$\phi = n\frac{1}{4}\pi\bar{d}^2 \quad (2.16)$$

The parallel type model (Scheidegger, 1974) in which the permeability is lowered by a factor of 3 gives permeability as:

$$k = \frac{\phi\bar{d}^2}{96} \quad (2.17)$$

For $\bar{d}$ in microns, porosity ϕ in fraction, and permeability k in md (Permadi and Susilo, 2009), Eq. (108) becomes:

$$k = 10.5625\phi\bar{d}^2 \quad (2.18)$$

2.5.1.2 Permeability from Mercury Injection Capillary Pressure (MICP) Methods

Permeability has been determined using a number of empirical correlations from mercury injection capillary pressure (MICP) measurements based on Washburn equation (see 2.5.3.1). As these correlations are based on Washburn equation, they may apply strictly to single phase flow (displacement of air by mercury in the pore space of reservoir rocks) (Rezaee *et al*, 2012). However, they are often applied to the case of two-phase flow.

Purcell (1949) using the graphical integral of the curve of mercury saturation versus reciprocal capillary pressure squared related capillary pressure empirically to air permeability. Swanson (1981) empirically expressed the relationship between permeability and the hyperbola of the log–log mercury injection capillary pressures curve, having observed earlier (Swanson, 1977) that the complete saturation of effectively interconnected pore spaces with a non-wetting phase (Wood's metal) corresponded to the apex of the hyperbola of a log–log mercury injection capillary pressures curve (Eq. 2.19).

$$K_{air} = 339 \left(\frac{S_{HG}}{P_c}\right)^{1.691}_{apex} \quad (2.19)$$

where K_{air} is air permeability (md), $S_{HG}$is the mercury saturation (%) corresponding to the apex of the hyperbola and P_c is capillary pressure (psi).

Katz and Thompson (1986) reported a relationship between permeability and conductivity at a threshold pressure (Eq. 2.20).

$$K = \frac{1}{226}(l_c^2)\left(\frac{C_o}{C_w}\right) \quad (2.20)$$

where l_c is the characteristic pore size (e.g. the calculated pore size (mm) for the threshold pressure at which mercury forms a connected pathway through the sample), and C_o/C_w is the ratio of rock conductivity to the conductivity of the formation water.

An empirical relationship between permeability, porosity, and throat size corresponding to a mercury saturation of 35% (r_{35}) was developed by Winland (in Kolodzie, 1980) (Eq. 2.21).

$$\text{Log}\, r_{35} = 0.732 + 0.588 \log k - 0.864 \log \phi \quad (2.21)$$

Pitman (1992) using multi-regression analyses of mercury injection, permeability and porosity data for sandstone samples extended Windland's work to obtain the following correlation:

$$\text{Log}\, K = -1.221 + 1.415 \log \phi + 1.512 \log r_{25} \quad (2.22)$$

or

$$1.512 \log r_{25} = \log K + 1.221 - 1.415 \log \phi \quad (2.23)$$

To obtain the pore throat diameter from permeability and porosity, Equation 2.23 can be expressed as:

$$r_{25}^{1.512} = 10^{1.221} \left(\frac{K}{\phi^{1.415}}\right) \quad (2.24)$$

Rezaee *et al* (2006) using regression analysis also developed a set of relationships between permeability, porosity and pore throat size for 144 carbonate samples (Eq. 2.25). They indicated that pore throat radii corresponding to a mercury saturation of 50% (r_{50}) is the best permeability predictor for carbonates with complex pore networks.

$$\text{Log}\, K = -1.160 + 1.780 \log \phi + 0.930 \log r_{50} \quad (2.25)$$

or

$$r_{50}^{0.930} = 10^{1.160} \left(\frac{K}{\phi^{1.780}}\right) \quad (2.26)$$

All the correlations above are for conventional reservoirs, and in all of the equations r_i is the pore throat corresponding to i_{th} percentile, K is uncorrected air permeability (md) and ϕ is porosity (%). For tight gas sand reservoirs from MICP, Rezaee *et al.* (2012) used multi-regression analysis to develop an empirical equation for calculating permeability from porosity and pore throat radius (Eq. 2.27). They concluded that pore-throat radii corresponding to a mercury saturation of 10% is the best permeability predictor of MICP for tight gas sands. Equation 2.27 is the corresponding equation that uses r_{10}.

$$\text{Log}\, K = -1.92 + 0.949 \log \phi + 2.18 \log r_{10} \quad (2.27)$$

or

$$r_{10}^{2.18} = 10^{1.92} \left(\frac{K}{\phi^{0.949}}\right) \quad (2.28)$$

where k is the dry gas permeability (md), ϕ is porosity (%) and r_{10} is the pore throat size (micron) corresponding to the 10^{th} percentile of mercury saturation on a cumulative mercury injection plot.

Rezaee (2012) concluded that while Winland, Pittman and Rezaee's equations (Eqs. 2.21 – 2.26) overestimate permeability, permeability obtained from Equation 2.27 shows a relatively good agreement with the measured permeability for tight gas reservoirs.

2.5.1.2.1 Pore throat in permeability estimation

Pore throat is a critical element for fluid flow in porous medium, because it controls fluid movements and influences the hydraulic properties such as permeability, capillary pressure, fluid saturation, as well as, the displacement mechanisms of two immiscible fluids (Gunter *et al,* 2014; Li and Wardlaw, 1986; Mayer and Miller,

1992*;* Al-Raoush and Wilson, 2005; Roof, 1970). It is therefore of importance in many fields of applied science and technology, including fluid flow in porous media such as in the extraction of oil, gas and groundwater (Zhang *et al,* 2015), geological storage of waste product, as well as in fine particle filtration (Lin and Miller, 2000). It is also being used by exploration geologists to evaluate the sealing capacity of cap rocks, as the pore throat size that corresponds to displacement pressure can be determined from a mercury injection test.

Pore throats are constrictions in the pore space of a porous medium and as such modulate flow and offer hydraulic resistance to flow (Hammecker *et al*, 2004; Nelson, 2009). The ease with which the porous medium transmits fluids is measured by the permeability of the medium (Zou *et al.,* 2012; Rezaee *et al.,* 2012), which by analogy with electrical conductors represents the reciprocal of the resistance which the porous medium offers to flow. This indicates the relevance of the pore throat in studying the resistance to fluid flow in the porous medium.

Numerous studies have shown the relevance of the pore throat size in determining the permeability of a porous medium. Thompson *et al* (1987) expressed permeability in terms of a single effective pore diameter measured from mercury injection capillary pressure, and stated that this permeability relation is valid for essentially all porous rocks and for a broad class of porous media. Andersson *et al* (2011) using Katz–Thompson model (Katz & Thompson, 1986, 1987) accurately predicted the permeability for macroporous alumina materials with porosities of 46–76% and suggested that the permeability to fluid flow in these materials is governed by the smallest constrictions between connected pores: the critical pore throat diameter. Zou

et al. (2012) observed that the permeability of the tight gas sandstone is heavily affected by the pore throat connectivity. Amaefule *et al* (1993) using Poiseuille's and Kozeny-Carman's equations showed that permeability is not only a function of pore/pore-throat radius, but also depends on porosity, surface area, and tortuosity. For constant porosity, the Kozeny-Carman equation shows that permeability is directly proportional to pore throat radius (Salah, 2011). Swanson (1981), Pittman (1992) and Bryant *et al* (1993) observed that in many cases, pore/pore throat radius have an effect on permeability higher than that of porosity. Salah (2011) also recently showed experimentally the significant role of pore throat size in permeability estimation based on Hagen-Poiseuille and Darcy laws. With 219 sandstone and limestone samples a relationship of each pore throat size obtained for 25% (R25), 35% (R35), 50% (R50) and 75% (R75) mercury saturation, with permeability was established. The regression coefficients obtained in each case was excellent, demonstrating the high dependence of the permeability on pore throat size. It was therefore suggested that any of the four equations (Equations 2.29 to 2.32) obtained could be used to estimate permeability from pore throat size.

$$y = 4.4203x^{1.7561} \quad (2.29)$$
$R^2 = 0.9241$ (R25)

$$y = 6.7934x^{1.6996} \quad (2.30)$$
$R^2 = 0.9207$ (R35)

$$y = 13.073x^{1.694} \quad (2.31)$$
$R^2 = 0.9085$ (R50)

$$y = 82.254x^{1.5646} \quad (2.32)$$
$R^2 = 0.827$ (R75)

where, y is the permeability in millidarcy (md), and x is the effective radius in microns (μm) for the given mercury saturation. He suggested that this can also be extended to uncored wells, especially in tight rocks, by measuring the pore throat size on cutting samples to estimate permeability. We need to investigate further if this could be applicable in case of a highly porous medium.

The importance of the dominating influence of the pore throat on permeability has been accounted for by the preferential occurrence of cementation at pore throats instead of within pore bodies. Neasham (1977) and Wilson and Pittman (1977) observed that the presence of pore lining and/or pore-bridging clays may reduce permeability significantly by affecting pore/pore throat radius and surface area. Beard and Weyl (1973) believe that surface area, pore size, and shape (tortuosity) are strongly correlated with permeability because they are dependent on grain size and grain packing.

2.5.1.2.1.1 Pore throat identification

Pore throats of porous media are usually identified and defined in terms of the pore size, the pore throat being considered to have smaller pore diameter than the pore body. Martin *et al* (1997) classified the pores of the producing zones of reservoirs based on their pore throat sizes; megaports have throat sizes greater than 10 μm, macroports throat sizes range from 2.5 - 10 μm, mesoports have throat sizes of 0.5 - 2.5 μm, microports have throat sizes in the range of 0.01 – 0.5 μm and nanoports have throat sizes less than 0.01 μm. For conventional sandstones, Nelson (2009) defined pore throat size as pore sizes greater than 2 μm, tight gas sandstone pore throats range from 0.03 – 2 μm, while shales pore throat is in the range of 0.005 – 0.1 μm. Zou *et al* (2012) defined the pore throat of tight gas sandstone reservoirs to be

pore sizes less than 1 μm. These definitions based on pore size are dependent directly or indirectly on mercury injection capillary pressure measurements. Mercury injection porosimetry, which is the usual experimental method to determine pore throat size, actually measures the pore size distribution of a reservoir rock in which pores with similar pore sizes are grouped together. Based on the pore size distribution, the pore throat is then assigned to a group of pores with the smallest effective pore sizes.

2.5.1.3 Permeability from displacement pressure

Displacement pressure is that pressure which must be applied to a pore system before the nonwetting phase starts to displace the wetting phase. This technique is derived from the combination of work by Wyllie & Rose (1950) and Rose & Bruce (1949). From Wyllie and Rose,

$$F = \frac{R_o}{R_w} = \frac{\sqrt{\tau}}{\phi} = \approx \frac{1}{\phi^2} \tag{2.33}$$

where τ is the resistivity factor of the porous medium, R_o is the resistivity of the porous material saturated with brine, and R_w is the resistivity of the brine.

From Rose and Bruce,

$$\tau = \frac{\phi}{kt_s} * \frac{\gamma^2}{P_d} \tag{2.34}$$

where, τ is tortuosity, ϕ is porosity, k is permeability, t_s is a shape factor, γ is interfacial tension, and P_d is displacement pressure. Combining Equations 2.33 and 2.34 give the permeability (Eq. 2.35).

$$k = \frac{21\gamma^2\phi^3}{t_s P_d^2} \tag{2.35}$$

where, k is permeability in md, P_d is displacement pressure in psi, γ is surface tension in dynes/cm, t_s is a pore shape constant (usually about 2.25), and ϕ is porosity (fractional). The displacement pressure is the capillary pressure corresponding to about 95 percent water saturation (Raymer and Freeman, 1984).

2.5.2 Fluid Saturation

Several macroscopic transport properties such as relative permeability, capillary pressure and dispersivity, which are used traditionally to characterize multiphase transport in porous medium are found experimentally to depend on fluid saturations, saturation history, and fluid properties as well as pore space morphology (Mohanty and Salter, 1982). Fluid saturation of a porous medium is dependent on the fluid distribution in individual pores, which is controlled by the capillary forces acting on this microscopic scale.

The nonwetting phase saturation is a function of the capillary pressure between the nonwetting phase and the wetting phase in a two-phase fluid system in a porous medium.

If the capillary pressure (Eq. 2.36) between the two immiscible fluids is decreased, a portion of the nonwetting fluid may be mobilized and extracted from the system.

$$P_{nw} - P_w = \Delta P \tag{2.36}$$

where, P_{nw} is the pressure in the nonwetting phase and P_w is the wetting phase pressure. This is the basis of EOR by surfactant flooding. No matter how small the capillary pressure between the two fluids, the wetting phase does not replace completely the nonwetting phase. As the saturation of the nonwetting phase

decreases, capillary forces tend to pinch off isolated blobs of the nonwetting fluid in the pore spaces. The discontinuous nonwetting fluid becomes entrapped and is said to be in a state of residual saturation (Mayer and Miller, 1992). The nonwetting blobs, which are in a state of residual saturation, assume shapes that are influenced by the pore geometry. The blob sizes vary over several orders of magnitude and this size distribution can have significant effects on the transport properties of the nonwetting phase. For example, for liquid-liquid interface, such as in oil recovery, the viscous forces required to remove a blob are related to the blob length, blob volume, and the surface area distributions of the oil blob will determine, at least partially, the rate of nonwetting fluid dissolution into the aqueous phase (wetting fluid). Wardlaw and McKellar (1985) showed that if the liquid-phase properties are held constant, given a constant capillary number and constant density forces, then maximum stable blob length is dependent on the porous medium properties of permeability, k and pore throat, r_t.

Many investigations have been carried out on the influence of fluid saturation on resistance to fluid displacement in single pores. Most of them focus on the relationship between film thickness or residual saturation and the correlation group known as the capillary number, defined as the ratio of viscous force to capillary force (interfacial force). One of the most common forms of capillary number is that by Saffman and Taylor (1958) (Equation 2.37).

$$N_c = \frac{\nu\mu}{\sigma} \qquad (2.37)$$

where ν is the velocity of displacing phase (Darcy velocity) (ms^{-1}), μ is the viscosity (Pa.s), and σ is the interfacial tension between the displacing phase and the displaced phase (Nm^{-1}). ν is defined as $\nu = q/A$, with A being the cross-sectional area, m^2.

Another form of the capillary number is defined by Taber (1969) in terms of pressure drop between two points, the flow length, and the interfacial tension (Equation 2.38).

$$N_c = \frac{\Delta P}{\sigma L} \tag{2.38}$$

where, ΔP is the pressure drop (Pa), L is the flow length of the porous medium (m), and σ is the interfacial tension (Nm^{-1}).

The range of the flow velocities (from 0.26 to 1.29 m/day) used in calculations for storage sites is assumed to be the same as in the laboratory experiments (Polaka *et al.*, 2011).

Fairbrother and Stubbs (1935), in their pioneering work, found that in a capillary tube, an air bubble moves faster than the liquid being displaced due to the adhesion of a thin film on the walls of the tube. The magnitude of the residual liquid left behind was found to be a function of the balance between the viscous forces and the capillary forces. This was expressed through the capillary number Ca, as follows:

$$Ca = \frac{\mu v_b}{\sigma} \tag{2.39}$$

where, μ is the viscosity of the displaced fluid, v_b is the bubble velocity and σ is the surface tension of air–liquid. They introduced an empirical equation to determine the fraction of the liquid supported on the surface of the tube and was related to the capillary number as follows:

$$W = \frac{v_b - v_m}{v_b} = Ca^{1/2} \tag{2.40}$$

where, v_m is the average velocity of the liquid. This correlation is useful for 1.0E-3<Ca<1.0E-2. Taylor (1961) found that Eq. (2.40) can be extended to Ca=0.09 and W approaches an asymptotic value of 0.56.

Bretherton (1961) studied the motion of an inviscid bubble in a straight capillary tube. His results show that there is a thin film with constant thickness between the bubble and the tube wall, and the thickness of the film is a function of *Ca*. He proposed an equation to predict the film thickness, assuming that the bubble profile is of constant curvature except very near the wall, where the meniscus is deformed by viscous forces:

$$\frac{h}{r} = 0.643(3Ca)^{2/3} \qquad (2.41)$$

where, h is the film thickness and, r is the radius of the tube. Bretherton also carried out experiments to check the theory and found that the theory underpredicts the measured values of film thickness as *Ca* becomes small. He found that Eq. (2.41) is applicable for Ca>1.0E-4. Similar conclusions are reported from the experimental investigations of Schwartz, Princen & Kiss (1986). To follow up the work of Bretherton, Cox (1962) presented experimental results indicating that the ultimate value of W was about 0.6. Chen (1986) found that the film thickness decreased as the capillary number decreased until it approaches a constant value at low capillary number, from the measurement of the film thickness through a conductimetric technique. His results showed a deviation from Bretherton theory and he argued that such deviation was due to the roughness of the tube wall.

Recently, Lucas *et al* (2006) observed from experimental studies that in immiscible displacement of a non-wetting fluid by a wetting fluid in a capillary a thin precursor wetting film exists, which enables a piston-like motion of the meniscus (Figure 2.13).

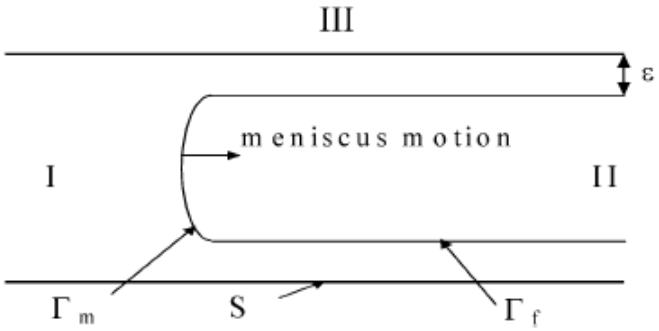

Figure 2.15: Model of interface displacement in circular capillary: ε tends to zero (Lucas et al, 2006). S and Γ_f – boundaries of thin film; ε – thickness of thin film; Γ_m – meniscus; I – wetting fluid; II – nonwetting fluid.

Gutenev *et al* (2003) suggested that the thin film thickness ε is given by:

$$\varepsilon = RCa^{2/3} \qquad (2.42)$$

where R is the mean meniscus curvature and Ca is the capillary number. When $Ca << 1$, capillary effect is important, and then the film thickness is negligible in front of the meniscus. That is, $\varepsilon << R$. As the film thickness is negligible at the front, the phenomenon can be described as a displacement in a capillary whose pores are parallel. Argüelles-Vivas and Babadagli (2014) experimented and quantitatively analysed film thickness (residual oil saturation) development in gas-oil displacements at low capillary numbers, for gas injection (isothermal) and steam assisted gravity drainage (SAGD) or steam injection (non-isothermal) oil or heavy-oil recovery processes in thick reservoirs using circular capillary tubes. The effects of injection (or flow) rate and temperature on the film development were investigated for temperatures between ambient (23.5^{o}C) and 85^{o}C. For horizontal displacement of kerosene by air at 23.5^{o}C and 85^{o}C they found that for Ca<1.0E-3, the film thickness (residual oil saturation) is practically independent of the temperature of the system, but depends on the capillary forces. For higher capillary number, the residual oil

saturation is predominantly dependent on the temperature and highly dependent on the gas injection rate. Initial water saturation resulted in increase in residual oil saturation, especially at high temperatures.

For air-heavy oil horizontal displacements at 55^{o}C and 85^{o}C, for low capillary numbers (Ca<1.0E-2), in the region for fluid flow in oil reservoirs, the residual oil saturation is not practically affected by temperature and gas flow rate, but just depends on the capillary forces. At higher capillary numbers, in the middle region zone (Ca>1.0E-2), the residual oil saturation is dependent of the temperature and gas flow rate, and therefore of the competition between capillary and viscous forces. This is also similar to the results obtained for air-kerosene displacement.

The investigation of Giavedoni and Saita (1997) covered the widest capillary number range, 5.0E-5<Ca<10, and found an excellent agreement with the Bretherton's theory for Ca≤1.0E-3. Modelling the low velocity region is still a challenge due to the complexity of solving the thin-film region (Dong and Chatzis, 2004). Low capillary numbers (Ca<1.0E-4) are characteristic of oil reservoirs (Schwartz *et al.,* 1986; Dullien, 1992). Bergslien and Fountain (2006) suggest that for capillary forces to dominate flow, the capillary number needs to be less than 10^{-4}. They defined capillary number, $N_{c,}$ as:

$$N_c = \frac{v_w \mu_w}{\gamma_{nw} \cos\theta} \qquad (2.43)$$

where, v_w is the water velocity, μ_w is the viscosity of water, γ_{nw} is the interfacial tension between the fluids and θ is the contact angle.

Although considerable investigations on the impact of capillary number on fluid saturation have been carried out we do not understand fully its impact on resistance

to displacement in the pores. For example, parameter such as contact angle were measured on flat surfaces and in most cases assumed to be constant, and the actual impact of pore structure is not clear. We need to investigate further on this.

2.5.3 Capillary or Displacement Pressure

Capillary pressure is the pressure difference existing across the interface holding movement of the interface of two immiscible fluids. It is expressed by the Young-Laplace equation (Equation 2.1).

The capillary pressure is described by Purcell (1949) as displacement pressure, which is analogous to injection pressure as described by Berg (1975). The displacement pressure is that force required in displacing the wetting phase (water) from the cylindrical pore and forcing the non-wetting phase (oil) filament through the pore. A change in any of the variables in Equation 2.1 will change the displacement pressure or the resistant force to displacement. The displacement pressure will increase with decrease in pore radius, increase in interfacial tension and decrease in contact angle. For non-cylindrical pores Smith (1966) defined the displacement pressure or breakthrough pressure as the minimum pressure required to establish a connected hydrocarbon filament through the largest interconnected water-saturated pore throats of the rock.

In order to determine the displacement or breakthrough pressure for a given nonwetting-wetting-solid system, the interfacial tension, wettability and radius of the largest connected pore throats must be measured or estimated.

The Young-Laplace equation assumes constancy of contact angle and must be applied with caution since contact angle is a function of capillary pressure as well as of interface type (Li and Wardlaw, 1986).

Reservoir initial fluid distribution and hydrocarbon recovery during primary or enhanced production are affected by capillary pressure. Fluids distribution in reservoir pores is a function of capillary forces, which in turn are related to pore geometry, system wettability, and fluid property. Capillary pressures data are used primarily to evaluate reservoir rock quality calculate the height of oil columns or estimate relative permeability characteristics (Rezaee *et al,* 2012). One of the most important and frequently used applications is to derive absolute permeability from some MICP data (as discussed in previous sections).

Understanding of the capillary pressure behaviour is also very essential in assessing the injectivity of CO_2 into hydrocarbon reservoirs (Bennion and Bachu, 2006a) or suitability and potential of CO_2 sequestration in deep saline aquifers (Plug and Bruining, 2007; Kumar *et al,* 2004; Shah *et al,* 2008). Capillary pressure behaviour has also been shown to be very important in mechanisms such as capillary trapping of CO_2 for underground storage (Kumar *et al,* 2005) and the alternate imbibition and drainage processes in heterogeneous media which results in capillary hysteresis. In addition, capillary pressure is a direct measure of wetting effects (Anderson, 1987a, van Lingen *et al,* 1996). This wetting behaviour is relevant for the integrity of the caprock as a geological seal (Kumar *et al,* 2005), and the seal capacity of the caprock is a measure of the sustainability of CO_2 sequestration. Furthermore, capillary pressure, interfacial tension and relative permeability have been shown to affect the

flow and storage of CO_2 as an immobile phase in the pore space at irreducible saturation (Kumar *et al*, 2004; Hassanizadeh and Gray, 1993; Reeves and Celia, 1996).

A number of techniques for measurement of capillary pressure at relevant pressure and temperature conditions are described in literature. Most techniques are based on the porous plate technique (Christoffersen and Whitson, 1995), the micro-pore membrane technique (Jennings *et al*, 1988), mercury drainage experiments (Anderson,1987a) and the centrifuge method (Newsham et al, 2004).

2.5.3.1 Measurement of Capillary Pressure – Mercury Porosimetry

Mercury Injection Capillary Pressure (MICP) measurement or Mercury Porosimetry is the most rapid method for measuring capillary pressure as a function of water saturation in rocks, and still remains as one of the standard petrophysical tests. Any sample shape can be used. The method also increases the range of pressure investigation; pores between 3 nm and 500 µm can be investigated *(Amyx et al*, 1960; Giesche, 2006). It also has an advantage of providing a wide range of information. Apart from measuring directly pore-throat size distribution (PSD) and the total pore volume or porosity, it can also indirectly evaluate other pore characteristics, such as total pore surface area and median pore diameter (Giesche, 2006).

The mercury capillary apparatus is as shown in Figure 2.16. The essential components of the apparatus are well described by Purcell (1949).

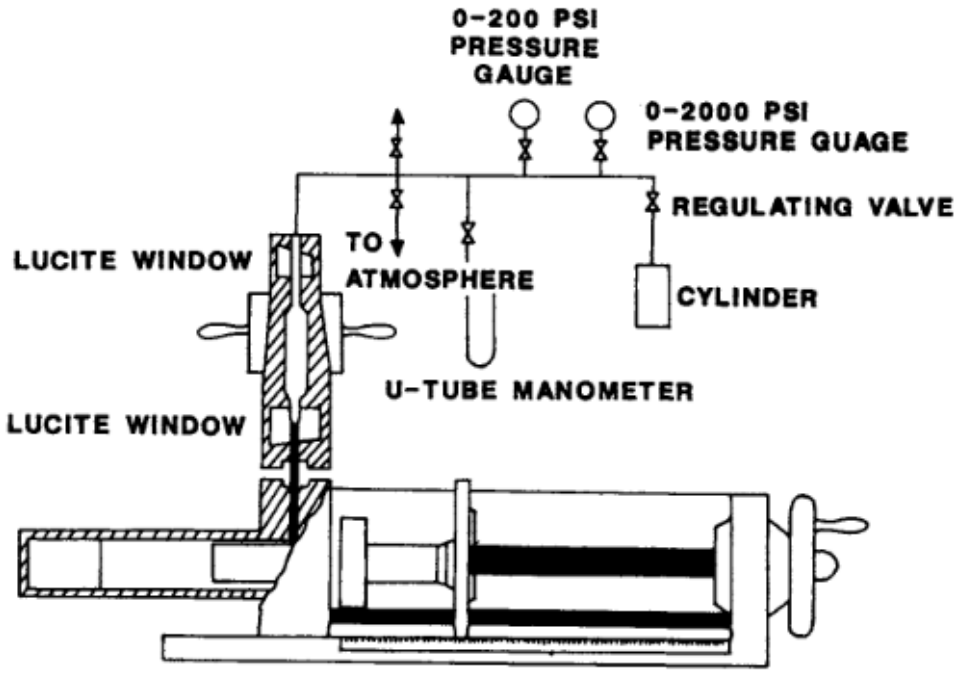

Figure 2.16: Equipment for mercury injection capillary pressure measurement (Tiab and Donaldson, 2015).

To conduct a test, a core is cleaned, dried, inserted in the sample chamber and evacuated. Incremental quantities of mercury are injected while the pressure required for injection of each increment is recorded. The volume of mercury injected at each pressure determines the nonwetting-phase saturation, because mercury is a non-wetting fluid, whereas the mercury vapour corresponds to a wetting phase. This procedure is continued until the core sample is filled with mercury or the injection pressure reaches some predetermined value. Each incremental pressure increase (P_c) is plotted versus the corresponding wetting-phase saturation to produce a curve of injection pressure versus fluid saturation from which a number of parameters can be extracted (Mian, 1992). Injection pressure values are directly converted into

corresponding pore size by using a modified Young-Laplace equation, which is most of the time referred to as the Washburn equation (1921).

A typical capillary pressure curve for tight gas sands is shown in Figure 2.17 and the pore throat size distribution from the mercury injection data is shown in Figure 2.18. Figure 2.16 shows that the dominant pore throat sizes for these sands range between 0.1 and 1 μm.

One of the most important limitations is the fact that it measures the largest entrance towards a pore, but not the actual inner size of a pore (Giesche, 2006). Other disadvantages are that, the core cannot be used for other tests after injection of mercury because the mercury cannot be removed safely from the rock, and mercury vapour is toxic, so strict safety precautions must be followed when using mercury. In addition, the mercury injection curve does not yield data on capillary hysteresis (Tiab and Donaldson, 2015).

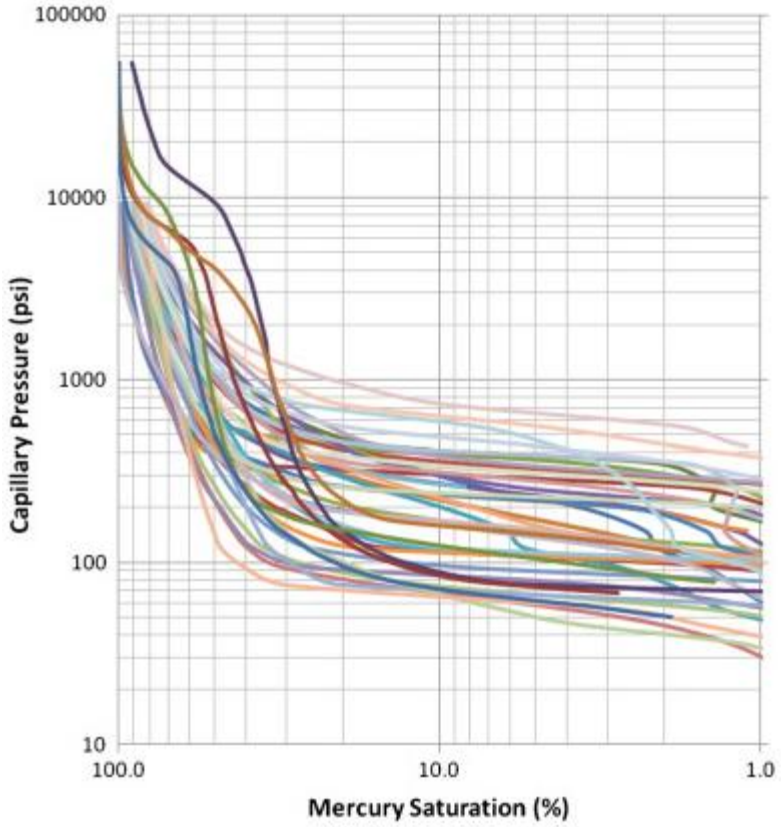

Figure 2.17: Mercury saturation versus injection pressure for tight gas sands (Rezaee et al, 2012).

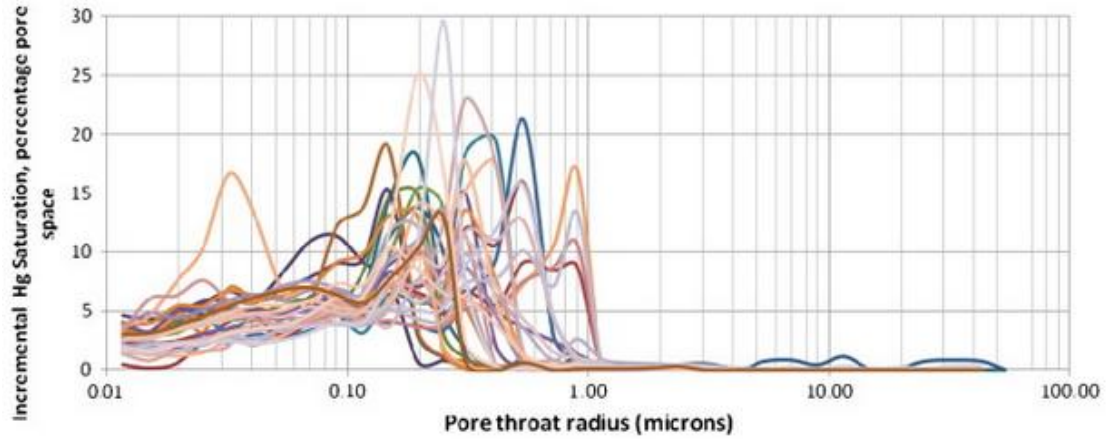

Figure 2.18: Pore throat size distribution (Rezaee et al, 2012).

2.5.4 Wettability

Wettability is the tendency of one fluid to adhere to a solid surface in the presence of other immiscible fluids (Anderson, 1986b and Buckley *et al,* 1997). It may also be defined as the work necessary to separate a wetting fluid from a solid. At the pore scale, it is determined by the local contact angle. Complete analysis of wettability provides a good insight into the multiphase flow in oil reservoirs (Maghzi *et al,* 2012).

The wettability of a porous medium such as a reservoir rock is dynamic and history-dependent. Most reservoir rocks are neither completely water-wet nor oil-wet. It has been observed from measurements of oil/water contact angle that most mineral surfaces, which were initially water-wet, become oil-wet after prolonged contact with crude oil (Wilhite, 1986; Dullien, 1992; Craig, 1993; Blunt, 1997), through the deposition of surface active components in the crude called asphaltenes (Buckley and Liu, 1998; Hui and Blunt, 2000). Craig (1993) showed that if crude oil and brine are left to age on a solid surface, the contact angle changes typically from a value much less than 90^o (water-wet) to about 150^o (oil-wet) after aging for 100 – 1000 hours.

Oil and gas recovery, geological CO_2 storage (Chalbaud et al, 2010; Plug and Bruining, 2007; Chalbaud et al, 2009; Chiquet et al, 2007; Hildenbrand et al, 2004) and methane production from hydrate bearing sediments (Seo et al, 2002; Sun et al, 2004; Watanabe et al, 2005) are influenced by macroscopic parameters, such as capillary pressure and relative permeability, which are controlled by wettability.

Many authors have documented that successful CO_2 EOR and CO_2 storage processes largely depend on the wettability of the CO_2-crude oil-reservoir brine-reservoir rock

system (Andreas and Nadja, 2011; Yang *et al,* 2008b; Emberly *et al,* 2004; Buckley and Liu, 1998). Wettability, on the other hand, depends on pore geometry, fluid composition and properties, and the interfacial tension among the reservoir brine, CO_2 and the reservoir minerals (Yang *et al,* 2008a; Chalbaud *et al,* 2006; Juanes *et al, 2006)* and has strong effect on capillary pressure (Yang *et al,* 2008a; Chalbaud *et al,* 2006, 2010; Juanes *et al,* 2006), relative permeability (Plug and Bruining, 2007; Juanes *et al,* 2006; Gaus, 2010), and phase distribution (Wu and Firoozabadi, 2010; Agbalaka *et al,* 2008; Drummond and Israelachvili, 2002; Van Oss and Giese, 1995; Morrow, 1990). The exact impact of each of these factors on pore wettability is yet to be fully understood because, to date, no relevant data on a single pore is available. Also, there are no data available regarding the change in pore wettability in non-flat surfaces caused by corrosive CO_2 (Li *et al,* 2005; Hildenbrand *et al,* 2002). It is therefore very difficult to accurately predict the displacement behaviour of CO_2 for geological storage and EOR. In order to facilitate the design of the CO_2 EOR and CO_2 storage processes it is pertinent to determine wettability in true geometry of the pore space and to determine the precise impact of the parameters on each pore.

2.5.4.1 Contact angle

Contact angle is the angle that the interface between two fluid phases makes with the solid surface. It is determined by the interactions across the three interfaces namely, solid/liquid, solid/gas and liquid/gas, and it is usually measured through the denser phase (Yuan and Lee, 2013; Miller and Neogi, 2008). Theoretically, it is expected to be characteristic for a given solid-liquid system in a specific environment (Snoeijer and Andreotti, 2008).

Contact angle is influenced by the surface energy of the solid surface, which varies greatly for different materials. The type and the intensity of the intermolecular forces acting inside the solid determine the surface energy of the solid surface. As a general rule, liquids with surface tension lower than the surface energy of the solid wet the substrate. Most metals and surfaces similar to silica have high surface energies and are therefore wetted by most liquids (Israelachvili, 1991), while polymers and waxes have low surface energies and their degree of wetting primarily depends on the surface tension of the liquid (Brandrup *et al.*, 1999).

The contact angle is usually measured on flat surfaces and for such surfaces it is measured from a drop of a suitable liquid resting on the surface. The droplet will completely spread out on the solid surface if the liquid is strongly attracted to the surface, and the contact angle will be close to zero degree. For example, a solid surface on which water droplet spreads easily is said to be hydrophilic. Less strongly hydrophilic solids will have a contact angle up to 90^o. Hydrophobic surfaces will have the contact angle greater than 90^o. When the contact angle is greater than 150^o the surface is said to be super hydrophobic. On such surfaces the water droplet simply rests on the surface without any significant wetting. Therefore, the contact angle directly provides information on the interaction energy between the surface and the liquid. In practice, external forces such as gravity deform the droplet; consequently, the contact angle is determined by a combination of surface tension and external forces (usually gravity). In capillaries the effect of gravity is negligible; as such contact angle is determined by surface tension.

A schematic of wettability levels on surfaces measured by contact angle is shown in Figure 2.19

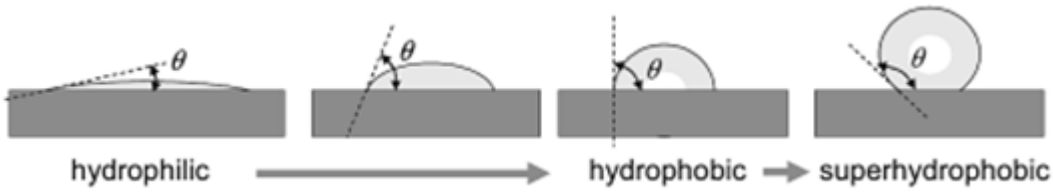

Figure 2.19: Schematic of different levels of wettability of surfaces (Förch *et al.*, 2009)

Thermodynamically, contact angle is related to the interfacial tension of the three interfaces namely, solid-gas (nonwetting) interfacial tension, γ_{SG}; solid-liquid (wetting) interfacial tension, $\gamma_{SL;}$ and liquid (wetting)-gas (nonwetting) interfacial tension, γ_{LG} by Young's equation (Young, 1805; Chow, 1998):

$$\gamma_{SG} = \gamma_{SL} + \gamma_{LG} \cos\theta \qquad (2.44)$$

where θ is the equilibrium contact angle. The interfaces are shown in Figure 2.20. The interface where solid, liquid, and vapour co-exist is referred to as the "three-phase contact line". The contact angle can also be related to the work of adhesion by the Young-Dupré equation:

$$\gamma(1 + \cos\theta) = \Delta W_{SLV} \qquad (2.45)$$

where ΔW_{SLV} is the solid-liquid adhesion energy per unit area when in the medium V.

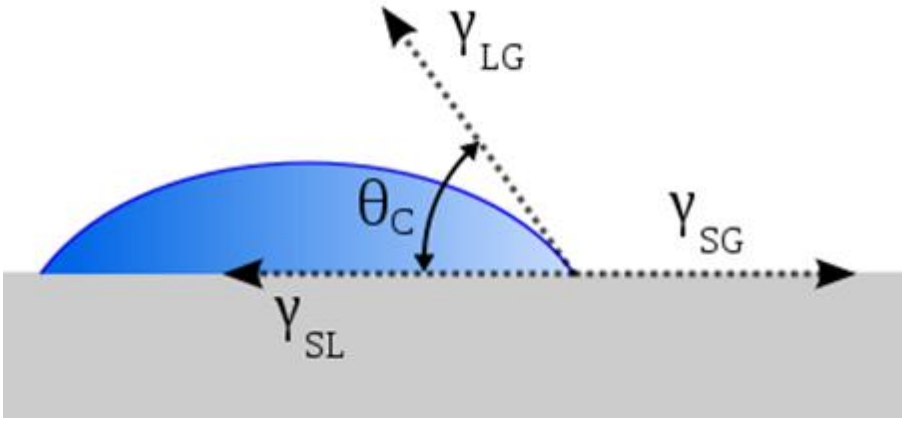

Figure 2.20: Schematic of a liquid drop showing the quantities in Young's equation

Young's equation assumes a perfectly flat surface but in many cases surface roughness and impurities cause a deviation in the equilibrium contact angle from the contact angle predicted by Young's equation. A drop will assume a wide spectrum of contact angles between the highest (advancing) contact angle, θ_A, and the lowest (receding) contact angle, θ_B, even in a perfectly smooth surface.

2.5.5 Pore Structure

The geometric and topological properties of the pores influence fluid transport on a microscopic scale (Silina *et al,* 2006; Sehbi *et al,* 2001; Wardlaw, 1980). Topology of the rock structure is concerned with the way the pores are connected together (pore connectivity). A reservoir rock contains pores connected by pore throats. As shown in Young-Laplace equation (Equation 2.1), the radius of the largest connected pore throats in the rock is a critical factor in estimating the displacement pressure of a given water-rock system. From the equation, the smaller the radius of the connected pore throats in a rock the grater the displacement pressure. The sizes and

arrangements of these pores and throats also strongly affect a wide range of reservoir properties such as permeability and formation factor, which represent the net effect of fluid interactions involving millions of pores and throats. The final geometry (sizes and shapes) of the pore, grain orientation and packing, and the degree of cementation and clay filling of pore spaces are controlled by diagenesis.

Heath *et al* (2012) observed that pore size and shape affect the magnitudes of capillary breakthrough pressures and permeability. Wardlaw (1980) showed experimentally how pore geometry may influence multiphase flow and recovery efficiency during immiscible displacements in pore casts. He reported that the non-wetting phase trapping caused by capillary forces is strongly dependent on the characteristics of the pore system of a reservoir rock, and that these characteristics can be identified quickly by visual observation of thin sections and pore casts. The characteristics of the pore system identified by Wardlaw are discussed in the following sections.

2.5.5.1 Pore system characteristics

As observed by Wardlaw (1980), the most important characteristics of the pore systems influencing fluid displacement are pore-throat size ratio, throat-to-pore coordination number, in addition to the type and degree of non-random heterogeneity and properties of pore surface.

2.5.5.1.1 Pore-throat size ratio

Pore-throat size ratio is defined as the ratio of the size of a pore body to the size of the pore throat connected to it. Dehghan *et al* (2009) showed that for all values of

coordination numbers, higher oil recovery is achieved at higher pore-throat size ratio. This is expected because higher pore-throat size ratio will lead to increased permeability. Wardlaw (1980) explained that decreasing microscopic displacement efficiency observed with decreasing porosity is due to increasing pore-to-throat size contrast. Increasing pore-to-throat size contrast accompanies decreasing porosity.

Chatzis *et al* (1983, 1984) in their pore network studies gave experimental evidence that increases in the pore aspect ratio (pore body size/pore throat size ratio) produced smaller blob sizes. Similarly, the theoretical studies of Mohanty *et al* (1987) and the experimental studies of Wardlaw and Yu (1988) found that the aspect ratio influence the formation of blobs. The blob sizes are found to have significant effects on the transport properties of the nonwetting phase. For high aspect ratios, the primary control on the trapping of blobs in the pore spaces was provided by the pore throat size. (More on blob sizes are discussed in section 2.5.5.2).

2.5.5.1.2 Coordination number or pore connectivity

The coordination number of a pore system is defined as the average number of throats which connect with each pore. It determines the connectivity of the network of throats and pores, as well as, the number of different pathways or access routes between pores. Researches have suggested that at low porosity, the effective coordination number of the pore space is low, giving rise to high residual non-wetting phase saturations and, therefore, lower microscopic displacement efficiency (Sehbi *et al*, 2001). Dehghan *et al* (2009) showed that final recovery efficiency is strongly affected by the coordination number of the pores, and increasing the coordination number value improves the final oil recovery.

The effect of pore coordination number on blob size distributions has been addressed by researchers. Chatzis *et al* (1983) observed that blob size was a relatively insensitive, inverse proportion of pore coordination number in experimental, etched-glass pore network studies. Larson *et al* (1981) had earlier established that the pore coordination and dimensionality used in percolation model did not significantly affect blob size.

2.5.5.1.3 Random and non-random heterogeneity

The types and degrees of heterogeneity in the arrangement of pores also affect the fluid displacement. Pores and throats of differing sizes may be distributed randomly in a porous medium (randomly heterogeneous) or they may be distributed non-randomly. In the non-random distribution, the larger pores may be clustered together in a section of the porous medium while the smaller pores may be clustered together in another section. Experimental investigations by Wardlaw and McKellar (1981) in glass micromodels showed that the amount of residual mercury following withdrawal is sensitive to the presence of certain types of non-random heterogeneity.

2.5.5.1.4 Properties of pore surfaces

Properties of the pore surfaces include composition and degree of roughness. The surfaces of pores in reservoir rocks may be smooth as commonly found in crystal surfaces of some dolomites or rough as in the commonly pitted or clay coated surfaces of many sandstones. Surface roughness affects advancing and receding contact angles.

2.5.6 Surface tension

Surface tension is caused by the imbalance of molecular force at the interface between two immiscible fluids. When two immiscible fluids are in contact, molecular attractions between similar molecules in each fluid are greater than the attractions between the different molecules of the two fluids. The boundary between the fluids has a region having properties different from those in the fluids farther from the boundary. Molecular attraction is greater on the side of the more dense fluid, and the surface of contact is drawn into a curvature which is convex toward the more dense fluid. This intermolecular force acting on the contact surface is called surface tension in the case of a gas in contact with a liquid or interfacial tension in the case of two liquids. The result of this force is to produce a pressure difference, called capillary pressure, across the contact surface. When an immiscible fluid is completely immersed in another fluid, it assumes a spherical shape of minimum surface area.

Figure 2.19 is an illustration of the intermolecular forces acting in a pure liquid. While each molecule in the bulk of the liquid is pulled equally in every direction by neighbouring liquid molecules, resulting in a net force of zero, the molecules exposed at the surface do not have neighbouring molecules in all directions to provide a balanced net force. They are rather pulled inward by the neighbouring molecules creating an internal pressure. Consequently, the liquid voluntarily contracts its surface area to maintain the lowest surface free energy. The surface tension forces acting on a droplet on a flat surface have been illustrated in Figure 2.21.

Figure 2.21: Unbalanced forces of liquid molecules at the surface causing surface tension (Yuan and Lee, 2013).

Interfacial tension can be defined as the work required per unit area to enlarge the interface between two immiscible fluids. Oil-water interfacial depends on the chemical composition of the oil, amount and type of surface-active agents, types and quantities of gas in solution, pH of the water, temperature, and pressure. Livingston (1938) observed that oil-water interfacial tension generally tends to decrease with increasing API gravity and decreasing viscosity. The effect of increasing temperature on oil-water interfacial tension is complex, but the general trend is for oil-water interfacial tension to decrease as temperature increases. Livingston (1938) reported that crude oil and formation water interfacial tension decreases between 0.1 and 0.2 mN/m/^{o}F. A decrease in interfacial tension of approximately 0.1 to 0.15 mN/m/^{o}F for crude oils between temperatures of 130 and 170 ^{o}F is documented by Hocott (1938). The effect of increasing pressure on oil-water interfacial tension is also complex, but in summary Schowalter (1979) concludes that the effect of pressure on crude oil-formation water interfacial appears small enough that it can be neglected.

Gas-water interfacial tension also varies with the amount of surface-active agents in the water, the amount of heavy hydrocarbons in solution in the gas, temperature, and pressure. At atmospheric pressure and temperature, methane gas-formation water interfacial tension is about 70 mN/m (Schowalter, 1979). Hough et al (1951) reported that gas-water interfacial tension decreases 5 to 10 mN/m/6.89-MPa pressure increase depending on the temperature and decreases with increasing temperature from 0.1 to 1.0 mN/m/^{o}F depending on the pressure. Estimates of methane-water interfacial tension, based on the effects of temperature and pressure from Hough et al (1951), and sufficiently accurate for exploration application to gas-water-rock displacement pressures, are available in nomographs. Excessive amounts of ethane, propane, and other heavy gases in the gas phase will decrease interfacial tension from that of the pure methane-water systems. Presently, a number of methods are available to measure surface tension.

2.5.6.1 Measurement of surface tension

Among the various ways to determine surface tension, Du Noüy ring method and Wilhelmy slide method are based on the separation of a solid object from the liquid surface, and Pendant drop method and Sessile drop or bubble method depend on the deformation of the spherical shape of a liquid drop .

2.5.6.1.1 Maximum Bubble Pressure Method (Bubble Pressure Method)

This is a useful method to measure dynamic surface tension of a system containing surfactants or other impurities. It depends on the deformation of the spherical shape of a liquid drop (Adamson and Gast, 1997).

The method involves the production of gas bubbles (e.g. air) at a constant rate from a bubble pressure tensiometer through a capillary of known radius immersed in a sample liquid. The gas bubbles within the liquids are compressed due to internal attractive forces of a liquid. The resulting pressure (bubble pressure) rises at a decreasing bubble radius (sita-process.com). The bubble pressure (P) increases continuously and the maximum value obtained is when the bubble has the completely hemispherical shape whose radius exactly corresponds to the radius of the capillary (krussUSA.com; sita-process.com).

A typical pressure profile from the experiment is as shown in Figure 2.22. At A bubble appears on the end of the capillary. As the bubble grows, its radius of curvature decreases as shown in B, while the pressure increases. C is the point of the maximum bubble pressure, Pmax. At this point the bubble has a complete hemispherical shape with a radius identical to the radius of the capillary denoted by Rcap.

The surface tension can be determined using the reduced form of the Young–Laplace equation (Eq.2.46) for spherical bubble shape within the liquid (krussUSA).

$$\gamma = \frac{\Delta P_{max} \times R_{cap}}{2} \qquad (2.46)$$

where, γ is the surface tension (N/m), ΔP_{max} is the maximum pressure drop (Pa), and R_{cap} is radius of the capillary (m).

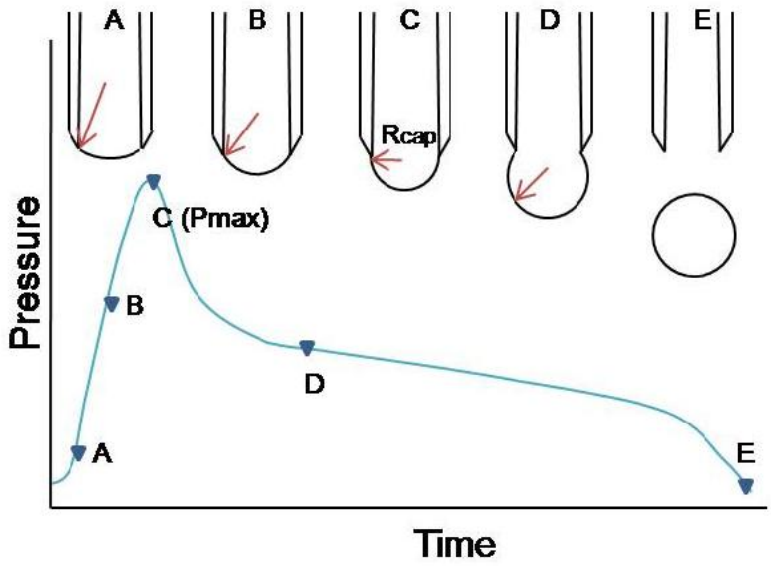

Figure 2.22: Change of pressure during bubble formation plotted as a function of time (krussUSA.com)

The pressure of the bubble decreases after the maximum pressure, and the radius increases as shown at D, until the bubble is detached from the end of the capillary (position E) and a new cycle begins. Section DE is not relevant to determine the surface tension (krussUSA).

Commercial tensiometers are available, that monitor the pressure needed to form a bubble, the pressure difference between inside and outside the bubble, as well as, the radius of the bubble. The surface tension of the sample is then calculated from these data.

Bubble pressure method does not require contact angle measurement and has high accuracy even though the measurement is done rapidly (Adamson and Gast, 1997; krussUSA).

This method is suitable for cases where a large amount of liquid sample is not required for measurement, such as in biological fluids like serum (Hubbard, 2002).

2.6 Summary

The analysis of literature on resistance to fluid displacement in porous medium reveals that it is very useful in processes such as oil recovery and geological storage of carbon dioxide. These processes occur in high permeability (low resistance) porous media such as conventional oil reservoirs and in low-permeability (high resistance) systems such as unconventional resources namely tight gas sandstones and shale gas.

It is of importance in trapping of fluids in oil and gas reservoirs for oil recovery, and in effectiveness of caprocks as seals for oil reservoirs and CO_2 storage. The storage safety is dependent on the caprock ability to prevent or seriously hinder CO_2 storage.

Resistance to fluid displacement is influenced by factors such as pore structure, fluid properties, fluid composition and wettability. These factors are interrelated and can be expressed by a simple equation such as the Young-Laplace equation.

Many researches have revealed the influence of the factors which affect resistance to displacement and conclude that the determination of the geometrical and transport properties of individual pores is therefore a key issue in view of practical applications. This is very necessary because the capillary forces which are known to control these processes act on the microscopic scale.

In order to understand better the impact of the factors affecting the resistance to fluid displacement this study proposes to carry out studies on single pores at different sizes.

2.7 References

Adamson, Arthur W.; Alice P. Gast (1997). Physical Chemistry of Surfaces (6th ed.). Wiley Interscience.

Agbalaka, C., A.Y. Dandekar, S.L. Patil, S. Khataniar, J.R. Hemsath, 2008. The effect of wettability on oil recovery: a review, in: Paper SPE 114496, SPE Asia Pacific Oil and Gas Conference and Exhibition, Perth, Australia, 20–22 October, 2008.

Al-Bazali, T. M., Zhang, J., Martin E. Chenevert, M. E., Sharma, M. M, 2009. Estimating the Reservoir Hydrocarbon Capacity through Measurement of the Minimum Capillary Entry Pressure of Shale Cap-Rocks. Paper SPE 121450 presented at the 2009 SPE Annual Technical Conference and Exhibition held in New Orleans, Louisiana, USA, 4–7 October 2009.

Al-Mansoori, S. K., Itsekiri, E, Iglauer, Pentland, C. A., Bijeljic, B., Blunt, M. J., 2010. Measurements of non-wetting phase trapping applied to carbon dioxide storage. Int'l J. of GHG Control 4(2010)283-288.

Almohsin, A., Bai, B., Imqam, A., Wei, M., Kang, W., Delshad, M., Sepehrnoori, K., 2014. Transport of Nanogel through Porous Media and its Resistance to Water. Paper SPE 169078 presented at the SPE Improved Oil Recovery Symposium held in Tulsa, Oklahoma, USA, 12-16 April.

Al-Raoush, Riyadh I., Clinton S. Willson., 2005. A pore-scale investigation of a multiphase porous media system. Journal of Contaminant Hydrology 77 (2005) 67–89.

Amaefule, J.O., Altumbay, M., Tiab, D., Kersey, D.G., Keelan, D.K., 1993. Enhanced reservoir description: using core and log data to identify hydraulic (Flow) units and predict permeability in uncored intervals/wells. Paper SPE 26436. SPE Annual Technical Conference and Exhibition Houston, TX, USA, October 3–5.

Amyx, J. W., Bass, D. M., Jr. and Whiting, R. L., 1960. Petroleum Reservoir Engineering. McGraw Hill Publishing Company, New York, NY.

Anderson, W. G., 1986b. Wettability Literature Survey – Part 2: Wettability Measurement. J. Pet. Technol. 1986,37,1246 - 1262.

Anderson, W. G., 1987a. Wettability Literature Survey – Part 4: The Effects of Wettability on Capillary Pressure. J. Pet. Technol. 1987, 39, 1283 – 1300

Andersson, Linnéa, Anthony C. Jones, Mark A. Knackstedt, and Lennart Bergstrom, 2011: Permeability, pore connectivity and critical pore throat control of expandable polymeric sphere templated macroporous alumina. Acta Materialia 59 (2011) 1239–1248.

Andreas Busch, Nadja Muller, 2011. Determining CO_2/brine relative permeability and capillary threshold pressures for reservoir rocks and caprocks: Recommendations for development of standard laboratory protocols, Energy Procedia 4 (2011) 6053 – 6060.

API Code 27, 1952. Recommended Practice for Determining Permeability of Porous Media, American Petroleum Institute, Division of Production, September, 1952.

Argüelles-Vivas, F.J. and Tayfun Babadagli, 2014: Drainage type oil and heavy-oil displacement in circular capillary tubes: Two- and three-phase flow characteristics and residual oil saturation development in the form of film at different temperatures. Journal of Petroleum Science and Engineering 118 (2014) 61–73.

Bachu, S, 2003. Sequestration of CO_2 in geological media in response to climate change: Capacity of deep saline aquifers to sequester CO_2 in solution, Energy Convers and Manage, 44(2003)20, 3151-3175

Bachu, S., 2000. Sequestration of CO_2 in geological media: Criteria and approach for site selection in response to climate change. Energy Convers Manage., 2000, 41(9), 953-970.

Bachu, S., 2002. Sequestration of CO_2 in geological media in response to climate change: Road map for site selection using the transform of the geological space into the CO_2 phase space. Energy Convers Manage, 2002, 43(1), 87-102.

Bachu, S., Gunter, W. D., Perkins, E. H., 1994. Aquifer Disposal of CO_2: hydrodynamic and mineral trapping. Energy Conversion Management 35(4), 269-279.

Bennion, B. and Bachu, S., 2006a. The Impact of Interfacial Tension and Pore-Size Distribution/Capillary Pressure Character on CO_2 Relative Permeability at Reservoir Conditions in CO_2 – Brine Systems. Paper SPE 99325 presented at the SPE/DOE Symposium on Improved Oil Recovery held in Tulsa, Oklahoma, U. S. A., 22 – 26 April.

Beard, D. C. and Weyl, P. K.: Influence of texture on porosity and permeability of unconsolidated sand. AAPG Bulletin (1973), 57, 349.

Bennion, D. B. and S. Bachu, 2006b. Dependence on Temperature, Pressure, and Salinity of IFT and Relative Permeability Displacement Characteristics of CO_2 Injected in Deep Saline Aquifers. Paper SPE 102138 presented at the SPE Annual Technical Conference and Exhibition held in San Antonio, Texas, U. S. A., 24 – 27 September.

Bennion, D. Brant and Bachu, Stefan, 2008. Drainage and Imbibition Relative Permeability Relationships for Supercitical CO_2/Brine and H_2S/Brine Systems in Intergranular Sandstone, Carbonate, Shale, and Anhydrite Rocks. SPE Reservoir Evaluation and Engineering, June, pp 487-496.

Berg, Robert R., 1975. Capillary Pressures in Stratigraphic Traps. The American Association of Petroleum Geologists Bulletin, v.59, No. 6 (June 1975), p. 939-956.

Bergslien, E. and Fountain, J., 2006. The effect of changes in surface wettability on two-phase saturated flow in horizontal replicas of single natural fractures. J. Contaminant Hydrology 88 (2006) 153-180.

Blunt, Martin J., 1997. Pore Level Modelling of the Effects of Wettability, SPE Journal, Vol. 2, December, 494-510.

Boschan A., I. Ippolito, R. Chertcoff, J. P. Hulin, H. Auradou, 2011. Characterization of fracture aperture field heterogeneity by electrical resistance measurement. J. Contaminant Hydrology 123 (2011) 65–74.

Brandrup, J., Immergut, E. H., Grulke, E. A., Abe, A. and Bloch, D. R., 1999. Polymer Handbook, John Wiley and Sons, Inc., New York.

Bretherton, F.P., 1961. The motion of long bubble in tubes. J. Fluid Mech.10, 166–188.

Bromhal, G. S., W. N. Sams, S. Jikich, T. Ertekin and D. H. Smith, 2005. Simulation of CO_2 sequestration in coal beds: The effects of sorption isotherms, Chem. Geol., 2005, 217(3-4), 201-211.

Bruant, R. G., Jr., M. A. Celia, A. J. Guswa, C. A. Peters, 2002. Safe Storage of CO_2 in Deep Saline Aquifers. Environ. Sci. Technol., 36 (11), 240A-245A.

Bryant, S., Cade, C. and Mellor, D., 1993. Permeability prediction from geologic models, AAPG Bulletin, 1993, 77, 1338-1350.

Buckley, J. S., Liu, Y., 1998. "Some Mechanisms of Crude Oil/Brine/Solid Interactions", J. Pet. Sci. Eng. 1998, 20, 155 – 160.

Buckley, J. S., Liu, Y., Xie, X., Morrow, N.R., 1997. Asphaltenes and crude oil wetting – the effect of oil composition. SPEJ, 2, 107 – 122.

Carman, P., 1937. Fluid flow through a granular bed. Trans. Inst. Chemical Eng., 15, 150-167.

Celia, Michael A., Paul C. Reeves and Lin A. Ferrand., 1995. Recent advances in pore scale models for multiphase flow in porous media. Reviews of Geophysics, Supplement, Pages 1049-1057, July 1995.

Chalbaud C, Robin M, Lombard J. M., Bertin J, Egermann P., 2010. Brine/CO_2 interfacial properties and effects on CO_2 storage in deep saline aquifers. Oil Gas Sci Technol – Rev IFP 2010; 65:541–55. http://dx.doi.org/10.2516/ogst/2009061.

Chalbaud C, Robin M, Lombard JM, Martin F, Egermann P, Bertin J., 2009. Interfacial tension measurements and wettability evaluation for geological CO_2 storage. Adv Water Resour 2009; 32:98109. http://dx.doi.org/10.1016/j.advwatres.2008.10.012.

Chalbaud, C., Robin, M., Egerman, P., 2006. Interfacial Tension Data and Correlations of Brine/CO_2 Systems under Reservoir Conditions. Paper SPE 102918 presented at SPE Annual Technical Conference and Exhibition, San Antonio, TX, September 24-27.

Chatzis, I., Kuntamukkula, M.S. and Morrow, N.R., 1984. Blob-size distribution as a function of capillary number in sandstones. Soc. Pet. Eng. AIME (Am. Inst. Min. Metall. Eng.) Meet, Dallas, TX, SPE 13213.

Chatzis, I., Morrow, N. R., and Lim, H. T., 1983. Magnitude and Detailed Structure of Residual Oil Saturation. Soc. Pet. Eng. J. 23, 311-326 (April 1983).

Chen, J. D., 1986. Measuring the film thickness surrounding a bubble inside a capillary. J. Colloid Interface Sci. 109, 34–39.

Chen, Jing-Den and Joel Koplik, 1985. Immiscible Fluid Displacement in Small Networks. Journal of Colloid and Interface Science, Vol. 108, No. 2, December 1985.

Chiquet, P., Broseta, D., Thibeau, S., 2007a. Wettability Alteration of Caprock Minerals by Carbon Dioxide. Geofluids 2007, 7, 112 – 122.

Chiquet, Pierre, Jean – Luc Daridon, Daniel Broseta and Sylvain Thibeau, 2007b. CO_2/water interfacial tensions under pressure and temperature conditions of CO_2 geological storage. Energy Conversion and Management 48 (2007) 736 – 744.

Chow, T. S., 1998. Wetting of rough surfaces. J. Phys.: Condens. Matter 10 (27), 445.

Christoffersen, K. R., Whitson, C. H., 1995. Gas/Oil Capillary Pressure of Chalk at Elevated Pressures. SPE FE 1995; 10(6): 153-9.

Costa, A., 2006. Permeability-porosity relationship: A re-examination of the Kozeny-Carman equation based on a fractal pore-space geometry assumption, Geophys. Res. Lett., 33, L02318, doi: 10.1029/2005GL025134.

Cox, B. G., 1962. On driving a viscous fluid out of a tube. J. Fluid Mech. 14, 81–96.

Cox, P. M., R.A. Betts, C. D. Jones, S. A. Spall, and I. J. Totterdell, 2000. Acceleration of global warming due to carbon-cycle feedbacks in a coupled climate model, Nature, Vol 408(6809) 184-187.

Craig, F. R., 1993. The Reservoir Engineering Aspects of Waterflooding, Society of Petroleum Engineers, New York.

Dehghan, R. Kharrat, M. H. Ghazanfari, S. A. Farzaneh, 2009: Studying the Effects of Pore Geometry, Wettability and Co-Solvent Types on the Efficiency of Solvent Flooding to Heavy Oil in Five-Spot Models. Paper SPE 123315 presented at 2009 SPE Asia Pacific Oil and Gas Conference and Exhibition held in Jakarta, Indonesia, 4-6 August, 2009.

Dong, M., and Chatzis, I., 2004. An experimental investigation of retention of liquids in corners of a square capillary. J. Colloid Interface Sci. 273, 306-312.

Doughty, C., 2007. Modelling geologic storage of carbon dioxide: comparison of non-hysteretic and hysteretic characteristic curves. Energy Conv Manage 2007; (6): 1768-81.

Drummond, C, Israelachvili J., 2002. Surface forces and wettability, J. Pet. Sc and Eng 33 (2002) 123-133.

Dullien, F. A. L. (1992). Porous Media: Fluid Transport and Pore Structure, 2nd ed. Academic Press, San Diego, CA.

Emberly, S., Hutcheon, I., Shevalier, M., Durocher, K., Gunter, W. D., Perkins, E. H., 2004."Geochemical Monitoring of Fluid – Rock Interaction and CO_2 Storage at the Weyburn CO_2 – Injection Enhanced Oil Recovery Site, Saskatchewan, Canada", Energy 2004, 29, 1393 – 1401.

Endo Y., Ngan, C. L. Y., Nandiyanto, A. S. B., Iskandar, F., Okuyama, K., 2009. Analysis of fluid permeation through a particle-packed layer using an electric resistance network as analogy. Powder Technology 191 (2009) 39-46.

Endo Yoshiyuki, Da-Ren Chen, David Y. H. Pui, 2001. Air and water permeation resistance across dust cakes on filters – effects of particle polydispersity and shape factor. Powder Technology 118 (2001) 24-31.

Ennis-King, J., Paterson, L., 2005. Role of Convective Mixing in the Long-term storage of Carbon dioxide in deep saline formations. SPE Journal 10(3), 349-356.

Fairbrother, F., Stubbs, J., 1935. Studies in electro-endosmosis. Part VI. The 'Bubble Tube' method of measurement. J. Chem. Soc. 1, 527–529.

Fenwick, Darry H. and Martin J. Blunt, 1998. Three-dimensional modelling of three phase imbibition and drainage. Advances in Water Resources 21, No. 2, pp. 121-143, 1998.

Fletcher, A. and Davis, J., 2010. How EOR Can Be Transformed by Nanotechnology. Paper SPE 129531 presented at the SPE Production and Operations Symposium, 23-26 March, Oklahoma City, Oklahoma, USA.

Gauglitz, P. A., St. Laurent, C. M., Radke, C. J., 1987. An Experimental Investigation of Gas-Bubble Breakup in Constricted Square Capillaries, JPT, September 1987, 1137 – 1146.

Gaus I., 2010. Role and impact of CO_2–rock interactions during CO_2 storage in sedimentary rocks. Int J Greenhouse Gas Control 2010; 4:73–89. http://dx.doi.org/10.1016/j.ijggc.2009.09.015.

Ghedan, S., 2009. Global Laboratory Experience of CO_2-EOR Flooding. Paper SPE 125581 presented at the 2009 SPE/EAGE Reservoir Characterization and Simulation Conference held in Abu Dhabi, U.A.E, 19 – 21 October 2009.

Giavedoni, M. D., and Saita, F. A., 1997. The axisymmetric and plane cases of a gas phase steadily displacing a Newtonian liquid – a simultaneous solution of the governing equations. Phys. Fluids 9 (8), 2420-2428.

Giesche, H., 2006. Mercury Porosimetry: a General (Practical) Overview. Part. Part. Syst. Charact. 23 (2006) 1-11.

Gluyas, J., Swarbick, R., 2004. Petroleum Geoscience. Blackwell Publishing. ISBN 978-0-632-03767-4.

Gunter, W. D.; Perkins, E. H.; Hutcheon, I., 2000. Appl. Geochem. 2000, 15, 1085-1095.

Gutenev, P.I., A.M. Pyatnitskii, N.V. Klimova, 2003. Liquid entrainment from the meniscus of a liquid wedge by a moving horizontal plate, Colloid Journal 65 (2003) 301–304.

Hammecker, C., L. Barbiero, P. Boivin, J. L. Maeght and E. H. B. Diaw, 2004. A Geometrical Pore Model for Estimating the Microscopical Pore Geometry of Soil with Infiltration Measurements. Transport in Porous Media 54: 193–219, 2004.

Hammond, Paul S. and Evren Unsal, 2009. Spontaneous and Forced Imbibition of Aqueous Wettability Altering Surfactant Solution into an Initially Oil-Wet Capillary. Langmuir 2009, 25(21), 12591–12603.

Hassanizadeh, S. M., Gray, W. G., 1993. Thermodynamic Basis of Capillary Pressure in Porous Media. Water Resour Res 1993; 29(10): 3389-405.

Heath, Jason E., Thomas A. Dewers, Brian J.O.L McPherson, Martin B. Nemer, Paul G. Kotula, 2012. Pore-lining phases and capillary breakthrough pressure of mudstone caprocks: Sealing efficiency of geologic CO2 storage sites. International Journal of Greenhouse Gas Control 11 (2012) 204-220.

Herzog H, Eliasson B, Karstad O., 2000. Capturing greenhouse gases. Scientific America, 2000, p.72– 79.

Hildenbrand A., Schlomer S., Kroos B. M., and Littke R., 2004. Gas breakthrough experiments on pelitic rocks: comparative study with N_2, CO_2 and CH_4. Geofluids (2004) 4, 61 – 80.

Hildenbrand A., Schlomer, S., Kroos, B. M., 2002. Gas breakthrough experiments on fine-grained sedimentary rocks. Geofluids (2002) 2, 3 – 23.

Hitchon, G., W. D. Gunter, T. Gentzis, and R. T. Bailey, 1999. Sedimentary basins and greenhouse houses: A serendipitous association, Energy Convers Manage, 1999, 40(8), 825-843.

Hite, R. J., Avasthi, S. M. and Bondor, P. L., 2005. Planning Successful EOR Projects. JPT March, 28-29.

Holloway, S., van der Straaten, R., 1995. Energy Convers Mgmt. 1995, 36, 519-522.

Hocott, C. R., 1938. Interfacial tension between water and oil under reservoir conditions. AIME Petroleum Trans, v. 32, 184-190.

Horseman, S. T., Harrington, J. F. and Sellin, P., 1999. Gas migration in clay barriers. Engineering Geology, 54 (1999) 139-149.

Hough, E. W., Rzasa M. J., Wood, B. B., 1951. Interfacial tensions at reservoir pressures and temperatures; apparatus and the water-methane system. Petroleum Trans, AIME, vol. 192, 57- 60.

Hubbard, Arthur T. (2002). Encyclopaedia of Surface and Colloid Science (Vol. 1). CRC press, pp. 814–815.

Hui, M. and Blunt, M. J., 2000. Pore-scale Modelling of Three-Phase Flow and the Effects of Wettability. Paper SPE 59309 presented at the 2000 SPE/DOE Improved Oil Recovery Symposium held in Tulsa, Oklahoma, 3-5 April.

International Energy Agency, 2004. "Prospects for CO_2 Capture and Storage", IEA/OECD, Paris, France, 249 p.

Israelachvili, J., 1991. Intermolecular and Surface Forces. Academic Press, San Diego.

Jennings, J. W., McGregor, D. S., Morse, R. A., 1988. Simultaneous Determination of Capillary Pressure and Relative Permeability by Automatic History Matching. SPE FE 1988; 3(3): 322-8.

Juanes, R., Spiteri, E. J., Orr, F. M. Jr., Blunt, M. J., 2006. Impact of Relative Permeability Hysteresis on Geological CO_2 Storage. Water Resour. Res. 2006, 42, W12418, doi: 10.1029/2005WR004806.

Katz, A. J. and Thompson, A. H., 1986. Prediction of rock electrical conductivity from mercury injection measurements. Journal of Geophysical Research (1986), 92, 599.

Katz, A. J. and Thompson, A. H., 1986. Quantitative prediction of permeability in porous rock. Physical Review B (34) 8179-8181.

Katz, A. J. and Thompson, A. H., 1987. Prediction of rock electrical conductivity from mercury injection measurements. Journal of Geophysical Research (1987), 92, 599.

Katz, D. L. and Ibrahim, M. A., 1971. Threshold displacement pressure – considerations for caprocks of abnormal pressure reservoirs. Paper SPE 3222 presented at the Drilling and Rock Mechanics Conference, 5-6 January, Austin, Texas.

Keller, A., Roberts, P.V., Blunt, M. J., 1999. Effect of fracture aperture variations on the dispersion of contaminants. Water Resources Research Vol 35(1), 55–63.

Kokal, Sunil and Abdulaziz Al-Kaabi, 2010. Enhanced oil recovery: challenges and opportunities. World Petroleum Council Official Publication on Global Energy Solutions.

Kolodzie, Stanley Jr, 1980. Analysis of Pore Throat Size and Use of the Waxman-Smits Equation to Determine OOIP in Spindle Field, Colorado. Paper SPE 9382 presented at the 55th Annual Fall Technical Conference and Exhibition of the Society of Petroleum Engineers of AIME, held in Dallas, Texas, September 21-24, 1980.

Kovscek A. R. and M. D. Cakici, 2005. Geologic Storage of Carbon dioxide and Enhanced Oil Recovery. II. Cooptimisation of Storage and Recovery. Energy Conversion and Management 46(2005) 1941-1956.

Kovscek A. R., and Y. Wang, 2005. Geologic Storage of Carbon dioxide and Enhanced Oil Recovery. I. Uncertainty quantification employing a streamline based proxy for reservoir flow simulation, Energy Convers and Manage, 46(2005) 1920-1940.

Kozeny, J., 1927. Uber kapillare Leitung der Wasser in Boden, Sitzungsber. Akad. Wiss. Wien, 136, 271-306 (In: Scholwater, 1979).

Krooss, B. M., Leythaeuser, D., Schaefer, R. G. (1992). The quantification of diffusive hydrocarbon losses through cap rocks of natural gas reservoirs—a re-evaluation. AAPG Bulletin, 76, 403–406.

KrussUSA.com @ https://www.kruss.de/services/education-theory/glossary/bubble-pressure-tensiometer/

Kumar, A., Noh M., Pope, G. A., Sepehrnoori, K., Bryant, S., and Lake, L. W., 2004. Reservoir simulation of CO_2 storage in deep saline aquifers. Paper SPE 89343 presented at the SPE/DOE 14th Symposium on Improved Oil Recovery, Tulsa, OK, U. S. A., April 17 – 21, 2004.

Kumar, A., R. Ozah, M. Noh, G. A. Pope, S. Bryant, K. Sepehrnoori, and L. W. Lake, 2005. Reservoir Simulation of CO_2 Storage in Deep Saline Aquifers. SPEJ, September, 336-348.

Lackner, K. S., 2003. A guide to CO_2 sequestration. Science, 2003 300(5626) 1677-1678.

Larson, R.G., Davis, H.T. and Scriven, L.E., 1981. Displacement of residual nonwetting fluid from porous media. Chem. Eng. Sci., 36: 75-85.

Lenormand, R. and Zarcone, C., 1984. Role of roughness and edges during imbibition in square capillaries, Paper SPE 13264, Proceedings of the 1984 SPE Annual Technical Conference and Exhibition, Houston, TX, September.

Lenormand, R., C. Zarcone, and A. Sarr, 1983. Mechanisms of the displacement of one fluid by another in a network of capillary ducts, J. Fluid Mech., 135,337-353, 1983.

Li X, Fan X, Askounis A, Wu K, Sefiane K, Koutsos V., 2013. An Experimental Study on Dynamic Pore Wettability. Chem Eng Sci. 2013; 104:988-97.

Li X, Fan X, Brandani S., 2014. Difference in pore contact angle and the contact angle measured on a flat surface and in an open space. Chem Eng Sci. 2014; 117:137-45.

Li Yu (Y. Li) and Norman Claude Wardlaw, 1986. The Influence of Wettability and Critical Pore-Throat Size Ratio on Snap-off. Journal of Colloid and Interface Science, Vol. 109, No. 2, February 1986, pp. 461-472.

Li, S., Dong, M., Li, Z., Huang, S., Qing H. and Nickel, E., 2005. Gas breakthrough pressure for hydrocarbon reservoir seal rocks: implications for the security of long-term CO_2 storage in the Weyburn field. Geofluids (2005) 5, 326-334.

Li, Zhaowen, Dong, Mingzhe, Li, Shuliang, Huang, Sam, 2006. CO_2 Sequestration in Depleted Oil and Gas Reservoirs – Caprock Characterization and Storage Capacity. Energy Convers Manage 47 (2006) 1372 – 1382.

Lin, C.L., J.D. Miller, 2000. Network analysis of filter cake pore structure by high resolution X-ray microtomography. Chemical Engineering Journal 77 (2000) 79–86.

Lin, H., Fujii T., Takisawa, R., Takahashi, T., and Hashida, T., 2008. Experimental Evaluation of Interactions in Supercritical CO_2/water/rock minerals system under

geologic CO_2 sequestration conditions. J. Mater Sci (2008) 43(7): 2307-2315. DOI 10.1007/s10853-007-2029-4.

Lindeberg, E., Wessel-Berg, D., 1997. Vertical Convection in an Aquifer Column under a Gas Cap of CO_2. Energy Conversion Management 38 (1), 5229-5234.

Liu, Y. Z., Bai, B. J., Wang, Y. F., 2010. Applied Technologies and Prospects of Conformance Control Treatments in China. Oil Gas Sci Technol 2010: 65:1.

Livingston, H. K., 1938. Surface and interfacial tension of oil-water systems in Texas oil sands. AIME Tech. Paper 1001.

Lucas Y., Mikhail P., Buès M., 2006. Prolongation of two phases in the model of fluid displacement through a capillary. C. R. Mecanique 334 (2006) 196–204.

Maghzi, Ali, Saber Mohammadi, Mohammad Hossein Ghazanfari, Riyaz Kharrat, Mohsen Masihi, 2012. Wettability alteration by silica nanoparticles during water flooding to heavy oils in five-spot systems: A pore-level investigation. Experimental Thermal and Fluid Science. Volume 40, July 2012, Pages 168–176.

Marshall, P., Horseman, S., and Gimmi, T., 2005. Characterization of gas transport properties of the Opalinus clay, a potential host rock formation for radioactive waste disposal. Oil and Gas Science and Technology – Rev. IFP, Vol. 60 (2005), No. 1, pp. 121-139. DOI: 10.2516/oust: 2005008.

Matsuki, K., Chida, Y., Sakaguchi, K., Glover, P. W. J., 2006. Size effect on aperture and permeability of a fracture as estimated in large synthetic fractures. International Journal of Rock Mechanics and Mining Sciences Vol. 43(5), 726–755.

Mayer, Alex S. and Cass T. Miller, 1992. The influence of porous medium characteristics and measurement scale on pore-scale distributions of residual nonaqueous-phase liquids. Journal of Contaminant Hydrology, 11 (1992) 189-213.

McCain, W. D. Jr., 1991. Soc Pet. Eng J. Reservoir Eng., 1991, 6, 266-272.

Méheust, Y., Schmittbuhl, J., 2000. Flow enhancement of a rough fracture. Geophysical Research Letters Vol. 27 (18), 2989–2992.

Mian. M. A., 1992. Petroleum Engineering Handbook for the Practicing Engineer Volume I, PennWell Publishing Company, Tulsa, Oklahoma, pp. 139-154.

Miller, C. A., and Neogi, P., 2008. Interfacial Phenomenon: Equilibrium and Dynamic Effects, Second Edition, Book Series: Surfactant Science Series, Vol. 139, pp. 61-107, CRC Press – Taylor and Francis Group, Boca Raton, Florida.

Mohanty, K.K., Davis, H.T. and Scriven, L., 1987. Physics of oil entrapment in water-wet rock. Soc. Pet. Eng. Reservoir Eng., 2: 113-128.

Mohanty, K. K. and Salter, S. J., 1982. Multiphase Flow in Porous Media: II. Pore-Level Modelling. Paper SPE 11018 presented at the 57th Annual Fall Technical Conference and Exhibition of the Society of Petroleum Engineers of AIME, held in New Orleans, LA, Sept 26-29, 1982.

Moore, T. F., and Slobod, R. L., 1955. Displacement of Oil by Water - Effect of Wettability, Rate, and Viscosity on Recovery. Paper 502-G, Presented at 30th Annual Fall Meeting, Petroleum Branch, AIME, New Orleans, La. (Oct. 2-5, 1955).

Moore, T. F., and Slobod, R. L., 1956. The effect of viscosity and capillarity on the displacement of oil by water. Producers Monthly (Oct. 1956) 20, 20-30.

Moritis G., 2006. CO_2 Injection Gains Momentum. Oil and Gas Journal, 2006, v.104, Issue 15, 37 – 41, April 17, 2006.

Moritis, G., 2010. CO_2, Miscible, Steam Dominate EOR Processes. Oil and Gas J., April 2010.

Morrow, N. R., 1990. Wettability and Its Effect on Oil Recovery. J. Pet. Technol. 1990, 42, 1476 – 1484.

Neasham, J. W., 1977. The morphology of dispersed clay in sandstone reservoirs and its effect on sandstone shaliness, pore space and fluid flow properties. Trans. AIME, (1977), SPE 6858, 8.

Nelson, Philip H, 2009. Pore-throat sizes in sandstones, tight sandstones, and shales, AAPG Bulletin, v. 93, no. 3 (March 2009), pp. 329–340.

Newsham, K. E., Rushing, J. A., Lasswell, P. M., Cox, J. C., Blasingame, T. A., 2004. Comparative Study of Laboratory Techniques for Measuring Capillary Pressures in Tight Gas Sands. Paper presented at SPE Annual Technical Conference and Exhibition, Houston, Texas, 26-29 September, 2004.

Oritz-Arango, J. D. and A. Kantzas, 2011. Pore-Level Investigation of Oil-Mobility Enhancement in Heavy-Oil Reservoirs. Journal of Canadian Petroleum Technology, May 2011, pp. 59-74.

Orr, F. M., Jr., 2004. Storage of carbon dioxide in geologic formations. J. Pet. Technol., 2004 56(9), 90-97.

Ortoleva, Peter J., 1994. Basin compartments and seals. AAPG Memoir (AAPG) 61: 34. Retrieved 15 March 2012.

Perera, M. S. A., Ranjith, P. G., Viete, D. R. and Choi, S. K., 2012. Parameters influencing the flow performance of natural cleat systems in deep coal seams experiencing carbon dioxide injection and sequestration. International Journal of Coal Geology. doi: 10.1016/j.coal.2012.03.010.

Perkins, M., Jr., 1957. An investigation of role of capillary forces in laboratory waterflood, F. SPE 840-G, November, 1957.

Permadi, P. and Susilo A., 2009. Permeability Prediction and Characteristics of Pore Structure and Geometry as inferred from Core data. Paper SPE 125350 presented at the 2009 SPE/EAGE Reservoir Characterization and Simulation Conference held in Abu Dhabi, UAE, 19-21 October 2009.

Pickell, J. J., Swanson, B. F., and Hickman, W. B., 1966. Applications of Air-Mercury and Oil-Air Capillary Pressure data in the study of Pore Structure and Fluid Distribution. SPEJ (March 1966) 55-61; Trans., AIME, 237.

Pini, R., Krevor, S., Benson, C. M., Sally, M., 2012. Capillary pressure and heterogeneity for the CO_2/water system in sandstone rocks at reservoir conditions. Advances in Water Resources 38 (2012) 48-59.

Pittman, E.D., 1992. Relationship of porosity and permeability to various parameters derived from mercury injection-capillary pressure curves for sandstone. AAPG 76 (2), 191–198.

Plug, W. J., Bruining, J., 2007. Capillary pressure for the sand-CO_2-water system under various pressure conditions. Application to CO_2 sequestration. Advances in Water Resources 30 (2007) 2339-2353.

Polaka S., Yildiray Cinarc, Torleif Holta and Ole Torsæterb, 2011. An experimental investigation of the balance between capillary, viscous, and gravitational forces during CO_2 injection into saline aquifers. Energy Procedia 4 (2011) 4395–4402.

Pruess, K., T. Xu, J. Apps, and J. Garcia, 2003. Numerical modelling of aquifer disposal of CO_2, Soc. Pet. Eng. J., 2003, 8(1), 49-60.

Purcell, W.R., 1949. Capillary pressures—their measurement using mercury and the calculation of permeability therefrom. T.P. 2544, Petroleum Transactions, AIME, Feb., 186, 39-48.

Qi, R., Laforce, T., Blunt, M. J., 2009. Design of carbon dioxide storage in aquifers. Int'l J. of GHG Control 3(2), 195-205.

Rao, D. N., Ayirala, S. C., Kulkarni, M. M., and Sharma, A. P., 2004. Development of the Gas Assisted Gravity Drainage (GAGD) Process for Improved Light Oil Recovery. Paper SPE 89357 presented at the SPE/DOE Fourteenth Symposium on Improved Oil Recovery, Tulsa, OK, April 17 – 21.

Raymer, L. L. and Freeman, P. M., 1984. In-Situ Determination of Capillary Pressure, Pore Throat Size and Distribution, and Permeability from Wireline Data. SPWLA Twenty-Fifth Annual Logging Symposium, June 10-13, 1984.

Reeves, P. C., Celia, M. A., 1996. A Functional Relationship between Capillary Pressure, Saturation and Interfacial Area as revealed by a Pore-scale network model. Water Resour Res 1996; 32(8): 2345-58.

Rezaee Reza, Ali Saeedi, Ben Clennell, 2012. Tight gas sands permeability estimation from mercury injection capillary pressure and nuclear magnetic resonance data. Journal of Petroleum Science and Engineering 88–89 (2012) 92–99.

Rezaee, M.R., Jafari1, A., Kazemzadeh, E., 2006. Relationships between permeability, porosity and pore throat size in carbonate rocks using regression analysis and neural networks. J. Geophys. Eng. 3, 370–376.

Roof, J.G., 1970. Snap-off of Droplets in Water-Wet Cores. SPEJ (March 1970) 85-90; Trans., AIME, 249.

Rose, W. D. and Bruce, W. A., 1949. Evaluation of Capillary Character in Petroleum Reservoir Rock. Trans., AIME (1949) 186, 127.

Saffman, P.G. and Taylor, G., 1958. The Penetration of a Fluid into a Porous Medium or Hele-Shaw Cell containing a more Viscous Fluid. Proceedings of the Royal Society of London, Series A, Mathematical and Physical Sciences, Vol. 245, Issue 1242, pp. 312-329, June 1958.

Salah, A., 2011. The impact of pore geometry aspects on porosity-permeability relationship – A critical review to evaluate NMR estimated permeability. Paper presented at the 10th Offshore Mediterranean Conference and Exhibition in Ravenna, Italy, March 23-25, 2011.

Sang, Qian, Yajun Li, Long Yu, Zhenquan Li, Mingzhe Dong, 2014. Enhanced oil recovery by branched-preformed particle gel injection in parallel-sandpack models. Fuel 136 (2014) 295–306.

Scheidegger, Adrian E., 1974. The Physics of Flow through Porous Media, 3rd Edition, University of Toronto Press, Toronto and Buffalo, Printed in Great Britain.

Schowalter, T. T. 1979. Mechanics of secondary hydrocarbon migration and entrapment. AAPG Bulletin, 63, 723–60.

Schwartz, L.W, Princen, H. M., Kiss, A. D., 1986. On the motion of bubbles in capillary tubes. J. Fluid Mech.172, 259–275.

Sehbi, Baljit S., Scott M. Frailey, and Akanni S. Lawal, 2001. Analysis of Factors Affecting Microscopic Displacement Efficiency in CO2 Floods. SPE paper 70022 presented at the SPE Permian Basin Oil and Gas Recovery Conference held in Midland, Texas, 15–16 May 2001.

Seo Y, Lee H, Uchida T., 2002. Methane and carbon dioxide hydrate phase behaviour in small porous silica gels: three-phase equilibrium determination and

thermodynamic modelling. Langmuir 2002; 18:9164–70. http://dx.doi.org/10.1021/la0257844.

Shah Virenkumar, Daniel Broseta, Gerard Mouronval, François Montel, 2008. Water/acid gas interfacial tensions and their impact on acid gas geological storage. International J. of Greenhouse Gas Control 2(2008) 594-604.

Silina, Dmitriy, Tad Patzek, 2006. Pore space morphology analysis using maximal inscribed spheres. Physica A 371 (2006) 336–360.

Sita-process.com @ http://www.sita-process.com/information-service/process-parameter.

Smith, D. A., 1966. Theoretical considerations of sealing and non-sealing faults. AAPG Bull., v.50, 363-374.

Socolow, R. H., 2005. Can we bury global warming? Scientific America, v. 293, no. 1, 49 – 55.

Snoeijer, J. H., and Andreotti, B., 2008. A microscopic view on contact angle selection. Physics of Fluids 20, 05710.

Stosur, G.J., 2003. EOR: Past, Present and What the Next 25 Years May Bring. Paper SPE 84864, presented at the SPE IOR Conference in Asia Pacific, Kuala Lumpur, Malaysia, October 20-21, 2003.

Sun C. Y., Chen G. J., Yang L. Y., 2004. Interfacial tension of methane + water with surfactant near the hydrate formation conditions. J Chem Eng Data 2004; 49:1024–5. http://dx.doi.org/10.1021/je049948p.

Swanson, B. F., 1981. A simple correlation between permeabilities and mercury capillary pressure curve, J. Pet. Tech. (1981), 2488-2504.

Swanson, B.F., 1977. Visualizing Pores and Nonwetting Phase in Porous Rock. Society of Petroleum Engineers Annual Fall Technical Conference. SPE Paper 6857 presented at the SPE-AIME Annual Fall Technical Conference and Exhibition, held in Denver, 1977.

Sweatman, R., Crookshank, S., and Edman, S., 2011. Outlook and Technologies for Offshore CO_2 EOR/CCS Projects. Paper OTC 21984 presented at the Offshore Technology Conference held in Houston, Texas, USA, 2-5 May.

Taber, J. J., 1969. Dynamic and static forces required to remove a discontinuous oil phase from porous media containing both oil and water. Soc. Pet. Eng .J. 9, 3–12.

Taylor, G. I., 1961. Deposition of a viscous fluid on the wall of a tube. J. Fluid. Mech.10, 161–165.

Thompson, A.H., A.J. Katz and C.E. Krohn, 1987. The microgeometry and transport properties of sedimentary rock. Advances in Physics, Volume 36, Issue 5, 1987, pages 625-694. DOI: 10.1080/00018738700101062.

Thompson, A. H., A. J. Katz, and R. A. Raschke, 1987. Estimation of Absolute Permeability from Capillary Pressure Measurements. Paper SPE 16794 presented at the 62nd Annual Technical Conference and Exhibition held in Dallas, Texas, September 27-30, 1987

Thomas, L. K., Katz, D. L., and Tek, M. R., 1968. Threshold pressure phenomena in porous media. SPE Journal, 174-184.

Tiab, D., Donaldson, E. C., 2015. Petrophysics: Theory and Practice of Measuring Reservoir Rock and Fluid Transport Properties. 4th Edition, Gulf Professional Publishing, Amsterdam.

Tzimas, G. C., T. Matsuura, D.G. Avraam, W. Van Der Brugghen, G.N. Constantinides, A.C. Patyatakes, 1997. The combined effect of the viscosity ratio and the wettability during forced imbibition through nonplanar porous media, Journal of Colloid and Interface Science, 189, 27–36.

Van der Meer, L. G. H., 1995. Energy Convers Mgmt. 1995, 36, 513-518.

Van Lingen, P. P., Bruining, J., van Kruijsdijk, CPJW, 1996. Capillary Entrapment Caused by Small-scale Wettability Heterogeneities, SPERE 1996; 11 (2): 93-100.

Van Oss, C.J., R.F. Giese, 1995. The hydrophilicity and hydrophobicity of clay minerals, J. Clays Clay Miner. 43 (4) (1995) 474–477.

Vavra, L., Kaldi, J., Sneider, M., 1992. Geological Applications of Capillary Pressure: a Review. American Association Petroleum Geologists, v 76/6, 1992.

Wardlaw, N.C., 1980. The Effects of Pore Structure on Displacement Efficiency in Reservoir Rocks and in Glass Micromodels," First Joint SPE/DOE Symposium on Enhanced Oil Recovery, Tulsa, OK, April 20-23, 1980, SPE #8843.

Wardlaw, N. C. and M. McKellar, 1981. Mercury Porosimetry and the Interpretation of Pore Geometry in Sedimentary Rocks and Artificial Models. Powder Technology 29 (1981) 127 – 143.

Wardlaw, N.C. and McKellar, M., 1985. Oil blob populations and mobilization of trapped oil in unconsolidated packs. Can. J. Chem. Eng., 63: 525-532.

Wardlaw, N.C. and Yu, L., 1988. Fluid topology, pore size and aspect ratio during imbibition. Transport Porous Media, 3: 17-34.

Washburn, E.W., 1921. Note on a method of determining the distribution of pore sizes in a porous material. Proceedings of the National academy of Sciences of the United States of America 7, 115–116.

Watanabe K, Imai S, Mori Y. H., 2005. Surfactant effects on hydrate formation in an unstirred gas/liquid system: an experimental study using HFC-32 and sodium dodecyl sulfate. Chem Eng Sci 2005; 60:4846–57. http://dx.doi.org/10.1016/j.ces.2005.03.043.

Watts, N. L., 1987. Theoretical aspects of cap-rock and fault seals for single- and two-phase hydrocarbon columns, Marine and Petroleum Geology, 4, 274-307.

Wilhite, G. P., 1986. Waterflooding, Society of Petroleum Engineers, Richardson, TX.

Wilson, M. D. and Pittman, E. D., 1977. Authigenic clays in sandstones: recognition and influence on reservoir properties and paleoenvironmental analysis. Journal of Sedimentary Petrology (1977), 47, 3**.**

Wu, S., A. Firoozabadi, 2010. Permanent alteration of porous media wettability from liquid-wetting to intermediate gas-wetting, J. Transp. Porous. Med. 85 (2010) 189–213.

Wyllie, R. J. and Rose, W. D., 1950. Some Theoretical Considerations Related to the Quantitative Evaluation of the Physical Characteristics of Reservoir Rock from Electrical Data. Trans., AIME (1950) 189, 105-118.

Yang, Daoyong, Yongan Gu, and Paitoon Tontiwachwuthikul, 2008a. Wettability Determination of the Reservoir Brine – Reservoir Rock System with Dissolution of CO_2 at High Pressures and Elevated Temperatures. Energy and Fuels 2008, 22, 504-509.

Yang, Daoyong, Yongan Gu, and Paitoon Tontiwachwuthikul, 2008b. Wettability Determination of the Crude Oil – Reservoir Brine – Reservoir Rock System with Dissolution of CO_2 at High Pressures and Elevated Temperatures. Energy and Fuels 2008, 22, 2363 – 2371.

Young, T, 1805. An Essay on the Cohesion of Fluids. Philos. Trans. R. Soc. Lond., 95, 65-87.

Yuan, Y. and Lee, R. T., 2013. Contact Angle and Wetting Properties. G. Bracco, B. Holst (eds.), Surface Science Techniques, Springer Series in Surface Sciences 51, DOI 10.1007/978-3-642-34243-1_1, © Springer-Verlag Berlin Heidelberg 2013.

Zhang, Li-juan and Yue, Xiang-an, 2007. Mechanism for Viscoelastic Polymer Solution Percolating through Porous media. Journal of Hydrodynamics, Ser.B, 2007, 19(2):241-248.

Zou, Caineng, Rukai Zhu , Keyu Liu, Ling Su, Bin Bai, Xiangxiang Zhang, Xuejian Yuan, Jinhong Wang, 2012. Tight gas sandstone reservoirs in China: characteristics and recognition criteria. Journal of Petroleum Science and Engineering 88–89 (2012) 82–91

Chapter 3: Materials and methods

3.1 Experimental method

3.1.1 Measurement of resistance of flow path to fluid interface in a single pore

Enhanced oil recovery and CO_2 storage are geological scale engineering, but controlled by the displacement of pore fluids (oil or saline water) at pore scale. Understanding the influence of flow path resistance in the displacement process in the porous medium is very crucial in determining the efficiency of the displacement, because it affects both the microscopic and macroscopic displacement efficiency (Green and Willhite, 1998). In this study, a method was developed to measure the resistance pressure profiles to multiphase flows, including the resistance to single phase flow, and to interfaces, in a single tapered pore or capillary, and to image the fluid movement, particularly the interfaces. The impact of each parameter such as pore geometry, interfacial tension, viscosity, fluids/gas composition and contact angle, on the resistance to the displacement can be studied using this method. The experimental data obtained may be very useful in gaining a better insight into microscopic displacement.

The experimental setup (Figure 3.1) includes a liquid delivery pump (LC-20 AD, Shimadzu), which can deliver liquids over flow rates from 0.00010 ml/min to 10 ml/min, a digital pressure transducer (DPI 280, Druck) with a resolution of 0.01 mbar to measure resistance pressure, a long working distance microscope (Brunel Microscopes Ltd, 10x objective) fitted with a digital camera (AM7023 Dino-Eye,

Dino-Lite Digital Microscope) to record fluid motion in the capillaries, particularly the motion of gas-water and liquid-liquid interfaces. The elapsed time and the pressure transducer outputs are displayed directly on the computer using LabView software. Figure 3.2 clearly shows the capillary exiting into the atmosphere.

Figure 3.1: Experimental setup for measurement of resistance to flow path in a capillary: (1) water reservoir (2) pump, (3) digital pressure display, (4) stainless steel cylinder, (5) transducer, (6) glass tube with tapered capillary at the end under a travelling microscope, (7) digital camera, (8) computer with LabView.

The displacing liquid (water) is delivered from a reservoir by means of a tube with a filter to ensure that the solvent flow line is not contaminated with any solid particle that may block the flow line. The pump delivers the liquid at a set flow rate to a

stainless steel cylinder containing water and fitted with the micropipette (tapered single pore or capillary) (Figure 3.3). The pressure transducer is fitted between the cylinder and the capillary, which is positioned between a light source and the long working distance microscope. The computer is used to acquire the digital image (micrographs) of the interface inside the capillary. The interface is curved to the capillary radius and the computer is able to process the photographic data.

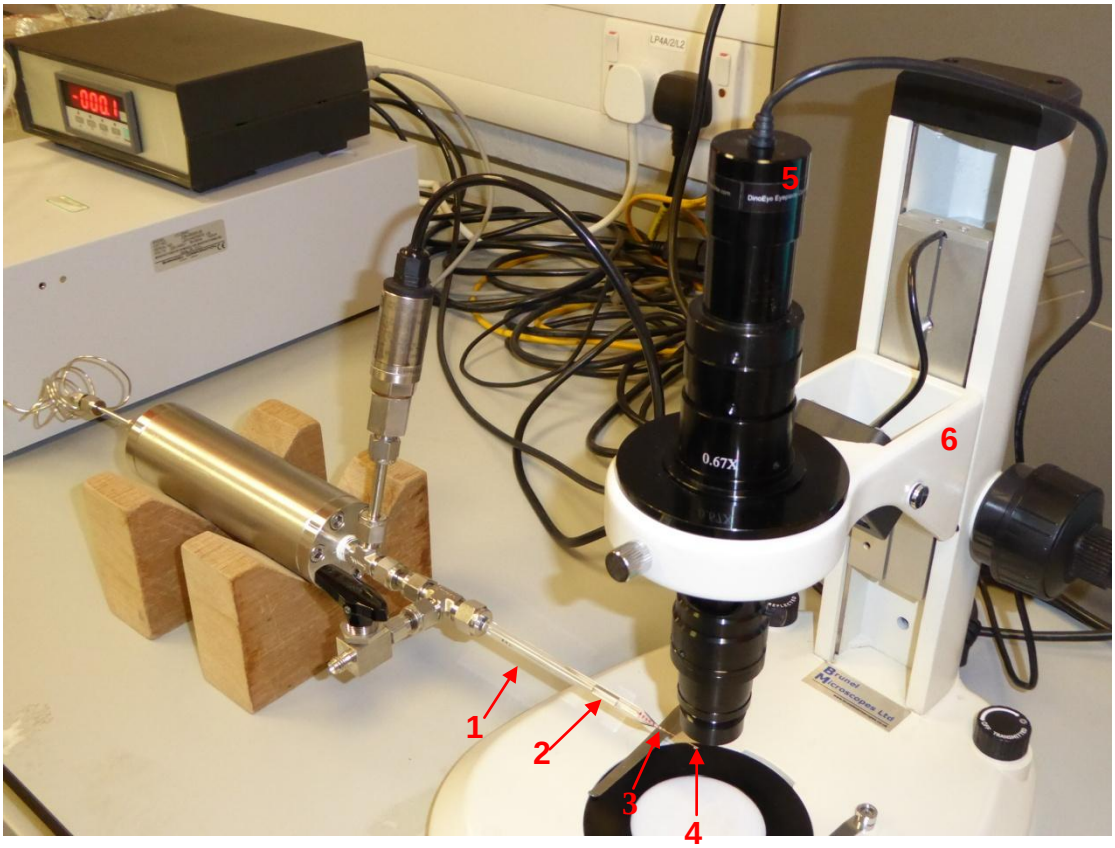

Figure 3.2: Experimental setup showing the tip of a tapered capillary with a gas bubble in the glass tube: (1) glass tube, (2) gas bubble, (3) tapered capillary, (4) capillary tip, (5) digital camera, (6) travelling microscope

Figure 3.3 shows a tapered glass capillary filled with deionised water only (no gas phase); the pore size decreases towards the capillary tip. The illumination of the glass capillary wall appears as three distinct shades of colour, with the external wall being

dark and fades gradually to white in the internal wall. The internal capillary wall is therefore clearly defined by a white line. This is the same observation for all the hundreds of glass capillaries used. Borosilicate glass used in fabricating these capillaries is hydrophilic, so water is in direct contact with the glass wall. When a gas phase displaces water, it also makes a direct contact with the glass wall, as shown in Figures 4.4a-g and 4.5. Similar images have been published in previous publications as shown in Figure 3.4 (Li et al, 2013; Li et al, 2014). There may be nanometer film of water on the glass wall in contact with the gas phase, but this can not be observed visually.

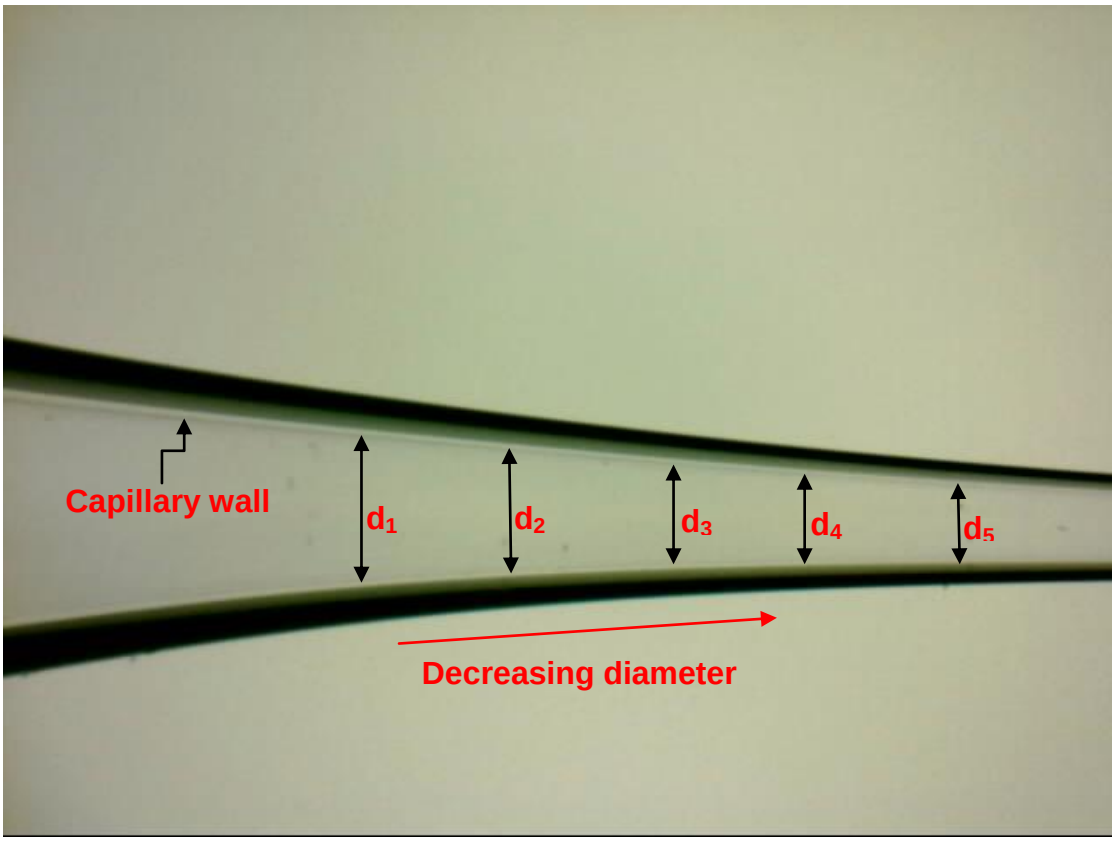

Figure 3.3: A tapered capillary filled with water and showing decreasing pore size towards the tip (diameter = 100 µm); (d_1= 506±30 µm; d_2= 430±30 µm; d_3= 355±30 µm; d_4= 304±30 µm; d_5= 279±30 µm).

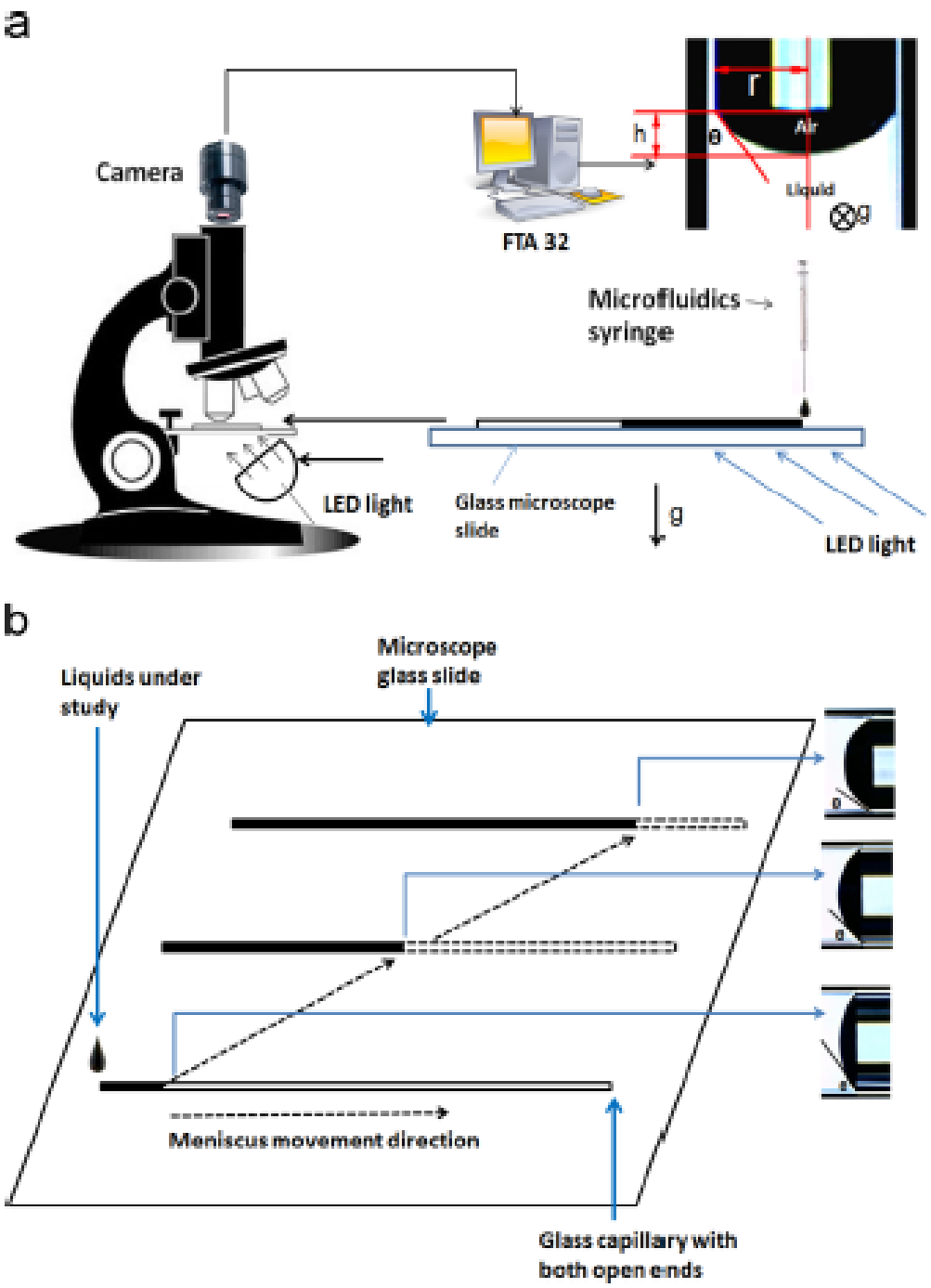

Figure 3.4: Meniscus movements in the measurement of air-glass contact angles in a glass capillary, showing a direct contact of the gas phase with the glass wall. (a) Microscopic imaging of contact angle of liquids in a pore (the vector ḡ shows the direction of gravity; (b) Dynamic contact angles under a microscope equipped with a camera (Li *et al*, 2013).

The diffraction at the walls of the capillary and the curvature of the glass itself introduce potential errors in the measurements of the curvature of the interface (Lee *et al,* 2001; Cheong *et al,* 2011). A LED white light source above and below the glass capillary and the high numerical aperture objective were used to optimize the digital image and minimize the optical diffraction at the interface. The entire experimental setup was mounted on a vibration-free horizontal workstation to minimize positional oscillations generated by vibration from external sources (Lee et al, 2001).

To measure the pore resistance to two-phase flow, the stainless steel cylinder was washed with hot detergent solution, rinsed thoroughly with tap water, and finally washed with deionised water (Fisher and Lark, 1979). It was then completely filled with the deionised water. First, the capillary was marked (Figure 3.5) at different intervals with an indelible marker pen to have suitable reference points for the interface position, and the micropipette was completely filled with deionised water, followed by an introduction of 0.1 ml of gas to create a gas-liquid interface.

The resistance to the fluid movement through the capillary is a combination of the resistance from capillary force and viscosity force (Chatzis and Dullien, 1983, Løvoll *et al,* 2005), and even in very slow displacements the displacement is controlled by the heterogeneity of the capillary force along the interface (Løvoll *et al,* 2005). The external force for driving the flow is provided by the liquid delivery pump, which is set at a slow flow rate to remove the effect of viscous force (Løvoll *et al,* 2005). The resistant pressure through the capillary was measured by the pressure transducer, and the LabView software recorded the variation of resistance pressure with time.

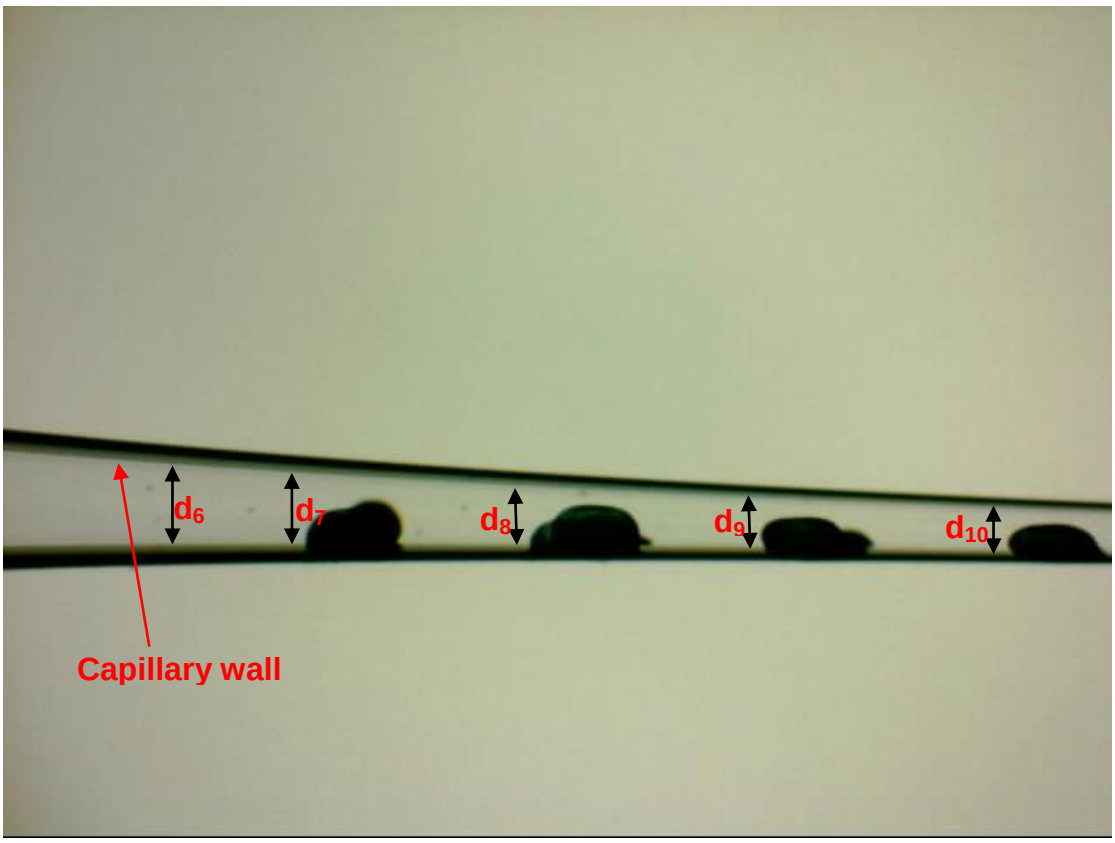

Figure 3.5: Posterior section of the tapered capillary filled with water, shown in Figure 3.3, marked with indelible ink (d_6= 253±30 µm; d_7= 228±30 µm; d_8= 203±30 µm; d_9= 177±30 µm; d_{10}= 165±30 µm).

The motion of the interface front was observed by viewing it horizontally with the optical microscope. The images and position of the interface before and after each marked position were captured with the digital camera attached to the microscope, and then recorded by the computer. When the interface moved out of the capillary the LabView output was analysed to obtain the resistant pressure.

To measure the resistance to gas-water interfaces, the resistance to the water single phase flow through the capillary and the resistance to gas-water two-phase flow were measured, respectively. The resistance to interface was then obtained by subtracting

the resistant pressure to the single phase water flow from the resistant pressure to gas-water flow.

3.1.2 Contact angle measurement in a micron-sized pore

A novel method developed in our laboratory, based on microscopic imaging technique, was used in this study to measure directly the contact angles of various interfaces in capillaries, by considering the effects of pore geometry, surface tension, viscosity (liquid's physical properties), its chemical structure and interface composition. This is similar to the method used by Li *et al* (2013 & 2014) to study pore static contact angle and pore dynamic contact angle.

The apparatus used in this study to measure contact angle in a non-uniform (tapered) capillary is shown in Figure 3.6. A long working distance microscope (Brunel Microscopes Ltd, 10x objective) equipped with a digital camera (AM7023 Dino-Eye, Dino-Lite Digital Microscope) was used to image the gas-liquid or liquid-liquid interface at different positions as it moves through the capillary, as shown in Figure 3.6.

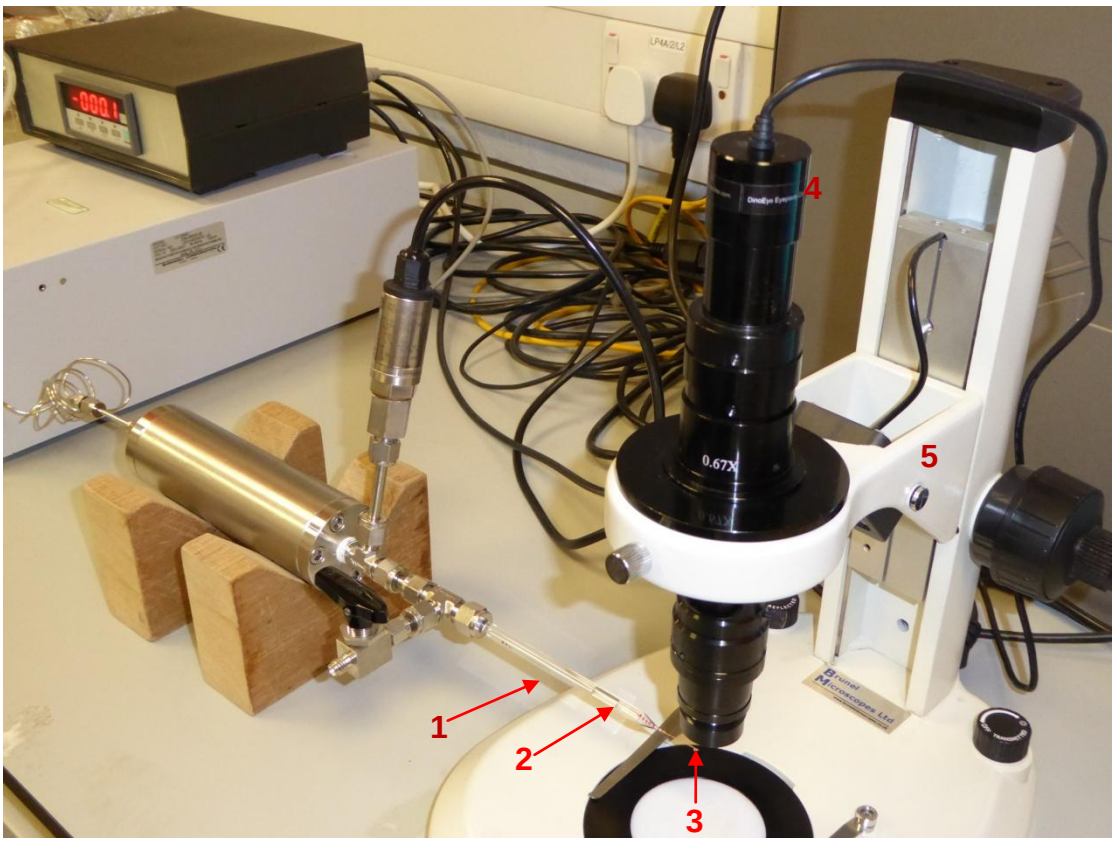

Figure 3.6: Measurement of pore contact angle in a tapered capillary: (1) glass tube with tapered capillary at the end, (2) gas-water interface, (3) capillary tip, (4) digital camera, (5) travelling microscope.

The use of glass material causes diffraction at the walls of the capillary, and as the capillary is cylindrical, the curvature of the glass is also a potential source of errors in the measurements of the curvature of the interface, as both may cause the image to be distorted (Lee *et al*, 2001; Cheong *et al*, 2011, Danişman *et al*, 2008).

As a caution by Cheong et al, the quality of the interface image of a small volume of liquid in a capillary depends strongly on the measurement method and illumination used. LED white light sources located below and above the glass capillary were used to illuminate the interface adequately to overcome the degree of image distortion, and thus improve and facilitate the contact angle measurements in a small pore. The principle used here is similar to the principle used by, Fan *et al* (2003) to measure

micron ice crystal size in aqueous solution, Fan *et al* (2004) to measure micron air-bubble size and Rosiñski *et al* (2002) to measure the size of a microcapsule or plant cell under a microscope, Kohonen (2006) to measure contact angle in water-conducting capillaries (tracheids) of plants, and Danişman *et al* (2008) to measure contact angle in micron-sized capillaries. The outermost boundary of the two-phase interface was lighted sufficiently and focused to obtain a clear two-phase interfacial line.

To initiate the contact angle measurement, a freshly fabricated tapered capillary is filled with deionised water and 0.1 ml of fluid (gas or liquid) is introduced into the uniform diameter (unstretched) section of the micropipette to create the gas/water or liquid/water interface. The interface front at this position is focused with the microscope and the image is taken. The contact angle obtained in this section should be fairly constant for all the capillaries since this section of the tube has a uniform diameter. A slight pressure was then applied temporarily by means of the liquid delivery pump to cause the interface to move. When the interface motion stops completely the meniscus is focused with the microscope to obtain the clear two-phase interfacial line and the image (micrograph) at this position is taken with the digital camera. This process is repeated until images of the interface are obtained at different sections of the tapered capillary, and the interface leaves the capillary. As the capillary is not uniform and tapers towards the tip, the distance between the microscope and the capillary is adjusted at every position of the interface to obtain a clear and focused image.

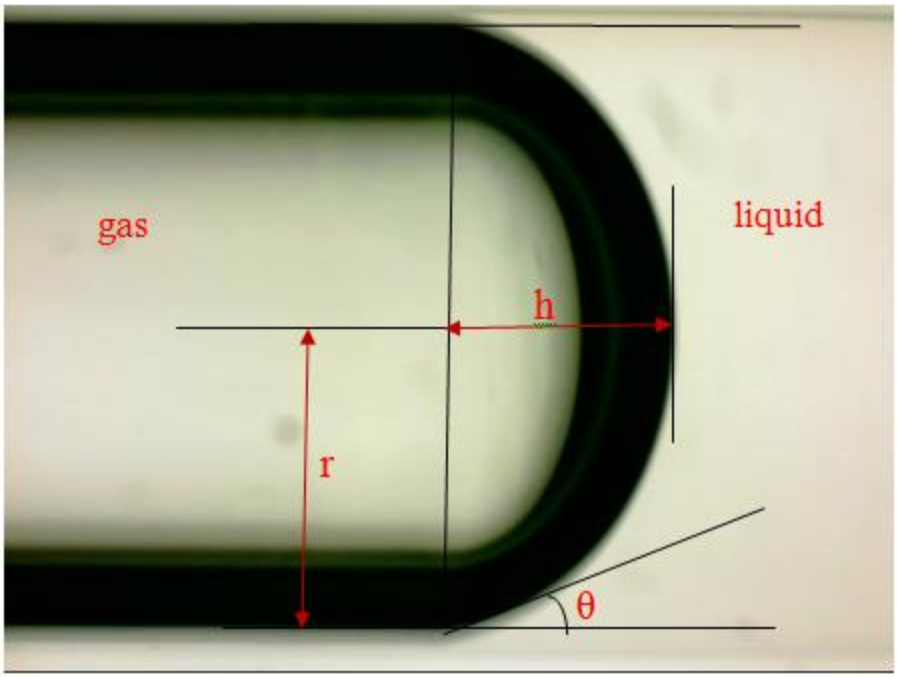

Figure 3.7: Measurement of contact angle of small liquid volume in a circular capillary (r = 2.015±0.03 mm).

To determine the contact angle of the interface, the micrographs obtained were analysed using the method proposed recently by Cheong *et al* (2011) to measure small liquid volumes in circular capillaries, which neglects gravity, and commercial software (FTA 32). Cheong et al method uses only the capillary radius, r and meniscus height, h (Figure 3.6) to obtain the contact angle, which is given by equation 3.1.

$$\theta = \tan^{-1}\left(\frac{r^2-h^2}{2rh}\right) \qquad (3.1)$$

where

h = height of the meniscus, mm

r = inner radius of the capillary, mm

θ = contact angle, rad

The assumptions in deriving this equation are that there is no effect of gravity and the volume of liquid involved is small (Cheong *et al,* 2011; Zheng *et al,* 2005). This is very true for our experiment where the flow is horizontal and the size of the capillaries used is very small. The effect of image distortion on contact angle estimation by this method can be minimized since the effect of image distortion on meniscus height is not significant (Cheong *et al,* 2011).

The error in measurement can be estimated by rearranging Equation 3.1 and differentiating into Equation 3.2

$$\delta\theta = \left(-\frac{r^2+h^2}{2rh^2(1+\tan\theta)}\right)\delta h = -\frac{2r}{r^2+h^2}\delta h \qquad (3.2)$$

Knowing that $h = r\,(1-\sin\theta)/\cos\theta$, Equation 3.2 can be written as

$$\delta\theta = \frac{-2K}{r}\delta h, \text{ where } K = \frac{1+\sin\theta}{2} \qquad (3.3)$$

Equation 3.3 shows that the sources of error are from the dimension of the capillary, r, the wetting characteristics of the liquid, K, and the imaging spatial resolution of the microscope system, δh. This implies that using larger radius will improve the accuracy of measuring the contact angle (Cheong *et al,* 2011), although there is a limit to increasing the radius at the expense of losing the capillary effect (Barr, 1923) and the ability to sustain small liquid volumes. The error in the measurement of contact angles in the pore sizes considered in this work (< 1000 μm to 100 μm) is ±0.003 to 0.03º.

3.2 Materials

3.2.1 Glass capillaries

Tapered capillaries with varying capillary tip sizes and gradients were made from standard glass tubes (borosilicate, bore size 3 mm, 0.5m long, 6 mm (ext.) diameter; FB51467 Fisher Scientific, UK). The standard glass tubes were cut into lengths of approximately 12 cm, and were washed by using hot 6 M NaOH and 6M HCl.

The tubes were then washed thoroughly using tap water until the washing water reached the natural water pH, and then rinsed with deionised water (C540 Deioniser, Veolia Water Solutions Technologies). The cleaned glass tubes were then heated under a 550^{o}C flame to remove any residue of organic contamination and kept in a dust-proof enclosure (Fisher and Lark, 1979). Single capillaries of various sizes were obtained by melting a middle section of the clean, dry glass tubes in a butane flame (Butane Battery, D2-BS 0167) and pulling it to create a suitable taper (Lee *et al*, 2001). This is similar to the technique used by Fisher and Lark (1979) to study liquid flow in fine capillaries and by Li *et al* (2013) to study dynamic pore wettability. By controlling the heat setting and pulling speed applied, capillaries with varying gradients and tip diameters can be obtained.

In this study, the minimum capillary tip size used was 100 µm, so as to obtain a good focus of the interface in all sections of the tapered capillary. With better focusing microscopes the tip size of the capillaries could be reduced to less than 100 µm. However, if the tip size becomes too small the resistant pressure to the interface motion may be too high and cause damage to the equipment, apart from the inherent elongation of the duration of each experiment. It is also important to note that it was

not possible to make, in a reproducible manner, series of capillaries of identical pore tip size and different gradients. This was due to the inability, to maintain the same degree of melting of the glass each time before pulling to make the capillaries and, to pull at a uniform speed, even for same degree of melting. The result is that capillaries of the same tip size but with differing pore gradient are obtained. As a result, it is difficult to compare accurately the impact of parameters on the resistance to flow. For example, to compare the impact of pore gradient on the resistant pressure it is necessary to obtain capillaries with same tip size but with varying pore gradient.

For a single uniform capillary with one diameter only one equilibrium point can exist. However, in a tapered capillary with varying gradients several equilibrium points can be obtained with applied pressure as the interface moves to a new position. The length of all the capillaries was fixed at about 2 cm to minimise any effect of capillary length on the resistant pressure (Li and Fan, 2013).

Borosilicate glass is strongly hydrophilic, so the glass capillaries used are water-wet.

3.2.2 Liquids

3.2.2.1 Fluids

The common reservoir liquids are saline water and crude oil. In this study, deionized water, silicone oil, n-decane and crude oil are used to represent the common reservoir liquids or saline aquifer. Silicone oil is used to investigate the effect of fluid viscosity on fluid displacement. The deionised water was obtained from (C540 Deioniser, Veolia Water Solutions Technologies). N-Decane was purchased from ACROS Organics (analytic grade, 99+% pure). Crude oil was sourced from MAPLLC

Petroleum Crude Oil (density: 659~818 kg/m3; surface tension: 20.0 mN/m; viscosity: 6.14×10-3 Pa·s).

3.2.1.2 Chemicals

Displacement in porous media is greatly influenced by liquid properties such as surface tension and viscosity, as both properties influence the dynamic contact angle which is related to the capillary number and the static contact angle (Li, 2015). The effect of surface tension on resistance to displacement and contact angle was studied using various concentrations of 1-propanol (99^{+} %, extra pure, ACROS Organics, New Jersey, U.S.A). 1-Propanol and its aqueous solutions and water give a good contrast in surface tension, with their surface tensions ranging from 24.4 mN/m for 1-propanol to 72.0 mN/m for water. However, their viscosities are very close, ranging from 8.94×10^{-4} Pa.s (water) to 1.94×10^{-3} Pa.s (1-propanol), so viscosity effect can be neglected to study the effect of surface tension on resistance. Their physical properties are shown in Table 3.1.

To investigate the effect of liquid viscosity on resistance to displacement, silicone oils with varying viscosities are used as shown in Table 3.2. These silicone oils have very close surface tensions ranging from 20.1 mN/m (10 cst) to 21.2 mN/m (1000 cst).

Table 3.1: Physical Properties of Aqueous Solutions of 1- propanol and de-ionised water

Mass fraction	Density (kg/m^3)	Viscosity (Pa.s)	Surface tension (mN/m)
0*	998.2	8.94×10^{-4}	72
0.05	987.9	1.10×10^{-3}	42.51
0.1	976.1	1.34×10^{-3}	34.86
0.2	953.3	1.84×10^{-3}	28.31
0.3	932	2.14×10^{-3}	26.41
0.7	854.2	2.54×10^{-3}	24.47
1	803.4	1.94×10^{-3}	23.69

0* Deionised water
Source: Li, 2015.

Table 3.2 Physical Properties of Oils

Name	Density (kg/m^3)	Viscosity (Pa.s)	Surface tension (mN/m)
Silicone oil (10 cst)	930	9.30×10^{-3}	19.4
Silicone oil (50 cst)	960	4.80×10^{-2}	20.8
Silicone oil (100 cst)	960	9.60×10^{-2}	20.9
Silicone oil (500 cst)	970	4.85×10^{-1}	21.1
Silicone oil (1000 cst)	970	9.70×10^{-1}	21.2
Crude oil	659-818	6.14×10^{-3}	20
n-Decane	730	9.20×10^{-4}	23.8

Source: Li, 2015.

3.2.3 Gases

3.2.3.1 Carbon dioxide (CO_2)

Apart from the growing need of CO_2 for geological storage in climate change mitigation, CO_2 is used for EOR (tertiary recovery). CO_2 injection for EOR is expected to rise with the increasing awareness of sequestering CO_2 and at the same time producing incremental oil.

CO_2 is a gas with a density of 1.8 kg/m^3 (air = 1.2 kg/m^3) at ambient surface temperature (25 ^oC) and pressure (0.1 MPa = 1 bar). It can be stored as a supercritical fluid at injection depths greater than ~800 m, assuming a geothermal gradient of 30 ^oC/km and a pressure gradient of 10.5 MPa/km (Bruant *et al*, 2002; Bachu and Gunter, 1994; Bachu, 2002; Holloway and van der Straaten, 1995). At 800 m depth, the density of supercritical CO_2 is approximately 260 kg/m^3 and this permits far greater quantities of CO_2 to be stored per unit volume than as a gas at shallower depths (Bruant *et al,* 2002). At this depth, the density of water with 15% total dissolved solids by mass is ~1100 kg/m^3 (McCain, 1991; Bachu and Gunter, 1994). This density difference generates buoyancy forces that drive injected CO_2 upward.

When CO_2 is dissolved in formation waters it is not subject to upward buoyant migration, and it is said to be trapped. The solubility of CO_2 decreases with increasing temperature and salinity, and increases with increasing pressure. At the surface conditions, the solubility of CO_2 in pure water is 1.3-1.7 kg/m^3 and at the higher temperature and pressure conditions at the depth of 800 m, the solubility of CO_2 in formation waters with 15% total dissolved solids by mass is ~35 kg/m^3 (Bruant *et al,* 2002).

In about 60% of the reservoirs in which CO_2 is injected the salinity of the aquifers ranges from 20,000 to 340,000 ppm (Bennion and Bachu, 2008). Usually, injection is into reservoirs (carbonate and sandstone formations) with porosity generally less than 12% and permeability on the order of millidarcy to tens of millidarcy.

CO_2 used in this study was purchased from C40-VB, BOC, Manchester. It has a purity of 100% and was supplied in a gas bottle (Figure 3.8). It was used to create interfaces of CO_2-water/aqueous solution in this study.

3.2.3.2 Methane (CH_4)

Methane is the simplest member of the alkane family and it is the major component of natural gas. It is considered to be an important greenhouse gas with a global warming potential of 34 compared to CO_2 over a 100-year period.

It is a colourless, odourless gas at room temperature and standard pressure. Its boiling point is −161 °C (−257.8 °F) at a pressure of one atmosphere and it is highly flammable over a range of concentrations in air at standard pressure. It is insoluble in water. It is lighter than air at ambient temperature.

Figure 3.8: Liquefied carbon dioxide and methane gases in bottles

CH_4 is a major component of natural gas. In shale gas recovery, water flooding is used to displace natural gas from porous rocks. Depleted gas/oil reservoirs have been seen as a place to store CO_2. The typical opinion is that the gas/oil reservoirs have sealed natural gas for million years; it should be able to store CO_2 gas. In this study, CH_4 was used to investigate the resistance to CH_4-water interface for advancing the understanding of water-natural gas displacement.

CH_4 (CP Grad (100%), BOC, Surrey) used in this study has a purity of 100% and was supplied in gas bottles (Figure 3.7).

3.2.3.3 Air

Air is a mixture of gases composed mainly of nitrogen (78 %), followed by oxygen (21 %) and others in trace amounts. Air is used for combustion processes in thermal oil recovery (tertiary recovery).

Atmospheric air obtained in syringes was used for this study.

3.3 Summary

A method developed to measure the resistant pressure to single phase flow in tapered pores, as well as, the resistance to two-phase flows, while imaging the fluid interface movement has been described. The method of determining contact angles of imaged interfaces was also described. The gas-water interface is in direct contact with the glass capillary wall, so the displacement is piston-like.

In the following chapters, the results, discussions and conclusions of the most important findings obtained in this experimental research are presented.

3.4 References

Bachu, S., 2002. Sequestration of CO_2 in geological media in response to climate change: Road maps for site selection using the transform of the geological space into the CO2 phase space. Energy Convers Mgmt. 2002, 43, 87-102.

Bachu, S., Gunter, W. D., Perkins, E. H., 1994. Aquifer Disposal of CO_2: Hydrodynamic and Mineral Trapping. Energy Convers and Mgmt 1994, 35, 269-279.

Barr, G, 1923. Capillary tube viscometers. Part 1. Journal of Scientific Instruments, 1923, Vol. 1, No. 3, pp 81-86.

Bennion, D. Brant and Bachu, Stefan, 2008. Drainage and Imbibition Relative Permeability Relationships for Supercritical CO_2/Brine and H_2S/Brine Systems in Intergranular Sandstone, Carbonate, Shale, and Anhydrite Rocks. SPE Reservoir Evaluation and Engineering, June, pp 487-496.

Bruant, R. G., Jr., M. A. Celia, A. J. Guswa, C. A Peters, 2002. Safe Storage of CO_2 in Deep Saline Aquifers. Environ. Sci. Technol., 36 (11), 240A-245A.

Chatzis, I. and F. A. L. Dullien, 1983. Dynamic Immiscible Displacement Mechanisms in Pore Doublets: Theory versus Experiment J. of Colloid and Interface Science, Vol. 91, No. 1, January 1983.

Cheong, Brandon Huey-Ping, Tuck Wah Ng, Yang Yu, and Oi Wah Liew, 2011.Using the Meniscus in a Capillary for Small Volume Contact Angle Measurement in Biochemical Applications. Langmuir 2011, 27, 11925–11929.

Danişman Mehmet F, Calkins Jacob A, Sazio Pier J. A., Allara David L, and Badding John V, 2008. Organosilane Self-Assembled Monolayer Growth from Supercritical Carbon Dioxide in Microstructured Optical Fibre Capillary Arrays. Langmuir. 2008, 24, 3636-3644.

Fan X, Ten P, Clarke C, Bramley A, Zhang Z., 2003. Direct Measurement of the Adhesive Force Between Ice Particles by Micromanipulation. Powder Technol. 2003; 131:105-10.

Fan X, Zhang Z, Li G, Rowson NA, 2004. Attachment of Solid Particles to Air Bubbles in Surfactant-free Aqueous Solutions. Chem Eng Sci. 2004; 59:2639-45.

Fisher, Leonard R. and Prosper D Lark, 1979. An Experimental Study of the Washburn Equation for Liquid Flow in Very Fine Capillaries. Journal of Colloid and Interface Science, Vol. 69, No. 3, May I979.

Green, D. W. and Willhite, G. P., 1998. Enhanced Oil Recovery, SPE, Richardson, TX, 1998.

Holloway, S., van der Straaten, R., 1995. The Joule II Project: The Underground Disposal of Carbon Dioxide. Energy Convers and Mgmt 1995, 36, 519-522.

Kohonen, M. M., 2006. Engineered Wettability in Tree Capillaries. Langmuir, 2006, 22(7), 3148-3153.

Lee, Sunghee, Dennis H. Kim, and David Needham, 2001. Equilibrium and Dynamic Interfacial Tension Measurements at Microscopic Interfaces Using a Micropipette Technique. 1. A New Method for Determination of Interfacial Tension. Langmuir 2001, 17, 5537-5543.

Li X, Fan X, Askounis A, Wu K, Sefiane K, Koutsos V., 2013. An Experimental Study on Dynamic Pore Wettability. Chem Eng Sci. 2013; 104: 988-97.

Li X, Fan X, Brandani S., 2014. Difference in pore contact angle and the contact angle measured on a flat surface and in an open space. Chem Eng Sci 2014; 117: 137-45.

Li, Xingxun and Xianfeng Fan, 2013. Experimental Studies on Multiphase Flow in Porous Media and Pore Wettability. World Academy of Science, Engineering and Technology Vol.74 2013-02-25.

Li, Xingxun, 2015. Experimental Studies on Pore Wetting and Displacement of Fluid by CO_2 in Porous Media, PhD Thesis, University of Edinburgh, United Kingdom.

Løvoll, Grunde, Yves Méheust, Knut Jørgen Måløy, Eyvind Aker, Jean Schmittbuhl, 2005. Competition of gravity, capillary and viscous forces during drainage in a two-dimensional porous medium, a pore scale study. Energy 30 (2005) 861–872.

McCain, W. D. Jr., 1991. Reservoir Fluid Property Correlations-State of the Art. Soc Pet. Eng J. Reservoir Eng., 1991, 6, 266-272.

Rosiñski S, Grigorescu G, Lewiñska D, Ritzén LG, Viernstein H, Teunou E, Poncelet D, Zhang Z, Fan X, Serp D, Marison I, Hunkeler D, 2002. Characterization of Microcapsules: Recommended Methods Based on Round-robin Testing. J Microencapsulation 2002; 19:641-59.

Zheng, Q.-S, Y. Yu, Z.-H. Zhao, 2005. Effects of Hydraulic Pressure on the Stability and Transition of Wetting Modes of Superhydrophobic Surfaces. Langmuir. 2005, 21 (26), pp 12207-12212.

Chapter 4: Pore resistant pressure profiles

4.1 Introduction

Although the profusion of experimental work pertaining to resistance to fluid flow in porous media has revealed many details of the mechanism of multiphase flow, there appear to be a few gaps to justify further experimental work. In particular, limited attempts have been made to study the exact impact of pore geometry on the resistant pressure (pressure drop) at the pore level and to determine the relationship between resistant pressure and factors that influence the fluid displacement. In this study, we have developed an experimental technique for measuring the resistant pressure profiles and pressure drop of fluid flow through single pores and then use the information to study the exact impact of factors such as pore geometry, surface tension, fluid properties, and wettability on the displacement.

4.2 Resistant pressure profiles for single phase flow and interface flow

To obtain the pressure profile of single phase flow and investigate the pore resistance to its flow, a micropipette was filled with deionised water and the water was allowed to flow through the capillary for a period of time, using the external force from the liquid delivery pump. The resistant pressure profile of the flow of water alone was measured. After the initial experiment, the micropipette was thoroughly rinsed with deionized water, dried, and re-used for the two-phase flow experiment. In order to

obtain the resistant pressure profile and investigate the pore resistance to two-phase flow, the micropipette was filled with deionized water and a gas-liquid interface was created by introducing 0.1 ml of the gas into the micropipette, and the resistant pressure profile through the capillary was measured. The motion of the interface front was observed by viewing it horizontally with the optical microscope.

Figures 4.1 and 4.2 show the pressure profiles for driving water, and CO_2-water, and CH_4-water, interfaces through two capillaries of tip sizes 150 µm (pore gradient = 4.762×10^{-3}) and 113 µm (pore gradient = 7.885×10^{-3}), respectively. The pore gradient or capillary gradient is defined as the pore diameter per unit length, determined between the effective pore diameter and pore tip diameter. Mathematically, it is the ratio of the difference between the effective pore diameter and pore tip diameter to the distance between them (Figure 4.3).

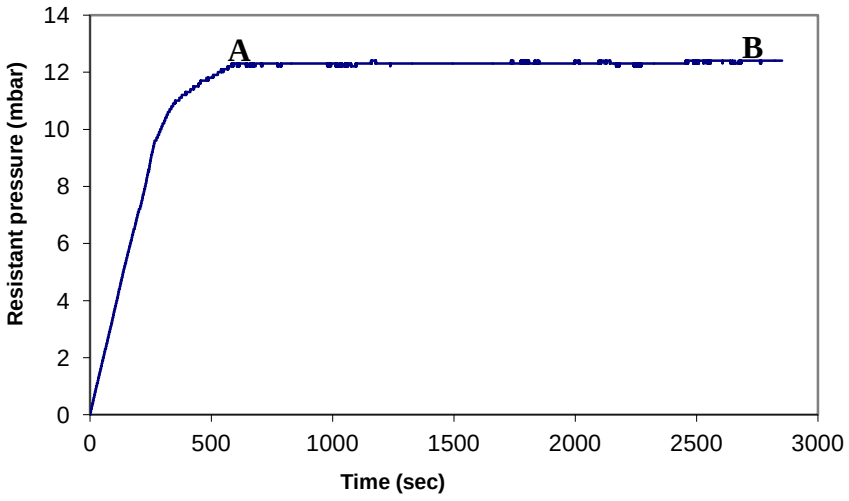

Figure 4.1a: Pressure profile for driving only water phase through a capillary of tip size 150 µm (capillary gradient: 4.762×10^{-3}).

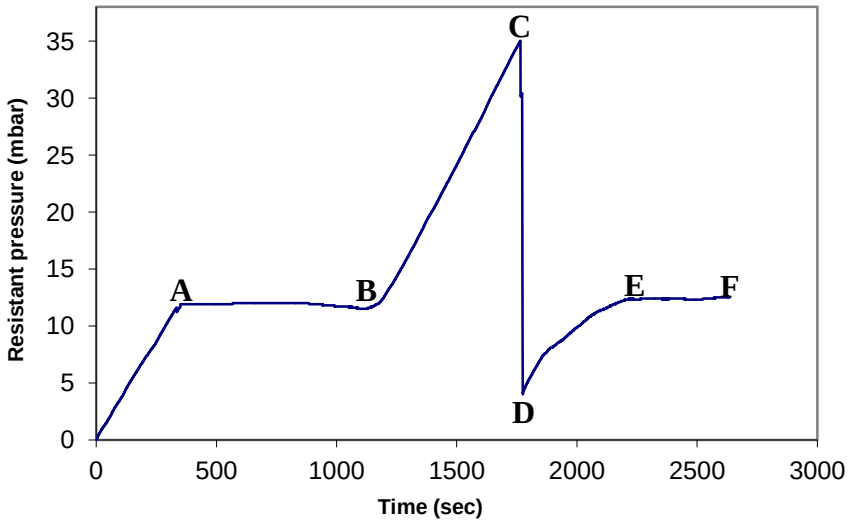

Figure 4.1b: Pressure profile for driving CO2-water interface through a capillary of tip size 150 µm (capillary gradient: 4.762×10^{-3}).

Figure 4.1a is the pressure profile for driving water phase only through the 150-µm capillary for about 1 hr and Figure 4.1b is the pressure profile for driving the CO_2-water interface through the same capillary for the same duration. Figures 4.1a and 4.1b are similar to the profiles in 113-µm capillary for water only, and CH_4-water interface, respectively (Figures 4.2a and 4.2b).

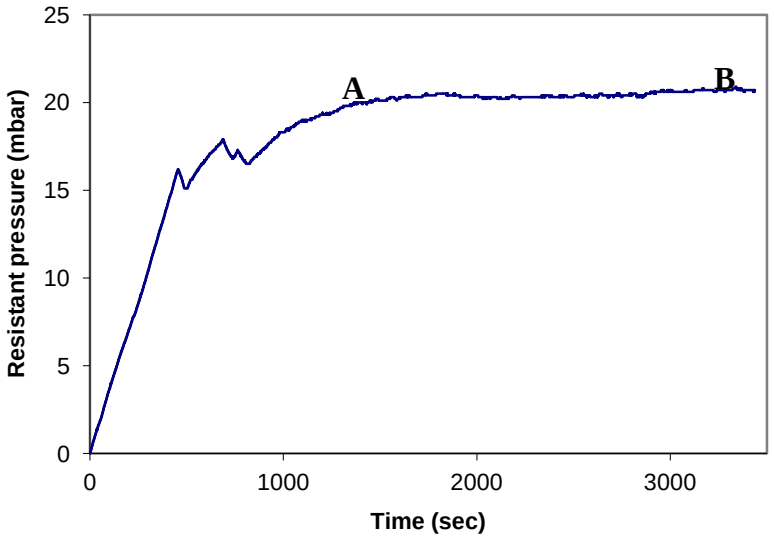

Figure 4.2a: Pressure profile for driving only water phase through a capillary of tip size 113 µm (capillary gradient: 7.885×10^{-3}).

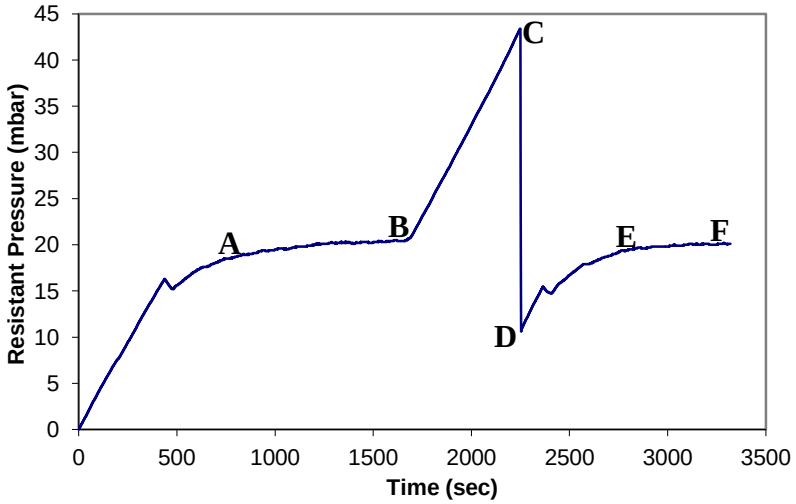

Figure 4.2b: Pressure profile for driving CH_4-water interface through a capillary of tip size 113 µm (capillary gradient: 7.885×10^{-3}).

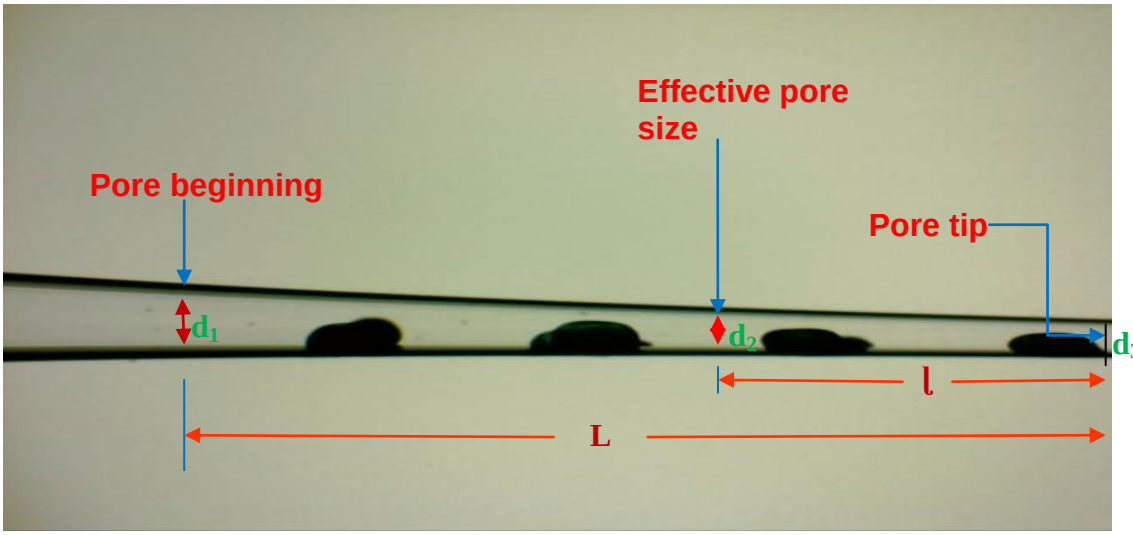

Figure 4.3: Tapered capillary illustrating the pore length, effective pore size and pore throat (d_1 < 1000 µm; l = pore throat length (mm); L = pore length (mm); d_2 = effective pore diameter (µm); d_3 = tip diameter (µm)).

Figures 4.1a and 4.2a show similar trends for flow of water through the two capillaries, while Figures 4.1b and 4.2b also show similar profiles for gas-water two-phase flow through the two capillaries.

Figure 4.1a shows that the pressure profile for driving water phase only has two sections, 0A and AB. The resistant pressure builds up from 0 mbar as the pump is started and increases linearly initially up to about 9.5 mbar at which the discharge of water from the capillary starts. Once water starts flowing out from the capillary, the increase in resistant pressure becomes non-linear until about 12.3 mbar, at which the pressure becomes constant. Section AB is the constant pressure (balanced pressure) section and the pressure remains the same irrespective of the duration of water flow through the capillary. The balanced pressure indicates that the rate of delivery of water by the pump is equal to the rate of discharge of water from the capillary. We

believe this is the maximum resistant pressure to water flow through this capillary at that condition.

The resistant pressure profile for CO_2-water flow in the same capillary (Figure 4.1b) is different from the resistant pressure profile for single phase water; the pressure profile has 6 sections. At the start of the pump, the resistant pressure increased linearly until water starts flowing out from the capillary. The increase continued, though not linear until point A (section 0A), from which the pressure becomes constant at about 12.3 mbar. Section AB is the constant (balanced) pressure section analogous with the case of single phase water flow (Figure 4.1a). In this section, the pore resistance to the flow is balanced by the pump driving force. At position B, the resistant pressure increased suddenly and this increase is linear up to position C, corresponding to the tip of the capillary. Position C is the maximum resistance to the interface flow, just before it comes out from the capillary. This drastic increase in the resistant pressure to interface flow is observed to occur only from a certain point in the tapered capillary, for a particular tip size and pore gradient. This point (B in Figures 4.1b and 4.2b) is the beginning of the pore throat effect, and the pore diameter corresponding to this point is the *effective* pore diameter. It is the pore size at which the pore has a dramatic effect on the pore resistance; the pore resistance increases rapidly from the effective pore size. The pore throat is the region of the pore from the effective pore diameter to the capillary tip. The rapid increase in pressure is observed in the entire pore throat. When the pore size is larger than the effective size, there is no throat effect, but when the pore size is less than the effective size, the resistant pressure will increase significantly. There is no smooth connection between these two regions. This observation is different from previous

theory. However, several hundreds of experiments have been conducted and this has been the observation in every experiment. This observation cannot be explained based on current theory, but it is a fact, so effective pore size is used to explain it and distinguish it with the traditional pore throat.

In a natural porous medium where the constriction of the pore occurs at one point, the effective pore size is same as the pore throat. Where the constriction occurs over a length of the pore, the pore throat extends from the effective size to the end of the constriction. This is the case with tapered capillaries. Therefore, in practical terms, the effective size is synonymous with the pore throat.

The next chapter will be devoted to discussions on the pore throat phenomenon. At position C, the CO_2-water interface started coming out of the capillary and the resistant pressure dropped suddenly to position D, as the interface leaves the capillary completely. The reduction in pressure occurs because of a sudden reduction of the excess pressure in the nonwetting phase as the interface leaves the capillary. Also, section CD shows the resistant pressure just before the interface leaves the capillary, when it starts leaving the capillary, and when it completely leaves the capillary. The resistant pressure starts dropping because the capillary which was occupied by the interface is now being taken over by the displacing water as the interface leaves. This indicates also that the resistance offered by the interface is higher than the resistance offered by either water or gas alone. From position D, the resistant pressure starts building up again as the water single phase flows out again, and this increase continues until the water single phase pressure attains the minimum resistant pressure at E. Section EF is a section of constant pressure value for the single phase water flow.

These results using tapered capillaries appear to be similar to the reverse of the result obtained in the Maximum Bubble Pressure Method (MBPM) to determine dynamic surface tension (see 2.5.6.1.1). In the Maximum Bubble Pressure Method, when a bubble grows at the tip of a uniform capillary, its radius of curvature decreases with a corresponding increase in bubble pressure up to a maximum pressure when its radius of curvature is same as the radius of the capillary (hemisphere). The radius then increases again accompanied with a pressure decrease (Figure 2.22). In the reverse MBP experiment, the bubble size in the uniform capillary decreases with a corresponding gradual increase in bubble pressure until the maximum bubble pressure is reached, at which the radius of the bubble equals the radius of the uniform capillary. The bubble pressure starts to decrease as the bubble radius becomes bigger than the uniform capillary radius until the bubble disappears (Figure 2.22).

In our tapered capillary experiment, although the capillary diameter decreases (decreasing interface radius) the interface pressure does not increase correspondingly. As observed in all the experiments, in the beginning section of the capillary where the size decreases appreciably, the resistant pressure remains fairly constant up till the effective pore size. At the effective pore size there is a dramatic increase in resistant pressure, which is linear up to the maximum pressure at the capillary tip. Once the maximum pressure is reached, the pressure drops drastically from maximum to about 0 mbar, as the interface exits the capillary (Figures 4.1b and 4.2b).

Comparing Figures 2.22 and 4.1b or 4.2b, it is observed that the pressure drop in reverse Figure 2.22 is not as drastic as the pressure drop in forward Figures 4.1b and

4.2b, neither are their pressure build-ups the same. The pressure build-up in the reverse MBP experiment is hemispherical, while in our tapered capillary experiment there are two distinct sections of constant pressure and linear increase in pressure. It should be noted also that there is no effect of contact angle on the bubble pressure in MBP experiment, whereas contact angle has a significant influence on the interface pressure in the tapered capillary.

Figure 4.2b shows a similar pressure profile for the CH_4-water interface. The different pressure profile observed for gas-water flow (as compared to single phase water flow) is attributed to the existence of the gas-water interface. The first two sections (0A and AB) are the same as what was measured when the single water phase moved in the capillary. In these first two sections, the gas-water interface was in the larger diameter section of the capillary (Figures 4.4a-f), and the resistant pressure to the flow was the same as what was measured for water flow (Figures 4.1a and 4.2a). The resistance to the gas-water phase was very small in this section and could not affect the overall profile. This may be the reason for wrongly applying the single phase pressure for two-phase pressure. However, when the gas-water interface reached point B (Figures 4.1b and 4.2b) where the pore diameter has reduced considerably (Figure 4.4g), about 206 μm for CO_2-water and 190 μm for the CH_4-water, the resistant pressure increased significantly. This is very different from the pore resistance to single water phase. We can conclude that the pore resistance to single water phase flow is quite small and that the resistance to interface is significantly higher than the resistance to single phase.

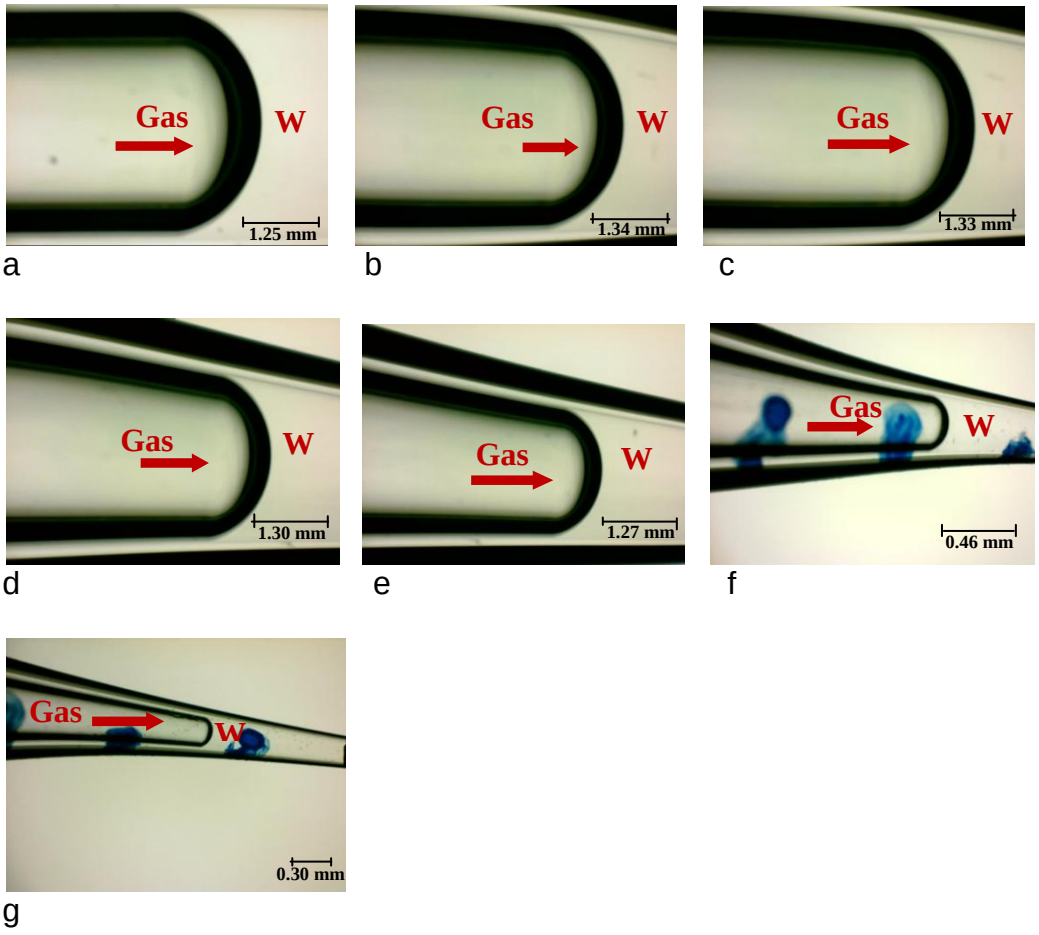

Figure 4.4: Approximate positions in micropipette of the initiation of the phenomenon shown in Figures 4.1b and 4.2b (tube internal diameter at inlet = 4.0 mm; interface diameter at inlet= 4.0 mm; W = water).

a) Start of displacement: gas-water interface is in the unstretched section of the tube (Position 0).

b) Motion of interface has started with the discharge of water after initial pressure build-up (0A). Interface is at the neck of the tube.

c) Interface has advanced further into the constricted section of the tube and interface motion has started to maintain a constant pressure from about this position (AB).

d) Interface just leaving the tube neck. Interface motion continues with constant pressure (AB).

e) Interface approaching start of capillary. Interface motion continues with constant pressure (AB)

f) Interface now moving in the capillary and has continued to maintain a constant pressure (AB).

g) Interface at the effective pore size. Sudden increase in pore resistant pressure begins (start of section BC).

The resistance to the interface movement through the capillary,ΔP, is the algebraic sum of the capillary resistance and the resistance from the viscosity force (Chatzis and Dullien, 1983).

$$\Delta P = \Delta P_c + \Delta P_v \quad (4.1)$$

where ΔP_c is the capillary pressure drop and ΔP_v is the viscous pressure drop. The magnitude of the viscous pressure drop is given by the application of the Hagen-Poiseuille (H-P) equation (Stegemeier, 1974):

$$\Delta P_v = \frac{128 q \mu l}{\pi D^4} \quad (4.2)$$

where D is the diameter of the capillary, l is the length of the flow path, μ is the viscosity of the fluid, and q is the volume flow rate.

For laminar flow, the viscosity μ of the fluid is defined as:

Viscosity = Shear stress/Strain rate

$$\mu = \frac{F/A}{v/l} \quad (4.3)$$

Rearranging Eq. 4.3,

$$F = \mu A \frac{v}{l} \quad (4.4)$$

Therefore, from Eq. 4.4 the force required for the motion is directly proportional to the viscosity of the fluid and velocity. The viscosities of water, air, CO_2, and CH_4 at ambient conditions are 1 cp (1 mPa.s), 18.27 μPa.s, 14.8 μPa.s, and 10.27 μPa.s, respectively, and are very small and negligible. Also, for very slow rate of displacement the velocity of the interface is very small. Therefore, the contribution of the viscosity force to the resistance to the motion of the interface is very small and negligible compared to the contribution by capillary resistance. Capillary force, therefore, is the main force responsible for the movement of the interface through the

capillary. The measured pressure, therefore, is equivalent to the capillary resistance to the two-phase flow. The magnitude of the capillary pressure across the interface boundary is given by the Young-Laplace equation (Equation 2.1).

As described by Li *et al* (2005), as the external force from the delivery pump is increased the pressure equilibrium across the gas-liquid interface is broken. That is, the differential pressure (Pnw – Pw) exceeds the resistance of the capillary, hence the nonwetting phase (gas) advances until it reaches a smaller section of the capillary where the differential pressure is balanced by a larger resistance (Figure 4.5).

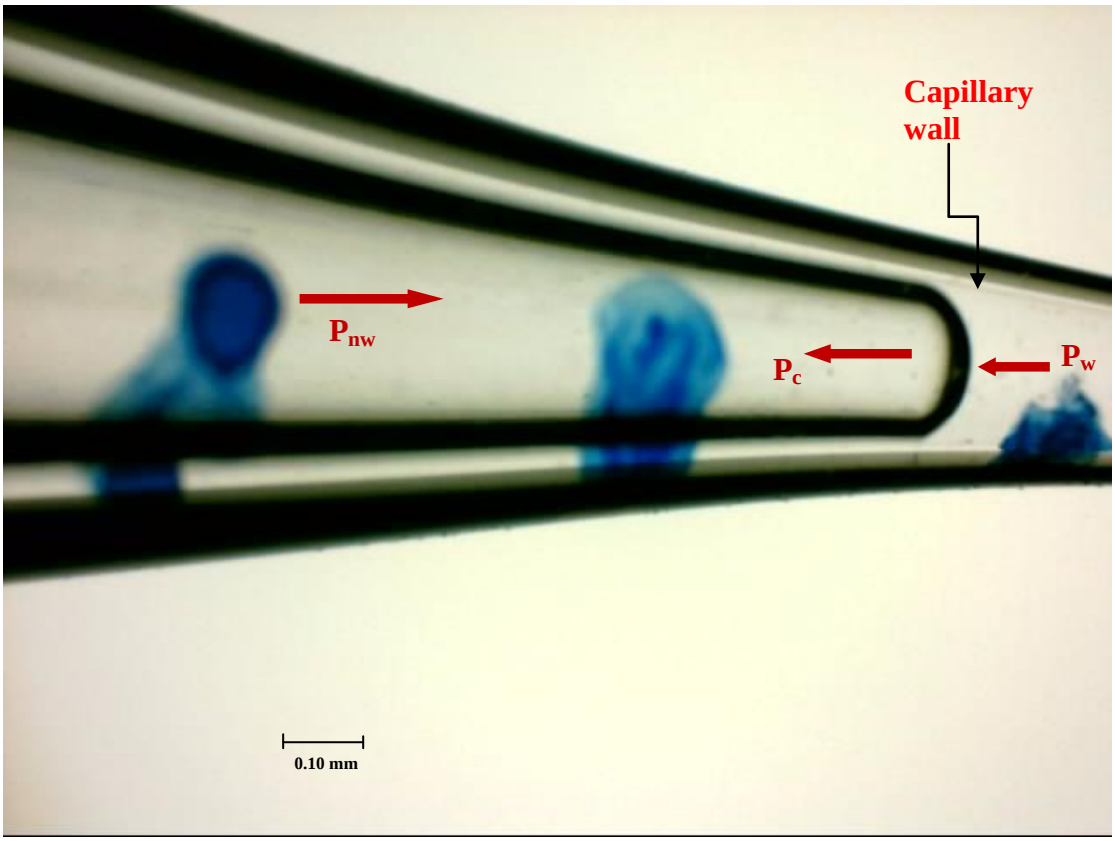

P_{nw} = pressure in the nonwetting phase
P_w = pressure in the wetting phase
P_c = capillary resistance across the nonwetting/wetting meniscus in the pore

Figure 4.5: Forces acting on an interface as it moves through a capillary

At this point the movement of the nonwetting phase is slowed down. This process is repeated as the pressure from the pump is increased until the interface is able to move through the smallest section of the capillary and the interface comes out. There is always a trace of water production at the capillary end, for each advancement of the interface. For larger capillary sizes the water production could easily be observed but for smaller capillaries it may not be observed since the amount of water in the pore space is small.

In the reservoir rock where there are interconnected pores of varying sizes, the same process takes place until the interface breaks through the smallest interconnected channel and then the gas begins to escape. This pressure is known as the breakthrough pressure.

4.2.1 Effect of gas type on the resistant pressure profile

In order to study the effect on pressure profile of the gas type used to create an interface, a micropipette was used to displace the air-water, CO_2-water, and CH_4-water interfaces, one after the other, respectively. A starting point of the displacements was marked on the micropipette and after each displacement the micropipette was thoroughly cleaned with deionized water and dried before re-use. It was important to use the same capillary so as to ensure that all the displacements took place in exactly same geometry. (Capillaries of same tip size may have different gradients and alter the geometry)

The resistant pressure profiles for air-water, CO_2-water, and CH_4-water, interface motion through a micropipette of tip size 105 μm (capillary gradient: 8.25×10^{-3}) are shown in Figure 4.6. All the interfaces show similar profiles as in Figures 4.1b and

4.2b, but their maximum resistant pressures are different and the positions of their effective pore diameter are slightly different. The air-water interface maximum resistant pressure was 49.7 mbar, while CO_2-water interface maximum pressure was 40.1 mbar, and CH_4-water maximum was 50.1 mbar. The results show that the resistant pressure varies slightly with the gas applied.

Hildenbrand *et al* (2004) observed differences in the breakthrough pressures of N_2, CO_2, and CH_4, in cylindrical sample plugs and attributed the differences to both, differences in the interfacial tension and contact angle of the three gases. Nitrogen had the highest displacement pressure with N_2-water interfacial tension of 110-135 mN/m, followed by CH_4 with CH_4-water interfacial tension of 66 mN/m, and the lowest displacement pressure was exhibited by CO_2 with CO_2-water interfacial tension of 42 mN/m, under the experimental conditions. They argued that for measurements performed on the same rock sample with different gases, it is implied from the Washburn equation that the observation of a lower capillary entry pressure for a certain gas is a result of a lower interfacial tension and/or a lower cos (θ) value. Although the experiments were performed under slightly different conditions, using statistical analyses and assuming a contact angle of zero (complete wetting) they concluded that the observed differences was due to the differences in their interfacial tension. Li et al (2005) also illustrated that the change of breakthrough pressure for N2/water, CO2/water and CH4/water is nearly proportional to the change in their interfacial tensions.

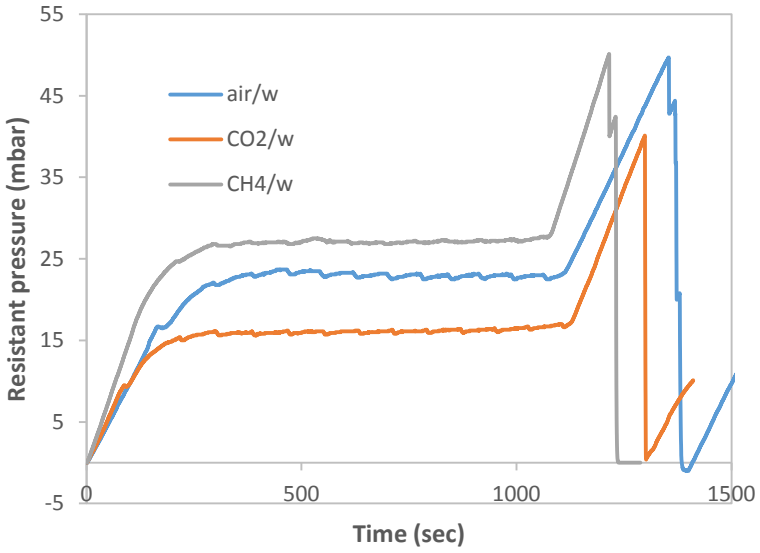

Figure 4.6: Resistant pressure profiles for air-water, CO_2-water, and CH_4-water interfaces in a tapered capillary (tip size: 105 µm; pore gradient: 8.25 × 10^{-3}).

The air-water interfacial tension is 72 mN/m at ambient conditions (23 ^{o}C, 1 atm), CO_2-water interfacial tension is 65 mN/m (Espinoza and Santamarina, 2010) and that of CH_4-water is 72-75.5 mN/m (Jennings and Newman, 1971; Hough *et al*, 1951). CH_4-water interfacial tension is higher than air-water and CO_2-water interfacial tensions under ambient conditions; the breakthrough pressure is therefore highest. This result supports experimentally the earlier observations by Hildenbrand *et al* (2004) and Li *et al* (2005). The influence of the gas type on the pore throat phenomenon will be investigated in the next chapter.

4.2.2 Effect of pore tip size and capillary gradient on resistant pressure profile

The effects of pore tip size and capillary gradient on the pressure profiles were studied by measuring the pressure profiles of the interface displacement through

tapered capillaries of varying tip sizes of about 100 µm to 300 µm with varying capillary gradient for the three gas-water interfaces. The capillary gradient of the tapered capillaries used varied between 6.89×10^{-3} and 1.65×10^{-2}.

Figures 4.7 to 4.9 show the resistant pressure profiles for air-water, CO_2-water, and CH4-water. Each profile shows a section of constant resistant pressure (balanced pressure), a point of sharp departure from the constant pressure and a linear increase in pressure, a point of maximum resistant pressure followed by a sharp decline in resistant pressure.

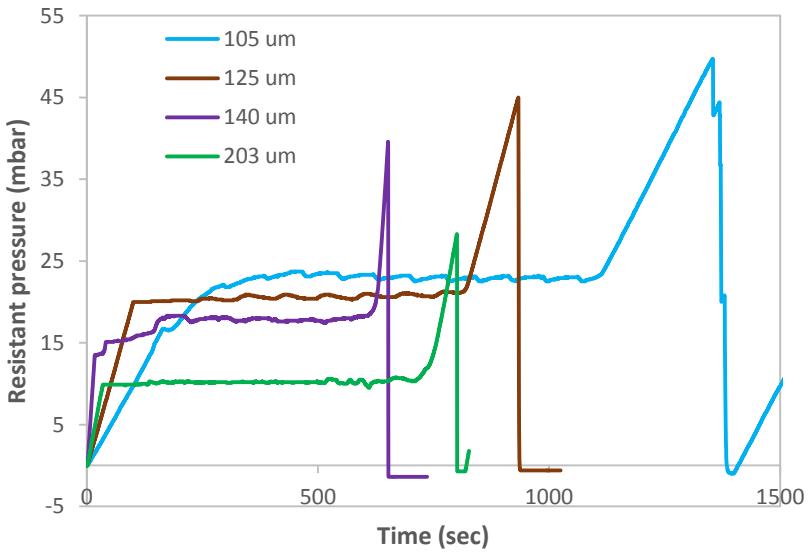

Figure 4.7: Resistant pressure profile for air-water displacement through capillaries of different tip sizes/capillary gradients (105 µm/8.25×10^{-3}; 125 µm/9.69×10^{-3}; 140 µm/1.16×10^{-2}; 203 µm/1.63×10^{-2}).

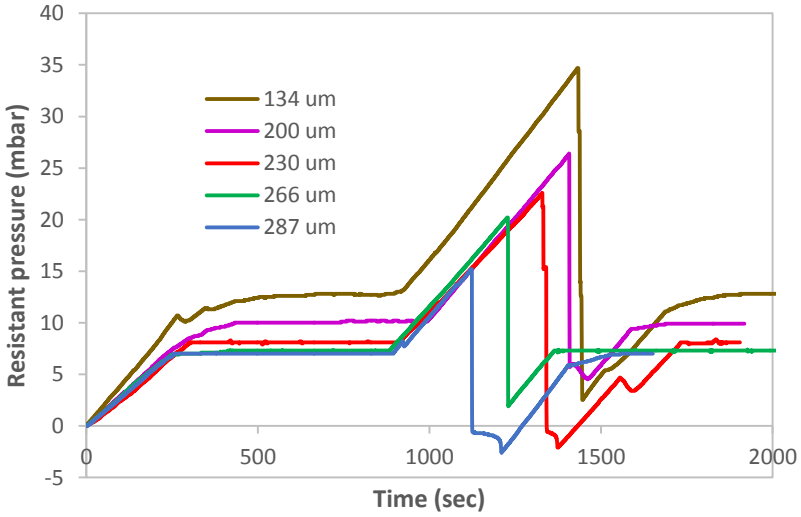

Figure 4.8: Resistant pressure profile for CO_2-water displacement through capillaries of different tip sizes/capillary gradients (134 µm/6.89 × 10^{-3}; 200 µm/1.35 × 10^{-2}; 230 µm/1.36 × 10^{-2}; 266 µm/1.52 × 10^{-2}; 287 µm/1.65 × 10^{-2}).

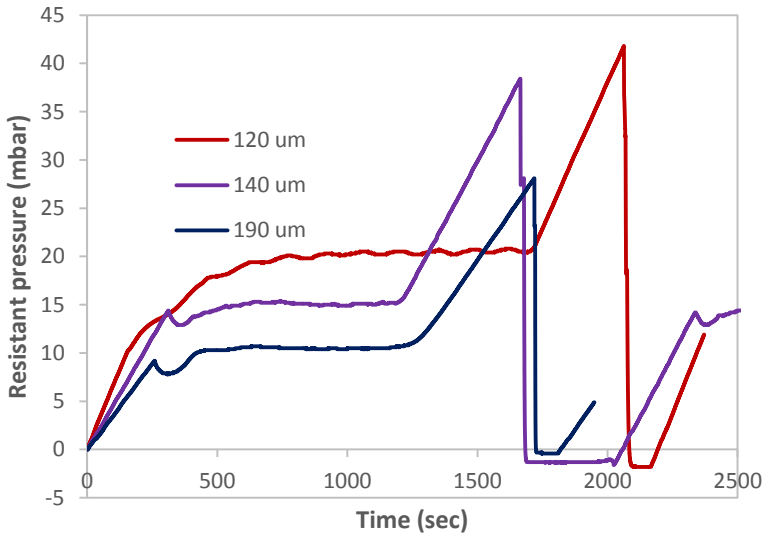

Figure 4.9: Resistant pressure profile for CH_4-water displacement through capillaries of different tip sizes/capillary gradients (120 µm/8.21 × 10^{-3}; 140 µm/9.05 × 10^{-3}; 190 µm/1.46 × 10^{-2}).

Our pressure profiles show a similar trend with the profiles obtained by conventional continuous injection approach method for measuring threshold capillary pressure of

heterogeneous rocks at in situ conditions (Figure 4.10) (Egermann *et al*, 2006; Rudd and Pandey, 1973). Pressure increased as the injection fluid moved from the coarse sandstone segment (Sample 1) to a finer grained siltstone (Sample 2) in an artificially laminated core sample and then decreased in the coarser sandstone segment (Sample 3).

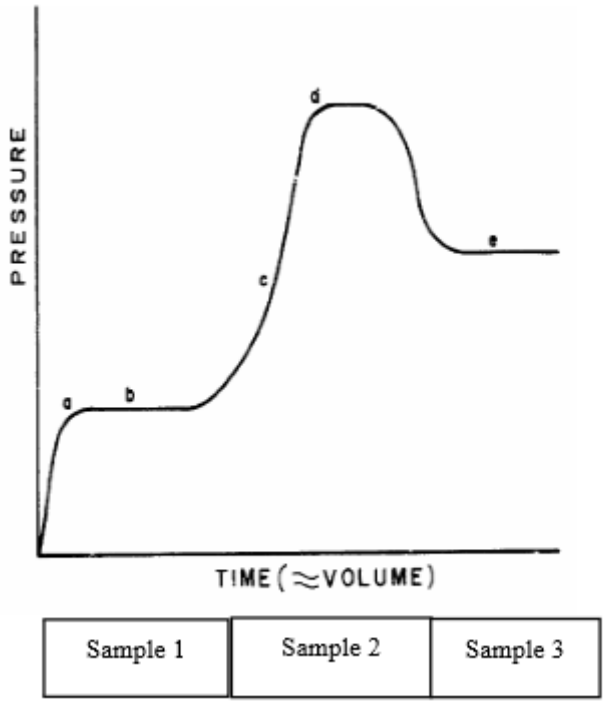

Figure 4.10: Pressure evolution as a function of time with continuous injection approach for a composite laminated core (Rudd et al., 1973).

Rose and Bruce (1949), McCreesh *et* al (1991), and Nelson (2009) have observed that the shape of the mercury injection curve (capillary pressure curve) may be primarily affected by the pore size. Chains of pores connected by the largest throats are penetrated first (at lower pressures), being the path of least resistance, followed by pores with smaller throats at higher pressures and then the pores with the smallest throats are filled with mercury at highest pressures. Nuclear Magnetic Resonance

(NMR) on samples of sandstones also show that macro pores fill at lower pressures (200-1000 psi), but the micro pores fill at very high pressures (1000 psi or greater**)** (Bowers *et al,* 1995). These indicate that pore size influence hydraulic resistance to flow and the pressure profile. Brown (1989) also made a similar observation of increased resistance to flow at reduced aperture by showing that the electrical resistance of a fracture saturated by a single conducting fluid is determined by the geometrical structure of the aperture field. He showed that the electrical aperture of fractures with fractal wall surfaces was lower than that for parallel plane walls of comparable size and distance, leading to a decrease in electrical resistance. This results from the increased tortuosity of the iso potential lines through the fractal wall surfaces (Boschan *et al,* 2011). Wenzel (1936) is of the view that the increase in the resistant pressure at the effective pore size could be attributed to increase in the roughness of the surface caused by thin film of liquid (water) on the walls of the capillary. The increased surface area to flow in this section coupled with the imposed roughness increase the surface energy, the contact angle, and hence the resistant pressure. The relationship between resistant pressure, surface energy and contact angle will be investigated further in Chapter 6.

4.3 Resistance to single phase flow and two-phase flow

Comparing the sections of the tapered capillary (micropipette) before and after the effective pore diameter, we have observed that the resistant pressure of the interface before the effective size is similar to the resistant pressure due to single phase water flow. However, in contrast to the single phase water flow, after the effective pore diameter the resistant pressure of the interface departs remarkably. This indicates that

pore size has a significant effect on the resistance to the interface compared to the resistance to the single phase.

4.4 Effect of pore size on resistant pressure in a tapered capillary

To study the variation of resistant pressure with the interface motion in a tapered capillary, the motion of the interface front was observed by viewing it horizontally with the optical microscope. The positions of the interface along the capillary were captured with the digital camera and the images were processed to obtain the corresponding diameter and pressure.

Figure 4.11 shows the variation of resistant pressure with pore size for an interface motion through a tapered capillary, for four different capillaries of pore tip sizes 115 µm, 140 µm, 190 µm, and 220 µm.

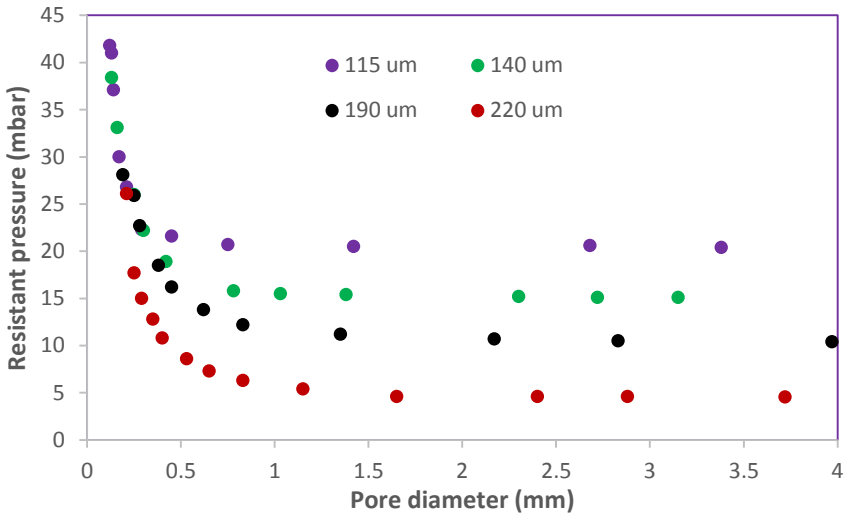

Figure 4.11: Change of resistant pressure with pore size in a tapered capillary for CH_4-water displacement.

It can be observed that for all the capillaries the resistant pressure (pressure across the interface of two immiscible fluids) is inversely proportional to the pore radius according to the Young-Laplace equation (Li et al, 2006). However, we observed that the resistance to single phase and interface is the same before the effective pore diameter but differ remarkably after the effective pore diameter. At the effective pore size the resistant pressure to interface is much higher than the resistant pressure to the single phase. The implication of this is that the Young-Laplace equation may not be applicable below the effective pore size for a two-phase flow.

In order to compare our measured single and two-phase resistances with theoretical two-phase resistance, the theoretical resistant pressures for air-water, CO_2-water, and CH_4-water interfaces in different pore sizes and capillary gradients were calculated using the Young-Laplace equation (Eq.2.1) (Tables 4.1 to 4.3). Figures 4.12 to 4.14 show comparisons between the theoretical resistant pressure and experimental resistant pressures for air-water, CO_2-water, and CH_4-water, interfaces, respectively.

Table 4.1: Resistant pressure from Young-Laplace equation for air-water interface

Pore tip diameter, d (µm)	Pore tip radius, R (µm)	Measured effective pore diameter dexp (µm)	Measured two-phase pressure Pmax (mbar)	Measured single phase pressure Pbal (mbar)	Pore length from effective diameter to pore tip l, (mm)	Capillary gradient (dimensionless)	Calculated interface pressure (Young-Laplace) Pcal (mbar)
105	52.5	180	49.7	23.04	9.09	0.008250825	24.49371429
111	55.5	205	46.5	21.98	13.12	0.007164634	23.16972973
125	62.5	226	45	20.65	10.42	0.009692898	20.57472
128	64	243	42.3	18.07	13.94	0.008249641	20.0925
140	70	278	39.6	17.95	11.85	0.01164557	18.37028571
157	78.5	305	31	15.7	13.61	0.010874357	16.3811465
167	83.5	320	27.6	11.57	16.3	0.009386503	15.40023952
170	85	338	27.5	11.2	15.12	0.011111111	15.12847059
184	92	368	27.2	10.73	13.7	0.013430657	13.9773913
203	101.5	442	26.3	10.13	14.64	0.016325137	12.66916256
216	108	453	24.9	9.89	17.09	0.013867759	11.90666667
230	115	486	23.9	8.09	17.06	0.015005862	11.18191304

Table 4.2: Resistant pressure from Young-Laplace equation for CO_2-water interface

Pore tip diameter, d (µm)	Pore tip radius, R (µm)	Measured effective pore diameter dexp (µm)	Measured two-phase pressure Pmax (mbar)	Measured single phase pressure Pbal (mbar)	Pore length from effective diameter to pore tip ļ (mm)	Capillary gradient (dimensionless)	Calculated interface pressure (Young-Laplace) Pcal (mbar)
105	52.5	171	45.1	20.85	8.06	0.008188586	22.23619048
111	55.5	198	43.7	19.6	12.61	0.006899286	21.03423423
125	62.5	223	43	18.27	10.18	0.009626719	18.6784
128	64	241	42	17.76	13.45	0.008401487	18.240625
140	70	264	39	15.1	11.24	0.011032028	16.67714286
157	78.5	292	28.9	10.59	12.21	0.011056511	14.87133758
167	83.5	293	26.6	8.71	15.51	0.008123791	13.98083832
170	85	314	25.6	8.3	14.45	0.009965398	13.73411765
180	90	358	25.1	8.25	14.09	0.012633073	12.97111111
184	92	355	24.9	8.2	12.97	0.013184271	12.68913043
203	101.5	398	24.3	8.1	14.48	0.013466851	11.50147783
230	115	450	22.5	8	16.21	0.013571869	10.15130435

Table 4.3: Resistant pressure from Young-Laplace equation for CH_4-water interface

Pore tip diameter, d (µm)	Pore tip radius, R (µm)	Measured effective pore diameter dexp (µm)	Measured two-phase pressure Pmax (mbar)	Measured single phase pressure Pbal (mbar)	Pore length from effective diameter to pore tip l, (mm)	Capillary gradient (dimensionless)	Calculated interface pressure (Young-Laplace) Pcal (mbar)
105	52.5	191	50.1	25.08	11.12	0.007733813	24.90780952
111	55.5	200	47.1	22.8	12.85	0.00692607	23.56144144
125	62.5	228	45.8	19.44	10.67	0.009653233	20.92256
128	64	248	43.6	18.92	14.6	0.008219178	20.4321875
140	70	253	40.5	16.8	12.48	0.009054487	18.68085714
157	78.5	283	31.2	16.6	14.36	0.008774373	16.65808917
167	83.5	295	28.8	13.3	16.3	0.007852761	15.6605988
170	85	338	28.2	12.1	15.12	0.011111111	15.38423529
184	92	389	27.9	10.83	14.06	0.01458037	14.21369565
203	101.5	447	27.7	10.26	14.82	0.016464238	12.88334975

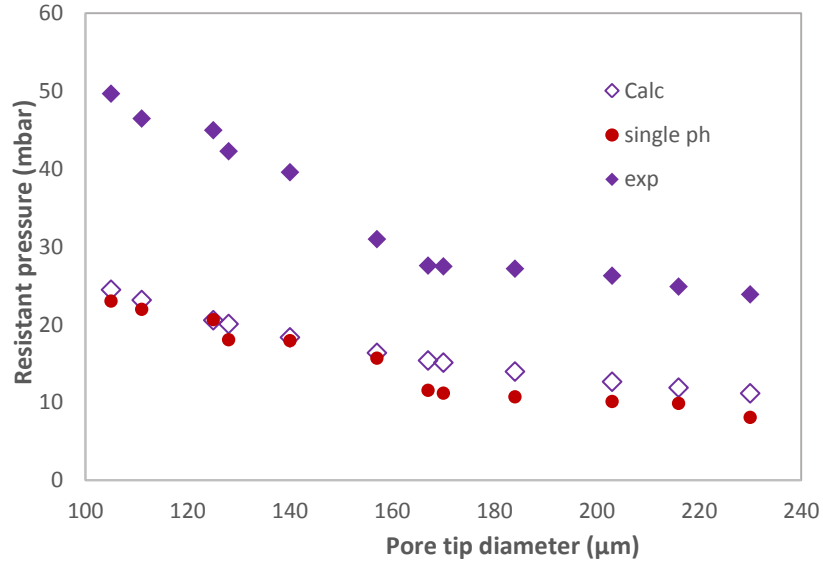

(a)

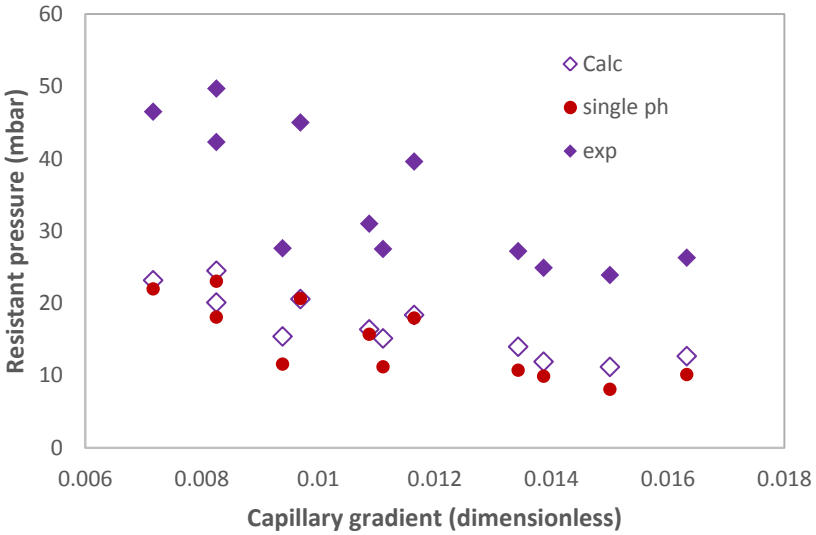

(b)

Figure 4.12: Comparison of measured resistant pressures with theoretical resistant pressure for air-water interface at ambient conditions

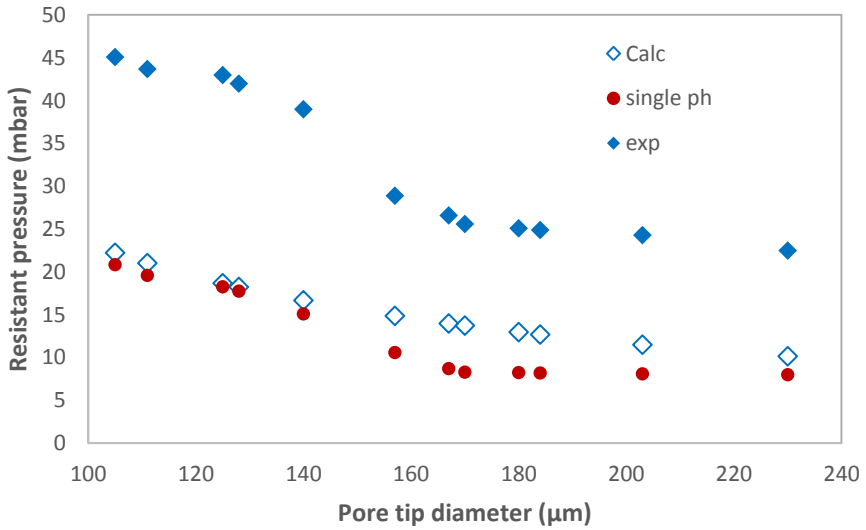

(a)

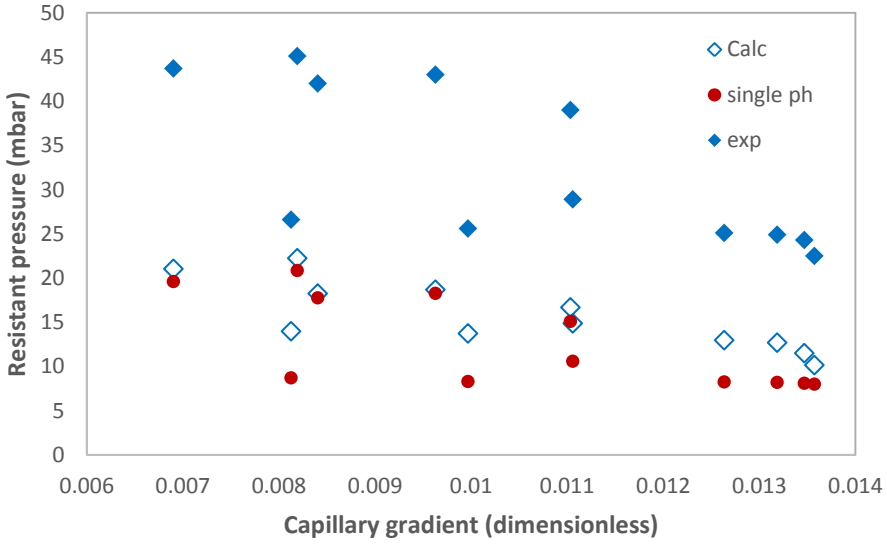

(b)

Figure 4.13: Comparison of measured resistant pressures with theoretical resistant pressure for CO_2-water interface at ambient conditions

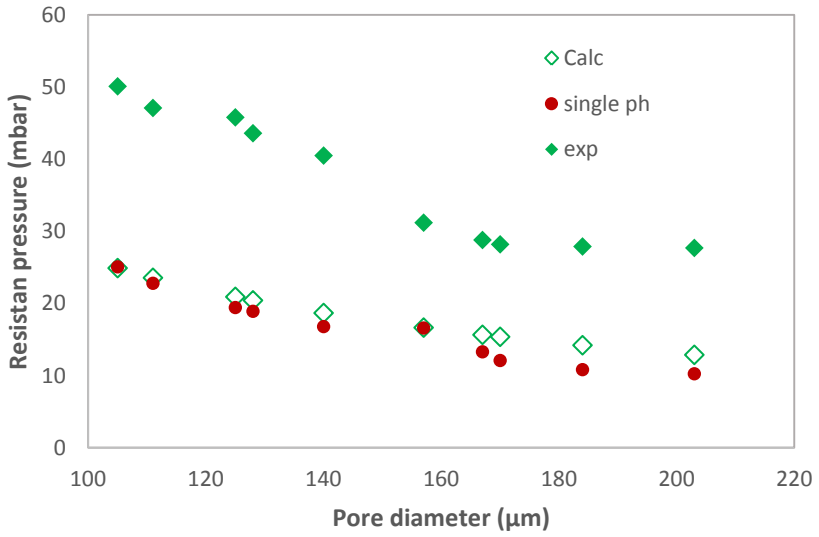

(a)

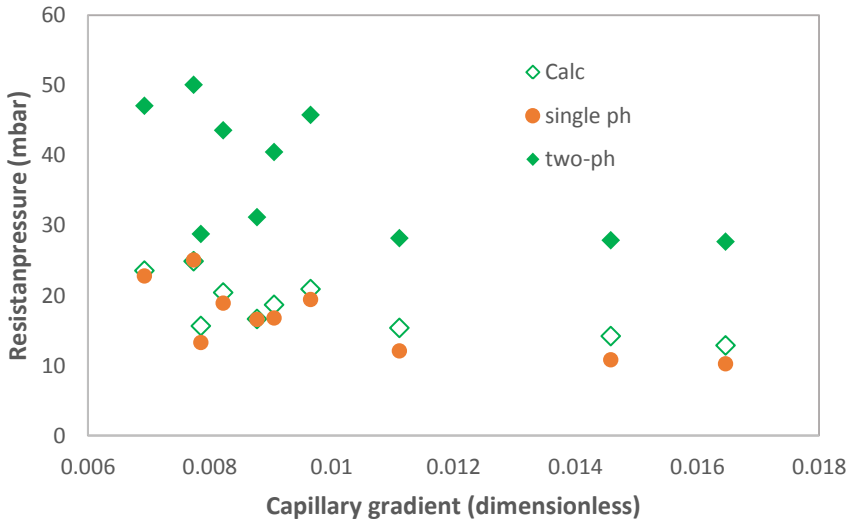

(b)

Figure 4.14: Comparison of measured resistant pressures with theoretical resistant pressure for CH_4-water interface at ambient conditions.

All the figures show that for any pore tip diameter or capillary gradient the measured resistance to two-phase flow is much higher than the predicted two-phase resistance using the Young-Laplace. The values of the predicted two-phase resistant pressures are rather very close to the measured resistance to single phase flow as shown in the

figures. We have shown experimentally that when the single phase moves through the capillary, the resistant pressure remains constant, and does not increase. However, the resistance to the interface is very different from the single phase resistance; it increases significantly when the interface reaches the effective pore diameter. It is, therefore, difficult to predict the interface resistance in capillaries by Young-Laplace equation. It becomes very important to clearly understand the factors that influence the resistance and the effective pore diameter.

The difference in the measured two-phase resistance and the theoretical Young-Laplace two-phase resistance generally increases as the pore diameter or capillary gradient decreases. This indicates that as capillary effect becomes significant the Young-Laplace equation becomes weaker in the prediction of resistance to two-phase flow. Our results also indicate that the resistances calculated for multiphase flow in capillaries in literature may not be true in all cases; they may have been over-simplified by using the resistances for single phase flow. This needs to be further investigated. This study has shown that for the tapered capillaries considered the effective pore size lies below 500 μm, approximately 300 μm, irrespective of the pore tip size (Figure 4.11). This diameter corresponds to the pore size about which the contact angle becomes fairly constant as reported by Li *et al* (2013, 2014).

4.5 Summary

In this chapter the resistant pressure profiles for gas-water interfaces have been presented and explained. The measured resistant pressures have been compared with the theoretical resistant pressures using the Young-Laplace equation. The results indicate the following:

1. A drastic increase in resistant pressure occurs at the effective pore size which marks the beginning of the pore throat effect. When the pore size is less than the effective size, no throat effect occurs, but when pore size is less than the effective size there is throat effect characterised by the increased resistance. This observation cannot be explained based on current theory, but this is true for several hundreds of experiments conducted.

2. The pressure profiles for single phase flow and interface flow are similar for higher tube sizes but are significantly different as the tube sizes decreases to approximately 500 to 300 μm. Similarly, the pressure drop for larger diameter tubes are similar for both cases but are completely different for smaller diameters where capillary effects become prominent.

3. Measured resistance to single phase flow is different from resistance to two-phase flow. Both resistances are same before the effective diameter, but differ remarkably at the effective pore size; the two-phase resistance becomes much higher than the single phase pressure.

4. The maximum resistance to interface (breakthrough pressure) depends on the type of gas used and varies with the interfacial tension of the gas. Resistance increases with increase in interfacial tension of the gas.

5. Young-Laplace equation may not be sufficient to account for two-phase resistant pressure in smaller tube sizes where capillary effect becomes significant.

4.6 References

Boschan, A., I. Ippolito, R. Chertcoff, J.P. Hulin, and H. Auradou, 2011. Characterization of fracture aperture field heterogeneity by electrical resistance measurement. Journal of Contaminant Hydrology 123 (2011) 65–74.

Bowers, M.C., R. Ehrlich, J.J. Howard, and W.E. Kenyon., 1995. Determination of porosity types from NMR data and their relationship to porosity types derived from thin section. Journal of Petroleum Science and Engineering 13 (1995) 1-14.

Brown, S. R., 1989. Transport of fluid and electric current through a single fracture. J. Geophys. Res., 94 (1989), pp. 9429-9438.

Chatzis, I. and Dullien, F. A. L., 1983. Dynamic Immiscible Displacement Mechanisms in Pore Doublets: Theory versus Experiment. J. of Colloid and Interface Science, Vol. 91, No. 1, January 1983.

Egermann, P., Lombard, J. M., and Bretonnier, P., 2006. A fast and accurate method to measure threshold capillary pressure of caprocks under representative conditions. Paper SCA2006-07 presented at the International Symposium of the Society of Core Analysts held in Trondheim, Norway, 12-16 September.

Espinoza, D. N., Santamarina, J. C., 2010. Water-CO2-mineral systems: Interfacial tension, contact angle, and diffusion – Implications to CO2 geological storage. Water Resources Research, Vol. 46, W07537, 1-10.

Hildenbrand, A., Schlömer, S., Kroos, B. M., and Littke, R., 2004. Gas breakthrough experiments on pelitic rocks: comparative study with N_2, CO_2 and CH_4. Geofluids (2004) 4, 61 – 80.

Hough, E. W., Rzasa M. J., and Wood, B. B., 1951. Interfacial tensions at reservoir pressures and temperatures; apparatus and the water-methane system. Petroleum Transactions, AIME, Vol. 192, 1951, 57- 60.

Jennings Jr., H. Y., and Newman, G. H., 1971. The Effect of Temperature and Pressure on the Interfacial tension of water against methane-Normal Decane Mixtures. Soc. Petrol. Eng. J. June 1971, 171-175.

Li, S., Dong, M., Li, Z., Huang, S., Qing H. and Nickel, E., 2005. Gas breakthrough pressure for hydrocarbon reservoir seal rocks: implications for the security of long-term CO_2 storage in the Weyburn field. Geofluids (2005) 5, 326-334.

Li, Zhaowen, Dong, Mingzhe, Li, Shuliang, Huang, Sam, 2006. CO_2 Sequestration in Depleted Oil and Gas Reservoirs – Caprock Characterization and Storage Capacity. Energy Convers Manage 47 (2006) 1372 – 1382.

Li Xingxun , Xianfeng Fan, Alexandros Askounis , Kejian Wu , Khellil Sefiane , Vasileios Koutsos., 2013. An experimental study on dynamic pore wettability. Chemical Engineering Science 104 (2013) 988–997.

Li Xingxun, Xianfeng Fan, Stefano Brandani, 2014. Difference in pore contact angle and the contact angle measured on a flat surface and in an open space. Chemical Engineering Science 117(2014)137–145.

McCreesh, C. A., Ehrlich, R. and Crabtree, S.J., 1991. Petrography and reservoir physics II: relating thin section porosity to capillary pressure, the association between pore types and throat size. Am. Assoc. Pet. Geol. Bull., 75(10): 1563-1578.

Nelson, Philip H, 2009: Pore-throat sizes in sandstones, tight sandstones, and shales, AAPG Bulletin, v. 93, no. 3 (March 2009), pp. 329–340.

Rose, W. D. and Bruce, W. A., 1949. Evaluation of capillary character in petroleum reservoir rock. Trans., AIME (1949) 186, 127.

Rudd, N., and Pandey, G. N., 1973. Threshold pressure profiling by continuous injection. Paper SPE 4597 presented at the 1973 Annual Technical Conference and Exhibition held in Las Vegas, Nevada, 30 September-3 October.

Stegemeier, G. L., 1974. Relationship of trapped oil saturation to petrophysical properties of porous media. Paper SPE 4754, presented at the SPE-AIME Improved Oil Recovery Symposium, Tulsa, OK, April 22-24, 1974.

Washburn, E.W., 1921. Note on a method of determining the distribution of pore sizes in a porous material. Proceedings of the National Academy of Science, 115–116.

Wenzel, Robert N.: Resistance of Solid Surfaces to Wetting by Water. Industrial and Engineering Chemistry, August 1936, Vol. 28, No.8, pp. 988-994.

Chapter 5: Pore throat and flow resistance

5.1 Introduction

Pore throat in conventional, tight, and shale gas reservoirs, is a term used to identify hydraulic flow units (Ziarani and Aguilera, 2012). A hydraulic flow unit is the representative elementary volume of the total reservoir rock in which the geological and petrophysical properties that affect fluid flow are internally consistent and predictably different from the properties of other rock volumes (Hearn, 1984; Ebanks, 1987; Amaefule *et al,* 1993; Tiab and Donaldson, 2004). Each hydraulic flow unit can be characterized by an approximate range of pore throat (port) size, so that fluid flow properties are uniform.

Many studies of the porous media fluid displacement on core samples have not been able to unravel completely the mechanisms involved, because the fundamental behaviours of multiphase porous media systems are governed by the physical processes acting at the pore scale (Al-Raoush and Wilson, 2005). With the current research focus on pore level displacements, the definition and interpretation of the pore throat seem not to be clear. It is believed that a clearer definition and a better understanding of the displacement phenomena in a pore will help to improve the understanding of pore level processes such as in enhanced oil recovery beyond current limits. This will ultimately alleviate a number of issues related to global energy supply, and also help in making accurate assessments of the leakage risks of

stored CO_2. In this study we try to give a clearer understanding of the definition of the pore throat based on hydraulic resistance to fluid flow in a pore.

5.2 Effective pore size identification

Pore throat definition by mercury injection porosimetry, which is the usual experimental method to determine pore throat size, has a wide range of sizes for the pore throat. Although the significant effect of pore structure and pore geometry on fluid displacement is recognised by this method, it does not include the exact influence of the internal structure of the pore in the identification and estimation of the pore throat. In order to include the internal geometry of a pore and have a unified definition, we propose to define the pore throat based on the pore resistance to fluid displacement.

In a single pore we define the effective pore size as the pore size at which a sudden increase in resistance to interface motion occurs, marking the beginning of the pore throat. The pore throat starts from the effective pore size and ends at the narrowest section of the pore (that is, pore size less than the effective pore size). The pore throat is then defined to be the region of increased hydraulic resistance to interface motion through the pore. In this chapter we demonstrate experimentally that force resistance measurements may provide useful information in identifying the effective pore size and consequently the pore throat, estimating it, and predict its impact on fluid displacement. The pore throat diameters of single tapered capillaries (micropipettes) are identified and measured by using the resistance to interface flow measurement technique described earlier in Chapter 4. The effects of pore tip

size/pore gradient, surface tension, and viscosity on the pore throat diameter are investigated.

To identify the effective pore size, the resistant pressure profile of gas-water interface displacement through a single tapered capillary (micropipette) was measured for a period of time. The gas-water interface was created by introducing 0.1 ml of the gas into the micropipette already filled with deionized water.

Figure 5.1 is a typical pressure profile for driving a gas-water interface through a tapered capillary. This is a case of CO_2-water in a tapered capillary with a tip size of 150 µm (capillary gradient = 4.762×10^{-3}). It shows that the resistant pressure profile is completely different from the profile when only single phase water flows through the same capillary as shown in Chapter 4.

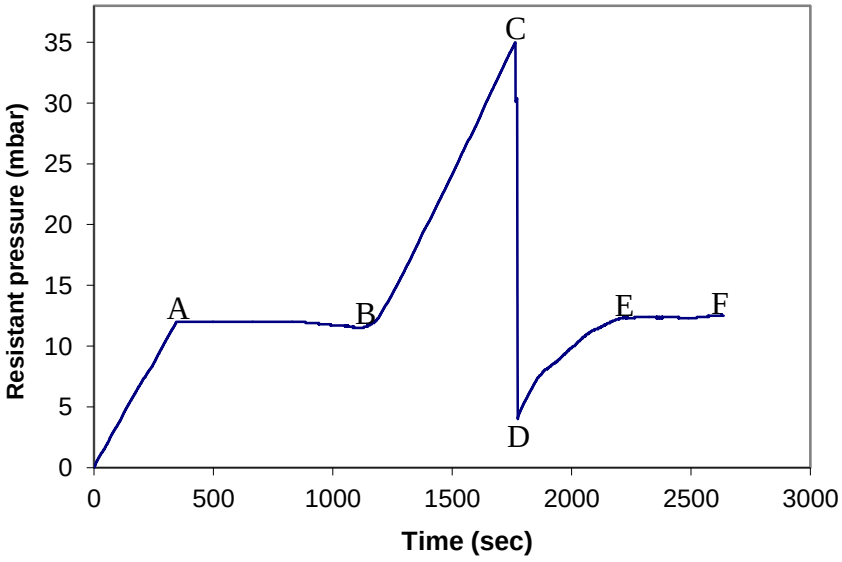

Figure 5.1: Resistant pressure profile of CO_2-water interface flow through a tapered capillary with a tip size of 150 µm (capillary gradient: 4.762×10^{-3}).

It is observed that the pressure increased initially from 0 to about 12 mbar at position A and remains approximately constant at this pressure up to position B. At position B the resistant pressure increased suddenly indicating an increase in hydraulic resistance to flow.

Position B is the position of the effective size of the capillary and the starting point of the pore throat. As the capillary is tapered with a gradient, and the hydraulic diameter decreases towards the tip, the resistant pressure continues to increase linearly up to position C, the tip of the capillary. BC corresponds to the distance from the effective size to the capillary tip, which is the pore throat length. CD is the section of the pore indicating a divergence in the pore size after the pore throat. The resistant pressure drops drastically because of this divergence in pore size. There is no further pore throat phenomenon from this section and the system attains the single phase resistant pressure profile in section EF. The phenomenon responsible for the resistance pressure profile is thought of as being the reverse of maximum surface pressure phenomenon in the determination of dynamic surface tension. However, both phenomena are slightly different because of the difference in the geometry of both systems as explained earlier (sec 4.2).

Figure 5.2 shows a comparison pressure profile for air-water, CO_2-water, and CH_4-water interface motions through a tapered capillary with a tip size of 105 µm and a gradient of 8.25×10^{-3}. The displacements of all the interfaces were started at a marked position in the micropipette, one after the other. All the interfaces show a similar profile; there is always a point of initiation of a marked increase in resistant pressure, which is the effective size and beginning of the pore throat. Figure 5.2

shows that the beginning of the pore throat phenomenon is slightly different for the three interfaces, suggesting that the composition of the interface can influence the effective pore size. Pore throat phenomenon sets off with CH_4-water interface earliest in the tapered capillary, followed by air-water interface and then the CO_2-water interface.

The Young-Laplace equation (Eq. 2.1) shows that the parameters influencing the resistant force to interface displacement are interfacial tension, contact angle and effective pore radius. The difference in the effective pore size (initiation of the pore throat phenomenon) exhibited by the three interfaces can be accounted for by the difference in their interfacial tensions. The interfacial tension of CH_4-water at ambient conditions is highest and that of CO_2-water is least. Therefore, the resistance to interface displacement is highest with CH_4-water interface, while that of the CO_2-water system is lowest in the same tapered capillary (Figure 5.2), according to the Young-Laplace equation. In the flat region of Figure 5.2 (section preceding the effective pore size) the contact angle is increasing (as will be shown in Chapter 6) and this is balanced by the decreasing pore size, hence, the resistant pressure remains constant in this region. From the effective pore size and through the entire pore throat, the contact angle remains fairly constant and the dominant factors on the resistance are the interfacial tension and pore size.

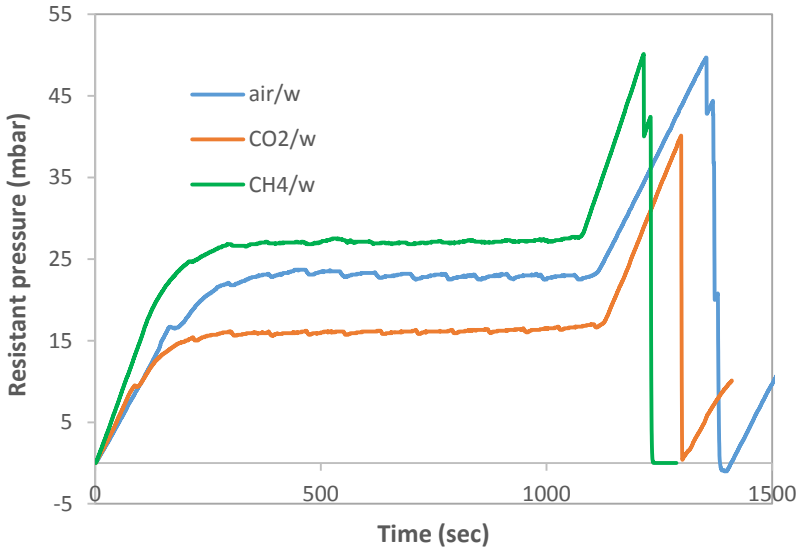

Figure 5.2: Pressure profiles for gas-water interfaces through a tapered capillary with a tip size of 105 µm and capillary gradient of 8.25×10^{-3}.

The pressure profiles when the interface moved through tapered capillaries with tip sizes ranging from 100 µm to 300 µm and capillary gradient from 6.89×10^{-3} to 1.65×10^{-2} were measured for three gas-water interfaces and oil-water interface to identify their effective pore sizes and estimate them. Air-water, CO_2-water, and CH_4-water and silicone oil-water interfaces were studied. The silicone oil-water interface was created by introducing about 0.3 ml of silicone oil into a tapered capillary already filled with distilled water. The motion of the interface front was observed by viewing it horizontally with the optical microscope, and the positions of the interface as it moved through the capillary were captured with the digital camera. The flow rate from the pump used to drive the fluids was 0.01 ml/min to minimize the effect of viscous force (Løvoll *et al*, 2005).

Figures 5.3 to 5.6 show the resistance pressure profile for air-water, CO_2-water, CH_4-water and silicone oil-water interfaces. Each pressure profile shows that as the

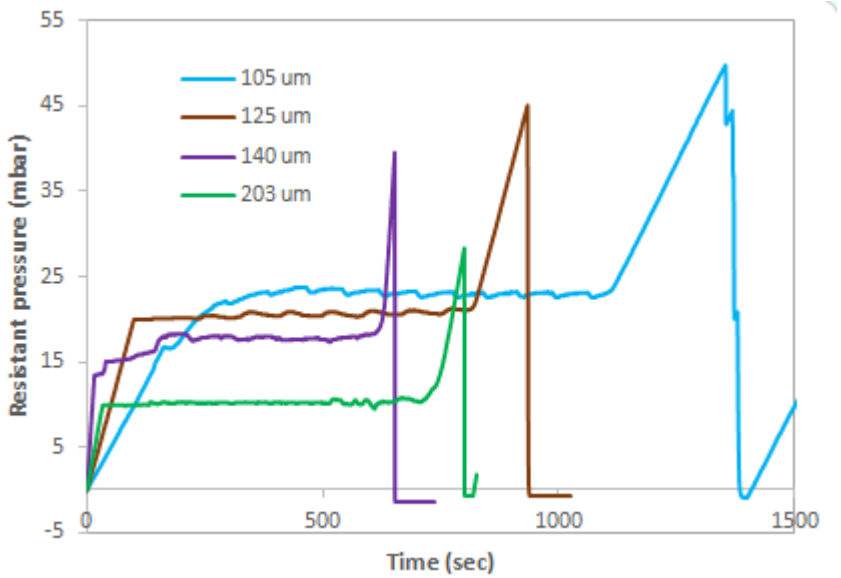

Figure 5.3: Resistant pressure profile for air-water interface displacement through capillaries with different tip sizes/capillary gradients (105 µm/8.25 × 10^{-3}; 125 µm/9.69 × 10^{-3}; 140 µm/1.16 × 10^{-2}; 203 µm/1.63 × 10^{-2}).

.

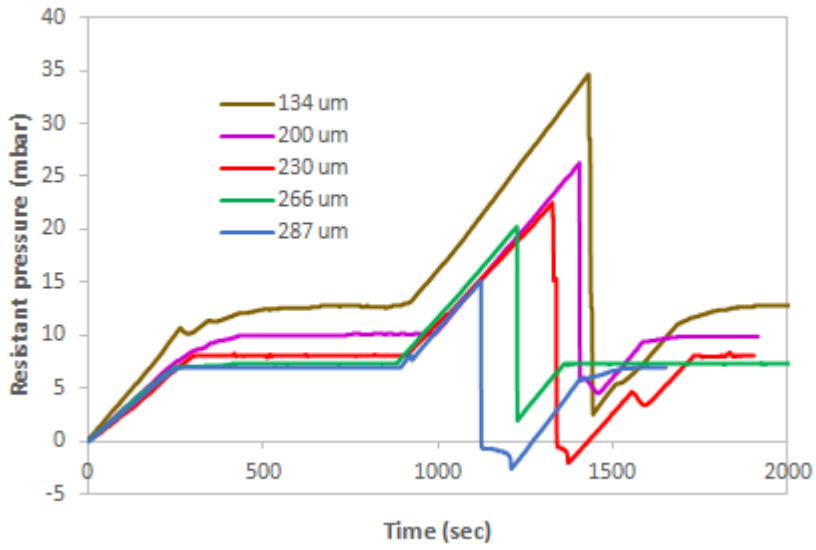

Figure 5.4: Resistant pressure profile for CO_2-water interface displacement through capillaries with different tip sizes/capillary gradients (134 µm/6.89 × 10^{-3}; 200 µm/1.35 × 10^{-2}; 230 µm/1.36 × 10^{-2}; 266 µm/1.52 × 10^{-2}; 287 µm/1.65 × 10^{-2}).

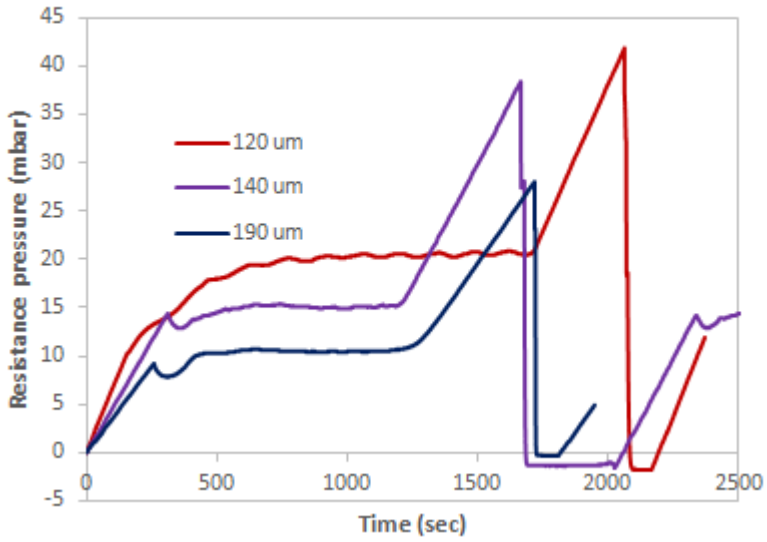

Figure 5.5: Resistant pressure profile for CH_4-water interface displacement through capillaries with different tip sizes/capillary gradients (120 µm/8.21 × 10^{-3}; 140 µm/9.05 × 10^{-3}; 190 µm/1.46 × 10^{-2}).

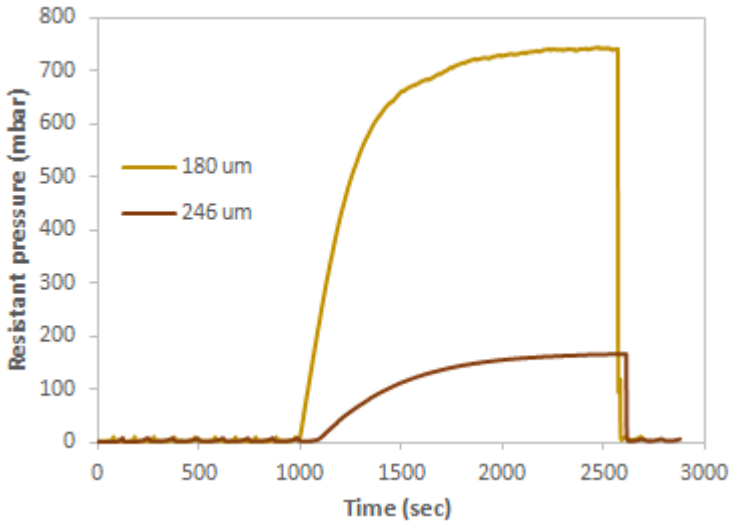

Figure 5.6: Resistant pressure profile of silicone oil-water interface displacement through two capillaries of different tip sizes/capillary gradients (180 µm/7.36 × 10^{-3}; 246 µm/1.63 × 10^{-2}). Oil viscosity: 500 cst

interface moves through the tapered capillary (micropipette) there is always an effective size; the point of a sudden increased resistance to the interface motion.

As the effective pore size is very significant in the control of fluid displacement in the porous medium its quantitative estimate was made, and the factors that may influence it were studied. The permeability of the medium was then estimated from the effective pore diameter obtained.

5.3 Estimation of the effective pore size

In order to quantify the effective pore diameter, the motion of the interface front was observed by viewing it horizontally with the optical microscope and the images of the front were taken at various positions until the interface exited the capillary. To obtain the effective pore diameter, the micrographs are processed to obtain the pressure, time and diameter corresponding to each position. The pressure-time profile is then converted to pressure-diameter profile and the effective pore diameter is obtained as the point of intersection of the constant pressure-diameter line and the linearly increasing pressure-diameter line.

As an illustration, a typical profile of a gas-water interface motion through a tapered capillary is as shown in Figure 5.7. In the pressure-time profile the effective pore diameter corresponds to position T, at which the resistant pressure to the interface suddenly increases and the pore at this point is acting as a throat to the interface. The balanced pressure section is AT, which is followed immediately by the pore throat section, TP.

A plot of pressure-diameter for sections AT and TP only of the pressure-time profile in Figure 5.7 is shown in Figure 5.8, from which the effective pore diameter is obtained. The effective pore diameter is obtained by intersection of AT and PT. The effective pore diameter in Figure 5.8 is at T, which is approximately 0.34 mm (340 µm).

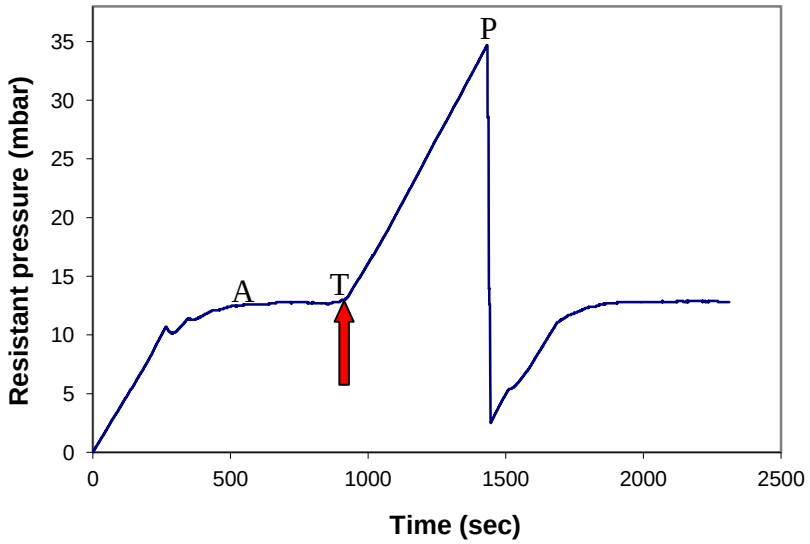

Figure 5.7: Pressure-time profile of a CO_2-water interface through a capillary with pore tip size of 134 µm and a gradient of 6.726×10^{-3}.

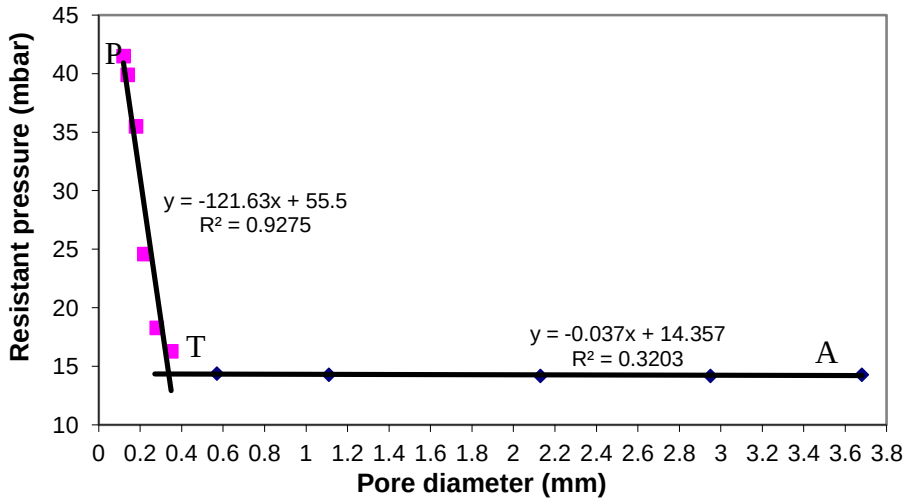

Figure 5.8: Pressure-diameter profile for sections AT and TP (refer to Fig. 5.7)

Another method of estimating the effective pore diameter is by solving the two simultaneous linear equations obtained from the pressure-diameter profile. Equations 5.1 and 5.2 are the two equations for lines AT and TP, respectively (Figure 5.8).

$$y = -0.037x + 14.357 \quad (5.1)$$

$$y = -121.63x + 55.5 \quad (5.2)$$

The value of x in Eq. 5.1 can be neglected because it is small compared to its value in Eq. 5.2. Therefore, equating the values of y from the two equations gives Equation 5.3.

$$14.357 = -121.63x + 55.5 \quad (5.3)$$

Solution of Eq. 5.3 gives the value of x as 0.338 mm (338 µm). This value is similar to the effective pore diameter obtained by intersection of sections AT and TP, and corresponds to the point T in Fig. 5.7.

The use of the simultaneous equations to estimate the pore throat diameter appears to be easier and less cumbersome, so it is the method adopted for our estimation of the pore throat diameters.

It should be noted that the value of y in Eq. 5.1 is the approximate value of the balanced pressure AT, which is equal to the resistant pressure to single phase flow. Instead of making a pressure-diameter plot for this section, we can obtain it from the original value of balanced pressure in the pressure-time plot (Figure 5.7).

In summary, to determine the effective pore diameter, the following steps are followed:

(i) Plot the pressure-time profile from the LabVIEW data. A plot of pressure (mbar) vs time (sec) is usually made.

(ii) Identify the balanced pressure section from the pressure-time profile.

(iii) Determine the balanced pressure by obtaining the average pressure for the balanced pressure section, if necessary.

(iv) From the micrographs, obtain the pressure, time and diameter corresponding to each position of the interface.

(v) Make a plot of pressure vs diameter for the pore throat section and obtain the linear equation for the section.

(vi) Using the balanced pressure obtained in (iii) above and the equation obtained in (v), solve for x to obtain the pore throat diameter.

The effective pore diameters were determined for air-water, CO_2-water, CH_4-water, silicone oil-water and crude oil-water interfaces in various tapered capillaries with

pore tip sizes varying from about 100 µm to 300 µm and capillary gradients varying from 6.901×10^{-3} to 2.153×10^{-2}. The results obtained are presented in Tables 5.1 to 5.3.

Table 5.1: Effective pore diameter for gas-water interfaces in glass capillaries

Capillary pore tip size (μm)±7.0	Air-water		CO_2-water		CH_4-water	
	Capillary gradient*	Effective pore diameter (μm)±7.0	Capillary gradient*	Effective pore diameter (μm)±7.0	Capillary gradient*	Effective pore diameter (μm)±7.0
105	8.250×10^{-3}	180	8.188×10^{-3}	171	7.733×10^{-3}	191
111	7.163×10^{-3}	205	6.901×10^{-3}	198	7.705×10^{-3}	210
125	9.688×10^{-3}	226	9.625×10^{-3}	223	1.031×10^{-2}	235
128	8.250×10^{-3}	243	8.398×10^{-3}	241	8.215×10^{-3}	248
140	1.164×10^{-2}	278	1.102×10^{-2}	264	1.209×10^{-2}	291
170	1.111×10^{-2}	338	1.038×10^{-2}	320	1.170×10^{-2}	347
180			1.242×10^{-2}	355		
184	1.343×10^{-2}	368	1.342×10^{-2}	358	1.457×10^{-2}	389
203	1.483×10^{-2}	420	1.346×10^{-2}	398	1.646×10^{-2}	447
216	1.386×10^{-2}	453				
230	1.500×10^{-2}	486				

* (dimensionless)

Table 5.2: Effective pore diameter for silicone oil-water interfaces in glass capillaries (Oil viscosity = 100 cst)

Capillary pore tip diameter (μm)±7.0	Silicone oil-water	
	Capillary gradient*	Effective pore diameter (μm)±7.0
150	3.233×10^{-3}	210
180	7.355×10^{-3}	254
207	1.271×10^{-2}	301
230	1.478×10^{-2}	359
246	1.633×10^{-2}	399
269	2.153×10^{-2}	483

* (dimensionless)

Table 5.3: Effective pore diameter for crude oil-water interfaces in glass capillaries

Capillary pore tip diameter (μm)±7.0	Silicone oil-water	
	Capillary gradient*	Effective pore diameter (μm)±7.0
109	3.796×10^{-3}	148
128	4.440×10^{-3}	165
142	1.245×10^{-2}	310

* (dimensionless)

In order to compare the measured effective pore diameter with existing correlation, theoretical effective pore diameters were calculated. Many correlations exist for estimating pore throat size, but they include bulk property of the porous medium such as porosity and permeability, which are routine parameters determined on core samples. As this is pore-level estimation, those correlations are not easily applicable.

Theoretical effective pore diameters were calculated using the Young-Laplace equation (Eq. 2.1). The measured pressure corresponding to the effective pore size (point T in Figure 5.8) was used to calculate R in the Young-Laplace equation.

Figures 5.9 to 5.13 show the comparison between the effective pore diameters obtained from our experiments with the theoretical effective pore diameter obtained using the Young-Laplace equation for air-water, CO_2-water, CH_4-water, silicone oil-water and crude oil-water, interfaces, respectively.

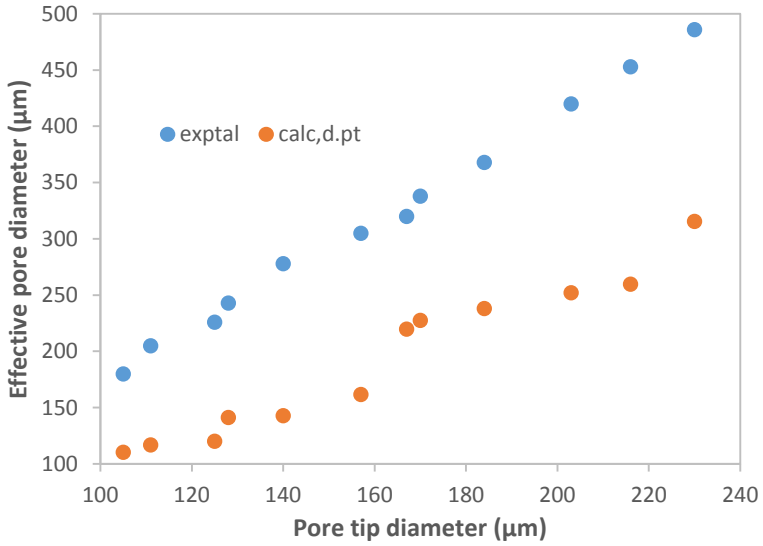

(a)Capillary tip size effect

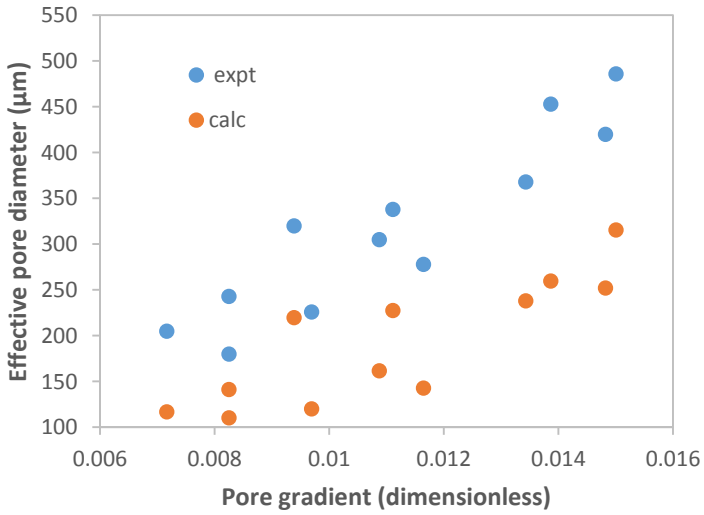

(b)Capillary gradient effect

Figure 5.9: Air-water interface – Comparison of experimental effective pore diameter with theoretical effective pore diameter using Young-Laplace equation

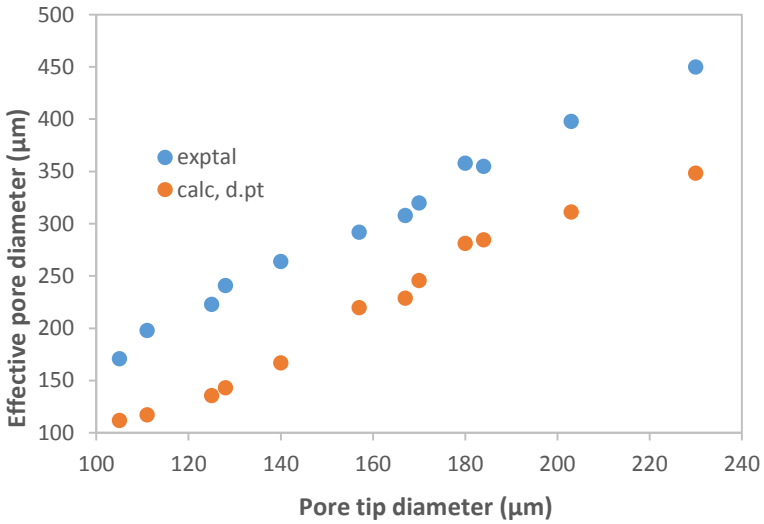

(a) Capillary tip size effect

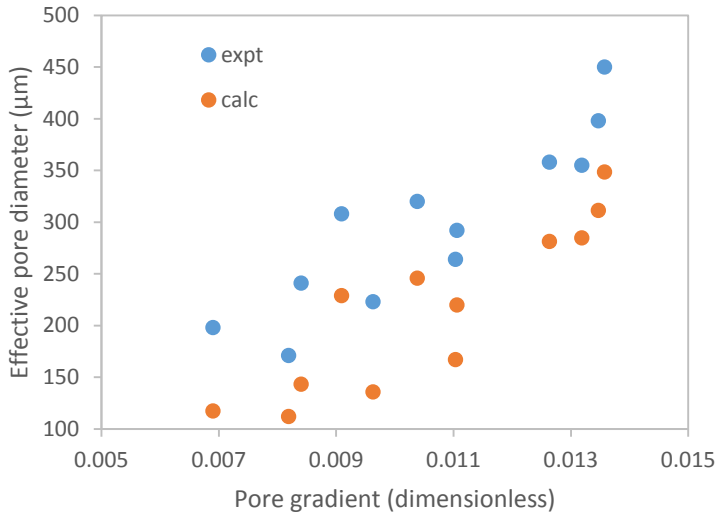

(b) Capillary gradient effect

Figure 5.10: CO_2-water interface – Comparison of experimental effective pore diameter with theoretical effective pore diameter using Young-Laplace equation.

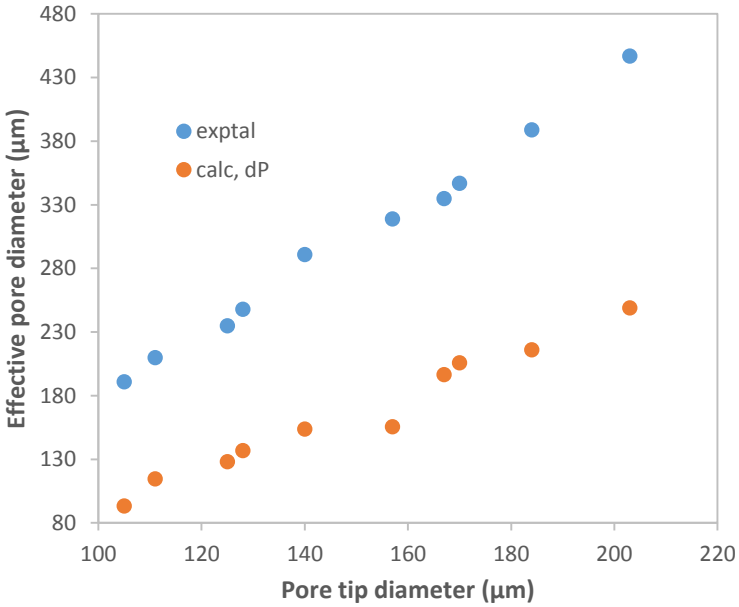

(a) Capillary tip size effect

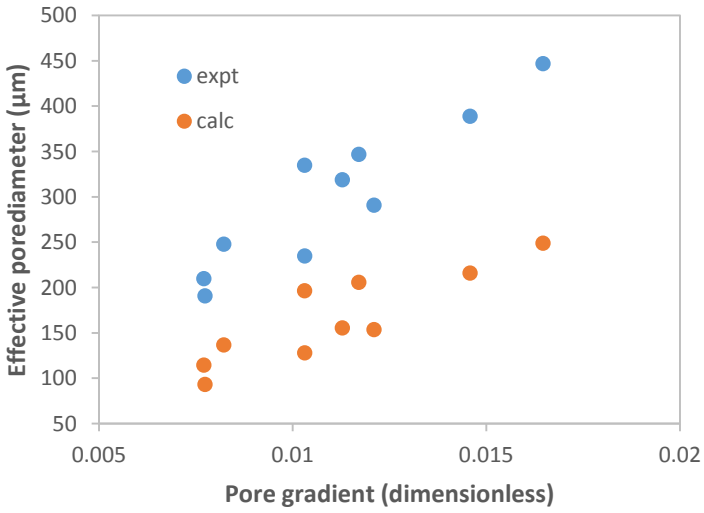

(b)Capillary gradient effect

Figure 5.11: CH_4-water interface – Comparison of experimental effective pore diameter with theoretical effective pore diameter using Young-Laplace equation.

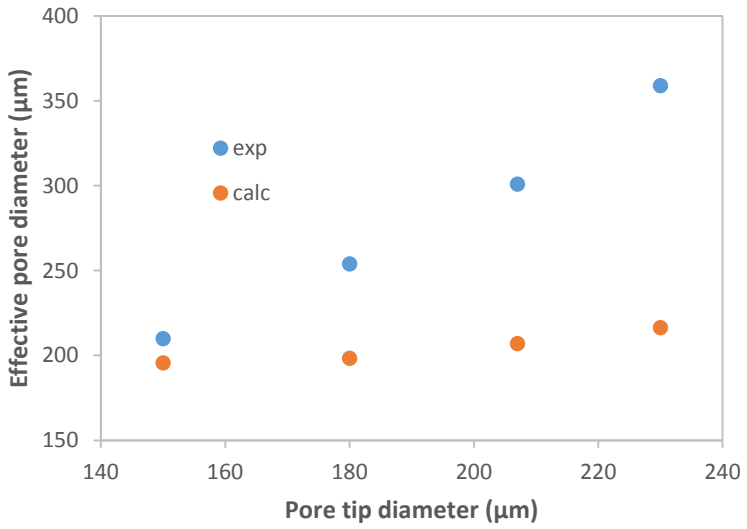

Capillary tip size effect

Figure 5.12: Silicone oil-water interface – Comparison of experimental effective pore diameter with theoretical effective pore diameter using Young-Laplace equation

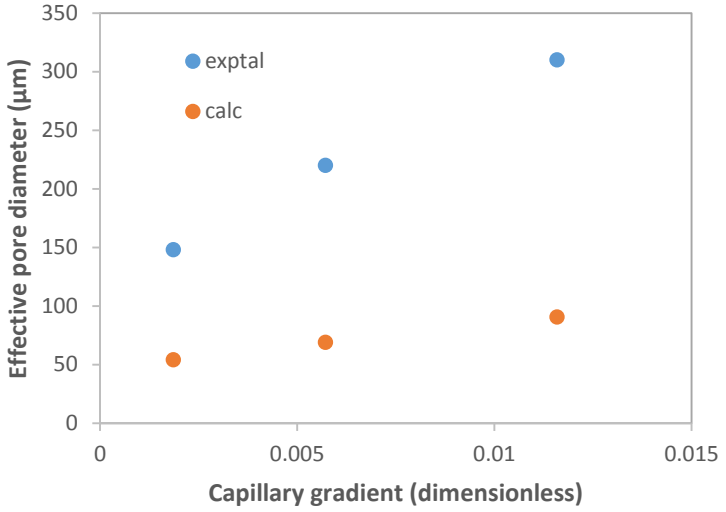

Capillary gradient effect

Figure 5.13: Crude oil-water interface – Comparison of experimental effective pore diameter with theoretical effective pore diameter using Young-Laplace equation

All the figures show that the experimental effective pore diameters are higher than the calculated effective pore diameters obtained from the Young-Laplace equation,

within the limits of experimental errors. Our results suggest that the Young-Laplace equation underpredicts the effective pore diameter for two-phase flow in a porous medium. The effective pore size is defined based mainly on the pore resistance to interface. We have shown previously (Chapter 4) that pore resistance to single phase is much smaller than the resistance to interface. The reason for the calculated effective pore diameter being lower than the measured value is because Young-Laplace equation does not consider the resistance to interface, but rather the resistance to single phase. Therefore, our experimental effective pore diameters are higher than the calculated effective pore diameter. This also confirms our previous finding (Chapter 4) that the theoretical resistant pressure obtained using the Young-Laplace equation may be applicable to single phase, and not for two-phase, displacements. As stated earlier, the equation was developed for single phase flow based on the capillary tube model and neglects the influence of conical flow in constrictions and expansions of flow channels (Scheidegger, 1974).

5.3.1 Effect of pore tip size and pore gradient on effective pore diameter

Pore tip size is important in determination of aspect ratio, which is defined as the ratio

of pore body size to pore throat size. It has been found that high aspect ratio favours oil recovery (Dehghan *et al,* 2009) and trapping under water-wet conditions (Wardlaw, 1982). Pore gradient is dependent on the length of the throat, and in a pore-throat system the length of a throat is important in causing trapping, as well as, the contrast in size between pores and throats (Wardlaw, 1982).

To study the effect of pore tip size (capillary pore tip) and pore gradient (capillary pore gradient) of different tapered capillaries with tip sizes ranging from 105 µm to 230 µm and with pore gradient of 6.901×10^{-3} to 2.153×10^{-2} were used for the motion of gas-liquid and liquid-liquid interfaces, as described in Chapter 3. Air-water, CO_2-water and CH_4-water were used to represent gas-liquid interface while silicone oil-water was used to represent liquid-liquid interface.

Figures 5.14 and 5.15 show the effects of pore tip size and capillary gradient, respectively on the effective pore diameter. For the pore tip sizes and capillary gradient considered, both figures show a linear relationship between the effective pore diameter and pore tip size, and capillary gradient; effective pore diameter increases with pore tip size and pore gradient for both the gas-liquid and liquid-liquid interfaces. However, it is observed that the gradient of the regression analysis for the effective pore diameter - capillary gradient relationship is far higher than that obtained for the effective pore diameter - pore tip diameter plot. We conclude that capillary gradient has a more dominant effect on the effective pore size than the pore tip size. This is true because we observed that two tapered capillaries may have same tip size but different capillary gradients and, as such offer different resistances to interface motion. It should be noted from our previous finding (Chapter 4) that for capillary effects to be significant the effective pore size should be less than 500 µm. Our effective pore sizes in these cases are therefore between 170 µm and 500 µm. This means that the pore within this size range will significantly affect the two-phase flow. The resistance of a pore with a size less than the effective diameter will become significant.

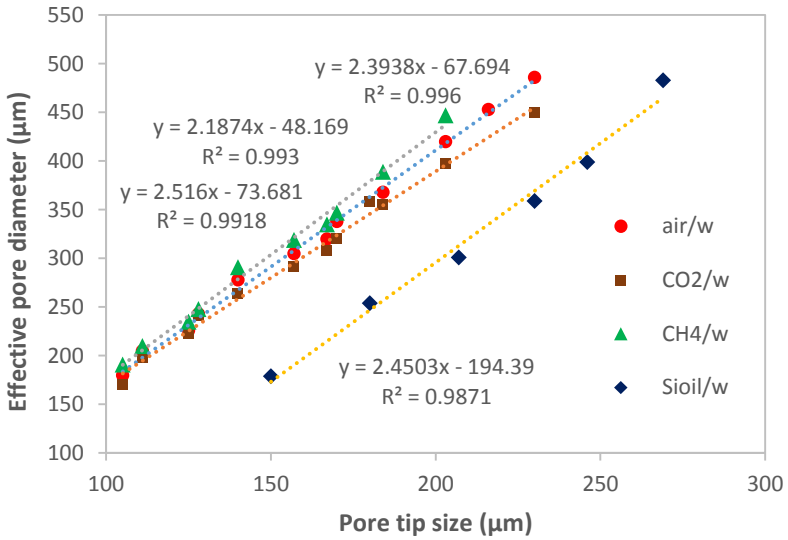

●air/w: y = 2.3938x – 67.694, R^2 = 0.996; ■CO_2/w: y = 2.1874x – 48.169, R^2 = 0.993; ▲CH_4/w: y = 2.516x – 73.681, R^2 = 0.9918;◆Si oil/w: y = 2.4503x – 194.39, R^2 = 0.9871

Figure 5.14: Effect of pore tip size on effective pore diameter for gas-liquid and liquid-liquid interfaces.

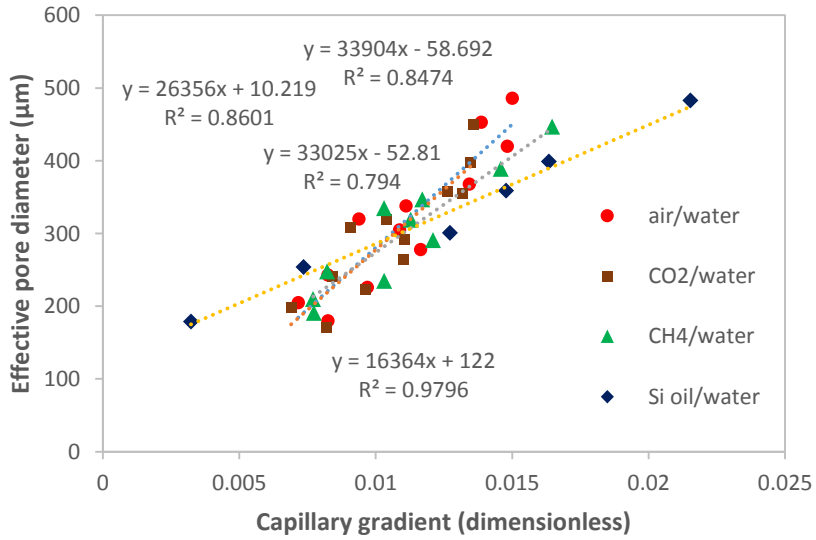

●air/water: y = 33904x – 58.692, R^2 = 0.8474;■CO_2/water: y = 33025x – 52.81, R^2 = 0.794;▲CH_4/water: y = 26356x – 10.219, R^2 = 0.8601;◆Si oil/water: y = 16364x + 122, R^2 = 0.9796

Figure 5.15: Effect of capillary gradient on effective pore diameter for gas-liquid and liquid-liquid interfaces.

The regression coefficients for the four interfaces are excellent and demonstrate the high dependence of the effective pore size on the tip size of the tapered capillary and the capillary gradient. The coefficients obtained for effective pore diameter – pore tip diameter relationship are 0.996, 0.993, 0.9918, and 0.9871 for air-water, CO_2-water, CH_4-water and silicone oil-water interfaces, respectively, while for effective pore diameter – capillary gradient relationship, the coefficients are found to be 0.8474, 0.794, 0.8601, and 0.9796 for air-water, CO_2-water, CH_4-water and silicone oil-water interfaces, respectively. For a tapered capillary of a known gradient the effective pore diameter can be estimated using any of the appropriate equations in Figure 5.15. The permeability of the porous medium can then be estimated using Equation 2.29.

Our results show that the effective pore size affects two-phase fluid flow significantly and supports Windland's observation. Winland recognized that "effective pore size" controls fluid movements in the reservoir and influences permeability measurements. Winland used the term "effective" pore size rather than "pore throat" size as measured by capillary pressure experiments. The effective pore size was defined as the pore size that effectively interconnects the pore system. (Gunter *et al,* 2014). Winland documented that in many cases, pore size is a function of crystal size, and large crystals were connected by large pores, and small crystals were connected by small pores. He noted that a more important observation is that even though larger intergranular and solution pores may be included within the intercrystalline storage system, the flow into and out of these larger pores is controlled mainly by the finer pore system. Winland's equation for calculation of average pore throat size shows that at a given porosity, larger pore throats in the pore result in greater flow-through and a larger permeability (Kolodzie, 1980). This

indicates that for a tapered capillary, larger pore tip size will give larger pore throat size (Ehrlich *et al.,* 1991a, Ehrlich *et al.,* 1991b; and McCreesh *et al.,* 1991) have shown that in sandstones the larger pores are commonly associated with larger pore throats.

Figure 5.14 shows clearly that the effective pore diameter of silicone oil-water interface is always smaller than the effective pore diameter of a gas-water interface through a capillary of the same size. This suggests that viscosity may not have any significant influence on the effective pore diameter. Washburn (1921) and Young-Laplace equations show that the radius of a pore is a direct function of the interfacial tension and the contact angle. The surface tension at ambient conditions of the silicone oil-water used is 20.9 mN/m and the air-water, CO_2-water and CH_4-water interfacial tensions are 72 mN/m, 65 mN/m and 75 mN/m, respectively (Li *et al,* 2013; Espinoza and Santamarina, 2010, Hough *et al*, 1951; Jennings and Newman, 1971). The interfacial tensions of the gas-water interfaces are higher than that of the silicone oil-water, leading to higher resistance to interface motion. This may be a possible reason for the higher pore throat diameter of the gas-water interfaces than that of the silicone oil-water interface for a corresponding pore tip diameter.

5.3.2 Effect of gas type on the effective pore diameter

The effect of gas type on the effective pore diameter was studied by using air, CO_2, and CH_4 to create interfaces with deionized water in capillaries with tip sizes of 100 – 300 µm and gradient of 6.901×10^{-3} to 1.646×10^{-2}. To obtain comparable results a tapered capillary of same tip size and gradient was used to study each of the three

interfaces, ensuring that the capillary was cleaned properly and dried before the next use.

Figure 5.16 shows the effect of the type of gas-water interface on the effective pore diameter. Figure 5.16a is the effective pore diameter – pore tip diameter plot and Figure 5.16b is the effective pore diameter – pore gradient plot for air-water, CO_2-water and CH_4-water interfaces. From Figure 5.16(a) it is seen that the effective pore diameter varies slightly with the gas applied. CH_4-water has the highest interfacial tension, and the effective pore size is larger than that in air-water and CO_2-water systems, while the effective pore size of air-water system with higher interfacial tension is larger than in CO_2-water system. Larger effective pore size (R), using tapered capillary of same capillary gradient for the different gas-water interfaces implies that the pore throat length is longer. Under the same conditions of pressure and temperature the resistance to interface will be higher. Our result implies that the resistance of a porous medium to CO_2-water interface is the least (lowest effective pore size) compared to CH_4-water and air-water systems. This confirms our finding in Chapter 4 that CH_4-water interface resistance is higher than air-water and CO_2-water systems. This may have serious implications on the geological storage of CO_2 in a depleted oil or gas reservoir. The common opinion is that the same reservoir that stored natural gas or oil could also store CO_2, after depletion of the hydrocarbon. Our finding shows that the depleted oil/gas reservoir may have lower pore resistance to CO_2 than to natural gas; the stored CO_2 could therefore escape. As a result, it is important to assess the integrity of a caprock that stored hydrocarbon before storing CO_2 in the same reservoir. The effect of interfacial tension on effective pore diameter will be investigated later.

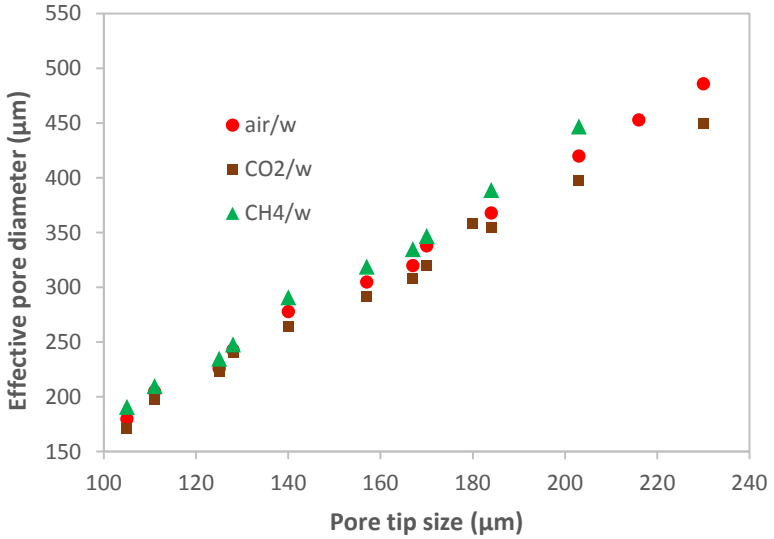

(a)

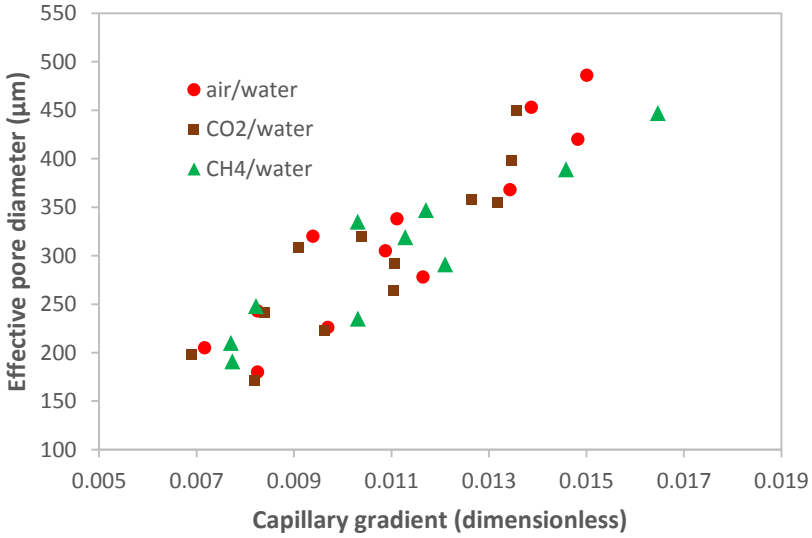

(b)

Figure 5.16: Effect of gas type on effective pore diameter

5.3.3 Effect of viscosity on effective pore diameter

To study the effect of viscosity on the pore throat diameter, the pore tip, pore gradient and surface tension were fixed. Silicone oil with viscosities ranging from 50 cst to 1000 cst and with surface tension from 20.1 to 21.2 mN/m was used to create interfaces with water. Two capillaries with pore tip sizes of 180 µm (capillary gradient: 7.355×10^{-3}) and 246 µm (capillary gradient: 1.634×10^{-2}) were used. The results are presented in Figure 5.17. The highest effective pore diameters were approximately 250 µm and 400 µm for the 180 µm and 246 µm capillaries, respectively and these remain fairly constant for the range of viscosities used, indicating that viscosity has a negligible influence on the effective pore diameter. This is in agreement with the Young-Laplace and Washburn equations. The difference in the effective pore diameter of the two capillaries at the same viscosity could be attributed to pore geometry effect as explained in the previous section. The surface tension difference between the various oil viscosities used is small, ranging from 0.1 mN/m to 0.5 mN/m. This may be the reason for slight variation in the effective pore diameter obtained for both pore sizes and pore gradient. This also gives an indication that surface tension may have a great influence on the pore throat diameter. This will be investigated further. The data from Figure 5.17 indicate that the effective size of the pore is controlled mainly by pore size and interfacial tension. Liquid viscosity does not affect the effective pore size significantly.

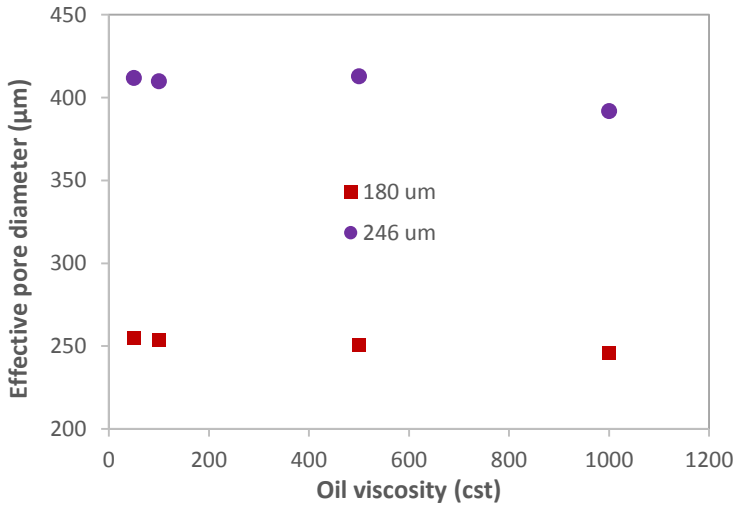

Fig. 5.17: Variation of effective pore diameter with silicone oil of different viscosities in the same capillary

5.3.4 Effect of surface tension on effective pore diameter

The effective pore diameter is the pore size that marks the beginning of the pore throat. It is characterised by a sudden increase in the resistance to two-phase displacement in a pore. To study the effect of surface tension on effective pore diameter, gas-water interface was created by using 0 %, 0.05 %, 0.1 %, and 0.2 % 1-propanol solution in deionized water. Their measured interfacial tensions are 72.0 mN/m, 42.51 mN/m, 34.86 mN/m, and 28.31 mN/m, respectively. For each tapered capillary, gas-0 % 1-propanol (water) interface was displaced first, followed by the gas-0.05 % 1-propanol, gas-0.1 % 1-propanol, and finally gas-0.2 % 1-propanol to obtain comparable results. Figure 5.18 shows the results for air-water interface. The figure shows an appreciable reduction in the effective pore diameter as the surface tension is reduced. This indicates that interfacial tension has a significant influence on the effective pore diameter.

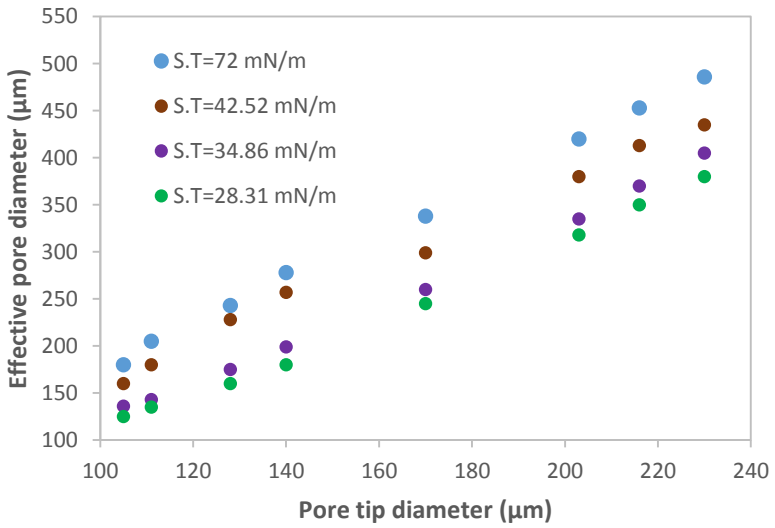

Figure 5.18: Effect of surface tension on effective pore diameter for air/propanol interface

5.4 Permeability prediction from pore throat diameter

Permeability of the porous media has been established to be mainly dependent on the pore throat radius, with the pore body contributing a little. For steady laminar flow in a uniform and smooth-walled tube of radius r, the permeability from the Hagen-Poiseuille and Darcy's laws is given by (Amyx *et al*, 1960; Oritz-Arango and Kantzas, 2011; Salah, 2011):

$$k = \frac{r^2}{8} \qquad (5.21)$$

This was also expressed by Scheidegger (1974) as:

$$k = \frac{\pi d^4}{128} \qquad (5.22)$$

Absolute permeability was estimated from Equation 5.21 using the effective pore radius obtained for the different interfaces in different capillaries. Permeability were calculated using the effective pore radius (initiation of the pore throat) and the effective radius at the capillary tip (end of the pore throat).

Figures 5.19 to 5.21 show the variation of permeability from the beginning of the pore throat radius to the end of pore throat radius (capillary tip) for air-water, CO_2-water and CH_4-water systems. The permeability at the effective pore radius (initiation of the pore throat) is always higher (bigger radius) than the permeability at the termination of the pore throat (capillary tip - smaller radius). For such systems the permeability will lie between the initiation of the pore throat and the termination of the pore throat

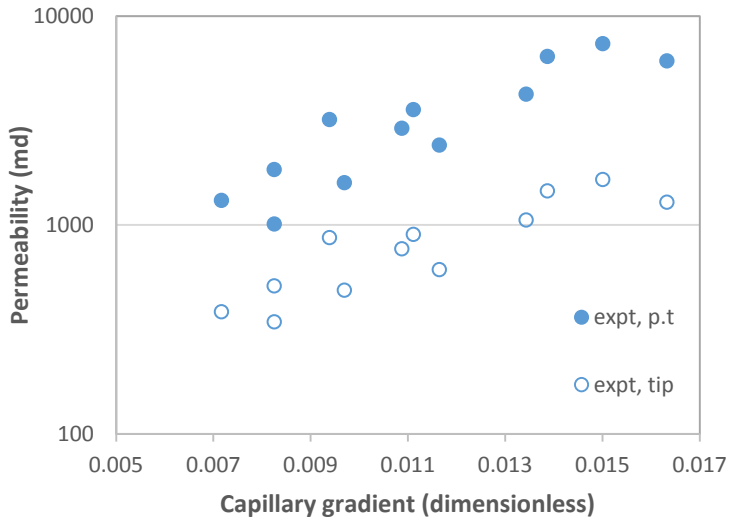

Figure 5.19: Permeability limits in tapered capillaries for air-water system

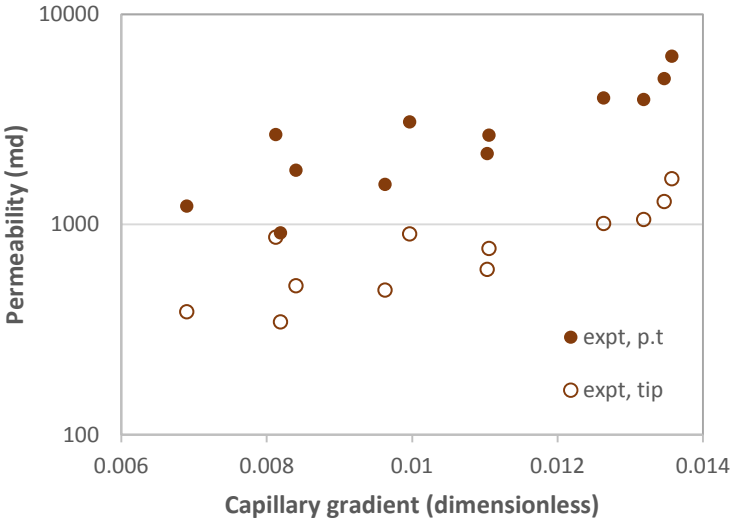

Figure 5.20: Permeability limits in tapered capillaries for CO_2-water system

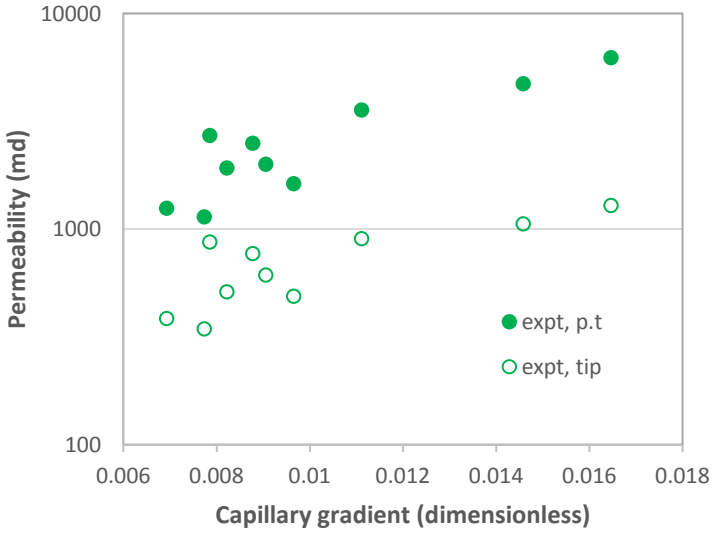

Figure 5.21: Permeability limits in tapered capillaries for CH_4-water system

5.5 Summary

The experimental results reported here demonstrate that the variation of the overall pressure resistance with pore size during an immiscible displacement experiment provides quantitative information about the aperture of the porous medium.

Effective pore size of a single pore has been identified and estimated using the resistance to two-phase flow. Effective pore diameter for air/water, CO_2/water, and CH_4/water interfaces are similar for a given pore tip size and pore gradient, especially at smaller pore tip sizes of about 100 to 140 microns. However, the effective pore size for CH_4/water is slightly higher than that of air/water, which in turn is higher than that of CO_2/water. This indicates that the energy needed to displace an interface through a pore space of the same size decreases in the order: CH_4/water > air/water > CO_2/water. It follows that CO_2 will break through more easily than methane or air.

For a given capillary size and gradient the effective pore diameter of a gas-water interface is always higher than that of silicone oil-water interface.

Effective pore diameter increases with the pore tip size and the pore gradient. However, the effect of the pore gradient is more dominant.

The effective pore diameter is influenced greatly by interfacial tension; it increases with interfacial tension. Surfactants lower the interfacial tension and consequently decrease the effective pore diameter. Viscosity does not have any significant effect on the effective pore diameter.

Effective pore diameter is very significant in determining the permeability of a porous medium. Absolute permeability for a single pore has been estimated based on pore throat size.

5.6 References

Al-Raoush, Riyadh I., Clinton S. Willson., 2005. A pore-scale investigation of a multiphase porous media system. Journal of Contaminant Hydrology 77 (2005) 67–89.

Amaefule, J.O., Altumbay, M., Tiab, D., Kersey, D.G., Keelan, D.K., 1993. Enhanced reservoir description: using core and log data to identify hydraulic (Flow) units and predict permeability in uncored intervals/wells. Paper SPE 26436. SPE Annual Technical Conference and Exhibition Houston, TX, USA, October 3–5.

Amyx, J. W., Bass, D. M., Jr. and Whiting, R. L., 1960. Petroleum Reservoir Engineering. McGraw Hill Publishing Company, New York, NY.

Boschan, A., I. Ippolito, R. Chertcoff, J.P. Hulin, H. Auradou, 2011. Characterization of fracture aperture field heterogeneity by electrical resistance measurement. Journal of Contaminant Hydrology 123 (2011) 65–74.

Bowers, M.C., R. Ehrlich, J.J. Howard, W.E. Kenyon., 1995. Determination of porosity types from NMR data and their relationship to porosity types derived from thin section. Journal of Petroleum Science and Engineering 13 (1995) 1-14.

Brown, S. R., 1989. Transport of fluid and electric current through a single fracture. J. Geophys. Res., 94 (1989), pp. 9429-9438.

Chatzis, I., Morrow, N. R., and Lim, H. T., 1983. Magnitude and Detailed Structure of Residual Oil Saturation. Soc. Pet. Eng. J. 23, 311-326 (April 1983).

Dehghan A. A., R. Kharrat, M. H. Ghazanfari, S. A. Farzaneh, 2009. Studying the Effects of Pore Geometry, Wettability and Co-Solvent Types on the Efficiency of Solvent Flooding to Heavy Oil in Five-Spot Models. Paper SPE 123315 presented at 2009 SPE Asia Pacific Oil and Gas Conference and Exhibition held in Jakarta, Indonesia, 4-6 August, 2009.

Ebanks, W. J., 1987. Flow unit concept – integrated approach to reservoir description for engineering projects. AAPG Meeting Abstracts, 1(5), 521–522.

Egermann, P., Lombard, J. M., and Bretonnier P., 2006. A fast and accurate method to measure threshold capillary pressure of caprocks under representative conditions. Paper SCA2006-07 presented at the International Symposium of the Society of Core Analysts held in Trondheim, Norway, 12-16 September.

Ehrlich, R., S. J. Crabtree, K. O. Horkowitz, and J. P. Horkowitz, 1991a. Petrography and reservoir physics I: objective classification of reservoir porosity. AAPG Bulletin, v.75, no. 10, 1547-1562.

Ehrlich, R., Etris, E.L., Brumfield, D., Yuan, L.P., and Crabtree, S.J., 199lb. Petrography and reservoir physics III: physical models for permeability and formation factor. Am. Assoc. Pet. Geol. Bull., V.75, No. 10 (October 1991): p.1579-1592.

Espinoza, D. N., Santamarina, J. C., 2010. Water-CO2-mineral systems: Interfacial tension, contact angle, and diffusion – Implications to CO2 geological storage. Water Resources Research, Vol. 46, W07537, 1-10.

Gao, Zhiye and Qinhong Hu, 2013. Estimating permeability using median pore-throat radius obtained from mercury intrusion porosimetry. Journal of Geophysics and Engineering, 10 (2013) 025014 (**7**pp).

Gielen, T., S. N. Hassanizadeh, C. T. Miller, M. W. Farthing, W. G. Gray and G. F. Pinder, 2004. A pore-scale network approach to investigate dynamic effects in multiphase flow. Computational Methods in Water Resources, Vols. 1 and 2, 55:83-94.

Gunter, G.W., D.R. Spain, E.J. Viro, J. B. Thomas, G. Potter and J. Williams., 2014. Winland Pore Throat Prediction Method - A Proper Retrospect: New Examples from Carbonates and Complex Systems. SPWLA 55rd Annual Logging Symposium, held in Abu Dhabi, United Arab Emirates, May 18-22, 2014.

Hearn, C. L., 1984. Ecological factors influencing reservoir performance of the Harfzog Drawfield. Journal of Petroleum Technology, 1335–1346.

Hough, E. W., Rzasa M. J., Wood, B. B., 1951. Interfacial tensions at reservoir pressures and temperatures; apparatus and the water-methane system. Petroleum Transactions, AIME, Vol. 192, 1951, 57- 60.

Jennings Jr., H. Y., Newman, G. H., 1971. The Effect of Temperature and Pressure on the Interfacial tension of water against Methane-Normal Decane Mixtures. Soc. Petrol. Eng. J. June 1971, 171-175.

Kolodzie, Stanley Jr, 1980. Analysis of Pore Throat Size and Use of the Waxman-Smits Equation to Determine OOIP in Spindle Field, Colorado. Paper SPE 9382 presented at the 55th Annual Fall Technical Conference and Exhibition of the Society of Petroleum Engineers of AIME, held in Dallas, Texas, September 21-24, 1980**.**

Li X., Fan X., Askounis A., Wu K., Sefiane, K., Koutsos, V., 2013. An experimental study on dynamic pore wettability**.** Chemical Engineering Science 104 (2013) 988–997.

Løvoll, Grunde, Yves Méheust, Knut Jørgen Måløy, Eyvind Aker, Jean Schmittbuhl, 2005. Competition of gravity, capillary and viscous forces during drainage in a two-dimensional porous medium, a pore scale study. Energy 30 (2005) 861–872.

Martin, A. J., Solomon, S. T. and Hartmann, D. J., 1997: Characterisation of petrophysical flow units in carbonate reservoirs. AAPG Bulletin (1997), 81, 734.

McCreesh, C. A., Ehrlich, R. and Crabtree, S.J., 1991. Petrography and reservoir physics II: relating thin section porosity to capillary pressure, the association between pore types and throat size. Am. Assoc. Pet. Geol. Bull., 75(10): 1563-1578.

Nelson, Philip H, 2009. Pore-throat sizes in sandstones, tight sandstones, and shales, AAPG Bulletin, v. 93, no. 3 (March 2009), pp. 329–340.

Oritz-Arango, J. D. and A. Kantzas, 2011. Pore-Level Investigation of Oil-Mobility Enhancement in Heavy-Oil Reservoirs. Journal of Canadian Petroleum Technology, May 2011, pp. 59-74.

Rudd, N. and Pandey, G.N., 1973. Threshold pressure profiling by continuous injection. Paper SPE 4597 presented at the Technical Conference and Exhibition, Las Vegas, Nevada, 30 September-3 October, 1973.

Salah, A., 2011. The impact of pore geometry aspects on porosity-permeability relationship – A critical review to evaluate NMR estimated permeability. Paper presented at the 10th Offshore Mediterranean Conference and Exhibition in Ravenna, Italy, March 23-25, 2011.

Scheidegger, Adrian E., 1974. The Physics of Flow through Porous Media, 3rd Edition, University of Toronto Press, Toronto and Buffalo, Printed in Great Britain.

Slatt, Roger M, 2013: Stratigraphic Reservoir Characterisation for Petroleum Geologists, Geophysicists, and Engineers – Origin, Recognition, Initiation, and reservoir Quality, Chapter 6. Development in petroleum Science, Vol. 61, Pages 1-671.

Thompson, A.H., A.J. Katz and C.E. Krohn, 1987. The microgeometry and transport properties of sedimentary rock. Advances in Physics, Volume 36, Issue 5, 1987, pages 625-694. DOI: 10.1080/00018738700101062.

Tiab, D., Donaldson, E. C., 2004. Petrophysics Theory and Practice of Measuring Reservoir Rock and Fluid Transport Properties. Elsevier Press, Oxford 112-132.

Toledo, P. G., Scriven, L. E. and Davis, H. T.: Pore space statistics and capillary pressure curves from volume-controlled porosimetry. SPE Formation Evaluation (1994), March, 46.

Tsakiroglou, C. D. and Payatakes, A. C., 2000. Characterization of the pore structure of reservoir rocks with the aid of serial sectioning analysis, mercury porosimetry and network simulation. Advances in Water Resources 23 (2000) 773-789.

Wardlaw, N.C., 1982. The Effects of Geometry, Wettability, Viscosity and Interfacial Tension on Trapping in Single Pore-Throat Pairs. J. Cdn. Pet. Tech., (May-June 1982) 21, 21-27.

Washburn, E.W., 1921. Note on a method of determining the distribution of pore sizes in a porous material. Proceedings of the National academy of Sciences of the United States of America 7, 115–116.

Wenzel, Robert N., 1936. Resistance of Solid Surfaces to Wetting by Water. Industrial and Engineering Chemistry, August 1936, Vol. 28, No.8, pp. 988-994.

Zhang, Wenjuan, Jun Yao, Hai Sun, 2015. Electrokinetic coupling in single phase flow in periodically changed capillary with a very small throat size. International Journal of Heat and Mass Transfer, Volume 84, May 2015, Pages 722-728.

Ziarani Ali S., Roberto Aguilera, 2012. Pore-throat radius and tortuosity estimation from formation resistivity data for tight-gas sandstone reservoirs. Journal of Applied Geophysics 83 (2012) 65–73.

Chapter 6: Pore wettability and flow resistance

6.1 Introduction

Wetting describes the contact between a liquid and a solid surface, which results from intermolecular interactions when the two are brought together. The wetting phase adheres more readily to the surface, while the non-wetting phase adheres less readily to the surface. The wetting phase occupies the smallest areas of the pore-space such as small pores, the corners of larger pores and as connected thin films residing on the walls of the solid surface (Schowalter, 1979). The non-wetting phase occupies the largest areas of the pore-space, principally in the centres of large pores.

As a thermodynamic process, whether or not wetting will proceed spontaneously, the rate, and the extent it can progress against the external forces that may be brought into play to resist it, or alternatively, how large an external force may be needed to overcome the initial resistance to wetting, is determined by the magnitude of the free energy change involved. As observed by Wenzel (1936), wetting replaces an area of the solid-gas interface by an equal area of solid-liquid interface and is generally also accompanied by an extension of the liquid-gas interface. Each interface has its own specific surface energy content, and as such, wetting, with its accompanying change in the extent of each interface, results in a net decrease or increase in total surface energy.

6.2 Contact angle and flow resistance in pores

Capillary force is negligible in two-phase flows in macrochannels while the inertia and viscous forces dominate, but as the tube diameter becomes smaller capillary forces become significant, and in that case the surface forces become very prominent (Lee and Lee, 2008). David and Neumann (2014) and Cubaud and Ho (2004) have also reported that in microfluidic and nanofluidic devices where the surface forces become dominant, the flow characteristics such as pressure drop, heat transfer, and mass transfer depend upon how the two fluids are distributed (flow pattern or regime), which ultimately depends on contact angle (Barajas and Panton, 1993). Several works have been reported on the effect of tube materials on the flow pattern of two-phase mixtures (Barajas and Panton (1993), Iguchi and Terauchi (2000, 2001a, b), Lee and Lee (2008), and Rapolu and Son (2007) and consequently on the pressure drop. All these are reported based on measurement of contact angles on the flat surface of the tube material in an open space. Data on the influence of geometry of wall materials of a pore space are still lacking.

Studies on contact angle have been limited to mainly observations on flat surfaces due to lack of a technique for measuring the contact angle in a small pore. Recent studies by Li *et al* (2013), Li *et al* (2014), and Li and Fan (2013), have revealed that contact angles in glass pores differ largely from the contact angles measured on flat glass surfaces. For various liquids studied, they observed that the contact angle of a liquid in a uniform glass pore increases as the pore size decreases from 1000 μm to about 300 μm. However, for pores of diameter from 300 μm to 100 μm investigated, the contact angle is fairly constant and there is no significant inconsistency regarding

the dependence of contact angle on glass pore size within this size range. We need to investigate further the effect of contact angle on the resistance to two-phase flow in pores of micron sizes.

6.3 Pore contact angle in tapered capillaries

In order to investigate the effect of contact angle on resistance to interface displacement, the static contact angles of the interface were measured in different sections of a tapered capillary. In this study, owing to the limitation of the optical microscope used it is difficult to obtain a clear image of the liquid meniscus in the tapered capillary for pore size less than 100 μm. Figures 6.1 to 6.3 show the variation of contact angle with pore size in various tapered capillaries for air-water, CO_2-water, and CH_4-water, interfaces, respectively.

All the figures show that generally, contact angle increases as the pore size decreases along the tapered capillary but tends to remain fairly constant from a pore size of about 300 μm. For the air-water interface (Figure 6.1), the contact angle increases from approximately $22^o \pm 0.003^o$ to $29.7^o \pm 0.03^o$, while for CH_4-water interface (Figure 6.3) it increases from about $23^o \pm 0.003^o$ to $30^o \pm 0.03^o$, as the glass pore size decreases from 1000 to 300 μm**.** The contact angle of the CO_2-water interface (Figure 6.2) increases from approximately $21^o \pm 0.003^o$ to $29^o \pm 0.03^o$ as the glass pore size decreases from 1000 to 300. From about 300 μm to 100 μm the change in contact angle is not significant and remains at approximately $29° \pm 0.03^o$, $29.7^o \pm 0.03^o$, and $30° \pm 0.03^o$ for CO_2-water, air-water, and CH_4-water systems, respectively.

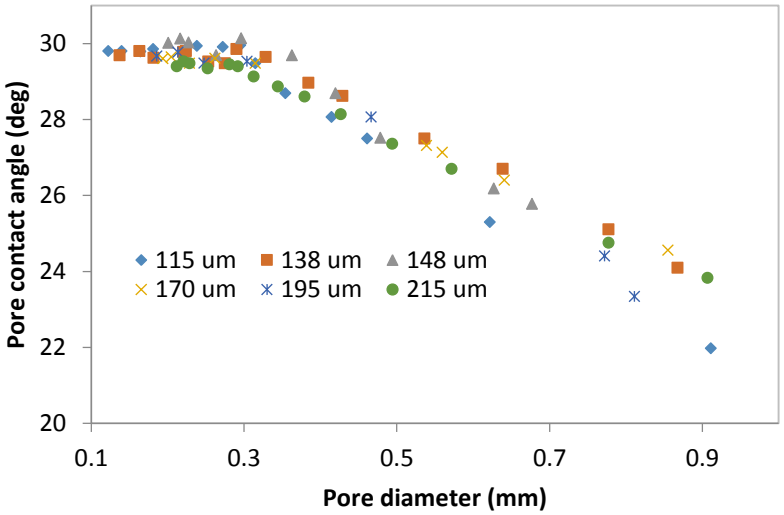

Figure 6.1: Effect of pore size on air/water contact angle in tapered capillaries with varying tip sizes/capillary gradient of 115 µm/7.155 × 10^{-3}, 138 µm/1.16 × 10^{-2}, 148 µm/1.09 × 10^{-2}, 170 µm/1.11 × 10^{-2}, 195 µm/1.63 × 10^{-2}, and 215 µm/1.39 × 10^{-2}.

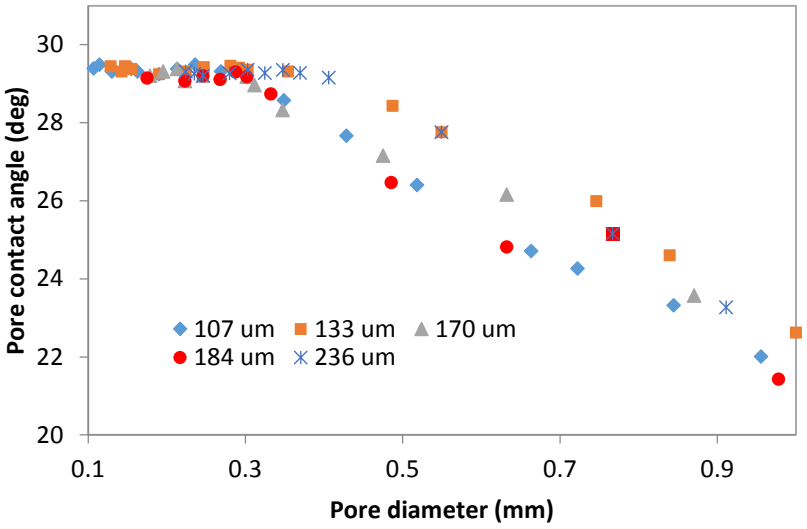

Figure 6.2: Effect of pore size on CO_2/water contact angle in tapered capillaries with varying tip sizes/capillary gradients of 107 µm/8.10 × 10^{-3}, 133 µm/8.40 × 10^{-3}, 170 µm/9.96 × 10^{-3}, 184 µm/1.31 × 10^{-2}, and 236 µm/1.36 × 10^{-2}.

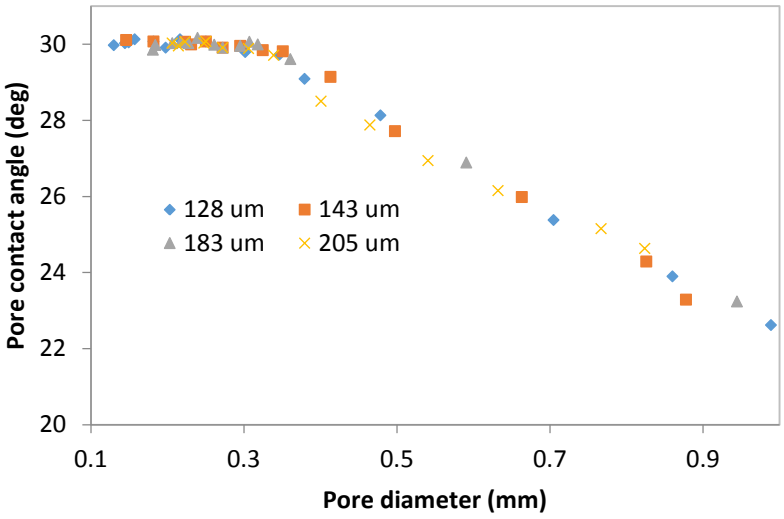

Figure 6.3: Effect of pore size on CH_4/water contact angle in tapered capillaries with varying tip sizes/capillary gradients of 128 µm/8.22 × 10^{-3}, 143 µm/9.05 × 10^{-3}, 183 µm/1.46 × 10^{-2}, 205 µm/1.65 × 10^{-2}.

The difference in the contact angle of the different interfaces could be attributed to the differences in their interfacial tensions. The CH_4-water interfacial tension is slightly higher than air-water interfacial tension, which in turn is higher than the CO_2-water. Wu *et al* (2007) have shown that as the interfacial tension increases the pressure at the three-phase contact line is increased, resulting to increased contact angle.

These results are similar to the results obtained by Li *et al* (2014), Li and Fan (2013, 2014) and Li *et al* (2013). Li and Fan (2013, 2014) and Li *et al* (2014) observed that for all liquids studied (water, 1-propanol, n-decane and crude oil), the static contact angle in uniform glass capillaries of various sizes increased as the glass pore size decreased from 1000 to 300 µm, but for pore size of roughly between 300 and 100 µm, the change of pore contact angle with pore size, though consistent, is not

remarkable. A similar observation was made by Li *et al* (2013) on the effect of pore size on dynamic contact angle in uniform glass capillaries.

They related the apparent dependence of contact angle on glass pore size within the size range of about 300 to 1000 μm to the effect of curvature of three-phase line. They concluded that, although there is no significant inconsistency regarding the dependence of contact angle on glass pore size range from 100 to 300 μm, the effect of curvature of three-phase line cannot support the results for the pore contact angles within this glass pore size range.

In this section of the capillary (that is approximately 300 μm and less) where the contact angle is highest and remain fairly constant, we have also observed a corresponding sudden increased resistance to the gas-liquid interface motion. This point of the beginning of the peak in the contact angle in the tapered capillary corresponds to the effective pore size of the tapered capillary. We have also shown in the previous chapter (Chapter 4) that the effective pore diameter in our tapered capillary lies somewhere less than 500 μm.

The magnitude of the resistant force to interface displacement in a cylindrical pore as expressed by the Young-Laplace equation is determined by the radius of the rock pore, the gas-water interfacial tension (surface energy), and wettability as expressed by the contact angle of the interface against the solid pore walls, measured through the water phase. As the gas-water contact angle is greater than zero, it is expected that the resistant pressure should theoretically decrease for the system. We have observed in this study that the interface pressure in tapered capillaries remains constant as the interface moves in a certain section of the capillary (the section just

before the effective pore radius - start of pore throat), but in the pore throat where the pore size is further reduced the interface pressure increases drastically. We suggest that this resistant pressure trend could be attributed to the trend of change of contact angle in the tapered capillary. In the section of the capillary preceding the effective pore radius (constant pressure section), the contact angle keeps increasing (that is, decreasing cos θ in Young-Laplace equation). The decrease in cos θ is balanced by the corresponding decrease in the pore size. Therefore, the interface pressure, ΔP, remains constant. At the effective pore radius, we observe that the interface pressure increases suddenly. The contact angle, which is at its peak at this point, remains fairly constant (cos θ constant) until the interface moves out of the capillary. The sudden increase in interface pressure from the effective pore radius is therefore not influenced by the contact angle but can be attributed to the effect of the decreasing pore size alone for a constant interfacial tension. The observed trend of contact angle and resistant pressure in the tapered capillary will be elucidated further in the next section.

For all the capillary tip sizes used, the variation of contact angle with pore size in a tapered capillary from a size of about 300 μm and less is very small. This suggests that the capillary tip size does not have a significant influence on the contact angle variation in the tapered capillary.

6.4 Effect of pore size on pore contact angle and resistant pressure

The effect of pore size on contact angle and resistant pressure in the tapered capillary was studied by measuring the contact angle of the interface in various sections of the capillary, up to the capillary tip. The capillary was then rinsed with deionised water, dried, and used to measure the resistant pressure to interface displacement through it. Figures 6.4 to 6.6 show the change in contact angle and resistant pressure for air-water, CO_2-water and CH_4-water interfaces in tapered capillaries of tip sizes 115 µm, 107 µm, and 128 µm, respectively. The capillary gradients of the capillaries are 7.155×10^{-3}, 8.180×10^{-3}, and 8.220×10^{-3}, and their corresponding effective pore diameters are 203 µm, 170 µm, and 250 µm, respectively.

The contact angle of air-water interface (Figure 6.4) increased from approximately 22^o at the capillary size of 1000 µm (1 mm) to about 29.8^o at the effective pore size of about 200 µm. It remains fairly constant at this angle until the interface leaves the capillary. The resistant pressure is fairly constant at about 16 mbar from the pore size of 1000 µm and at the effective pore diameter of about 200 µm it increases rapidly to a maximum of 35 mbar at the capillary tip. Similarly, for CO_2-water interface (Figure 6.5) the contact angle increased from approximately 21^o at the capillary size of 1000 µm to about 29^o at the effective pore size of about 170 µm, and remains fairly constant at this angle until the interface leaves the capillary. The resistant pressure is fairly constant at about 15 mbar from the pore size of 1000 µm and at the effective pore diameter of about 170 µm it increases rapidly to a maximum of 40 mbar at the capillary tip. Figure 6.6 shows that for CH_4-water interface, its contact angle increased from approximately 23^o at the capillary size of 1000 µm to about 30.2^o at

the effective pore size of about 250 µm, and remains fairly constant at this angle until the interface leaves the capillary. Its resistant pressure is fairly constant at about 18 mbar from the pore size of 1000 µm and at the effective pore diameter of 250 µm it increases rapidly to a maximum of about 44 mbar at the capillary tip.

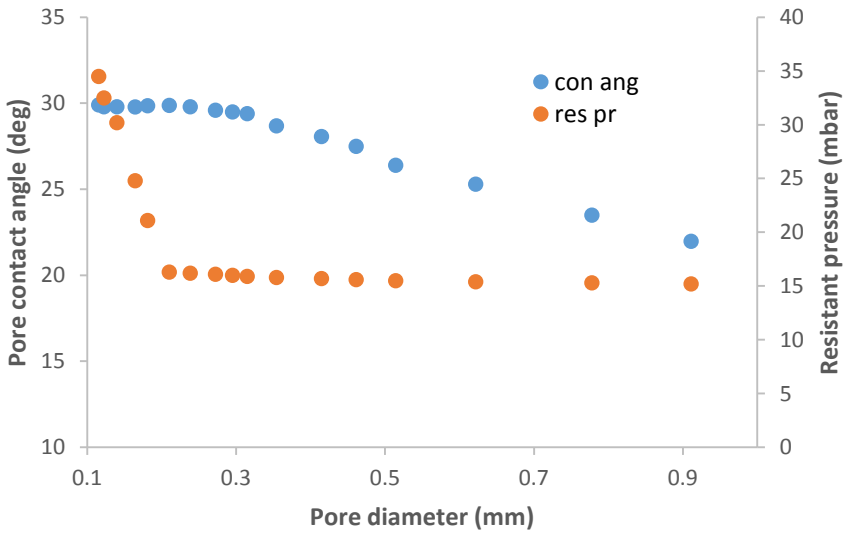

Figure 6.4: Air/water interface - Effect of pore size on contact angle and resistant pressure in a tapered capillary of tip size 115 µm and capillary gradient 7.155×10^{-3}.

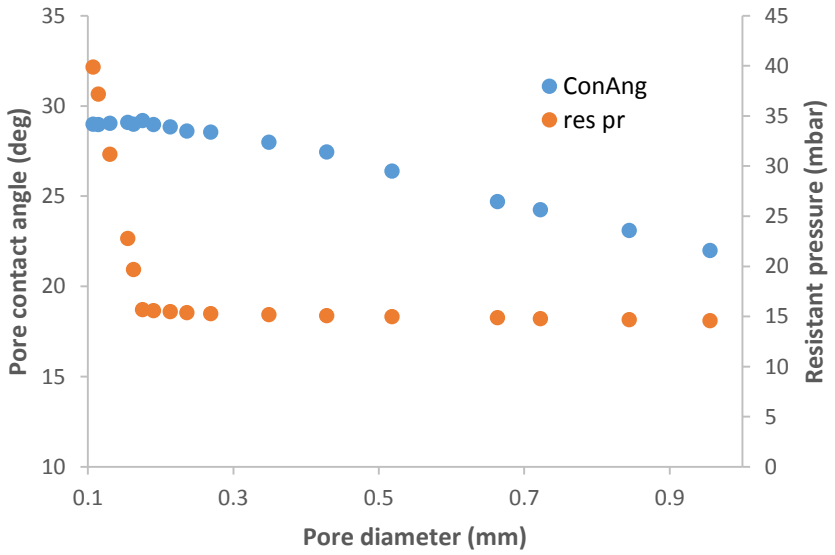

Figure 6.5: CO_2/water interface - Effect of pore size on contact angle and resistant pressure in a tapered capillary of tip size 107 µm and capillary gradient 8.180×10^{-3}.

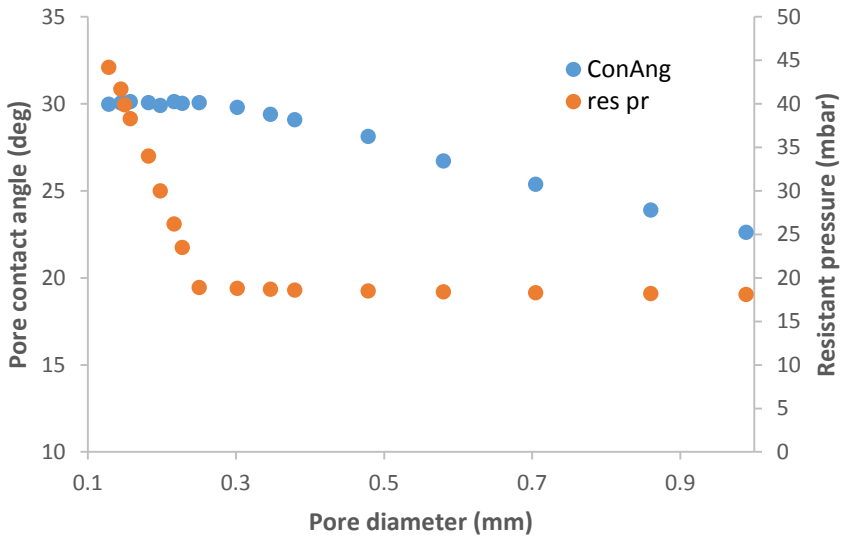

Figure 6.6: CH_4/water interface - Effect of pore size on contact angle and resistant pressure in a tapered capillary of tip size 128 µm and capillary gradient 8.220×10^{-3}

In all of the figures, the resistant pressure increase corresponds to constant contact angle, and constant resistant pressure corresponds to contact angle increase. This

may relate to the energy accumulation in the interface. When the contact angle remains constant the gas-water interface does not change, so energy does not accumulate in the interface, and the resistant pressure increases. Increasing contact angle means that the interfacial area of gas-water interface is increasing, consequently more energy is stored, so that the pressure does not increase.

6.5 Effect of surface tension on pore contact angle in a tapered capillary

To investigate the effect of surface tension of a liquid on the pore contact angle in a tapered capillary the effect of liquid viscosity should be minimized. In this study, water and aqueous solutions of 1-propanol are used. The surface tension of water is 72 mN/m while that of 5% wt 1-propanol is 42.51 mN/m, but their viscosities are small and close at 8.94×10^{-4} Pa.s and 1.10×10^{-3} Pa.s, respectively. The contact angles from about the effective pore radius to the tip of the capillary were focused on to understand more clearly the influence of surface tension on contact angle in the pore throat of a tapered capillary. Figure 6.7 illustrates the effect of surface tension of a liquid on the pore contact angle in a tapered capillary. It indicates that the contact angle for gas/water system is higher than that for the corresponding gas/5 wt% 1-propanol system. Within the pore size range considered the contact angles of the air/water systems were between 29.6^{o} and 29.8^{o} while those for corresponding air/5 wt% 1-propanol system lie between 22.9^{o} and 23.4^{o}, the contact angles of the CO_2/water system were between 28.8^{o} and 29^{o} and those of the corresponding CO_2/5 wt% 1-propanol were between 22.1^{o} and 22.6^{o}, and the contact angles of CH_4/water

system were between 29.9° and 30.2° while those of the corresponding CH_4/5 wt% 1-propanol system lie between 23.5° and 24°.

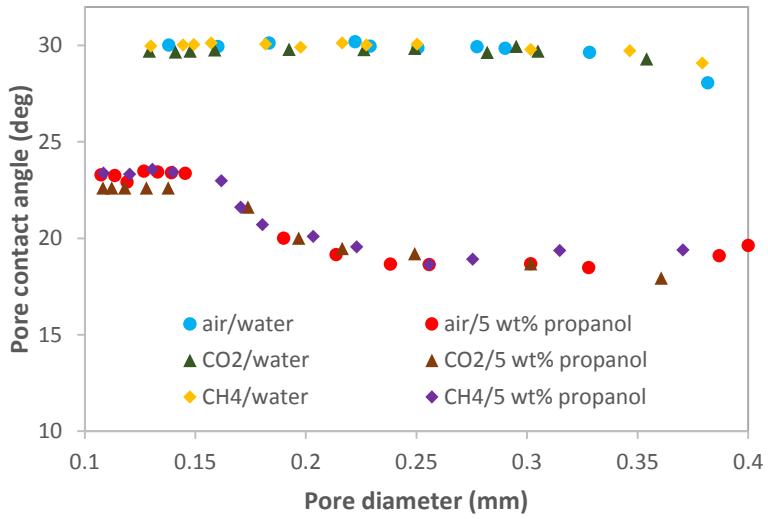

Figure 6.7: Surface tension effect on contact angle in a tapered capillary (water; γ = 72 mN/m, η = 8.94 × 10^{-4} Pa.s; 5 wt% propanol; γ = 42.51 mN/m, η = 1.10 × 10^{-3} Pa.s)

The difference in the contact angle between the gas/water system and the corresponding gas/5 wt% 1-propanol system is due to the difference in the surface tension of the liquids used in both systems. The surface tension of water was 72 mN/m while the surface tension of the aqueous solution of 1-propanol used was 42.51 mN/m. The effect of decreasing interfacial tension in the gas/aqueous 1-propanol systems is to decrease the contact angle (Shafrin and Zisman, 1960; Wu *et al*, 2007; Duzyol and Ozkan, 2014).

From Figure 6.4 the pore size range considered is within the pore throat of the tapered capillaries and the contact angles for the gas/water systems is fairly constant, as shown also previously in Figures 6.1 to 6.3. It is observed that in the gas/aqueous

1-propanol systems the contact angles also remained fairly constant from a pore size of about 150 μm. This indicates that apart from decreasing the contact angles, the decrease in surface tension of the liquid used also reduced the effective pore size. The implication of this is that the pore throat length will be reduced, with the resultant effect of reduced resistant pressure to interface motion.

6.6 Energy at interfaces between different phases

When gas forms an interface with water, for example air bubble trapped in water or water droplet in air, the water molecules at the air-water interface must be at a higher energy level than those in the bulk water. Water molecules in the bulk fluid can associate with other water molecules through hydrogen bonding and are therefore at a lower energy level. Molecules at the gas-water interface are at a higher energy state because they bind to fewer water molecules. The total energy at the interface is a product of the total surface area, A, and the surface tension, γ, between the two phases, as given in Equation 6.1 (Logan, 2012).

$$E = \gamma_{gw} A \tag{6.1}$$

where γ_{gw} is the gas-water interfacial tension (N/m) (air-water = 72 mN/m); A is in m^2.

The contribution to surface area by the interface curvature is small and can be ignored.

But, Energy (Work) = Force x distance

$$E = F \times d = PA \times d = PV \tag{6.2}$$

where E is in Joules, P is the pressure (N/m^2) exerted by the system and V (m^3) is the

volume of the system.

The capillaries used in this experiment can be simulated as a frustum of a right circular cone, as the capillaries are not uniform and are tapered towards the tip as shown in Figure 6.8.

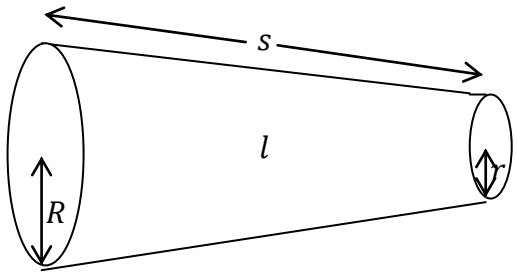

r - radius of the smaller end of the capillary
R - radius of the larger end of the capillary
l - capillary horizontal length from larger to smaller radius
s - slant length of capillary from larger to smaller radius

Figure 6.8: Enlarged tapered capillary simulated as a frustum

The volume of the frustum is given by

$$V = \pi \int_0^l [r(z)]^2 \, dz \tag{6.3}$$

But,

$$r(z) = R + (r - R)\frac{z}{l} \tag{6.4}$$

So,

$$V = \pi \int_0^l \left[R + (r - R)\frac{z}{l}\right]^2 dz \tag{6.5}$$

$$V = \frac{1}{3}\pi l(r^2 + rR + R^2) \tag{6.6}$$

where V is in m^3, r, R, and l are in m

Substituting for V in Equation (6.6) into Equation (6.2) yields

$$E = P\left[\frac{1}{3}\pi l(r^2 + rR + R^2)\right] \quad (6.7)$$

The lateral surface area, A_l

$$A_l = \pi(r + R)s \quad (6.8)$$

or

$$A_l = \pi(r + R)\sqrt{(R - r)^2 + l^2} \quad (6.9)$$

The total surface area, A

$$A = \pi(r + R)s + \pi r^2 + \pi R^2 \quad (6.10)$$

or

$$A = \pi(r + R)\sqrt{(R - r)^2 + l^2} + (\pi r^2 + \pi R^2) \quad (6.11)$$

where A is in m^2, r, R, and l are in m

Substituting for A in Equation (6.11) into Equation (6.1) yields:

$$E = \gamma_{gw}\left[\pi(r + R)\sqrt{(R - r)^2 + l^2} + (\pi r^2 + \pi R^2)\right] \quad (6.12)$$

where E is stored energy (Joules) and γ_{gw} is gas-water interfacial tension in N/m.

The experimental stored energy can be obtained using Equation (6.7), while the theoretical stored energy in interface can be obtained from Equation (6.12).

The energy stored in the interface was obtained by measuring the distance between two successive marked positions on the tapered capillary. The diameter and the corresponding pressure to the marked positions were measured as the interface moved. Owing to the difficulty of capturing distinct interface fronts in the entire capillary, measurements were focused from about the effective pore diameter to the capillary tip.

Figures 6.9 to 6.11 show plots of experimental stored energy in interface at each position in the capillary and the cumulative stored energy of the interface for air-water, CO_2-water, CH_4-water systems, respectively. All the figures show that the energy of the interface at every position is fairly constant for all the systems, while the cumulative stored energy increases as the interface advances towards the capillary tip. The increase in cumulative stored energy is as theoretically expected, because it is the addition of all the energies at the previous positions up to the current position.

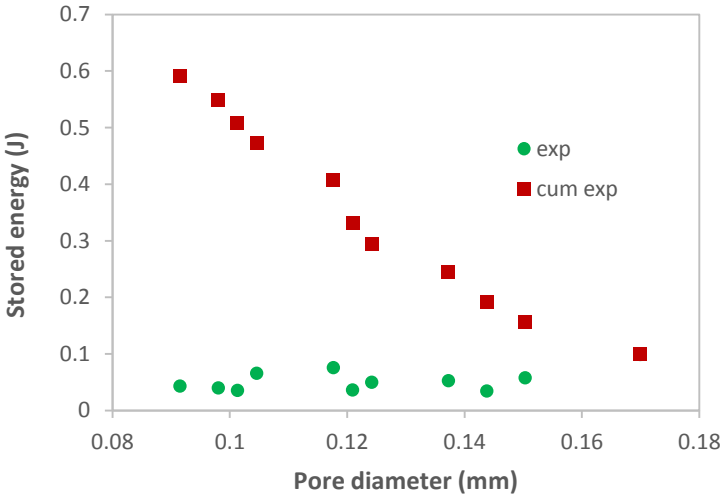

Figure 6.9: Experimental stored energy for air-water system

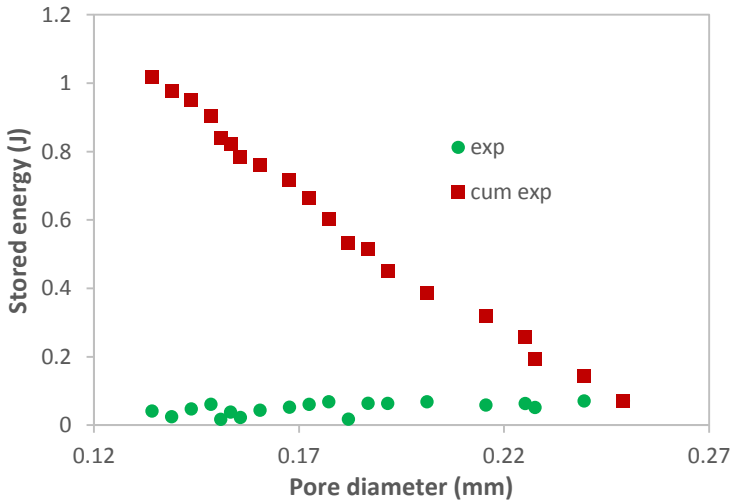

Figure 6.10: Experimental stored energy for CO_2-water system

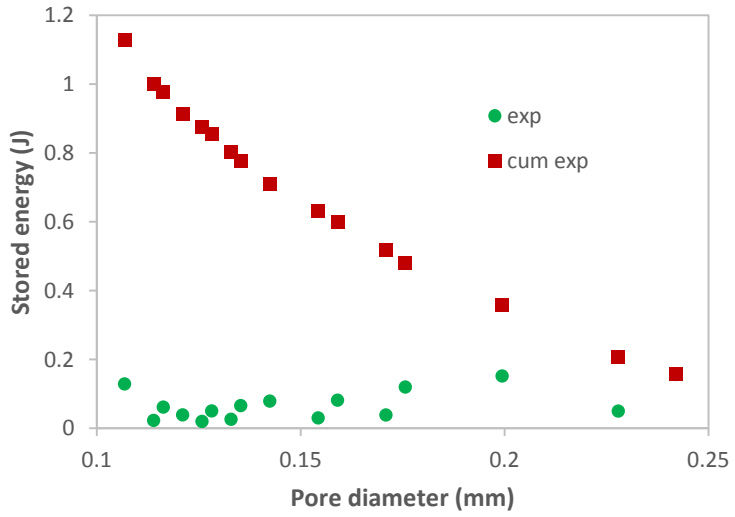

Figure 6.11: Experimental stored energy for CH_4-water system

Figures 6.12 – 6.14 show the comparison between the experimental and calculated cumulative stored energy in the interface for air-water, CO_2-water, CH_4-water systems, respectively. It is observed that the experimental and calculated stored energy seem to have a better agreement at higher pore sizes. This indicates that as the capillary effect becomes more significant, this model for stored energy of a

macroscopic scale displacement may not be suitable in the case of microscopic displacement. In addition, the experimentally measured energy is always higher than the calculated energy.

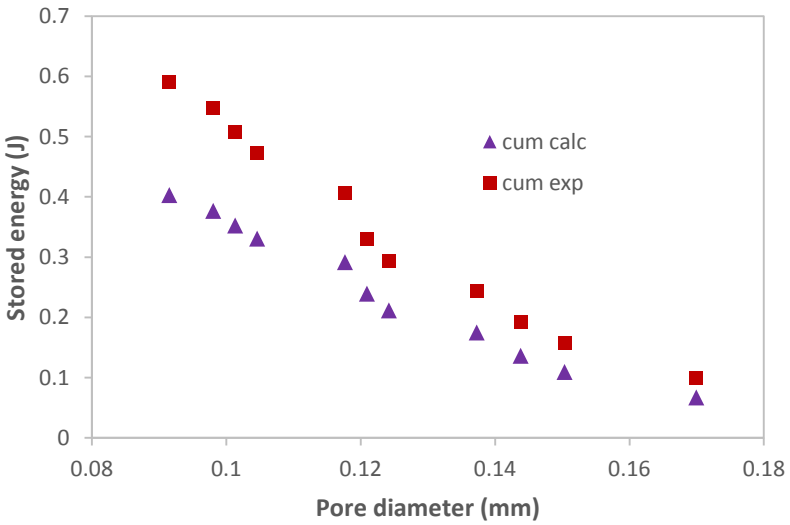

Figure 6.12: Cumulative experimental and calculated stored energy for air-water system

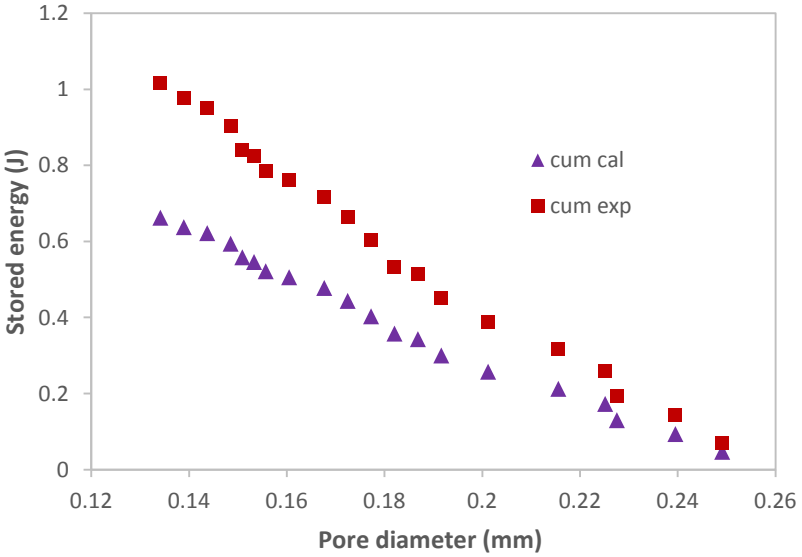

Figure 6.13: Cumulative experimental and calculated stored energy for CO_2-water system

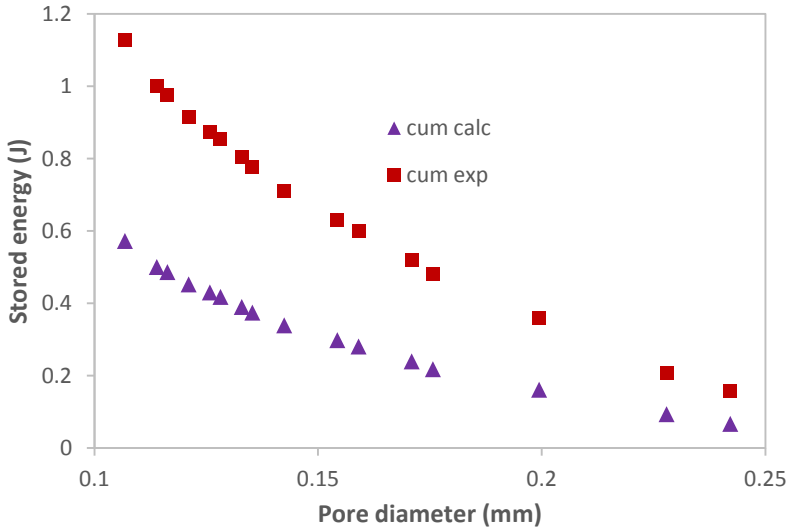

Figure 6.14: Cumulative experimental and calculated stored energy for CH_4-water system

6.7 Summary

The static contact angles of gas-liquid interfaces were measured in tapered capillaries to study the effect of contact angle on interface displacement by linking the measured contact angles to the resistant pressure to the displacement and stored energy in the interface. The results obtained indicate the following:

Pore contact angle has a significant influence on the resistant force to interface displacement in a porous medium and needs to be accurately determined rather than assuming it to be zero or constant value as had been done in many previous studies.

Contact angle increases with the decrease in the pore size, for all the systems studied but remains fairly constant after a certain pore size. It increases drastically about the effective pore size of the capillary and remains fairly constant after this point (that is, in the entire pore throat).

The section of the capillary where the contact angle is increasing corresponds to the section of constant resistant pressure while the section where the contact angle is constant corresponds to the section of rapid increase in the resistant pressure.

Contact angle in the tapered capillary decreases with decreasing interfacial tension. As the interfacial tension results in the decrease of the effective pore size it shifts the position of constant contact angle further towards the capillary tip, thus reducing the resistant pressure.

The tip size of a tapered capillary does not influence greatly the measured contact angle for any given interface. The contact angle depends largely on the pore size.

Energy stored at every position of the interface motion is fairly constant and does not depend on the contact angle, but the cumulative stored energy increases steadily throughout the interface displacement in the tapered capillary.

There seems to be no good agreement between the experimental and theoretical cumulative stored energy for the gas-water systems, especially at smaller pore sizes. This may also be an indication that the model for stored energy of a macroscopic displacement may not be suitable for microscopic displacement.

6.8 References

Barajas, A. M. and Panton, R. L., 1993. The effects of contact angle on two-phase flow in capillary tubes. Int. J. Multiphase Flow Vol. 19, No. 2, pp. 337-346, 1993.

Cubaud, T., Ho, C. M., 2004. Transport of bubbles in square microchannel, Physics of Fluids, 16(12), 4575-4585, (2004).

David R., and Neumann, A. W., 2014. Advances in Colloid and Interface Science 206 (2014) 46–56. Contact Angle Patterns on Low-Energy Surfaces.

Duzyol, S. and Ozkan, A., 2014. Effect of contact angle, surface tension and zeta potential on oil agglomeration of celestite. Minerals Engineering 65 (2014) 74-78.

Iguchi, M., Terauchi, Y., 2000. Rising behaviour of air–water two-phase flows in vertical pipe of poor wettability. ISIJ Int. (Iron Steel Inst. Jpn.) 40, 567–571.

Iguchi, M., Terauchi, Y., 2001a. Boundaries among bubbly and slug flow regimes in air–water two-phase flows in vertical pipe of poor wettability. Int. J. Multiphase Flow 27, 729–735.

Iguchi, M., Terauchi, Y., 2001b. Microgravity effects on the rising velocity of bubbles and slugs in vertical pipes of good and poor wettability. Int. J. Multiphase Flow 27, 2189–2198.

Lee, C. Y., and Lee, S. Y., 2008. Influence of surface wettability on transition of two-phase flow pattern in round mini-channels. International Journal of Multiphase Flow 34 (2008) 706–711.

Li Xingxun, Xianfeng Fan, 2013. Experimental Studies on Multiphase Flow in Porous media and Pore Wettability. World Academy of Science, Engineering and Technology 74, 739-743.

Li Xingxun, Xianfeng Fan, 2014. Pore Wetting Phenomena: Implications to Enhanced Oil Recovery and Geologic Carbon Storage. Energy Procedia 61 (2014) 2712-2715.

Li Xingxun, Xianfeng Fan, Alexandros Askounis, Kejian Wu, Khellil Sefiane, Vasileios Koutsos., 2013. An experimental study on dynamic pore wettability. Chemical Engineering Science 104 (2013) 988–997.

Li Xingxun, Xianfeng Fan, Stefano Brandani, 2014. Difference in pore contact angle and the contact angle measured on a flat surface and in an open space. Chemical Engineering Science 117(2014)137–145.

Logan, Bruce E., 2012. Environmental Transport Processes, 2nd Edition, John Wiley and Sons, Hoboken, New Jersey, Chap. 12, pp. 306 – 309.

Rapolu, P., Son, S. Y., 2007. Characterization of wettability effects on pressure drop of two-phase flow in microchannel, Exp Fluids (2011) 51:1101–1108. DOI10.1007/s00348-011-1129-8.

Schowalter, Tim T., 1979. Mechanics of Secondary Hydrocarbon Migration and Entrapment, American Association of Petroleum Geologists Bulletin, V.63, No. 5 (May 1979), p. 732-760.

Shafrin, E. G., and Zisman, W. A., 1960. Constitutive relations in the wetting of low energy surfaces and the theory of the retraction method of preparing monolayers. J. Phys. Chem. 64, 519-524.

Wenzel, Robert N., 1936. Resistance of Solid Surfaces to Wetting by Water. Industrial and Engineering Chemistry, August 1936, Vol. 28, No.8, pp. 988-994.

Wu, Jiyu, T. Farouk, and C. A. Ward, 2007. Pressure Dependence of the Contact Angle. J. Phys. Chem. B 2007, 111, 6169-6197.

Yuan, Y. and Lee, R. T., 2013. Contact Angle and Wetting Properties. G. Bracco, B. Holst (eds.), Surface Science Techniques, Springer Series in Surface Sciences 51, DOI 10.1007/978-3-642-34243-1_1, © Springer-Verlag Berlin Heidelberg 2013.

Chapter 7: Conclusion and recommendation for future work

7.1 Conclusion

This research is predicated on the premise that the fundamental behaviours of multiphase porous media systems are governed by the physical processes acting at the pore scale and that the flow and transport properties in each pore are strongly influenced by the roughness of the walls and spatial variations of their local aperture, in addition to the fractal nature of the porous medium.

The goal of this research, ultimately, is to advance the understanding of the resistance to multiphase fluid flow at the pore level using micron-sized pores, by providing data to interpret the impact of pore size, pore wettability, fluid properties and surface chemistry on fluid transport in the pores and give a clearer understanding of the exact impact of these factors on multiphase flow. The results obtained are of fundamental importance in the study of the leakage risk of stored carbon dioxide and enhanced oil recovery processes, and in addition provide fundamental data for pore-level modelling.

A novel technique is therefore developed for the measurement of resistant pressure profile in a single micron-sized pore, ensuring the ease of visualisation and monitoring of events. In addition, a novel technique to directly measure the contact angles of the interfaces (gas-liquid and liquid-liquid) in the micron-sized pore instead of the conventional contact angle measurements on a planar surface is employed. The

impact of each factor affecting fluid displacement such as pore geometry, fluid properties and wettability are studied at the pore level.

The resistant pressure profiles of gas-lquid and liquid-liquid interfaces were measuerd in various micron-sized tapered capillaries. The effective pore size of the single pores were identified and estimated for gas-liquid and liquid-liquid interfaces using the hydraulic resistance to flow, and the influence of pore geometry, gas type in the interface, interfacial tension and viscosity were investigated. Absolute permeability of the single pore was estimated from the pore throat radius. The pore contact angles of air-water, CO_2-water, and CH_4-water systems in micron-sized capillaries were measured and linked to the resistant pressure profiles and energy stored in the sytem.

The key conclusions resulting from this study are summarised as follows:

1. Glass capillaries are good options for pore-scale studies because of their ease of visualisation and monitoring of events in them. The optical effect on the glass capillary wall illuminated with white light clearly defines the internal capillary wall as a white line, while the outer wall is dark. This internal wall may appear visually as a thin water film, but this is deceptive. Any water film, if present, is infinitesimally small to be observed visually, and the gas phase being displaced by water is in direct contact with the capillary wall.

2. The resistant pressure profiles for all gas-lquid and liquid-liquid interfaces exhibit a similar pattern in single pores and this is completely different from the single phase resistant pressure profile. For the interface displacement, there is always a section of

constant pressure and a pore size of drastic increase in resistant pressure known as the effective pore size. Resistant pressure is influenced significantly by the pore geometry (pore tip size and pore gradient) and interfacial tension.

3. The effective pore size is the boundary between throat effect and non-throat effect. When the pore size is bigger than the effective size, no throat effect occurs and the resistant pressure remains constant, but when the pore size is less than the effective size, there is throat effect in which the resistant pressure increases significantly. There is no smooth connection between these two regions, so this observation is different from previous theory. This interesting observation is made in all the several hundreds of experiments conducted. This observation cannot be explained based on current theory, but it remains a fact. Therefore, effective pore size is used to explain this and distinguish it with the traditional pore throat.

4. The difference between the resistant pressure of single phase flow and two-phase flow in a single pore is observed at the effective pore size. While the resistant pressure to the single phase flow still remains constant at the effective radius and the entire pore throat, the resistant pressure to two-phase flow increases rapidly from the effective pore radius and the entire pore throat. Pore resistance to single phase flow is therefore much smaller than the resistance to two-phase flow.

5. Both the pore tip size and pore gradient influence the effective pore size but the influence of pore gradient is more dominant. Effective pore size is influenced significantly by interfacial tension; it increases with the interfacial tension. The influence of viscosity is not significant. The gas type used in the interface also

influences the effective pore size. The effective pore size of methane-water interface is highest, followed by air-water interface and then carbon dioxide-water interface.

6. Permeability of a porous medium is dependent on the pore throat diameter and its value lies between the effective pore radius and the pore tip diameter. The larger the pore throat diameter the higher the permeability.

7. Pore contact angle increases with the decrease in pore size and it is found to remain constant from the effective pore size to the pore tip. The region of constant contact angle coincides with the region of drastic increase in resistant pressure, while the region of constant pressure in the resistant profile coincides with the region of increasing contact angle. The stored energy increases steadily until the interface leaves the pore tip.

8. The difference in the contact angles of the air-water, CO_2-water and CH_4-water systems is not much. The difference in their observed resistant pressure is accounted for primarily by the differences in their interfacial tensions and the effective pore size.

9. Surfactants lower the resistant pressure and contact angle of the interface and shift the effective pore radius forward (decreasing effective radius).

Finally, this study has increased scientific knowledge and improved understanding of the multiphase processes in the porous medium.

7.2 Future work

A major limitation of this study is the lack of commercial micron-sized tapered glass capillaries. Use of standardized capillaries will make reproducibility and comparison of results easier and better. All the capillaries used were fabricated manually and it was difficult to obtain capillaries of exactly same geometry. For instance, two capillaries may have same tip size but different pore gradient and this difference will alter the results obtained and make comparison and interpretation of results difficult. It is suggested that standardized capillaries be used for future work outlined below.

1. It has been established that both pore tip size and pore gradient influence the effective pore diameter, and that the influence of the pore gradient is more dominant. However, the exact influence of pore gradient on the effective diameter has not been established because the capillaries used are not standardized. To establish the exact impact, standard tapered capillaries with same tip size but with varying gradients should be used. This was not possible to manufacture manually.

2. All the experiments so far are conducted at ambient conditions. Experimentation at higher pressures and temperatures are yet to be explored and these open up new directions of research. This will be applicable to specific cases of flow in porous medium such as the geological CO_2 storage and enhanced oil recovery.
A method needs to be devised to carry out the experiments in tapered capillaries at elevated temperatures and pressures to reflect the reservoir rock conditions.

3. A key success and better improvement on the result is to obtain a better camera. A high resolution camera should be used to measure clearer interface fronts as the

interface moves. The camera should be such that will have a self-adjusting mechanism to respond to the changes in the focused distance between the camera and the tapered capillary. This is very important because the size of the tapered capillary decreases towards the tip, thereby causing changes in the focused distance between the camera and the capillary. This will enable measurement of resistant pressure and dynamic contact angle at the same time. The camera used so far can only capture static contact angle after measurement of the resistant pressure.

4. The surfaces used for this study are high energy surfaces (water wetting). Low energy surfaces (oil wetting) should also be studied.

5. Due to the limitation of the magnification of microscope, the pore sizes used are large. A new system with high magnification to investigate pores with a size down to several microns and sub-microns would be the next stage of this research.